An EPR and DFT Investigation of the Products Formed in the Reaction of Group 11 Metal Atoms with Three-Membered Heterocyclic Compounds

By

Chad Orsini

A thesis submitted in partial fulfillment
of the requirements for the degree of
Master of Science (MSc) in Chemical Sciences

The Faculty of Graduate Studies
Laurentian University
Sudbury, Ontario, Canada

THESIS DEFENCE COMMITTEE/COMITÉ DE SOUTENANCE DE THÈSE
Laurentian Université/Université Laurentienne
Faculty of Graduate Studies/Faculté des études supérieures

Title of Thesis Titre de la thèse	An EPR and DFT Investigation of the Products Formed in the Reaction of Group 11 Metal Atoms with Three-Membered Heterocyclic Compounds
Name of Candidate Nom du candidat	Orsini, Chad
Degree Diplôme	Master of Science
Department/Program Département/Programme	Chemical Sciences
Date of Defence Date de la soutenance	March 29, 2016

APPROVED/APPROUVÉ

Thesis Examiners/Examinateurs de thèse:

Dr. Hélène Joly
(Supervisor/Directeur(trice) de thèse)

Dr. Gustavo Arteca
(Committee member/Membre du comité)

Dr. Stephan Siemann
(Committee member/Membre du comité)

Dr. Travis Fridgen
(External Examiner/Examinateur externe)

Approved for the Faculty of Graduate Studies
Approuvé pour la Faculté des études supérieures
Dr. David Lesbarrères
Monsieur David Lesbarrères
Dean, Faculty of Graduate Studies
Doyen, Faculté des études supérieures

ACCESSIBILITY CLAUSE AND PERMISSION TO USE

Abstract

Transition metals have been shown to be efficient catalysts in a variety of organic reactions. In particular, Group 11 metals have emerged as essential components in the carboxylation or metal-catalyzed ring expansion of three-membered heterocyclic compounds. Previous reports have speculated the presence of short-lived metal-substrate complexes and metallacyclic intermediates along the reaction path, yet to date there is no direct evidence for their existence.

Using cryogenic matrix isolation EPR spectroscopy, we were able to characterize several highly reactive intermediates formed in the reactions of Group 11 metal atoms, Cu, Ag, and Au, with small, strained, heterocyclic compounds, namely, oxiranes, thiiranes, and aziridines. Experimental data indicates that the major products formed are mononuclear metal complexes, M-$\overline{XCH_2CH_2}$ (X = O, S or NH). In addition, reaction mixtures containing Cu atoms and oxiranes or thiirane yield novel metallacycles, i.e., cupraoxetane and cuprathietane, respectively. DFT calculations were also used to support the structural assignments of the M-$\overline{XCH_2CH_2}$ complexes.

Dedication

This work is dedicated to my late nona, Theresa Orsini, who sadly passed away during the project. I love and miss you dearly.

Acknowledgements

I would like to thank all the people who contributed in some way to the work described in this thesis. First and foremost, I thank my academic supervisor, Dr. Hélène Joly for the opportunity to work in her group. During my tenure, she contributed to a rewarding graduate school experience with her strong mentorship, guidance and patience throughout the project. To my committee members Drs. G. Arteca and S. Siemann, thank you for your constructive criticism and helpful discussions. I would like to thank the department technologists Adam, Luc, Kevin, Paul and Frank for their assistance with equipment and certain supplies. To my lab mate Carter Hayes and all the other graduate students on the fourth floor, Rylan, Jessy, Becky, Calvin and Julie thank you for your encouragement, laughs and regular euchre games at lunch.

I would like to thank Laurentian University for affording me the Queen Elizabeth (II) Scholarship in Science and Technology during my studies and furthermore the Chemistry and Biochemistry Department for the Henrik & Regina Waern Graduate Bursary and Richard Sawicki Scholarship.

Additionally, I would like to thank my parents, Lise and Sylvio for their endless love and motivation while continuing my education. Finally, to my brother Shawn, my friends and extended family members, too numerous to list, I thank you for your enormous support over the last several year.

Table of Contents

List of Tables

List of Figures

Abbreviations, Constants and Symbols

a_{Nu}	Nuclear hyperfine interaction
AO	Atomic Orbital
β	Bohr Magneton
β_n	Nuclear Magneton
DFT	Density Functional Theory
DMF	Dimethylformamide
E	Energy
ECP	Electron Core Potential
EPR	Electron Paramagnetic Resonance
EZI	Electron Zeeman Interaction
G	Gauss
g	Effective g-value
h	Planck's Constant
H	Spin Hamiltonian
H_0	External magnetic field
I	Spin quantum number
IR	Infrared
J	Joule
K	Kelvin
kW	Kilowatt
m_I	Spin State Transitions
m_F	z-component of the total angular momentum
MHz	Megaherts
m.p.	Microwave Power
MO	Molecular Orbital
MOF	Metal-Organic Framework
mW	Milliwatts
NMR	Nuclear Magnetic Resonance
ρ_n	Electron Density
Q	Nuclear Quadrupole Interaction
SOMO	Singly-occupied Molecular Orbital
θ	Elevation angle
μ_I	Nuclear magnetic moment
v	Frequency
γ_n	Gyromagnetic ratio of the Nucleus
ψ	Wave function

1. Introduction

Harnessing and understanding the reactivity of three-membered heterocyclic compounds has fascinated chemists for decades.[1] Transition metals have long been implicated as crucial components of several catalytic transformations under both ambient and cryogenic conditions. As discussed below, there is a large literature on the metal-atom vapour cryosynthesis of novel copper (Cu), silver (Ag) and gold (Au) complexes, including both experimental as well as theoretical calculations. The latter have become an important tool, lending support to the unstable or highly reactive intermediates proposed in catalytic cycles. In the following section the importance of three-membered heterocyclic compounds, reactions catalyzed by Group 11 metal atoms, the cryosynthesis of Group 11 metal atom complexes and their characterization by EPR and DFT will be presented.

1.1. Reactivity of Three-Membered Rings

The three-membered heterocyclic compounds of interest for the work described in this thesis are oxirane, thiirane and aziridine. These small molecules can be prepared efficiently in high yields from simple starting materials.[2] They have similar structures; ethylene oxide and aziridine, for instance, are isoelectronic with 24 electrons each, and have an almost equilateral triangular structure with C-X-C bond angles of 60.58^{o} and 62.62^{o}, respectively.[2] Ethylene sulfide, on the other hand, contains 32 electrons, and exhibits a less rigid geometry about the sulfur center, resulting in a more acute C-S-C bond angle of 47.51^{o}.[2] The intrinsic ring strain of these molecules makes them an excellent choice as starting materials for the synthesis of more complex heteroatom-

containing products. The unique properties of these rings are exploited in the preparation of polymeric materials,[3,4] natural products[5] and other important molecules used every day, such as the synthesis of ethylene glycol from ethylene oxide.[6]

Three-membered rings are susceptible to nucleophilic ring opening.[7] The addition of certain transition metals to these reactions broadly expands the chemistry of these molecules.[8] Hundreds of syntheses employ transition metals as catalysts, both improving reaction conditions (lower temperatures or shorter reaction times) and leading to the production of molecules via complex processes not easily accomplished in their absence, Figure 1. Transition metals have the ability to facilitate several ring expansion reactions such as; (i) carbonylations (addition of CO), (ii) carboxylations (addition of CO_2), and (iii) cycloadditions (addition of unsaturated molecules). They can also undergo (iv) hydrogenations and (v) deoxygenation or desulfurization leading to acyclic products, just to mention a few.[8]

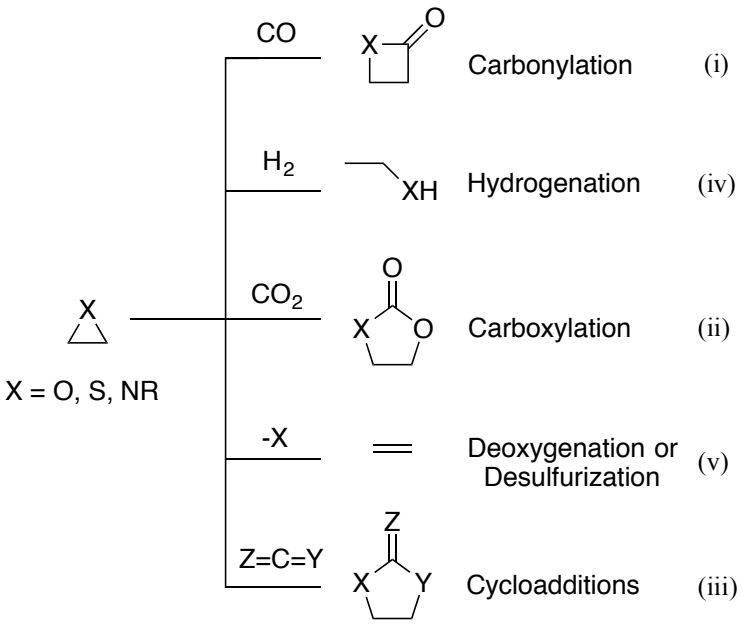

Figure 1. Transition-metal-catalyzed reactions of three-membered heterocyclic compounds

Of particular importance in this thesis are the reactions of Group 11 metals (Cu, Ag or Au) with three-membered heterocyclic compounds. A review of the literature revealed several cases whereby Group 11 metals can facilitate the catalytic ring expansion of oxiranes, thiiranes and aziridines.

For instance, ethylene or propylene carbonates can be synthesized from the corresponding epoxides with the aid of Cu(I) cyanoacetate ($NCCH_2CO_2Cu$).[9,10] It is believed that $NCCH_2CO_2Cu$ acts as a carrier of activated CO_2 since reacting Cu(I) cyanomethyl ($NCCH_2Cu$) and CO_2 gas with propylene oxide afforded the same propylene carbonate product. A theoretical study of the mechanism of the coupling reaction suggested the reaction proceeds by a two-step process.[11] The first step involves CO_2 insertion into the Cu(I)-C bond of $NCCH_2Cu$, generating the activated CO_2 carrier ($NCCH_2CO_2Cu$). The second step, shown in Figure 2, involves several intermediates (shown in brackets). Initially the epoxide coordinates to the $NCCH_2CO_2Cu$ molecule. This is followed by insertion of the Cu atom into the C-O bond forming a four-membered metallacycle which ultimately results in the formation of the carbonate product.

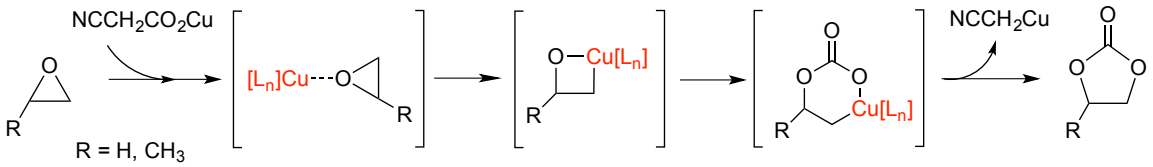

Figure 2. Cu-catalyzed carboxylation of oxiranes ($L_n = NCCH_2CO_2$)

Njardarson and coworkers have used Group 11 metal catalysts for the ring expansion of vinyl oxiranes,[12] thiiranes,[13] and aziridines,[14] Figure 3. The catalyst most frequently employed is Cu(II) hexafluoroacetylacetonate ($Cu(hfacac)_2$). It functions as a

pre-catalyst and undergoes a single-electron transfer reduction, *in situ*, forming a [Cu^{I}(hfacac)(substrate)] intermediate complex, with Cu bound to the heteroatom of the three-membered ring.[15] The next step in the catalytic cycle is thought to involve the formation of a metallacycle via C-X bond insertion. Subsequently, allylic transposition and reductive elimination steps lead to the formation of the corresponding five-membered 2,5-dihydrofuran, 2,5-dihydrothiophene or 2,5-dihydropyrrole products.

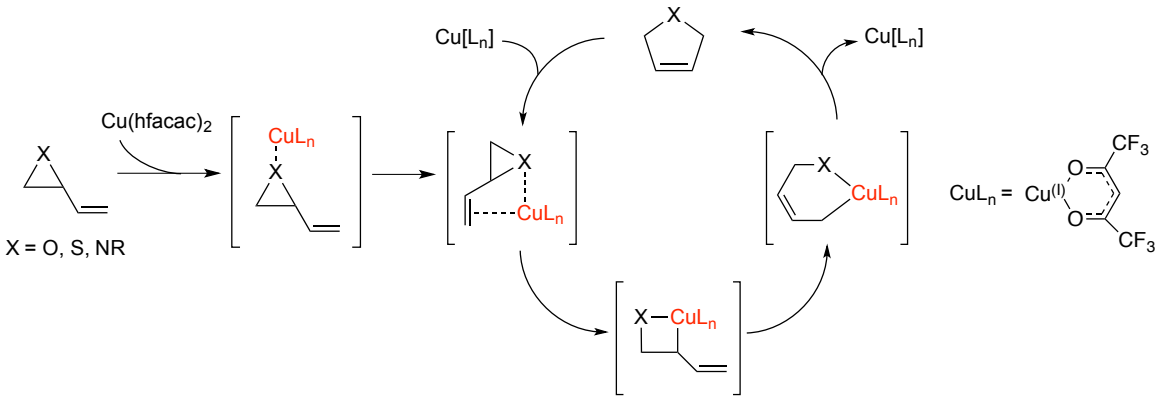

Figure 3. Cu-catalyzed ring expansion of vinyl oxiranes (X = O), thiiranes (X = S) and aziridines (X = NH).

Recent advances show that several Au complexes efficiently mediate the expansion of rings containing large substituents and multiple functional groups.[16,17] Besides catalytic ring expansion reactions, Ag and Au have also been implicated as important catalysts in the ammonolysis[18] and alkoxymetalation[19] of thiiranes. In the ammonolysis of substituted thiiranes, Figure 4, coordination of the Ag^{+} ion to the sulfur atom results in the weakening of the C-S bond facilitating the nucleophilic attack on the primary carbon atom and formation of the kinetically active ternary intermediate complex. The aminoethanethiol products are subsequently formed when the sulfur atom captures a free proton in the reaction mixture.

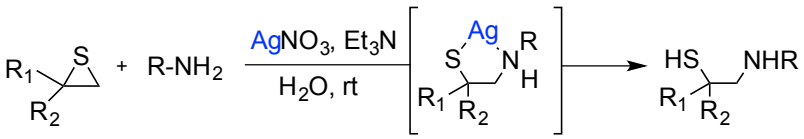

Figure 4. Ag-mediated ammonolysis of thiiranes

The reaction mechanism for the alkoxymetalation of ethylene sulfide and substituted thiiranes is thought to involve two intermediate species, I and II, Figure 5. First, complexation of the metal center to the sulfur atom occurs to form a metal-ring complex, I. A second gold-centered species (Au(OR)) is incorporated to deliver the alkoxy group to the ring, II, facilitating cleavage of the C-S bond yielding a 2-alkoxyethylsulfanylgold complex, III.

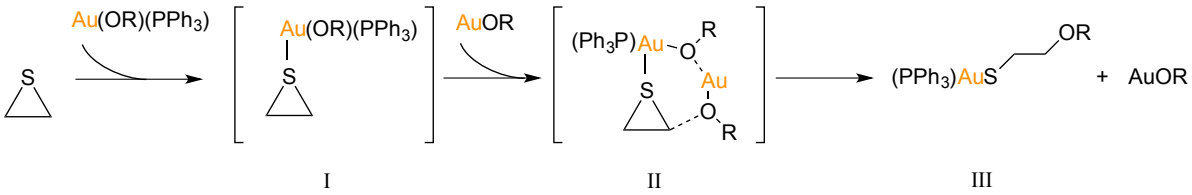

Figure 5. Au-mediated ring alkoxymetalation of thiiranes

Spectroscopic techniques such as infrared (IR), nuclear magnetic resonance (NMR) and electron paramagnetic resonance (EPR) spectroscopies, as well as the analysis of theoretically calculated energies of intermediates found along the reaction coordinate are all fundamental tools that have been employed to characterize unstable intermediates in reactions involving transition metals and three-membered heterocyclic compounds.[20,21] However, there is little evidence in support of the proposed role played by the Group 11 metal atoms in the mechanisms shown above. More specifically, successful isolation or spectroscopic evidence for one of the proposed intermediates has yet to be reported.

1.2. EPR Spectroscopy

Electron Paramagnetic Resonance (EPR) spectroscopy is an essential tool used to characterize and understand the electronic structure of paramagnetic molecules, including organic free radicals and metal-centered organometallic complexes. For brevity, this thesis will review only the pertinent aspects of EPR, namely, the nuclear hyperfine interaction, zero-field splitting, isotropic versus anisotropic EPR spectra and electron spin density.[22]

1.2.1. Principles of EPR

An unpaired electron possesses a net magnetic moment arising from the electronic spin angular momentum (S=1/2), and thus has two possible spin states, $m_s = \pm 1/2$.[23] In the absence of an external magnetic field, the two spin states are degenerate, i.e., of equal energy. However, when an external magnetic field is applied to the system the degeneracy of the spin states is lifted. A transition can be induced between the levels by applying an oscillating magnetic field of frequency, v, causing the spin to flip at a particular resonance field, according to equation (1):

$$E = hv = g\beta H_0 \qquad (1)$$

where h represents Planck's constant (6.6262×10^{-27} J•s), g is the g-value for a free electron (2.0023), β is the Bohr magneton (9.274×10^{-24} JG^{-1}) and H_0 is the external magnetic field strength (G). A low energy spin state (β, $m_s = -1/2$) results from alignment of the magnetic moment of the electron with the external magnetic field while a higher energy spin state (α, $m_s = +1/2$) results when the electron's magnetic moment opposes the

external magnetic field. The splitting between two energy states is known as the Electron Zeeman Interaction (EZI), Figure 6.

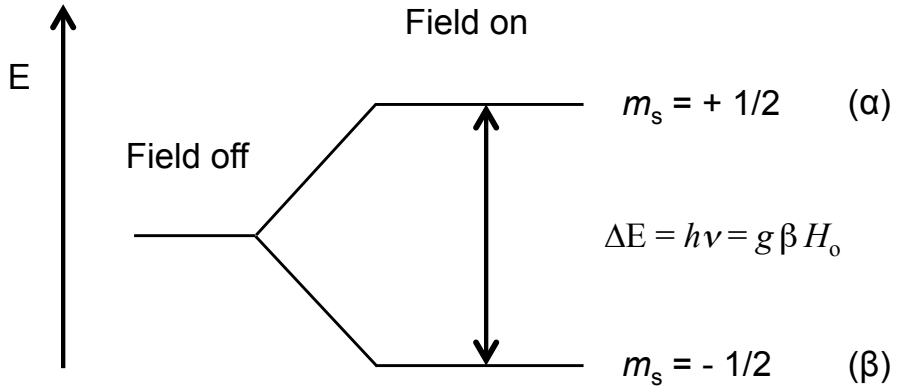

Figure 6. Electron Zeeman Interaction for a free electron in an external magnetic field (H_0)

1.2.2. Nuclear Hyperfine Interaction (a_{Nu})

The nuclear hyperfine interaction is one of the most important sources of information in EPR spectroscopy.[24] It characterizes the interaction between the magnetic moment of an electron and the nuclear magnetic moment (μ_I) of magnetic nuclei in its vicinity. Most elements have at least one stable isotope with a nuclear magnetic moment giving rise to hyperfine structure. If the magnetic moment of an unpaired electron interacts with the magnetic moment of a nucleus with a nuclear spin, I, the single EPR transition line observed will split into $2nI+1$ equally spaced lines, where n represents the number of equivalent magnetic nuclei. The sign of the nuclear hyperfine interaction is dependent on the sign of the nuclear magnetic moment (μ_I) according to equation (2):

$$\mu_I = gI\beta_n \qquad (2)$$

where β_n is the nuclear magneton (5.0510×10^{-24} J/G). The nuclear hyperfine interaction

is also proportional to the gyromagnetic ratio $\gamma_n = \mu\beta_n/I\hbar$, where $\hbar$ is $h/2\pi$ ($1.0545919 * 10^{-27}$ J.s). Therefore, the hyperfine interaction for the isotope of an element can be calculated from that of the other isotope based on the ratio of their respective gyromagnetic ratios.

The spin Hamiltonian ($\mathcal{H}$) for an isotropic system of one electron (**S**) and a nucleus of spin (**I**) in a magnetic field (**H**) is given by equation (3):

$$\mathcal{H} = g\beta\mathbf{H}\cdot\mathbf{S} + g\beta a\mathbf{I}\cdot\mathbf{S} - \gamma\mathbf{H}\cdot\mathbf{I} \qquad (3)$$

where a, the hyperfine interaction, is presented in gauss.[25] Neglecting the very small nuclear Zeeman term, $\gamma\mathbf{H}\cdot\mathbf{I}$ in equation (3), the energy levels ($E_{\pm}$) for the system are given exactly by the Breit-Rabi equations (4):[26]

$$\frac{E_{\pm}}{g\beta a} = -\frac{1}{4} \pm \frac{(2I+1)}{4}\left\{1 + \frac{4x m_F}{(2I+1)} + x^2\right\}^{1/2} \qquad (4)$$

where $x = 2H/a(2I+1)$ and m_F is the z component of the total angular momentum, $F = I \pm 1/2$. Figure 7 shows the energy levels as a function of H/a for the case of a nucleus with spin of 3/2 (i.e. $^{63/65}$Cu or ^{197}Au) and positive a. The four EPR transitions, labelled $m_I = +3/2, +1/2, -1/2$ and $-3/2$ are equally spaced and centered at $g \sim 2$ when the spectrometer frequency is greater than the zero-field splitting, $(I+1/2)a$. In this case, good approximations for g and a are obtained by iterative diagonalization of the spin Hamiltonian in equation 1. However, if v is less than the zero-field splitting there will only be two observable transitions in the EPR spectrum, the highest hyperfine component of the normal EPR transitions ($\Delta m_s = \pm 1$, $m_I = -I$) and an NMR transition ($m_s = -1/2$,

$m_I = -I \leftrightarrow -I + 1$).[27] This can be seen more clearly in Figure 8 which gives the resonant field strength, H, for the four transitions of the $I = 3/2$ system as a function of the hyperfine interaction, a (both H and a are dimensionless, in units of $\nu/g\beta$).

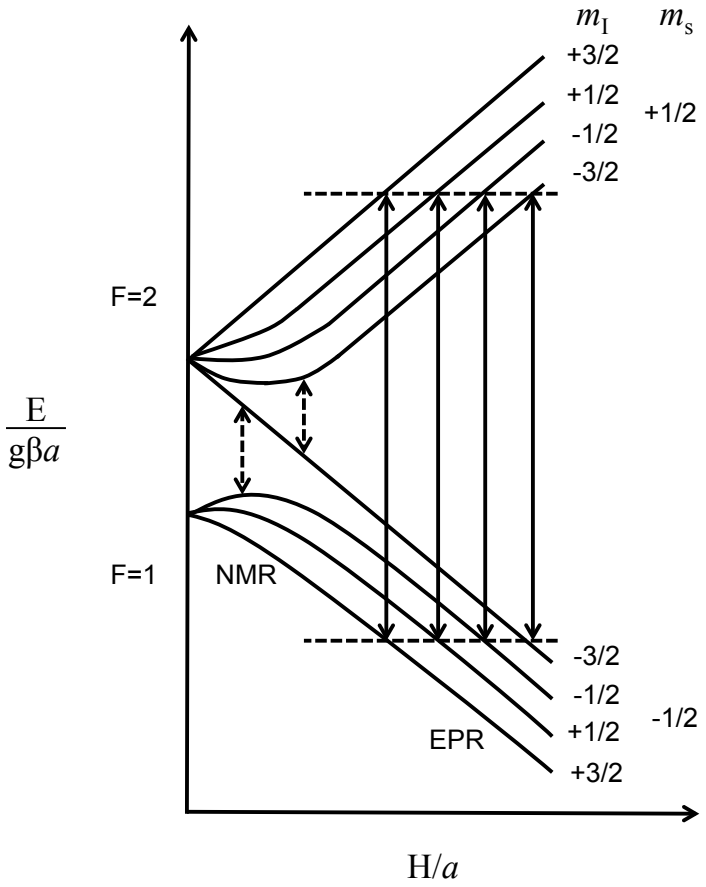

Figure 7. Energy levels for the system, S= 1/2, I = 3/2 with observable transitions for $\nu > 2a$ (solid arrows) and $\nu < 2a$ (dashed arrows).

In cases where only the highest field component is present in the spectrum, it becomes more difficult to obtain accurate values for a and g. However, Boate *et al.*[25] have demonstrated that an approximate value of a can still be obtained by equation (5):

$$a = \pm(2H - 2)/(2I + 1 - H) \qquad (5)$$

Isotopic substitution of nuclei in radicals does not significantly affect the g-value.

Therefore, it can be assumed that the *g*-value of a ^{65}Cu-containing radical where only the high field transition line is observed is approximately equal to that determined from the transition lines of the ^{63}Cu isotopomer.

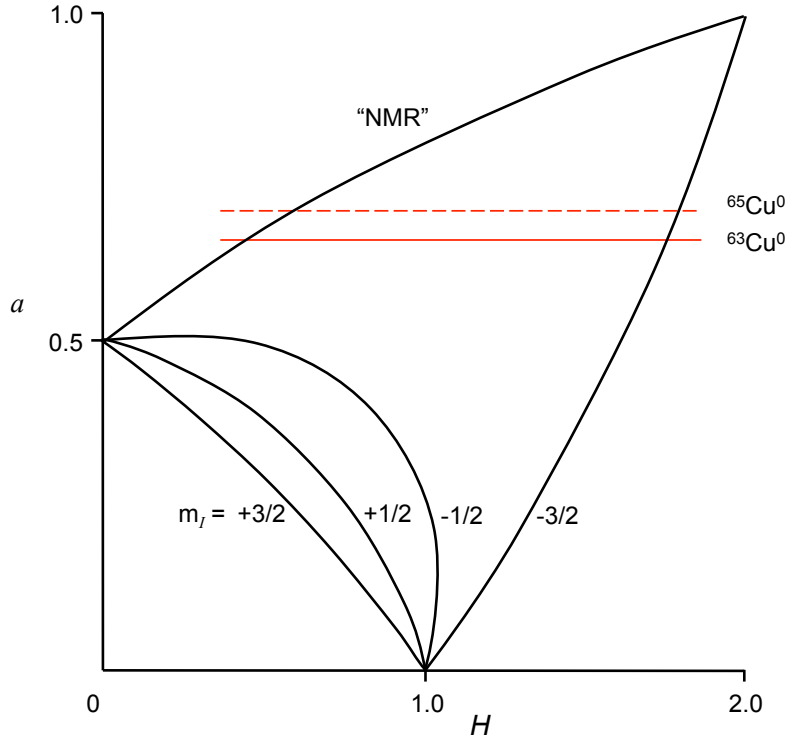

Figure 8. Resonant field strength as a function of hyperfine interaction for a S = 1/2, *I* =3/2 system. Actual positions observed with Cu atoms in an argon matrix are indicated with red lines.

1.2.3. Nuclear Quadrupole Interaction

Nuclei with $I \geq 1$ are characterized by a non-spherical charge distribution that may give rise to a nuclear electric quadrupole moment, *Q*.[28] This moment interacts with the electric field gradient at the nucleus caused by electrons and nuclei in its vicinity. In EPR spectra, nuclear quadrupole interactions cause resonance shifts in the transition lines of paramagnetic species and the appearance of otherwise forbidden transitions in isotropic nuclei. These small second-order effects are sometimes difficult to observe but

when present they can cause difficulties in the interpretation of EPR spectra.

1.2.4. Anisotropy

The samples prepared in this thesis are non-crystalline, meaning that the radicals are randomly oriented. When the rate of rotational motion is rapid, the orientation of the radicals is averaged and an isotropic spectrum is obtained. The magnetic parameters, a_{iso} and g_{iso}, will be an average of the principal values (eigen values) of the a and g tensors, equations (6) and (7):

$$a_{iso} = \frac{a_x + a_y + a_z}{3} \qquad (6)$$

$$g_{iso} = \frac{g_x + g_y + g_z}{3} \qquad (7)$$

The paramagnetic products discussed in this thesis were prepared and analysed at cryogenic temperatures. At low temperatures, the rate of rotational motion is slow and the radicals are randomly oriented with respect to the applied magnetic field. It follows that the magnetic properties of a molecule depend on the orientation of the paramagnetic species axis of symmetry with respect to the direction of the applied magnetic field, H_0, Figure 9. The orientation of the paramagnetic species in the applied magnetic field is defined with the aid of elevation (zenith) angle, θ, and the azimuth, φ. θ is the angle formed by the paramagnetic species' z-axis and the vector representing the magnetic field, H_0, while φ is the angle formed by the projection of H_0 in the xy plane and the x-axis.

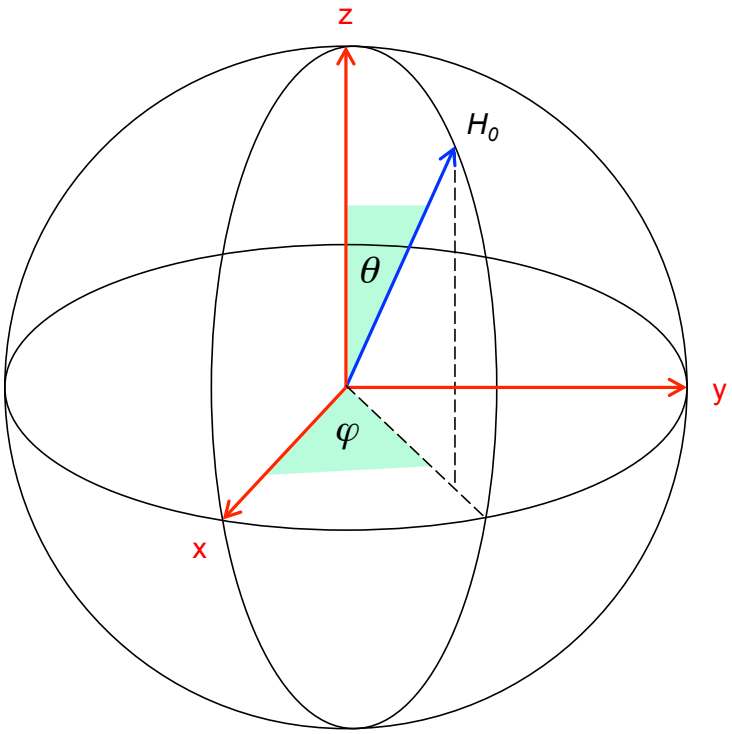

Figure 9. Orientation of a radical in a magnetic field (in spherical coordinates)

The effective g value is given by equation (8):

$$g_{eff}^2 = [\, g_x^2 \cos^2\varphi \sin^2\theta + g_y^2 \sin^2\varphi \sin^2\theta + g_z^2 \cos^2\theta] \quad (8)$$

where g_x, g_y and g_z are the principal values of the g_{eff} tensor. In cases where $g_x \neq g_y \neq g_z$ the symmetry of the g tensor is said to be orthorhombic. When the magnetic field is parallel to the axis of the paramagnetic species and it has axial symmetry, i.e., g_z is defined as $g_{\parallel}$ and $g_x = g_y$ are defined as $g_{\perp}$, equation (8) becomes (9):

$$g_{eff}^2 = [\, g_{\perp}^2 \cos^2\varphi \sin^2\theta + g_{\perp}^2 \sin^2\varphi \sin^2\theta + g_{\parallel}^2 \cos^2\theta] \quad (9)$$

which reduces to:

$$g_{eff}^2 = [\, g_{\perp}^2 \sin^2\theta + g_{\parallel}^2 \cos^2\theta] \qquad (10)$$

The effect of *g* anisotropy on the spectral pattern is shown in Figure 10. In an S = 1/2 system where $g_x = g_y = g_z$ a single line will be observed, Figure 10a. However, when the *g*-tensor is axial, i.e., $g_z \neq g_x = g_y$ or $g_{\|} \neq g_{\perp}$ the spectrum in Figure 10b results. Finally, in the case where the *g*-tensor is orthorhombic, $g_z \neq g_x \neq g_y$, the spectral pattern in Figure 10c will be observed.

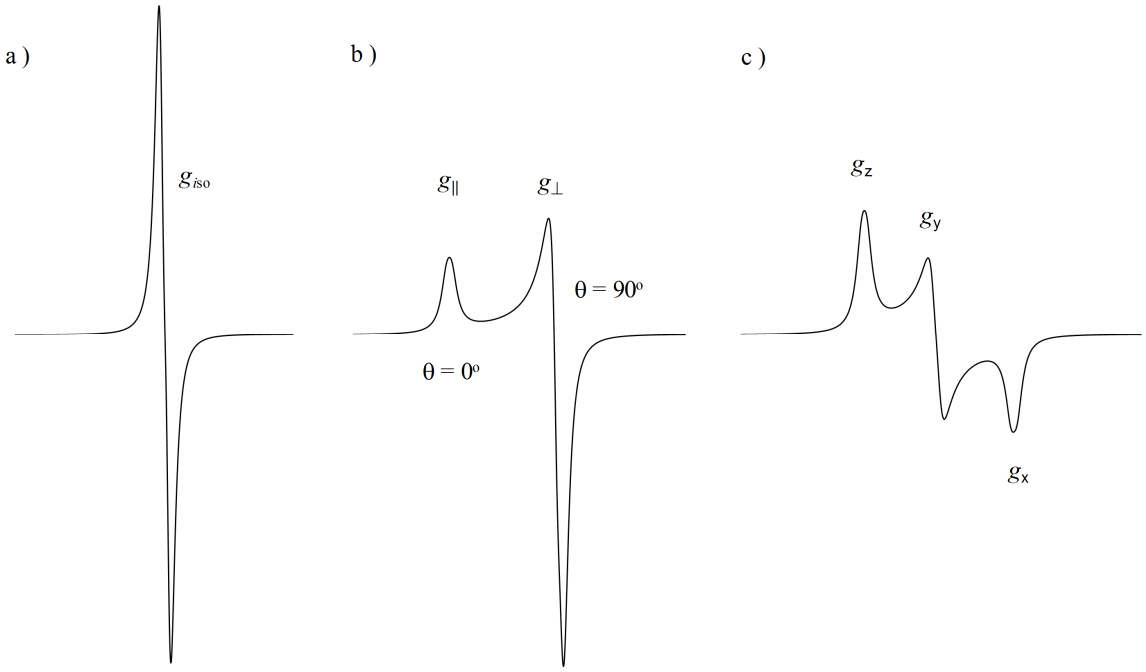

Figure 10. The effect of *g* anisotropy on the spectral pattern when the *g*-tensor is a) isotropic, b) axial and c) orthorhombic.

Similarly, anisotropy can arise in the nuclear hyperfine interaction, *a*. It is a consequence of the interaction of the nuclear and electronic magnetic moments and depends upon the orientation of the paramagnetic species with respect to the external magnetic field. It follows then:

$$a_{eff}^2 = [\, a_x^2 \cos^2\varphi \sin^2\theta + a_y^2 \sin^2\varphi \sin^2\theta + a_z^2 \cos^2\theta] \quad (11)$$

where a_x, a_y and a_z are the principal values (eigen values) of the *a*-tensor. An orthorhombic *a*-tensor results when $a_z \neq a_x \neq a_y$. For an axial *a*-tensor, i.e., $a_z = a_{||}$ and $a_x = a_y = a_\perp$, then:

$$a_{eff}^2 = [\, a_\perp^2 \sin^2\theta + a_{||}^2 \cos^2\theta] \qquad (12)$$

The expected EPR spectrum for an S = ½ system with a nucleus with I = ½ where the *a* and *g* tensors are isotropic, axial (i.e., $a_{||} > a_\perp$) and orthorhombic (i.e., $a_z > a_x > a_y$) are shown in Figure 11a, b and c, respectively.

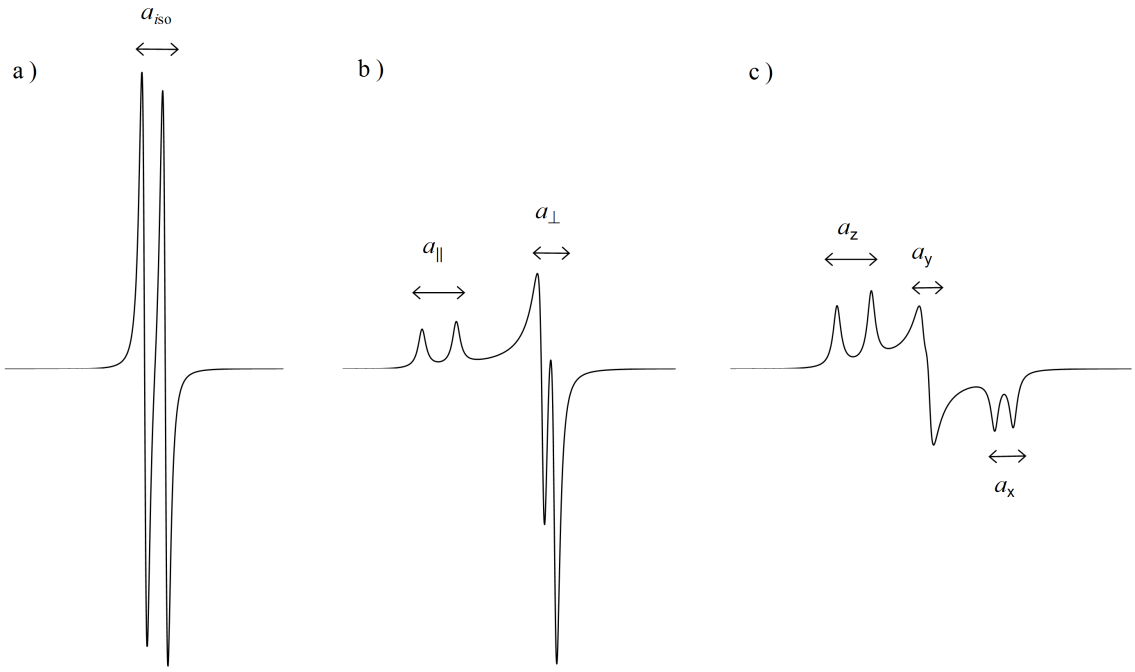

Figure 11. The effect of *a* anisotropy on the spectral pattern, for the case of an S = 1/2 system with a nucleus *I* = 1/2 where the *a*-tensor is a) isotropic, b) axial and c) orthorhombic.

The new spin Hamiltonians, representing deviations from spherical symmetry, are shown below, namely, equation (13) for paramagnetic species with axial symmetry and equation (14) for paramagnetic species with orthorhombic geometry:

$$\mathcal{H} = g_{\parallel}\beta H_z S_z + g_{\perp}\beta\left(H_x S_x + H_y S_y\right) + a_{\parallel} I_z S_z + a_{\perp}\left(I_x S_x + I_y S_y\right) \qquad (13)$$

$$\mathcal{H} = g_z\beta H_z S_z + g_x\beta H_x S_x + g_y\beta H_y S_y + a_z I_z S_z + a_x I_x S_x + a_y I_y S_y \qquad (14)$$

1.2.5. Spin Density

The electron spin density at a nucleus in a molecule is the unpaired-electron probability density at the nucleus. More specifically, it is the difference between the total probability densities of all electrons with spin α and spin β at the nucleus. The α and β spins in closed shells cancel, leaving only the contribution of the unpaired electron spin density.

The isotropic interaction, a_{iso}, is known as the Fermi contact interaction and depends upon the electron density at the nucleus, to which only *s* electrons significantly contribute, equation (15):

$$a_{\text{iso}} = \mathrm{g}_e\beta_e\mathrm{g}_n\beta_n\frac{8\pi}{3}|\psi(0)|^2 \qquad (15)$$

where $|\psi(0)|^2$ represents the spin density at the magnetic nucleus.[29] The unpaired "s" electron spin population for a molecule can then be calculated by dividing the experimental a_{iso} of the molecule by the theoretical a_{iso}^{o} of the gas phase atom:[30]

$$\rho_{ns} = a_{\text{iso}}\ (\text{molecule})/\ a_{\text{iso}}^{o}\ (\text{atom}) \qquad (16)$$

The dipolar interaction between the magnetic dipoles of the electron and the nucleus are represented as a_{dip}. If the spin density of the electron has spherical symmetry about the nucleus, this dipole-dipole interaction averages to zero. However, when there is angular

dependence (i.e., a is anisotropic) the dipolar hyperfine interaction, a_{dip}, can be calculated using equation (17):

$$a_{dip} = (a_{\parallel} - a_{\perp})/3 \qquad (17)$$

This parameter is divided by the theoretical values of a^{o}_{dip}, to estimate the unpaired spin population of *p*, *d* or *f* electrons:

$$\rho_{np/d/f} = a_{\text{dip}}\ (\text{molecule})/\ a^{o}_{\text{dip}}\ (\text{atom}) \qquad (18)$$

The parameters, a_{iso} and a_{dip} will be used to characterize the singly-occupied molecular orbital (SOMO) of paramagnetic molecules prepared in the present study, revealing important bonding information.

1.3. Reactions of Group 11 Metals via Matrix Isolation

Metal-vapour synthesis has made a significant contribution as a method to prepare new and unusual metal complexes in the fields of synthetic organic and inorganic chemistry.[31] The technique involves the condensation of metal atoms and substrate molecules on a reaction surface, under cryogenic conditions, where the product is formed and collected.

Information on the nature of bonding in metal σ- and π- complexes of small molecules has been obtained by adapting cryosynthetic methods in such a way as to accommodate a wide range of spectroscopic techniques.[32–34] This requires that the products are isolated in matrices. Similar to a solvent, the matrix functions as a means to separate the highly reactive intermediates or complexes, thus minimizing unwanted secondary reactions. IR and UV-Vis spectroscopy are best used with rare gas matrices

and allow for the examination of both paramagnetic and diamagnetic products. EPR spectroscopy can be used in combination with either rare gas or inert hydrocarbon matrices and is restricted to the study of paramagnetic species.

Cu, Ag, and Au represent the first, second and third row transition metals in Group 11 of the periodic table, with increasing radii reflecting the larger atomic number. They have similar ground state electronic configurations of $[Ar]3d^{10}4s^1$, $[Kr]\ 4d^{10}5s^1$ and $[Xe]4f^{14}5d^{10}6s^1$, respectively, and are all paramagnetic with the unpaired electron residing in the largest semi-filled s orbital.

In general, the matrix-isolated intermediates formed in the reactions of Group 11 transition metals and organic or inorganic molecules fall into three categories;[35]

1) σ- or π-complexation to the metal center
2) Addition of the metal to a carbon atom
3) Metal insertion into various (C-X, N-X, or X-F) bonds.

A summary of Group 11 metal complexes characterized by matrix-isolation EPR spectroscopy, including, a_{iso}, the *g*-value, and the calculated metal s spin population can be found in Tables 1, 2, and 3. The values for isolated atoms are also included for comparison.

Metal atoms reacted with unsaturated compounds such as alkenes, alkynes, cyanides, and alkylcyanides, were referred to as π complexes, whereas reactions between metals and substrates containing lone pairs, i.e., :CO, :SiO, $:NH_3$, or $:PF_3$, generate σ bonded complexes. Paramagnetic addition products are also formed when metal atoms add to one of the carbon atoms of the triple bond in alkynes, cyanides, alkyl cyanides,

and aryl cyanides or the double bond in allene or ketene. Finally, some interesting chemistry has been observed due to the insertion of Cu atoms into the N-H bond of NH_3, C-H bond of CH_4, H-F bond of HF, and the C-F bond of FCH_3 (see references in Table 1).

Table 1. Summary of isotropic hyperfine interaction values (a_{Cu}),[a] *g*-values, and metal s orbital spin population (ρ_{4s}) of Cu-containing radicals isolated in argon and adamantane matrices.

	Argon			Adamantane			Ref.
	g	a_{Cu}	ρ_{4s}[b]	*g*	a_{Cu}	ρ_{4s}[b]	
Isolated atoms							
$^{63}Cu^0$	1.9994	6151	-	2.0016	5745	-	27, 36
$^{65}Cu^0$	1.9994	6587	-	2.0016	6155	-	27, 36
π-Interactions							
$^{63}Cu(C_6H_6)$[c]	-	-	-	2.0033	4341	0.72	36
				2.0020	4155	0.69	
$^{63}Cu(C_2H_4)$	1.9900	3998	0.67	1.9930	3730	0.62	37, 38
$^{63}Cu(C_3H_6)$	1.9997	3962	0.66	-	-	-	39
$^{63}Cu(1\text{-}C_4H_8)$	-	-	-	1.9981	3825	0.64	40
				1.9879[d]	4036[d]	0.67[d]	40
$^{63}Cu(cis\text{-}C_4H_8)$	-	-	-	1.9989	3806	0.63	40
$^{63}Cu(trans\text{-}C_4H_8)$	-	-	-	1.9987	3910	0.65	40
$^{63}Cu(2\text{-}CH_3C_3H_5)$	-	-	-	2.0003	3800	0.63	40
$^{63}Cu(c\text{-}C_6H_{10})$	-	-	-	1.9995	3973	0.66	40
$^{63}Cu(c\text{-}C_6H_8)$	-	-	-	1.9992	3939	0.66	40
$^{63}Cu(c\text{-}C_8H_{14})$	-	-	-	~2.0000	~4133	0.69	40
$^{63}Cu(c\text{-}C_8H_{12})$	-	-	-	1.9966	3990	0.67	40
				1.9988[d]	3802[d]	0.63[d]	
$^{63}Cu(C_2H_2)$	1.9930	4072	0.68	-	4145	0.69	37, 41
$^{63}Cu(CH_3CCH)$	-	-	-	2.0056	3750	0.63	41
$^{63}Cu(CH_3CCCH_3)$	-	-	-	2.0007	3736	0.62	41
$^{63}Cu[(CH_3)_3CCCC(CH_3)_3]$		-	-	1.9932	3601	0.60	41
$^{63}Cu[HCN]$	-	-	-	2.0100-2.0200	3884-4218	0.68-0.73	42
$^{63}Cu[(CH_3)_3CCN]$	-	-	-	2.0057	3602	0.60	43
$^{63}Cu[C_6H_5CN]$	-	-	-	-	~3643	~0.61	43
$^{63}Cu(C_2H_4)_2$	2.0013	124	0.02	2.0010	123	0.02	37, 38
$^{63}Cu(C_2H_4)_3$		e		2.0047	91	0.02	38
$^{63}Cu(C_3H_6)_2$	2.0010	126	0.02	-	-	-	39

Table 1. (continued)

	Argon			Adamantane			Ref.
	g	a_{Cu}	ρ_{4s}[b]	g	a_{Cu}	ρ_{4s}[b]	
$^{63}Cu(1\text{-}C_4H_8)_2$	-	-	-	2.0017	123	0.02	40
$^{63}Cu(cis\text{-}C_4H_8)_2$	-	-	-	2.0067	128	0.02	40
$^{63}Cu(trans\text{-}C_4H_8)_2$	-	-	-	2.0067	128	0.02	40
$^{63}Cu(2\text{-}CD_3C_3D_5)_2$	-	-	-	2.0067	123	0.02	40
$^{63}Cu(C_2H_2)_2$	1.9970	127	0.02	2.0019	126	0.02	37, 41
$^{63}Cu(CH_3CCH)_2$	-	-	-	2.0000	~121	0.02	41
$^{63}Cu(CF_3CCH)_2$	-	-	-	1.9920	131	0.02	41
$^{63}Cu((CH_3)_3CCCH)_2$	-	-	-	1.9950	131	0.02	41
$^{63}Cu(CH_3CCCH_3)_2$	-	-	-	2.0000	~131	0.02	41
$^{63}Cu((CH_3)_3CCCC(CH_3)_3)_2$	-	-	-	2.0000	131	0.02	41
$^{63}Cu(C_6H_5CCC_6H_5)_2$	-	-	-	2.0000	~125	0.02	41
σ-Interactions							
$^{63}CuSiO$	2.0021	4238	0.71	-	-	-	44
$^{63}CuCO$	1.9960	4142	0.67	1.9966	3961	0.66	29, 45
$^{63}CuPF_3$	-	-	-	1.9990	4205	0.70	46
$^{63}CuNH_3$	2.0140	3632	0.61	-	-	-	47
$^{63}Cu(NH_3)_2$	2.0190	3365	0.56	-	-	-	47
$^{63}Cu(NH_3)_3$	2.0000	2920	0.49	-	-	-	47
$^{63}Cu[PMe_3]_3$	-	-	-	2.0018	120	0.02	48
$^{63}Cu[P(OMe)_3]_3$	-	-	-	2.0028	120	0.02	48
$^{63}Cu(CO)_3$	2.0004	71	0.01	2.0014	94	0.01	29, 49
$^{63}Cu(CN)_3^{3-}$	-	-	-	2.0034	137	0.02	50
$^{63}CuO_2$	2.0314	152	0.03	2.0290	120	0.02	51, 52
M-C Bonds							
$^{63}CuCH{=}\dot{N}$	-	-	-	2.0010[f]	1342[f]	0.22[f]	43
				2.0010	784	0.13	
				1.9980	1040	0.17	
$CH_3C(^{63}Cu){=}\dot{N}$	-	-	-	2.0044	981	0.16	43
				2.0025	822	0.14	
$(CH_3)_3CC(^{63}Cu){=}\dot{N}$	-	-	-	1.9984	951	0.16	43
				2.0022	1176	0.20	
$^{63}CuCH{=}\dot{C}H$		e		2.0020	537	0.09	41
$^{63}CuCH{=}\dot{C}CH_3$	-	-	-	2.0023	~443	0.07	41
$^{63}CuCH{=}\dot{C}CF_3$	-	-	-	2.0013	~387	0.06	41
$^{63}CuCH{=}\dot{C}C_6H_5$	-	-	-	2.0019[g]	375[g]	0.06[g]	53
$^{63}CuC[C(CH_3)_3]{=}\dot{C}C(CH_3)_3$	-	-	-	2.0007	1113	0.19	41
$^{63}CuC(C_6H_5){=}\dot{C}C_6H_5$	-	-	-	2.0012[f]	950[g]	0.16[g]	41
				2.0005[h]	720[h]	0.12[h]	
$CH_2C(^{63}Cu)CH_2$	-	-	-	2.0020[g]	36[g]	<0.01[g]	54
$CH_2C(^{63}Cu)O$	-	-	-	2.0025	32	<0.01	55

Table 1. (continued)

	Argon			Adamantane			Ref.
	g	a_{Cu}	ρ_{4s}[b]	g	a_{Cu}	ρ_{4s}[b]	
Bond Insertion							
$H^{63}CuNH_2$	2.0727	247	0.04	-	-	-	47
$H^{63}CuCH_3$[c]	2.0200	328	0.05	-	-	-	56
$F^{63}CuCH_3$	2.2123	2681	0.45	-	-	-	57
	2.2301[i]	2688[i]	0.45[i]				
$H^{63}CuF$	2.2633[i]	2396[i]	0.40[i]	-	-	-	57
$F^{63}CuF$	2.3717	1541	0.26	-	-	-	58
$^{63}CuCH_2$	2.0009[i]	305[i]	0.05[i]	-	-	-	59
Other Species							
$^{63}Cu + CH_2CHCN$	-	-	-	2.0050	376	0.06	43

[a]Hyperfine in MHz. [b]Calculated from a_{Cu}/5995 MHz (Free atom value for ^{63}Cu).[30] [c]No matrix. [d]Additional trapping site. [e]Not observed in the reaction. [f]Trans isomer. [g]Cyclohexane matrix. [h]Cis isomer. [i]Neon matrix.

Table 2. Summary of isotropic hyperfine interaction values (a_{Ag}),[a] g-values, and metal s orbital spin population (ρ_{5s}) of Ag-containing radicals isolated in argon and adamantane matrices.

	Argon			Adamantane			Ref.
	g	a_{Ag}	ρ_{5s}[b]	g	a_{Ag}	ρ_{5s}[b]	
Isolated atoms							
$^{107}Ag^0$	1.9998	1810	-	2.0014	1772	-	27, 36
				2.0018[c]	1682[c]	-	
$^{109}Ag^0$	1.9998	2089	-	2.0023	2039	-	27, 36
				2.0020[c]	1938[c]	-	
π-Interactions							
$^{107}Ag(C_6H_6)$[d]	-	-	-	2.0004	1698	0.93	36
$^{107}Ag(C_6H_6CH_3)$	-	-	-	2.0004[e]	1591[e]	0.87[e]	36
$^{107}Ag(C_6H_6OCH_3)$	-	-	-	2.0009[e]	1645[e]	0.90[e]	36
$^{107}Ag(C_6H_6(CH_3)_3)$	-	-	-	2.0004[e]	1575[e]	0.86[e]	36
$^{107}Ag(C_2H_4)$	1.9980	1659	0.91	2.0001	1618	0.88	37, 60
$^{107}Ag(C_3D_6)$	1.9990[f]	1573[f]	0.86[f]	-	-	-	39
$^{107}Ag(1\text{-}C_4H_8)$	-	-	-	1.9980	1550	0.85	40
$^{107}Ag(cis\text{-}C_4H_8)$	-	-	-	1.9992	1551	0.85	40
$^{107}Ag(trans\text{-}C_4H_8)$	-	-	-	1.9993	1594	0.87	40
$^{107}Ag(2\text{-}CH_3C_3H_5)$	-	-	-	1.9992	1501	0.82	40
$^{107}Ag(c\text{-}C_6H_{10})$	-	-	-	2.0004	1636	0.89	40
$^{107}Ag(c\text{-}C_6H_8)$	-	-	-	1.9993	1576	0.86	40
$^{107}Ag(c\text{-}C_8H_{14})$	-	-	-	2.0010	1601	0.87	40
				2.0006	1522	0.83	40
$^{107}Ag(c\text{-}C_8H_{12})$	-	-	-	1.9986	1561	0.85	40

Table 2. (continued)

	Argon			Adamantane			Ref.
	g	a_{Ag}	ρ_{5s}[b]	g	a_{Ag}	ρ_{5s}[b]	
$^{107}Ag(C_2H_2)$	2.0000	1753	0.96		G		37
$^{107}Ag(CH_3CCH)$	-	-	-	1.9960	-1500	0.82	41
				2.0000[c]	-1568[c]	0.86[c]	41
$^{107}Ag(CH_3CCCH_3)$	-	-	-	2.0002	-1560	0.85	41
$^{107}Ag[(CH_3)_3CCCC(CH_3)_3]$		-	-	1.9920	-1553	0.85	41
$^{107}Ag(C_6H_5CCC_6H_6)$	-	-	-	1.9960	-1133	0.62	41
$^{107}Ag(C_2H_4)_2$	2.0017	46	0.03	2.0017	46	0.03	37, 61, 60
$^{107}Ag(CH_2CO)$	-	-	-	2.0008	1567	0.85	55
$^{107}Ag[HCN]$	-	-	-	2.0010[h]	-1598[h]	0.87[h]	42
				1.9994[i]	-1297[i]	0.71[i]	
$^{107}Ag[CD_3CCN]$	-	-	-	1.9990[h]	-1422[h]	0.78[h]	43
				1.9950[i]	-972[i]	0.53[i]	
$^{107}Ag[(CH_3)_3CCN]$	-	-	-	1.9988[h]	-1422[h]	0.78[h]	43
				1.9950[i]	-972[i]	0.53[i]	
$^{109}Ag[C_6H_5CN]$	-	-	-	2.0024	-1555	0.85	43
σ-Interactions							
$^{107}AgSiO$	1.9995	1363	0.74	2.0001	1226	0.67	44, 63
$^{107}AgSi_2O_2$	1.9993	909	0.50	1.9968	902	0.49	44, 63
$^{107}AgSi_3O_3$	-	-	-	1.9999	750	0.41	63
$^{107}AgCO$	2.0001	1787	0.98	2.0020	1682	0.92	64, 65, 42
$^{107}Ag(CO)_2$	-	-	-	2.0010	1646	0.90	65
$^{107}Ag(CO)_3$	1.9954	23	0.01	1.9954	23	0.01	64, 66, 65
$^{107}Ag(CO)_3$[c]		f		2.0009	1587	0.86	50, 42
$^{107}Ag(CN)_3^{3-}$	-	-	-	2.0019	116	0.06	50
$^{107}AgPF_3$	-	-	-	2.0020	1685	0.92	67
$^{107}AgPN$	-	-	-	1.9987	1116	0.61	68
$^{107}AgGeO$				1.9987	1096	0.60	68
$^{107}AgO_2$	2.0282	27	0.01	2.0230	14	<0.01	51, 52
M-C Bonds							
$^{107}AgCH=\dot{N}$	-	-	-	2.0011[j]	-518[j]	0.31[j]	43
				-	-280[k]	0.15[k]	
$CD_3C(^{107}Ag)=\dot{N}$	-			1.9990[j]	-521[j]	0.28[j]	43
$(CH_3)_3CC(^{107}Ag)=\dot{N}$	-	-	-	1.9990[j]	-522[j]	0.29[j]	43
$C_6H_5C(^{107}Ag)=\dot{N}$	-	-	-	-	-280[k]	0.15[k]	43
$^{107}AgCH=\dot{C}H$	2.0027	356	0.19	1.9988	-422	0.23	37, 53
$^{107}AgCH=\dot{C}CH_3$	-	-	-	~2.0000	-448	0.24	41
$^{107}AgCH=\dot{C}CF_3$	-	-	-	2.0000	-460	0.25	41

Table 2. (continued)

	Argon			Adamantane			Ref.
	g	a_{Ag}	ρ_{5s}[b]	g	a_{Ag}	ρ_{5s}[b]	
$^{107}AgCH=\dot{C}C(CH_3)_3$	-	-	-	1.9966[j]	-419[j]	0.23[j]	41
				1.9988[k]	-310[k]	0.17[k]	41
$^{107}AgCH=\dot{C}C_6H_5$	-	-	-	2.0014[d]	-307[d]	0.17[d]	53
$^{107}AgC[C(CH_3)_3]=\dot{C}C(CH_3)_3$		-	-	-	~-420[j]	0.23[j]	41
				2.0004[k]	-287[k]	0.16[k]	41
$^{107}AgC(C_6H_5)=\dot{C}C_6H_5$	-	-	-	2.0054	-304	0.17	41
$CH_2C(^{107}Ag)CH_2$	-	-	-	2.0045[d]	20[d]	<0.01[d]	54
$CH_2C(^{107}Ag)O$	-	-	-	2.0046	6.2	<0.01	55
Other Species							
$^{107}Ag + CH_2CHCN$	-	-	-	2.0010	-383	0.21	42
$^{107}Ag + B_2F_4$	-	-	-	2.0008	1371	0.75	69
$CH_2CO^{107}Ag$	-	-	-	1.9940	339	0.22	55
$^{107}Ag + SiS$	-	-	-	2.0013	1599	0.87	68
				1.9994	1226	0.67	
				1.9993	975	0.53	
				2.0006	712	0.39	
				2.0003	358	0.19	
$^{107}Ag + GeO$	-	-	-	2.0014	1599	0.87	68
				2.0002	1517	0.83	

[a]Hyperfine in MHz. [b]Calculated from a_{Ag}/1831 MHz (Free atom value for ^{107}Ag).[30] [c]Additional trapping site. [d]No matrix. [e]Cyclohexane matrix. [f]Neon matrix. [g]Not observed in the reaction. [h]Side-on bonding. [i]End-on bonding. [j]Trans isomer. [k]Cis isomer.

Table 3. Summary of isotropic hyperfine interaction values (a_{Au}),[a] g-values, and metal s orbital spin population (ρ_{6s}) of Au-containing radicals isolated in argon and adamantane matrices.

	Argon			Adamantane			Ref.
	g	a_{Au}	ρ_{6s}[b]	g	a_{Au}	ρ_{6s}[b]	
Isolated atoms							
$^{197}Au^0$	2.0012	3138	-	2.0017	2932	-	27, 36
				2.0022[c]	2881[c]	-	36
				2.0016[c]	2854[c]	-	36
π-Interactions							
$^{197}Au(C_6H_6)$[d]	-	-	-	2.000	2693	0.94	36
$^{197}Au(C_2H_4)$	1.9020	1734	0.60	-	-	-	70
$^{197}Au(C_3H_6)$	1.9303	1735	0.60	-	-	-	39
$^{197}Au(1\text{-}C_4H_8)$	-	-	-	1.9940	1718	0.60	40
$^{197}Au(cis\text{-}C_4H_8)$	-	-	-	1.9390	1659	0.58	40
$^{197}Au(trans\text{-}C_4H_8)$	-	-	-	1.9750	1686	0.59	40
$^{197}Au(2\text{-}CH_3C_3H_5)$	-	-	-	1.9690	1665	0.58	40
$^{197}Au(c\text{-}C_6H_{10})$	-	-	-	1.9527	1714	0.60	40

Table 3. (continued)

	Argon			Adamantane			Ref.
	g	a_{Au}	ρ_{6s}[b]	g	a_{Au}	ρ_{6s}[b]	
$^{197}Au(c\text{-}C_6H_8)$	-	-	-	1.9630	1724	0.60	40
				1.9990[c]	2313[c]	0.80[c]	
$^{197}Au(c\text{-}C_8H_{12})$	-	-	-	1.9533	1995	0.69	40
$^{197}Au(C_2H_2)$	1.9453	1859	0.65	-	-	-	71
$^{197}Au(CH_3CCH)$	-	-	-	1.9802	1691	0.59	41
$^{197}Au(CH_3CCCH_3)$	-	-	-	1.9708	1740	0.61	41
				1.9802[c]	1788[c]	0.62[c]	
$^{197}Au[CH_2CO]$	-	-	-	1.9930	1611	0.56	55
$^{197}Au[(CH_3)_3CCN]$	-	-	-	2.0280	1892	0.66	43
$^{197}Au[CD_3CCN]$	-	-	-	2.0275	1918	0.67	43
$^{197}Au(C_2H_4)_2$	2.0033	72	0.03	2.0087[e]	60[e]	0.02[e]	71, 40
$^{197}Au(C_3H_6)_2$	2.0000	72	0.03	-	-	-	39
$^{197}Au(1\text{-}C_4H_8)_2$	-	-	-	1.9990	71	0.02	40
σ-Interactions							
$^{197}AuSiO$	1.9636	1559	0.54	-	-	-	44
$^{197}AuCO$	1.9334	1705	0.59		f		72
$^{197}AuO_2$	2.0373	92	0.03	2.0310	272	0.03	51, 52
M-C Bonds							
$^{197}AuCH{=}\dot{N}$	-	-	-	1.9970	751	0.26	43
$(CH_3)_3CC(^{197}Au){=}\dot{N}$	-	-	-	1.9923	696	0.24	43
$CD_3C(^{197}Au){=}\dot{N}$	-	-	-	2.0000	709	0.25	43
$C_6H_5C(^{197}Au){=}\dot{N}$	-	-	-	-	~701	0.24	43
$^{197}AuCH{=}\dot{C}H$	2.0020	617	0.21	1.9938	628	0.22	71, 53
$^{197}Au\dot{C}{=}CH_2$	-	-	-	1.9938	1083	0.38	53
$^{197}AuCH{=}\dot{C}CH_3$	-	-	-	~1.9830	~544	0.19	41
$^{197}AuCH{=}\dot{C}C(CH_3)_3$	-	-	-	1.9931[g]	611[g]	0.21[g]	41
				-	448[h]	0.16[h]	
$^{197}AuCH{=}\dot{C}C_6H_5$	-	-	-	1.9970[g]	530[g]	0.18[g]	53
				-	300[h]	0.10[h]	
$^{197}AuC(C_6H_5){=}\dot{C}C_6H_5$	-	-	-	2.0054	502	0.17	41
$CH_2C(^{197}Au)CH_2$	-	-	-	2.0020[e]	18[e]	<0.01[e]	54
$CH_2C(^{197}Au)O$	-	-	-	2.0047	9	<0.01	55
Other Species							
$^{197}Au + CH_2CHCN$	-	-	-	1.9982	610	0.21	42

[a]Hyperfine in MHz. [b]Calculated from a_{Au}/2876 MHz.[30] [c]Additional trapping site. [d]No matrix. [e]Cyclohexane matrix. [f]Not observed in the reaction. [g]Trans isomer. [h]Cis isomer.

1.3.1. σ- or π-Complexation to Metal Centers

The ^{63}Cu, ^{107}Ag and ^{197}Au atoms have been co-condensed with several alkenes, such as ethylene,[37,38,60,70,71] propylene,[39] 1-butene,[40] *trans*-2-butene, [40] *cis*-2-butene,[40] 2-methylpropene,[40] cyclohexene,[40] 1,4-cyclohexadiene,[40] *cis*-cyclooctene,[40] and 1,5-cyclooctadiene.[40] Results show that both mono- and di-ligand complexes form between the Cu and Au metals and substrates, with Ag forming mainly weakly bound mono-ligand complexes. According to Kasai,[37] Ag forms pseudo-complexes, with ethylene and propylene bound by a van der Waals interaction, as the value of the hyperfine interaction is only slightly smaller than that observed for trapped atoms in argon. Howard,[60] on the other hand, believes that bona fide complexes were obtained in solid hydrocarbon matrices, since the *a*-values are significantly lower than those observed in argon and well resolved ^{13}C nuclear hyperfine splitting was observed when ^{13}C labelled ethylene and propylene were used. Di-ligand complexes were not observed for reactions of Ag with alkenes, with the exception of ethylene itself.

The bonding in the metal-alkene complexes are believed to follow that of the Dewar-Chatt-Duncanson type.[73,74] This involves the counter electron flow of two dative interactions, i.e., electron donation from the alkene π-orbital into an empty sp_y hybridized orbital on the metal and back-donation of d-electron density from the metal d_{xy} orbital into the empty π_y* orbital of the alkene, Figure 12. The unpaired electron is located in the sp_y orbital pointing away from the alkene.

For the di-ligand complex, the unpaired electron is located in the metal p_x orbital and bonding occurs by the electron donation from alkene π_y orbital into metal s and p_y

orbitals with back-donation from metal d_{xy} and semi-filled p_x orbitals into the vacant π^* orbital. In other words, the unpaired spin population of the metal mono-ligand complexes remains mainly on the metal center, while for di-ligand complexes there is more delocalization of electron density onto the ligands.

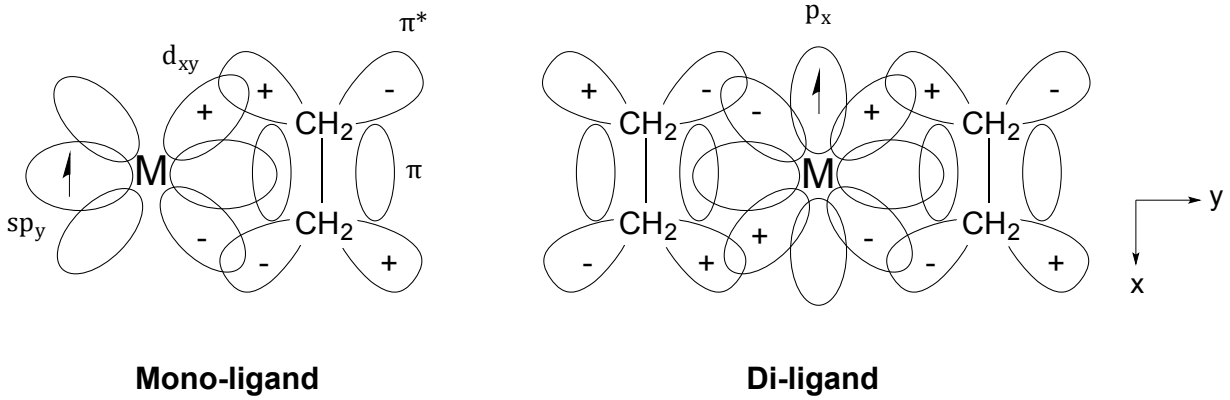

Figure 12. Dewar-Chatt-Duncanson model of bonding in mono- and di-ethylene complexes.

Mono- and di-ligand complexes are also formed when Cu, Ag, and Au atoms react with alkynes,[37,41,53,71] (acetylene, methylacetylene, (trifluoromethyl)acetylene, dimethylacetylene, di-*tert*-butylacetylene, diphenylacetylene, bis(trifluoromethyl)acetylene), cyanides,[42,43] (hydrogen cyanide, methyl cyanide, methyl-d_3 cyanide, *tert*-butyl cyanide, phenyl cyanide) and ketene.[55] The Cu, Ag and Au atoms reacted with alkynes to give mono-substituted complexes, while only Cu formed di-ligand complexes. All three metals formed mono-ligand complexes with alkyl cyanides, Ag forming both side-on and end-on complexes. The side-on complex exhibits greater stability because of the increased d-π^* overlap between the metal and ligand. EPR spectra from the reactions with ketene revealed stable complexes with Ag and Au, Ag[CH_2CO] and Au[CH_2CO], respectively. However, interestingly, no complexes were formed with Cu atoms.

Sigma-type dative interactions have been observed in reactions of CO and SiO with Cu, Ag, and Au atoms.[44,45,63–65,72] Mono-ligand complexes between the metal and CO or SiO involve the lone-pair electrons of the ligand and a vacant sp-hybrid orbital on the metal center, with π –type back-donation from metal d_π orbitals into π^* orbitals of the ligand. The unpaired electron resides in an sp_σ orbital of the metal pointing away from the ligand, Figure 13. Di- and tri-ligand complexes were also present in reactions of Ag and CO or SiO in adamantane matrices, formed by the empty 5p orbitals of Ag progressively accepting electron pairs from the σ orbitals of up to three ligands. Two conformers of $Ag(CO)_3$ have been observed, a pyramidal structure with larger hyperfine (only observed in adamantane) and a planar structure (observed in both argon and adamantane). The more stable planar structure was also observed in reactions with Cu but no pyramidal conformer was found. The bonding in $M(CO)_3$ (M = Cu or Ag), follows similar σ-type dative-interactions described for the mono-ligand complexes, where the lone pair electrons from the ligands are donated into three sp^2 orbitals in the xy plane, with the unpaired electron almost completely located in the metal p_z orbital (perpendicular to the molecular plane). Howard *et al.* were successful in preparing planar isostructural $M(CN)_3^{3-}$ molecules, by γ-irradiation of single crystals of the corresponding salt, $K_3M(CN)_4$, showing strong similarities to the $M(CO)_3$ structures.[50]

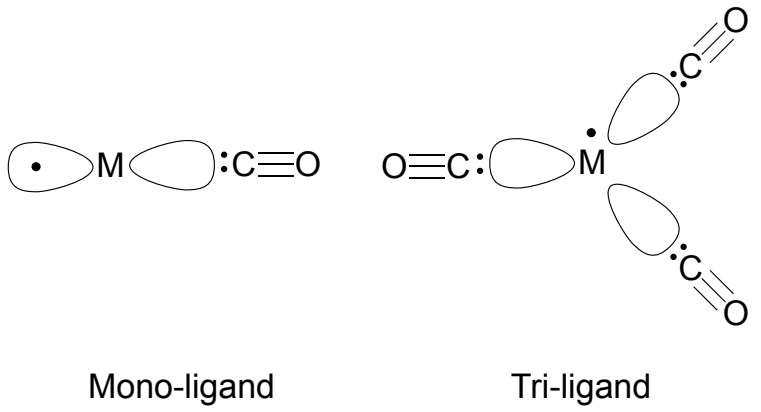

Figure 13. Bonding scheme for the σ-type dative-interactions of metal atoms and CO.

Mono-ligand, i.e., $CuNH_3$, $CuPF_3$, $AgPF_3$ and tri-ligand, i.e., $Cu[P(OCH_3)_3]_3$ and $Cu[P(CH_3)_3]$ complexes, comparable to those of MCO and $M(CO)_3$, have been observed by EPR spectroscopy. The $CuNH_3$ and MPF_3 complexes are held together by the overlap and mixing of the ligand σ donor orbital with the metal sp-hybridized orbital, directly placing unpaired spin population in the ligand σ system.[46,47,67] The unpaired electron is thus located in the second sp orbital on the metal pointing away from the ligand. The $Cu(PR)_3$ planar π-radicals arise from the donation of three lone pairs from phosphorous ligands into the empty Cu hybridized sp^2 orbitals with the unpaired electron occupying the remaining $4p_z$ orbital perpendicular to the molecular plane.[48] In this case, there is less back donation of unpaired spin population towards the ligand, in comparison to the complexes formed with CO.

1.3.2. Metal-Carbon Bonds

Metal-carbon (M-C) bonds in organometallic vinyl (MHC=ĊR or MRC=ĊR), and iminyl (MRC=Ṅ) adducts, arise from the addition of Group 11 metal atoms to the carbon atom in the C-X triple bond of hydrogen cyanide, alkyl cyanides, benzyl cyanide,

acetylene, phenyl acetylene and other mono- or di-substituted acetylene molecules. The Ag and Au atoms were more reactive than Cu toward addition to the C-C triple bond of acetylene, as photoexcited Cu atoms were essential in generating the β-substituted vinyl.[37,41,53,71] The reaction of Au atoms and acetylene in adamantane resulted AuHC=ĊH which subsequently isomerized to AuĊ=CH_2 by a rapid 1,2-hydrogen shift. The relative stability of the β-substituted vinyls were determined to be AgCH=ĊH > AuCH=ĊH > CuCH=ĊH. All three metal atoms react with phenylacetylene to give β-substituted α-styryls (MCH=ĊC_6H_5) from addition of the metal atoms to the unsubstituted carbon atom of the alkyne. In the Au atom reaction, the isomer was also observed. These radicals have a planar structure with the unpaired electron located in the p_y orbital on the α-carbon.[53] Organometallic vinyls were also formed in the reaction of all three metals with other monosubstituted alkynes, (methylacetylene and (trifluoromethyl)acetylene) and disubstituted alkynes (dimethylacetylene, di-*tert*-butylacetylene, diphenylacetylene, and bis(trifluoromethyl)acetylene).[41] The metal s orbital spin population in MRC=ĊR and MHC=ĊR are comparable to those of MHC=ĊH, with the exception of those formed with Cu atoms, i.e., CuRC=ĊR radicals showed larger contributions (16 - 19 %) than CuHC=ĊR (6 – 9 %).

The isoelectronic σ-bonded metal iminyls trapped in adamantane or cyclohexane matrices from reactions with hydrogen cyanide, methyl-d_3 cyanide, *tert*-butyl cyanide, and phenyl cyanide can exist as cis or trans stereoisomers at cryogenic temperatures with the unpaired electron spin population on nitrogen residing in an orbital with a significant s contribution.[43] While Cu and Ag atoms form both isomers (referring to the position of

the metal with regards to the orbital containing the unpaired electron), cis being the most stable, reactions with Au atoms yield only the cis isomer.

The formation of M-C bonds, by addition of Cu, Ag or Au atoms to the central carbon atom in allene and ketene, has been reported in solid hydrocarbon matrices.[54,55] The regioselective addition of the metals producing 2-metal substituted allyls and oxallyls are due to low-lying empty p orbitals of the metal atoms.[75] In the case of allene, it is believed that the metal atom approaches the central carbon at an angle of 45^{o} to the two π systems. Two subsequent interactions take place. First, the two lobes of a d orbital of opposite sign overlap with both π* systems at the central carbon leading to a population of the π* orbitals by electrons from the filled d orbitals. Secondly, the unfilled metal p orbitals overlap with the two-π systems forming sigma bonds. In this case, electrons leave the bonding π orbitals for the metal. For ketene, the metal atom forms a mono-ligand π-complex with the electrons of the C=O, and migration of the metal towards the central carbon forms the 2-metal-oxallyl.

1.3.3. Metal Insertion into Covalent Bonds

It is well-known that metal atoms can insert into the covalent bonds of various small molecules under cryogenic conditions. IR studies of Cu, Ag and Au metal atom reactions, in particular, have revealed they insert into N-H,[76] N-F,[77] O-H,[78] C-N,[79] C-H,[80] C-F,[81] C-Cl,[82] and C-Br[82] bonds. However, this section will focus solely on bond insertion products characterized by EPR spectroscopy.

As previously mentioned, Cu atoms have reacted with NH_3,[47] CH_4,[56] HF,[57] DF,[57] and CH_3F,[57] forming the corresponding, $HCuNH_2$, $HCuCH_3$, HCuF, DCuF, and $FCuCH_3$

radicals. N-H and C-H insertion products were formed after photoexcitation of Cu atoms ($^2P \leftarrow {}^2S$) isolated in a matrix containing the substrates listed above. In the reaction of Cu atoms with NH_3, the intensity of the transition lines for the trapped mono-ligand Cu-NH_3 complex diminished when irradiated with UV light ($\lambda = 325 \pm 50$ nm) and signals due to H atoms and $\dot{N}H_2$ radicals appeared. Spectral features, although partially obscured by the $\dot{N}H_2$ and H atom transition lines, were indicative of a molecule with ionic character, $(H^-)Cu^{++}(NH_2^-)$, where the unpaired electron resides in the Cu $3d_z^2$ orbital. The insertion product is believed to have formed through a photoinduced isomerization process, whereby the energy produced by the high pressure Xe-Hg lamp excites the unpaired electron into a vacant Cu 4p orbital allowing for an intramolecular hydrogen atom abstraction. Methyl copper hydride, $HCuCH_3$, is formed in a similar fashion after photoirradiation of the Cu/CH_4 matrix at $\lambda = 315$ nm. A number of observations led Ozin *et al.*[56] to conclude the molecule is best described as, $(H^-)Cu^{++}(CH_3^-)$, with linear geometry and essentially normal Cu-C and C-H bonds. The dominant hyperfine interaction in the EPR spectrum is that of a_{63Cu}, due to the coupling of the unpaired electron with the Cu nucleus. The magnitude of a_{63Cu}, along with the observed anisotropy, suggests the electron to reside mainly in a d-type orbital on Cu. The values for the hyperfine interaction of ^1H and ^{13}C nuclei are much smaller, indicating tiny contributions of electron density from hydrogen 1s and carbon 2s orbitals to the SOMO (ρ_{ns} equals 0.07 and 0.03, respectively, *cf.* equation (16)).

Insertion of Cu atoms into C-F and H-F bonds were carried out using a different technique. Laser sputtering of a thin film of the reactant gas condensed on a Cu metal

target vaporizes the reactant film and metal in a simultaneous high-energy process that could initiate certain metal reactions that do not occur under normal conditions (i.e., resistive heating). Knight *et al.* consider the paramagnetic Cu-insertion products formed to be the divalent copper molecules, $(F^-)Cu^{++}(CH_3^-)$ and $(H^-)Cu^{++}(F^-)$.[57] EPR evidence suggests that Cu 4s and $3d_z^2$ orbitals contribute the majority of the electron spin density in the molecules.[57] The small ligand hyperfine interaction signifies a closed shell ligand environment, and lends a reasonable explanation to the ionic character of the structure with the unpaired electron in a hybridized $4s/3d_z^2$ orbital.

In many cases, proposed bonding schemes involve not only experimental EPR evidence but also theoretical quantum chemical methods to predict the spin density contributions of specific orbitals and the relative energies of molecular orbitals in the molecule.[45] More recent EPR investigations couple both experimental and theoretical calculations, carried out using density functional theory, as a tool for predicting IR absorbance frequencies, nuclear hyperfine interaction values and also internal energies of proposed structures.[21]

1.4. Quantum Mechanical (DFT) Calculations

Density functional theory (DFT) is a method used for studying the properties of molecules using electron density, $\rho(\mathbf{r})$, instead of the wave-function based methods ("*ab initio*") that solve the Schrödinger equation.[83] The Kohn-Sham approach to DFT is quite popular and uses a molecular orbital representation to build electron density, $\rho(\mathbf{r})$, and estimates the kinetic and potential contributions to the total molecular energy.[84] The different DFT models vary in the way they represent the so-called exchange-correlation

potential. Several hybrid approximations ("functionals"), mixing the exact-exchange Hartree-Fock (HF) theory with exchange and correlation from other sources, have been designed using the Kohn-Sham approach to locate local minima along the potential energy surface, i.e., the most stable nuclear geometry. The most common functional used is B3LYP, where the acronym stands for Becke, 3-parameter hybrid functional[85] with Becke 1988 exchange functional[86] and Lee-Yang-Par-correlation functional.[87] Other exchange-correlation hybrid functionals were developed to expand the Kohn-Sham DFT. These include BHandHLYP,[88] similar to B3LYP yet includes local spin density approximations (LSDA), and M06,[89] found to improve accuracy in transition-metal bonding and organometallic molecules.

Computational DFT methods represent the Kohn-Sham (KS) orbitals using a basis set of atomic orbitals (AOs).[90] The KS molecular orbitals (MOs) are computed by linearly combining AOs that are usually represented as either Slater type orbitals (STO) or Gaussian type orbitals (GTOs). The former describes the shape of the AOs in a physically more accurate way while the GTOs have the advantage of being faster and easier to compute. In fact, combinations of GTOs are often used to describe STOs. The basis sets used in this report are of split valence, i.e., the so-called "Pople split-valence type" (or double-zeta), which allow one to specify a different number of GTOs for core and valence electrons. The notation of the basis sets is K-LMG, where, K = number of sp-type inner (core) shell GTOs, while L and M indicate the number of GTOs used in two sets of functions for each outer valence orbitals. The final "G" indicates the use of GTOs. For example, 6-31G is a double zeta basis with two functions per atomic orbital in the outer shell and 6-311G is a triple zeta with three different STOs/GTOs for outer valence

electrons. Pople basis sets can be modified to obtain better approximations to describe systems by adding polarization functions (allowing AOs to deviate from their original shape by having higher angular momentum), indicated by a letter in brackets following the G, and also possibly a number of diffuse functions (letting electrons spread farther away from the nucleus) in the form of "+" in front of the G. Diffuse functions, as the name indicates, are associated with smaller Gaussian exponents (the "zeta") that allows one to describe the outer region of a molecule. For example in 6-311+G(d), "(d)," adds d-type functions on to all atoms except hydrogen and f-type functions on to transition metals, while "+" signifies the addition of diffuse functions on to all atoms except hydrogen.

Elements beyond the second row of the periodic table with d electrons require more elaborate basis sets when conducting *ab initio* or DFT calculations. More specifically, first row transition metals are well described by the Wachters-Hay all electron basis set (15s11p6d1f),[88] consisting of Wachters primitive set (14s9p5d),[91] supplemented with one s, two p, and one d diffuse functions and a single f polarization function.[92] Unfortunately, this basis set has limitations and cannot be applied to second and third row transition metals. However, the basis of Wadt and Hay[93–95] includes Effective Core Potentials (ECPs) to better describe the AOs in these larger elements. All these approaches will be used in this thesis.

2. Proposed Research

After an extensive literature search, it is quite clear that Group 11 metals are implicated in several important reactions involving three-membered heterocyclic compounds. The mechanisms proposed for these reactions typically involve mononuclear-metal complexes and metallacycles as intermediates. Direct evidence for the existence of these reactive intermediate species is difficult to obtain. Cryogenic studies, involving the reaction of Group 11 metal atoms, have been shown to yield complexes with small molecules (see Tables 1, 2 and 3). Thus we propose to react Group 11 metal atoms ($^{63/65}$Cu, $^{107/109}$Ag and ^{197}Au) with several three-membered heterocyclic compounds, namely, oxiranes, thiiranes and aziridines, in an adamantane matrix, at cryogenic temperatures, to capture any highly reactive intermediates formed, Figure 14.

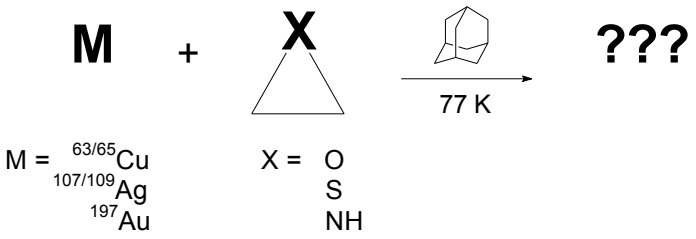

Figure 14. Proposed synthesis

The paramagnetic products formed in the metal atom reactions will be characterized by EPR spectroscopy. This technique will identify what type of bonding interactions occur between the metal atom and the heterocyclic compound. Information on the relative stability of the paramagnetic products will be obtained by studying the persistence of the EPR signal of the products as a function of temperature. When possible, isotopic substitution will be used to confirm EPR spectral assignments of

proposed organometallic products formed in the reaction. In addition, DFT will be used in combination with the experimental work in order to make structural assignments. More specifically, a DFT method will be developed to predict isotropic nuclear hyperfine interactions of ^{63}Cu-containing radicals. The experimental a_{63Cu} values for Cu-containing radicals reported in the literature will first be used to test this method.

3. Experimental

3.1. Materials

Ethylene oxide, 1,2-epoxybutane, styrene oxide, ethylene sulfide, adamantane, 2-chloroethylamine, phthalimide-^{15}N potassium salt, and ethylene carbonate-d_4, were purchased from Sigma-Aldrich Canada Ltd. (Oakville, Ontario). Isotopic forms of ethylene oxide (ethylene oxide-1,2-$^{13}C_2$ (99%) and ethylene oxide-d_4 (98%)) were purchased from Cambridge Isotope Laboratories (Tewksbury, MA). Copper turnings were purchased from BDH Chemicals Ltd. (Poole, England), silver powder from Goodfellow Metals (U.K.) and gold kindly provided by Dr. C. M. Hurd (NRC, Ottawa).

3.2. Synthesis

3.2.1. Synthesis of Aziridine

Aziridine was synthesized in a single step by the N-alkylative ring closure of 2-chloroethylamine,[96] Figure 15.

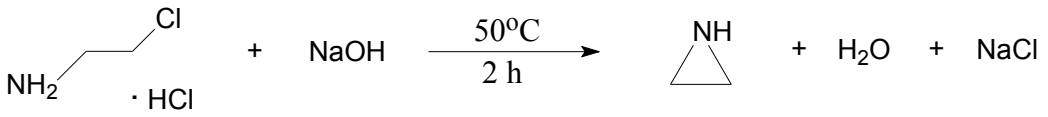

Figure 15. N-alkylative ring closure of 2-chloroethylamine.

2-Chloroethylamine hydrochloride (4.25 g, 36.6 mmol) was added to 25 mL of a 3.79 mM aqueous NaOH solution in a pear-shaped flask equipped with a reflux condenser. The reaction mixture was heated to 50°C via a glycerol bath and mechanically

stirred for 2 h. The condenser was replaced by a short path vacuum distillation apparatus. The distillate was collected between 70 to 78^{o}C at 300 Torr. The distillate was dried over NaOH pellets and kept in a freezer overnight. This resulted in a phase separation. The upper aziridine containing layer was withdrawn with a Pasteur pipette and the drying process repeated until water was not detected by NMR spectroscopy (0.98 g, 62% yield). ^{1}H NMR (200 MHz, $CDCl_3$): δ (ppm) 1.61 (4H). The NMR data is in agreement with that found in the literature.[96]

3.2.2. Synthesis of Aziridine-^{15}N

A three-step process was used to prepare aziridine-^{15}N, Figure 16. The first step involved the reaction of phthalimide-^{15}N with 1,2-dichloroethane to form 2-(2-chloroethyl)-1*H*-isoindole-1,3-(2*H*)-dione-2-^{15}N **1** via the Gabriel synthesis.[97] In the second step, hydrolysis of **1** yielded 2-chloroethylamine-^{15}N hydrochloride, which underwent N-alkylative ring closure when treated with sodium hydroxide in the third step forming aziridine-^{15}N.

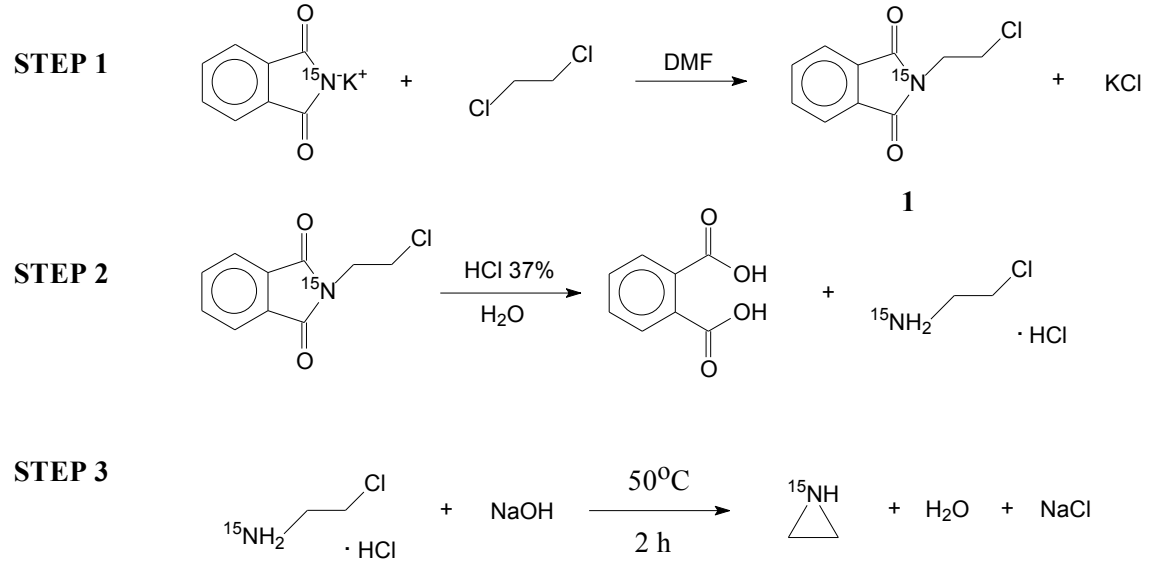

Figure 16. Overview of aziridine-^{15}N synthesis

3.2.3. Synthesis of 2-(2-chloroethyl)-1*H*-isoindole-1,3(2*H*)-dione-2-^{15}N

The procedure used by Betley and Peters[98] to prepare 2-phenyl-1*H*-isoindole-1,3(2*H*)-dione was modified to synthesize 2-(2-chloroethyl)-1*H*-isoindole-1,3-(2*H*)-dione-2-^{15}N. First, 10.0 g (54.0 mmol) of phthalimide-^{15}N potassium salt was added to 8.0 g of 1,2-dichloroethane in a 500 mL round-bottom flask. Next, 70 mL of DMF was added and the resulting solution was mechanically stirred and heated under reflux for 19 h. At this point, the solution was allowed to cool to room temperature and four, 100 mL portions of distilled water were added to the flask. Once the contents of the flask had again reached room temperature (~ 2 h), the precipitate was collected in a Büchner funnel and washed with two, 50 mL portions of distilled water. The crystals were transferred to a 150 mL round-bottom flask and dried in vacuo over night to afford the title product as an off-white solid (7.37 g; 65 % yield).

3.2.4. Synthesis of 2-chloroethylamine-^{15}N hydrochloride

2-Chloroethylamine-^{15}N hydrochloride was prepared using the procedure reported for the generation of 2,2-difluoroethylamine hydrochloride.[99] The crude 2-(2-chloroethyl)-1*H*-isoindole-1,3-(2*H*)-dione-2-^{15}N (7.37 g, 35.2 mmol), prepared in section 3.2.3 above, was added to 50 mL of distilled water in a 150 mL round-bottom flask and treated with 50 mL of 37 % hydrochloric acid. The reaction mixture was heated under reflux and mechanical stirring for 20 h. The reaction mixture was allowed to cool to room temperature and filtered to remove the solid material, i.e., phthalic acid. The phthalic acid was washed with a few mL of cold distilled water and the filtrate was concentrated to dryness under reduced pressure in a 100 mL round-bottom flask. The resulting white

solid, crude 2-chloroethyamine-^{15}N hydrochloride, (3.54 g, 90% yield), was used in the final step without further purification.

3.2.5. N-alkylative Ring Closure of 2-Chloroethylamine-^{15}N hydrochloride

The procedure outlined in section 3.2.1 was used to prepare aziridine-^{15}N, with the exception that 2-chloroethylamine-^{15}N hydrochloride (3.54 g, 82.2 mmol) was added to a 3.79 mM NaOH solution (3.23 g of sodium hydroxide in 21.3 g of distilled water). As expected, the NMR spectrum of the product (0.94 g, 71% yield) was similar to that attained for the aziridine-^{14}N. ^{1}H NMR (200 MHz, $CDCl_3$): δ (ppm) 1.62 (4H).

3.2.6. Synthesis of Ethylene sulfide-d_4

Following a modified protocol of the method published by Quack *et al.*,[100] 1.70 g (17.5 mmol) of ground potassium thiocyanate was added to a 5 mL round-bottom flask connected to a jacketed short-path distillation apparatus and vacuum line. The contents of the flask were heated, using a glycerol bath set at 100^{o}C, while maintaining a reduced pressure of ~50 Torr. After 30 min the pumping and heating were stopped (replacing the vacuum line with a drying tube) and the flask cooled to room temperature. Once cooled, ethylene carbonate-d_4 (0.97 g, 11.0 mmol) was added to the flask and heating resumed. Distillation of the product began when bubbles, due to CO_2 production, formed in the flask. The product was collected over 30 min in a second 5 mL round-bottom flask between 37 and 45^{o}C. Ethylene sulfide-d_4 (37.2 mg, 33% yield) was obtained as a colourless liquid. Based on NMR, the chemical shift present at 2.37 ppm was not observed, consistent with deuteration.[100]

3.3. Sample Preparation

Substrates, present in the liquid state at ambient temperature, were transferred into glass bulbs specifically designed for use with vacuum systems, Figure 17a. Aziridine, ethylene sulfide, 1,2-epoxybutane, or styrene oxide were placed in 10 mL bulbs and degassed, prior to use, by multiple freeze-thaw cycles. This involved connecting the bulbs to a vacuum line via a B10 male Quickfit joint, freezing the contents of the bulbs with liquid nitrogen, and pumping on the contents of the bulbs, first with a roughing pump and then a diffusion pump. Once rid of all trapped air, the bulbs were sealed by closing the Teflon stopcock and the contents thawed to room temperature by immersing the bulb in a methanol bath. This process was repeated several times until there was no observable deflection on the Penning vacuum gauge. The substrates remained under vacuum in the bulbs until used on the rotating cryostat.

The gaseous substrates, ethylene oxide, ethylene oxide-d_4, or ethylene oxide-$^{13}C_2$ were condensed in 2000 mL glass bulbs, Figure 17b. Mixtures of ethylene oxide-1,2-$^{13}C_2$:He (0.6:1), and ethylene oxide-d_4:He (0.3:1) were prepared by a former laboratory member. First, the 2000 mL glass bulb was attached to the vacuum line and evacuated following the method mentioned above. A lecture bottle, containing the gaseous substrate, was connected to the vacuum system. The system was isolated from the vacuum pump and the desired amount of gas was added into the system based on the pressure influx measured by a transducer. The cold finger of the bulb was then submerged into liquid nitrogen and the gas was condensed. Any uncondensable substances were removed from the system with the aid of a roughing pump followed by a

diffusion pump. The system was once again isolated from the vacuum pump and helium was introduced into the vacuum line in order to obtain the desired ratio of substrate to helium. In the final step, the stopcock was closed and the content of the bulb was thawed to room temperature by immersing the bulb in a methanol bath.

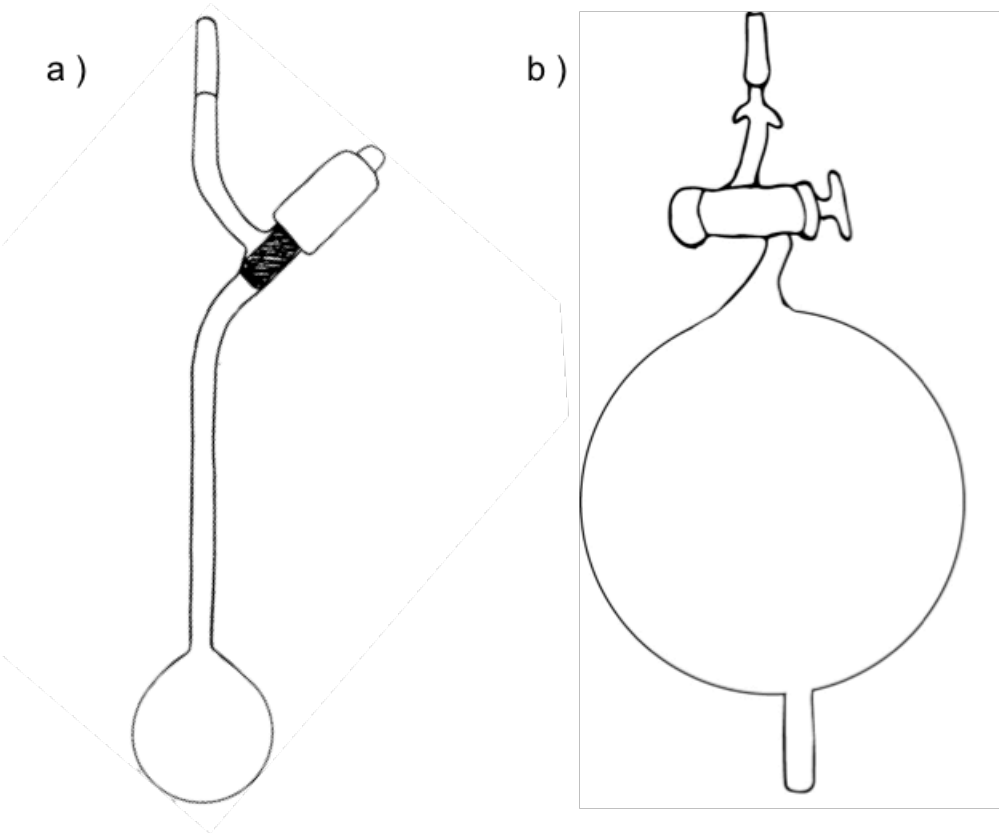

Figure 17. Pyrex glass bulbs designed for use with vacuum systems. a) 10 mL capacity bulb fitted with a male B10 Quickfit joint and a rotoflow stopcock. b) 2000 mL capacity bulb with male B10 Quickfit joint, vacuum stopcock and glass finger.

3.4. Reaction of Group 11 metal atoms with Heterocyclic Compounds

The reactions of $^{63/65}$Cu, $^{107/109}$Ag and ^{197}Au metal atoms with aziridine, ethylene sulfide, ethylene oxide, styrene oxide, or 1,2-epoxybutane were carried out in a metal atom reactor known as a rotating cryostat.[34] This device allows for the synthesis and trapping

of highly reactive intermediates at cryogenic temperatures (77 K) in an inert solid matrix. The heart of this instrument is the stainless steel drum situated in a stainless steel vessel with multiple portholes allowing for the introduction of the reactants, metal atoms, matrix material as well as the monitoring of the reaction progress. Setting up the experiments began by mounting the metal and corresponding evaporation source between the two electrodes on the high temperature furnace assembly. Copper turnings and silver powder were evaporated from a molybdenum pouch, while a tungsten basket (Micro Metallurgical LTD, Ontario) was used to evaporate gold metal. The matrix inlet, substrate inlet and furnace occupied three of the portholes around the reaction vessel. Once all access points to the inside of the reaction vessel were blocked, the reaction vessel was evacuated with the aid of a roughing pump. When the pressure inside the cryostat reached approximately 4.5×10^{-2} Torr, an oil diffusion pump was engaged reducing the pressure further to $<10^{-6}$ Torr.

Next, the furnace was heated by passing current through the electrodes of the furnace to remove any volatile impurities on the metal surface, prior to the reaction. The hollow drum and hollow ring-shaped reservoir inside the reaction vessel were filled with liquid nitrogen. A water bath set at 80^{o}C was placed under the bulb containing the adamantane (matrix material) to maintain a vapour pressure of approximately 1 Torr during the experiment. When everything had been set up, the drum was slowly rotated to a speed of 2000 rpm.

At this point, adamantane was deposited for 2 min on the surface of the cold drum. Next, the metal atoms and substrate were simultaneously co-condensed on the surface of the cold drum, Figure 18. The approximate molar ratio of metal atoms,

substrate and adamantane was 1:10:100. The substrate concentration was regulated by using a constant temperature bath, to maintain the substrates vapour pressure at *ca*. 0.1 Torr throughout the experiment, Table 4. Helium:substrate gas mixtures were regulated with a needle valve assembly that was coupled to the glass bulb.

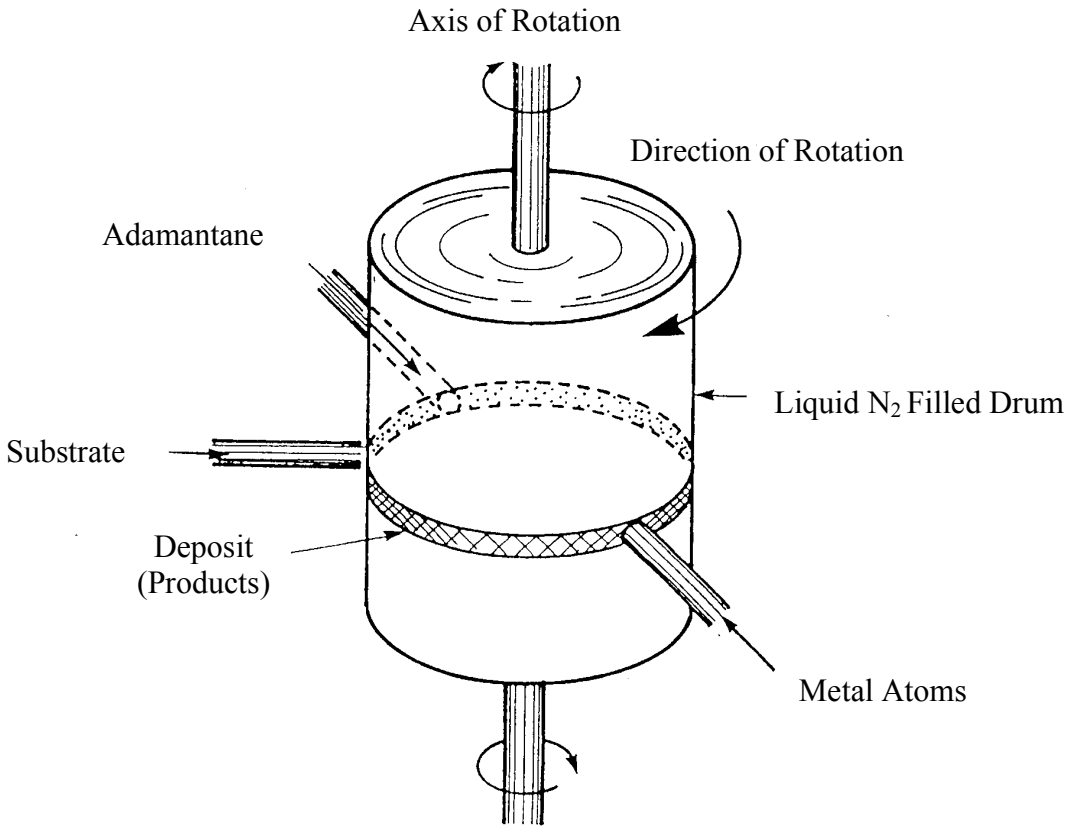

Figure 18. Schematic representation of the rotating stainless steel drum

Table 4. Temperature baths used to regulate substrate concentration

Substrate	Composition of Bath	Temperature
Ethylene oxide	Ethanol + N_2 (*l*)	-117^{o}C
Ethylene sulfide	Ethyl acetate + N_2 (*l*)	-84^{o}C
1,2-Epoxybutane	Ethyl acetate + N_2 (*l*)	-84^{o}C
Aziridine	Isopropanol + N_2 (*l*)	-88^{o}C
Styrene oxide	Chlorobenzene + N_2 (*l*)	-44^{o}C

The final step entailed collecting the sample from the drum. After a deposition time of approximately 12 min (2 min of just adamantane followed by 10 min of adamantane, metal atoms, and chosen substrate) rotation of the drum was stopped. The deposit was scraped off the drum's surface, with a knife, into a quartz tube and subsequently sealed under vacuum at 77 K.

3.5. Identification of reaction products

The newly synthesized matrix-isolated products were immediately analyzed at 77 K on a Varian E 109 EPR spectrometer operating at X-band. A signal from the spectrometer indicates that there are paramagnetic species present in the reaction mixture. Spectra were calibrated using a Varian gaussmeter and a Systron-Donner 6016 frequency counter. After initial analysis, the samples were stored in liquid nitrogen. At a later date, EPR spectra of the samples were recorded at 10 K intervals from 77-250 K, or until a signal was no longer visible, using a variable temperature accessory.

3.6. Photoirradiation Experiments

Reaction mixtures of $^{63/65}$Cu atoms and ethylene oxide, ethylene oxide-D_4 or 1,2-epoxybutane in adamantane, were subjected to UV-irradiation at 77 K before being subjected to temperature studies. A schematic of the experimental set up can be found in Figure 19. The samples (**E**) were placed in a quartz finger Dewar (**D**), containing liquid nitrogen, approximately 13 cm away from the 1 kW high-pressure Hg-Xe lamp housing (**A**). An Edmund Optics UV band pass filter (**B**, λ_{max} = 330 nm) and a focusing lens (**C**) were placed between the lamp and the Dewar. The light from the arc lamp was focused

onto the sample in the finger Dewar as it was spun with the aid of a motor (**F**), allowing for even photoirradiation. Samples were exposed to UV light for a total of 6 h and EPR spectra were recorded at 0 h, 3 h, and 6 h to monitor any changes.

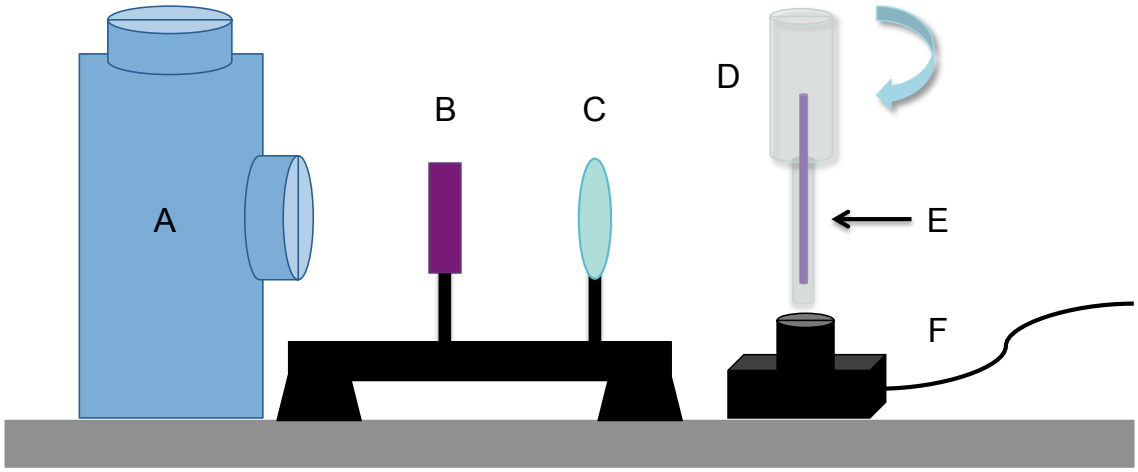

Figure 19. Photoirradiation set up. A) Lamp housing with high-pressure Hg-Xe arc lamp (1 kW). B) UV band pass filter (λ_{max} = 330 nm). C) Focusing lens. D) Cold finger Dewar (containing sample and N_2 (l)). E) EPR sample. F) Motor to rotate the sample.

3.7. Computational Methods

Computer-based calculations were performed to help characterize the paramagnetic products found in the reaction mixtures. The programs used served several functions, such as, determining EPR parameters (nuclear hyperfine interaction values (a_{Nu}) and *g*-values), constructing simulations of the experimental spectra, and predicting geometries theoretically with density-functional calculations.

3.7.1. Determination of Magnetic Parameters

Isotropic magnetic parameters, a_{iso} and g_{iso}, of paramagnetic products, observed in the EPR spectra, were determined using the FORTRAN program ESRLSQ.[101] This required providing the program with the experimental magnetic field position of each transition line (G), obtained from calibrated spectra, along with the corresponding microwave frequency (MHz) and gyromagnetic ratio (γ) of the magnetic nuclei. Execution of the ESRLSQ program resulted in the exact solution of the spin Hamiltonian, yielding values of a_{iso}, g_{iso} as well as the corresponding standard deviations.

Anisotropic magnetic parameters, $a_{||}$, $a_{\perp}$, $g_{||}$, and $g_{\perp}$, of paramagnetic products observed in the EPR spectra were determined with a second FORTRAN program, ANISO.[101] The spin quantum number (I), gyromagnetic ratio (γ), parallel and perpendicular components of the $m_I = \pm I$ transition lines (G) obtained from calibrated spectra and corresponding microwave frequency (MHz) were entered into the program, yielding values of $a_{||}$, $a_{\perp}$, $g_{||}$, and $g_{\perp}$.

3.7.2. Spectral Simulations

Experimental spectra were simulated using the programs ISOPLOT[101] and EPR-NMR.[102] ISOPLOT was used to simulate compounds with relatively small isotropic hyperfine interactions. Magnetic parameters, a_{iso} and g_{iso}, estimated from the experimental spectra were used as initial input for the spectral simulation program, ISOPLOT, along with the microwave frequency (MHz) at which the spectrum was recorded and the line width (G) of the transition lines. The simulation was compared to the experimental spectrum and if

needed the a_{Nu} and or *g*-values were adjusted. This process was repeated until the best fit between the experimental and simulated spectra was obtained.

EPR-NMR is a multifunction program capable of simulating isotropic, axial and orthorhombic spectra. A spectral simulation required providing the EPR-NMR input file with a_{Nu} and *g*-values, determined with the FORTRAN computer programs ESRLSQ or ANISO, the corresponding spectrometer operating frequency (MHz) at which the experimental spectrum was recorded, and the line width of the transition lines (MHz).

3.7.3. DFT Calculations

All quantum-mechanical calculations were carried out using density functional theory (DFT) with the Gaussian09W program.[88] Three different hybrid functionals, B3LYP,[85,87] M06[89] and BHandHLYP[88] were used in combination with several basis sets. The 6-311G, 6-311+G, 6-311+G(d), EPR-III, and 6-31++G(d,p) basis sets were used for C, H, N, O, S and Si atoms. Cu atoms were treated with the 6-311G, 6-311+G, or 6-311+G(d) basis sets. The pseudo-potential Los Alamos ECP plus DZ basis set (LANL2DZ) was also used for Cu, Ag and Au atoms. Geometries were fully optimized and harmonic vibrational frequencies calculated with analytical second derivatives of the total potential energy. Structure-specific internal energies and hyperfine interaction values (with the exception of those containing Ag or Au) were recorded from the output files of the Gaussian program. All optimized geometry information (bond lengths, angles and dihedral angles) of molecules used in this thesis can be found in the Appendix section (see sections 8.1.1 and 8.1.2).

4. Results

4.1. Reaction of Copper Atoms with Three-Membered Heterocyclic Compounds

4.1.1. Oxiranes

4.1.1.1. Ethylene oxide

The reaction of $^{63/65}$Cu atoms (I = 3/2) with ethylene oxide in an adamantane matrix at 77 K produced a dark red-brown deposit on the drum. A sample of the deposit was collected and analyzed at 77 K by EPR spectroscopy. Trapped $^{63/65}$Cu atoms, evident by the ^{63}Cu NMR transition (m_s = -1/2, m_I = -3/2 $\leftrightarrow$ -1/2) at 1234 G (ν = 9137 MHz) and $^{63/65}$Cu EPR transitions ($\Delta m_s = \pm 1$, m_I = -3/2) at 5602 G and 5726 G (ν = 9139 MHz), two large quartets, ^{63}Cu-EO-1 and ^{63}Cu-EO-2 and finally a small central feature, A, were detected in the EPR spectrum, Figure 20a. In addition, transition lines of ^{65}Cu-EO-1 and ^{65}Cu-EO-2 at m_I = -1/2 and m_I = -3/2 were apparent. The transitions at m_I = 1/2 and 3/2 were not visible because the spectrometer frequency is less than the zero-field splitting, (I +1/2)$g\beta a$,[25] where I is the spin quantum number and β is the Bohr magneton. The natural abundance[24] of the ^{63}Cu and ^{65}Cu isotopes, 30.91% and 69.09%, respectively, are reflected in the intensity of the transition lines corresponding to the respective copper-containing products. The magnetic parameters corresponding to $^{63/65}$Cu-EO-1 and $^{63/65}$Cu-EO-2 were determined using the magnetic field positions of their transition lines, Table 5, and the ESRLSQ program. Paramagnetic products containing the ^{65}Cu isotope have a larger nuclear hyperfine interaction, a_{Cu}, than ^{63}Cu radicals based on the ratio of the gyromagnetic ratios for ^{65}Cu and ^{63}Cu, i.e. $\gamma_{65Cu}/\gamma_{63Cu}$ = 1.071. A simulated spectrum of $^{63/65}$Cu-EO-1 and $^{63/65}$Cu-EO-2 was constructed using the EPR-NMR program and the

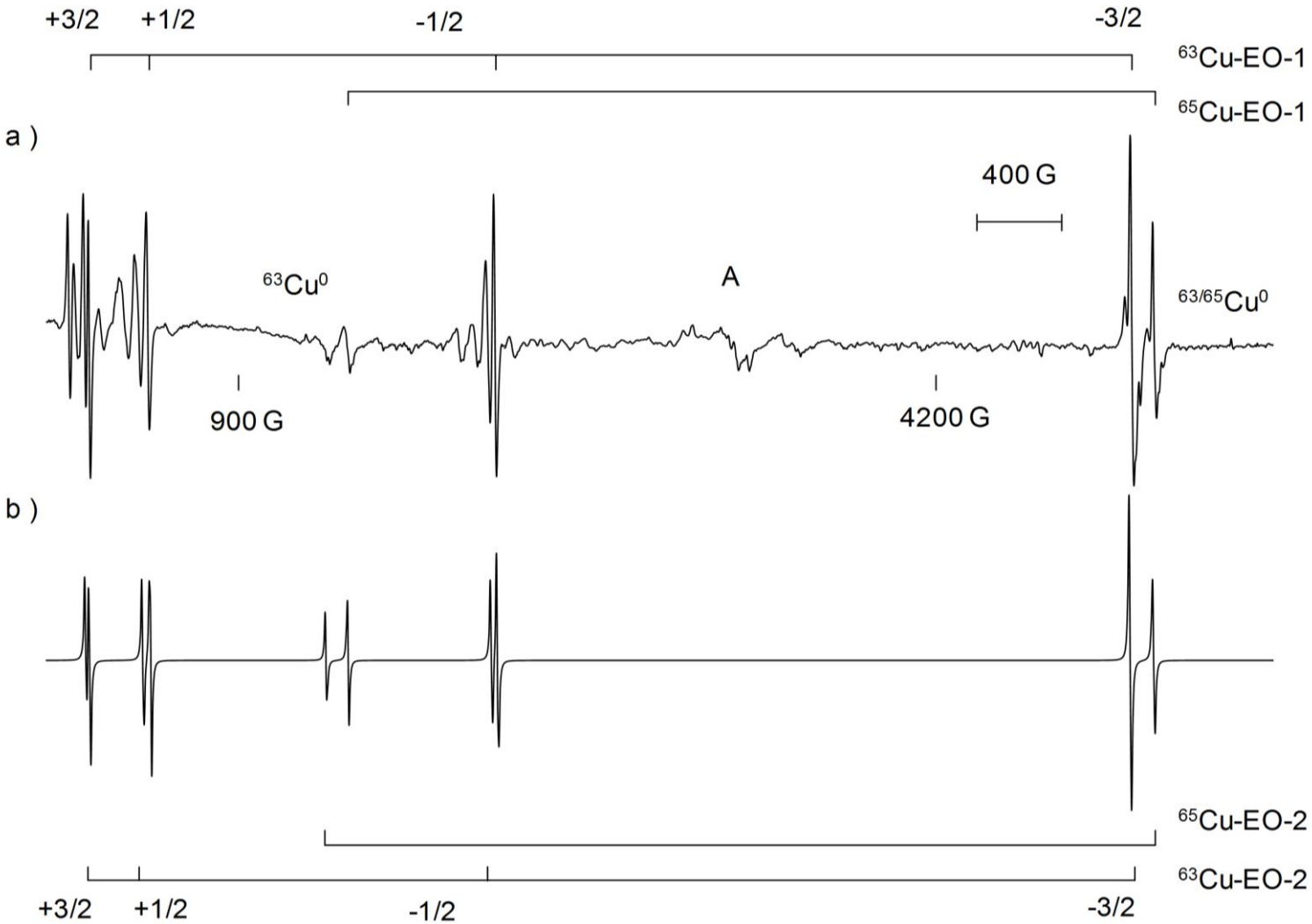

Figure 20. a) EPR spectrum recorded at 77 K (ν = 9138 MHz, microwave power, m.p. = 2 mW) of the paramagnetic products, $^{63/65}$Cu-EO-1, $^{63/65}$Cu-EO-2 and A, formed in the reaction of $^{63/65}$Cu atoms with ethylene oxide in an adamantane matrix. b) Simulated spectra of $^{63/65}$Cu-EO-1 and $^{63/65}$Cu-EO-2 using the magnetic parameters listed in Table 5.

parameters in Table 5, Figure 20b.

Table 5. The magnetic field positions of $^{63/65}$Cu-EO-1 and $^{63/65}$Cu-EO-2, formed in the reaction of $^{63/65}$Cu atoms and ethylene oxide in adamantane, as well as the corresponding magnetic parameters[a] determined with ESRLSQ.

	Transition	Magnetic Field Position (G)	a_{Cu} (MHz)	g
^{63}Cu-EO-1[a]	+3/2	191.34	4349 ± 1.6	2.0091 ± 0.0005
	+1/2	470.95		
	-1/2	2115.49		
	-3/2	5128.66		
^{65}Cu-EO-1[a]	+3/2	-	4656	2.0088
	+1/2	-		
	-1/2	1417.80		
	-3/2	5234.96		
^{63}Cu-EO-2[b]	+3/2	163.83	4368 ± 2.5	2.0096 ± 0.0007
	+1/2	411.78		
	-1/2	2067.18		
	-3/2	5126.78		
^{65}Cu-EO-2[b]	+3/2	-	4678	2.0095
	+1/2	-		
	-1/2	1253.71		
	-3/2	5234.29		

[a]Calculated at 77 K, ν = 9137 MHz. [b]Calculated at 100 K, ν = 9120 MHz.

When the sample was annealed from 77 K to 100 K, Figure 21, the resolution of the spectrum improved greatly and notably the transitions associated with $^{63/65}$Cu-EO-1 disappeared, Figure 21b. When examining the spectra one can see that the m_I = -3/2 transition of ^{63}Cu-EO-1 and ^{63}Cu-EO-2 were superimposed at 77 K due to the almost identical g-values and the small differences (19.4 MHz, 0.4%) in their respective hyperfine values.

The central region of the spectrum, 2850-3650 G, consists of several transition lines that are 1/6 the intensity of $^{63/65}$Cu-EO-1 and centered at g ~ 2.007, Figure 22a. One can see that there is not much change in the spectrum between 77 and 120 K with the intensity remaining relatively constant, Figure 22b and c.

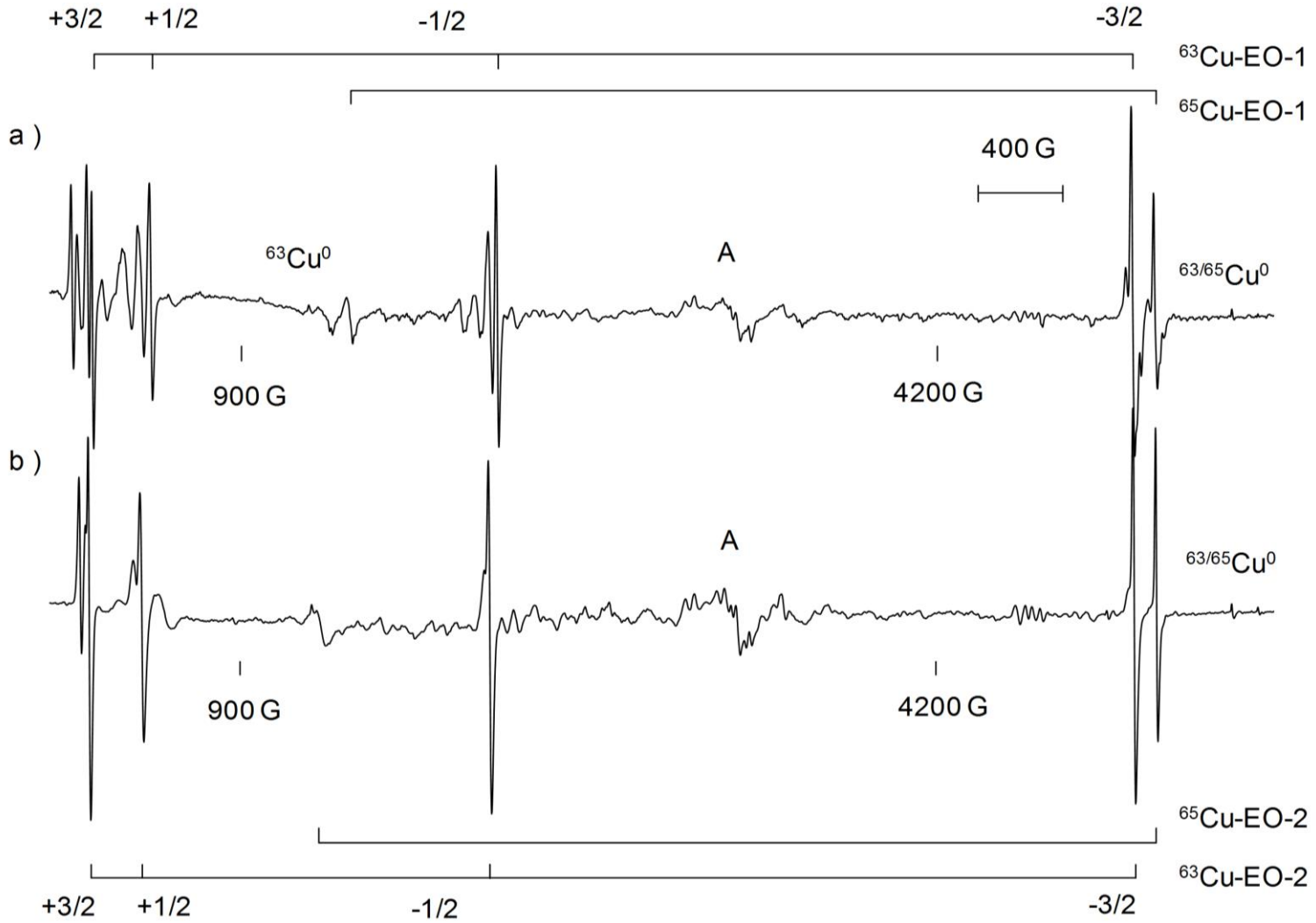

Figure 21. Comparison of the EPR spectra of the paramagnetic products formed in the reaction of $^{63/65}$Cu atoms with ethylene oxide in adamantane recorded at a) 77 K (*v* = 9138 MHz, m.p. = 2 mW) and b) 100 K (v = 9120 MHz, m.p. = 2 mW).

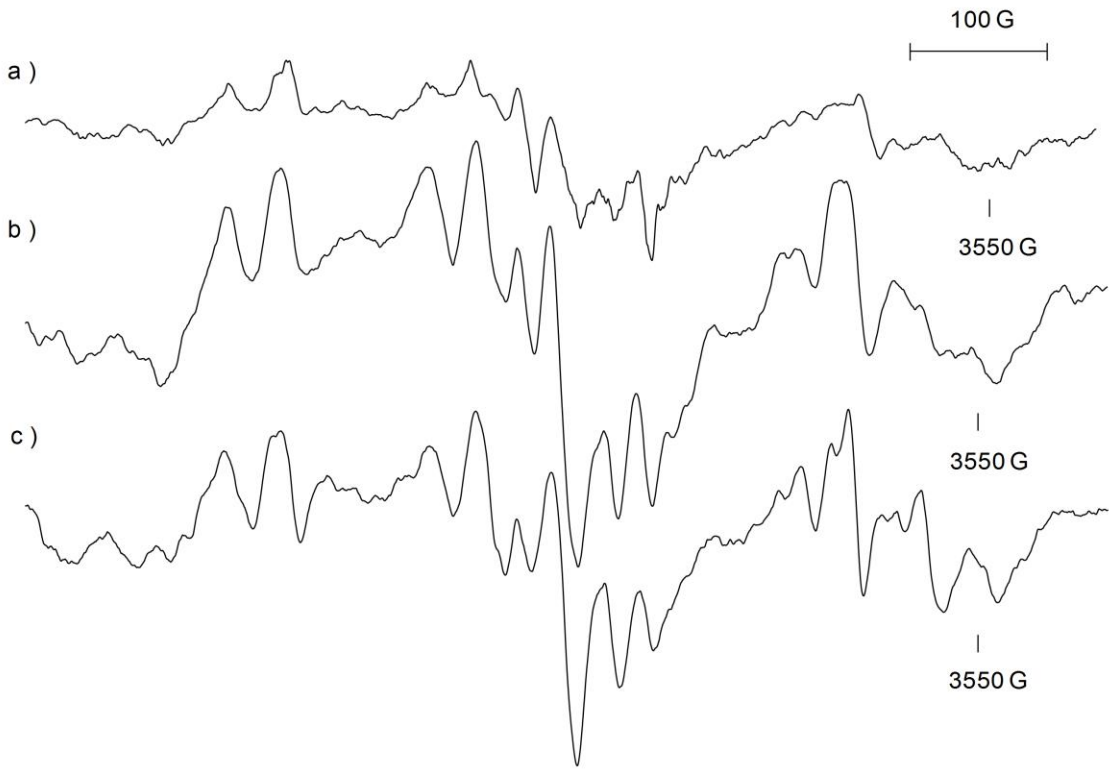

Figure 22. EPR spectrum of the central region from the reaction of $^{63/65}$Cu atoms with ethylene oxide at a) 77 K (ν = 9139 MHz, m.p. = 2 mW) b) 100 K (ν = 9120 MHz, m.p. = 10 mW) and c) 120 K (ν = 9120 MHz, m.p. = 10 mW).

In a subsequent experiment, the sample of the $^{63/65}$Cu atom-ethylene oxide reaction mixture, previously annealed to 130 K, was irradiated for 5 h with a Hg-Xe lamp and a band pass filter (λ_{max} of 330 nm). Although there was no significant difference in the intensity and appearance of $^{63/65}$Cu-EO-2 EPR transition lines after irradiation of the sample, the region between 3000 and 3500 G did change slightly, Figure 22a and Figure 23a. Comparison with the EPR spectrum for the photoirradiation of the $^{63/65}$Cu atoms-ethylene oxide-d_4 sample (Figure 31, section 4.1.1.2) led us to detect the weak quartet, A-UV, centered at g = 2.0005 with a_{63Cu} = 188.6 MHz and a_{65Cu} = 202.0 MHz (see simulation in Figure 23b).

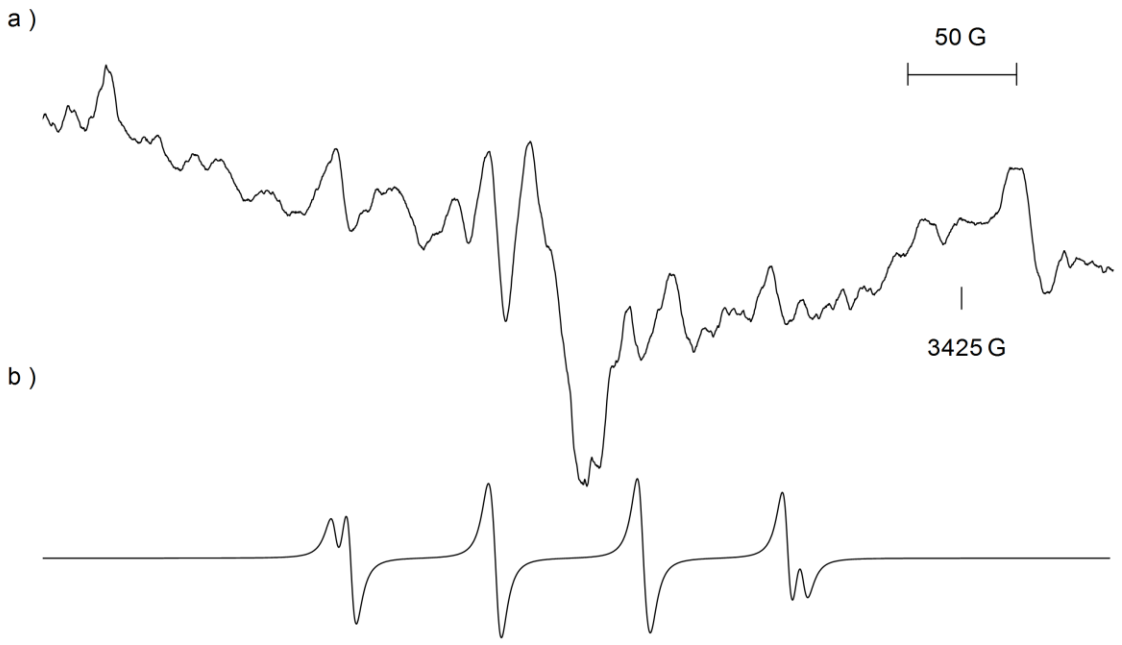

Figure 23. a) EPR spectrum of A-UV at 77 K after 5 h of UV exposure, λ_{max} = 330 nm (ν = 9087 MHz, m.p. = 2 mW). b) Simulation of the experimental EPR spectrum of A-UV using ISOPLOT, with the parameters, g = 2.0005, $a_{^{63}Cu}$ = 188.6 MHz and $a_{^{65}Cu}$ = 202.0 MHz.

4.1.1.2. Ethylene oxide-d_4

The $^{63/65}$Cu (I = 3/2) atom reaction was repeated with ethylene oxide-d_4. A sample of the dark red-brown deposit was collected and analyzed at 77 K by EPR spectroscopy, Figure 24. As in the case for the $^{63/65}$Cu-ethylene oxide reaction, a ^{63}Cu NMR transition (1259 G, ν = 9088 MHz) and $^{63/65}$Cu EPR transitions (5573 G and 5731 G, ν = 9088 MHz), indicative of trapped $^{63/65}$Cu atoms, were observed. Similarly a large quartet, labelled ^{63}Cu-EO-d_4-1, the m_I = -1/2 and -3/2 transition lines corresponding to ^{65}Cu-EO-d_4-1, and the central feature, A-d_4, were detected. The a_{Cu} and g-values of $^{63/65}$Cu-EO-d_4-1, determined from the magnetic field position of the transition lines, are found in Table 6.

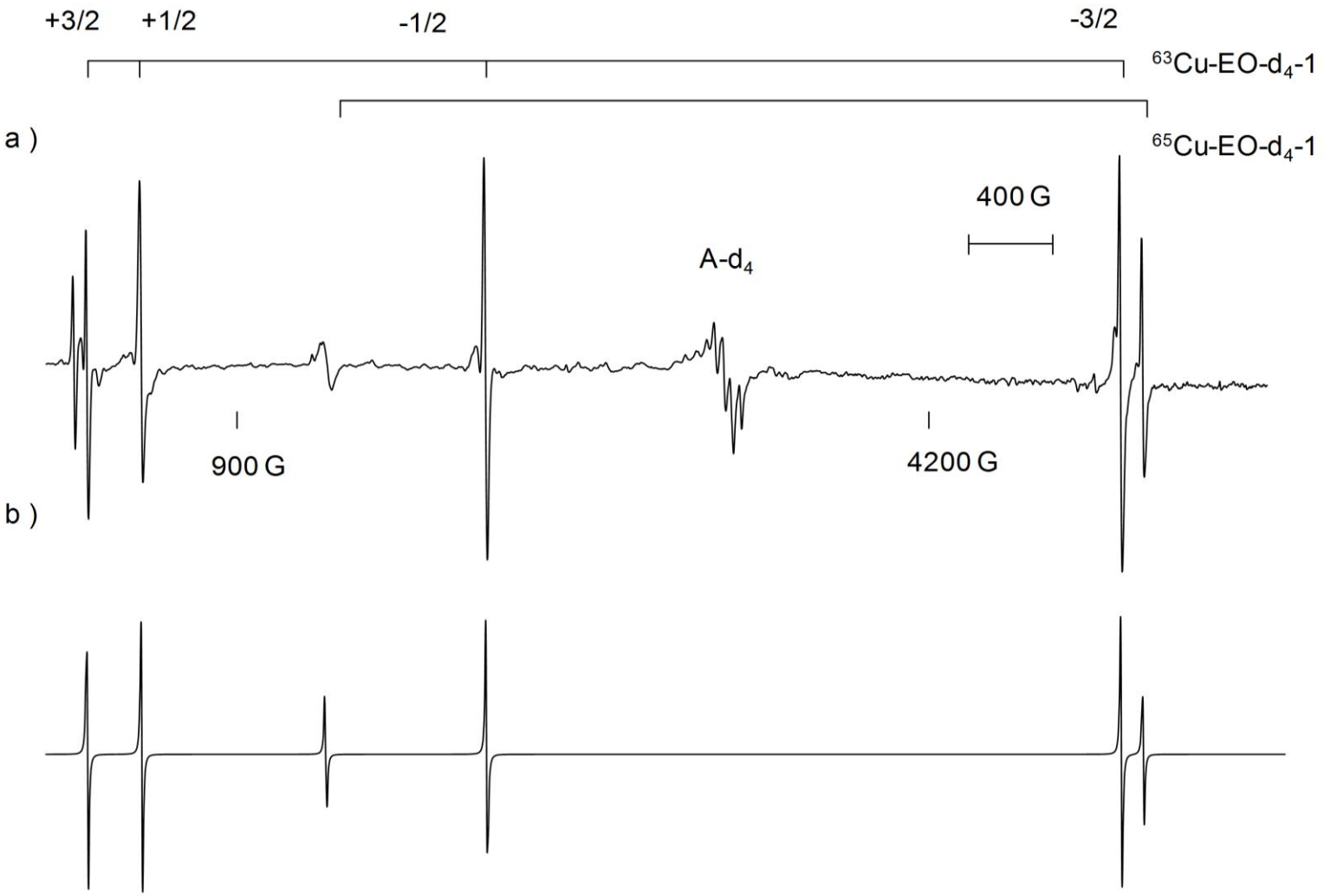

Figure 24. a) EPR spectrum recorded at 77 K (ν = 9086 MHz, m.p. = 2 mW) of the paramagnetic products, $^{63/65}$Cu-EO-d$_4$-1 and A-d$_4$, formed in the reaction of $^{63/65}$Cu atoms with ethylene oxide-d$_4$ in an adamantane matrix. b) Simulated spectra of $^{63/65}$Cu-EO-d$_4$-1 using the magnetic parameters listed in Table 6.

The ratio of the hyperfine interaction of ^{65}Cu-EO-d$_4$-1 and ^{63}Cu-EO-d$_4$-1, i.e. a_{65Cu}/a_{63Cu}, is equal to 1.071 respecting the ratio of the gyromagnetic ratios of ^{65}Cu and ^{63}Cu atoms.

Table 6. The magnetic parameters of $^{63/65}$Cu-EO-1, $^{63/65}$Cu-EO-2, $^{63/65}$Cu-EO-d$_4$-1, ^{63}Cu-EO-d$_4$-2, $^{63/65}$Cu-EO-^{13}C-1, and ^{63}Cu-EO-^{13}C-2, formed in the reactions of $^{63/65}$Cu atoms with ethylene oxide or its isotopomers, ethylene oxide-d$_4$ and ethylene oxide-^{13}C$_2$ in adamantane.

Ethylene oxide	a_{Cu} (MHz)	g	Temperature	ν (MHz)
^{63}Cu-EO-1	4349 ± 1.6	2.0091 ± 0.0005	77 K	9137
^{65}Cu-EO-1	4656	2.0088		
^{63}Cu-EO-2	4368 ± 2.5	2.0096 ± 0.0007	100 K	9120
^{65}Cu-EO-2	4678	2.0095		
Ethylene oxide-d$_4$	a_{Cu} (MHz)	g	Temperature	ν (MHz)
^{63}Cu-EO-d$_4$-1	4337 ± 4.7	2.0098 ± 0.0014	77 K	9087
^{65}Cu-EO-d$_4$-1	4647	2.0098		
^{63}Cu-EO-d$_4$-1	4371 ± 3.5	2.0110 ± 0.0010		
^{65}Cu-EO-d$_4$-1	4674	2.0093	120 K	9121
^{63}Cu-EO-d$_4$-2	4033 ± 1.7	2.0105 ± 0.0006		
Ethylene oxide-^{13}C$_2$	a_{Cu} (MHz)	g	Temperature	ν (MHz)
^{63}Cu-EO-^{13}C-1	4347 ± 1.9	2.0095 ± 0.0005	77 K	9088
^{65}Cu-EO-^{13}C-1	4677	2.0098		
^{63}Cu-EO-^{13}C-1	4370 ± 3.0	2.0103 ± 0.0009		
^{65}Cu-EO-^{13}C-1	4701	2.0097	110 K	9120
^{63}Cu-EO-^{13}C-2	4030 ± 7.2	2.0101 ± 0.0020		

As the sample was warmed to 120 K in the cavity of the spectrometer four additional transition lines corresponding to a Cu-centered radical, ^{63}Cu-EO-d$_4$-2, appeared, Figure 25. The intensity of the m_I = -3/2 transition line of ^{63}Cu-EO-d$_4$-2 is 1/11 that of ^{63}Cu-EO-d$_4$-1. It is therefore not surprising that the transition lines of the ^{65}Cu-EO-d$_4$-2 species are not visible. It is however possible to estimate the ^{65}Cu hyperfine interaction value from the ^{63}Cu hyperfine interaction, Table 6, and the ratio of the gyromagnetic ratios of ^{65}Cu and ^{63}Cu, i.e., $a_{65Cu} = a_{63Cu} \times \gamma_{65Cu}/\gamma_{63Cu} \approx 4319$ MHz. The ^{63}Cu hyperfine interaction values determined from data collected at 120 K, Table 6, for

^{63}Cu-EO-d$_4$-1 and ^{63}Cu-EO-d$_4$-2, differ by ~ 339 MHz (7.8%) while the *g*-values are the same within experimental error.

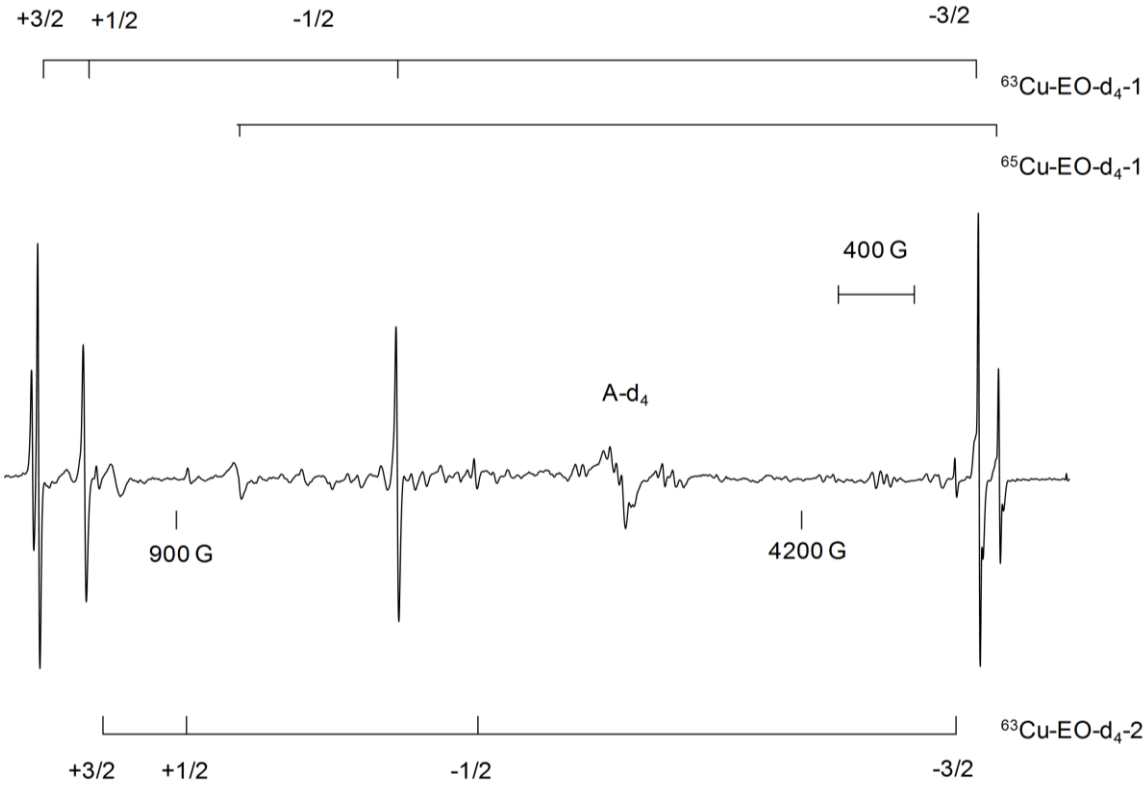

Figure 25. EPR spectrum recorded at 120 K (*ν* = 9120 MHz, m.p. = 2 mW) of the paramagnetic products, $^{63/65}$Cu-EO-d$_4$-1, ^{63}Cu-EO-d$_4$-2 and A-d$_4$, formed in the reaction of $^{63/65}$Cu atoms with ethylene oxide-d$_4$ in an adamantane matrix.

The difference in the hyperfine values of ^{63}Cu-EO-d$_4$-1 at 77 K and 120 K, is another observation worth noting. Closer examination of the spectra in Figure 26 shows that, as the temperature increases from 100 K to 160 K, the m_I = +3/2 and +1/2 transitions of ^{63}Cu-EO-d$_4$-1 shift to lower field, while the position of ^{63}Cu^0 remains unchanged. On the other hand, the m_I = -1/2 and -3/2 transitions, were found to shift to lower and higher field, respectively, as the temperature of the sample was increased. Therefore, between 77

K and 120 K, there is a 47 MHz (1%) increase in the hyperfine value of ^{63}Cu-EO-d$_4$-1. Finally, the Cu-centered radicals, ^{63}Cu-EO-d$_4$-1 and ^{63}Cu-EO-d$_4$-2, persisted to 180 K.

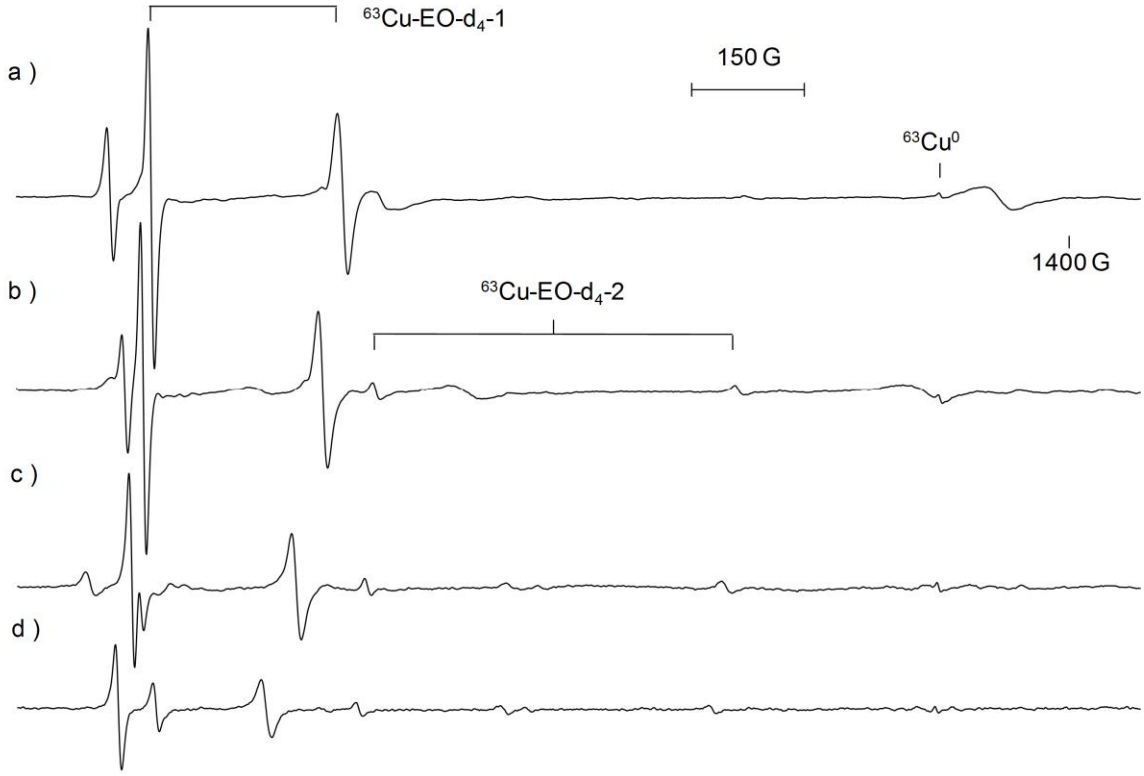

Figure 26. Array of low field EPR spectra showing a shift in the m_I = +3/2 and +1/2 transition lines of ^{63}Cu-EO-d$_4$-1 and ^{63}Cu-EO-d$_4$-2 at a) 100 K, b) 120 K, c) 140 K and d) 160 K. All spectra recorded at ν = 9120 MHz and m.p. = 2 mW.

The features in the central region of the EPR spectrum recorded at 77 K, A-d$_4$, Figure 27a, are characteristic of a $^{63/65}$Cu-centered radical with axial symmetry. A good simulation of the experimental spectrum was obtained by assuming $a_{\|}$ (^{63}Cu) = 137.7 MHz, $a_{\|}$ (^{65}Cu) = 147.4 MHz, $a_{\perp}$ (^{63}Cu) = 109.9 MHz, $a_{\perp}$ (^{65}Cu) = 117.6 MHz, $g_{\|}$ = 2.1217 and $g_{\perp}$ = 2.0075, Figure 27b. The intensity of the A-d$_4$ transitions decreases as the temperature is increased, Figure 28. Weak lines appeared at ~ 3015 and ~3475 G which in the absence of additional information could not be assigned.

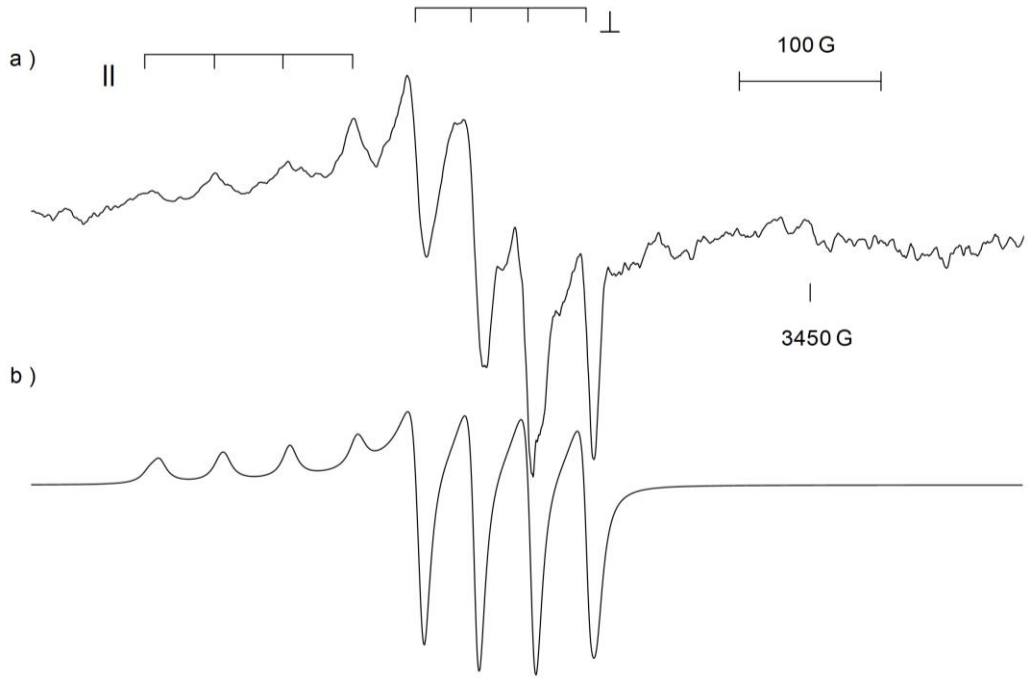

Figure 27. a) The central region, A-d4, of the EPR spectrum of the $^{63/65}$Cu atom-ethylene oxide-d$_4$ reaction mixture recorded at 77 K (ν = 9088 MHz, m.p. = 2 mW). b) Simulation of A-d$_4$ using the parameters reported in the text (LW = 20 MHz).

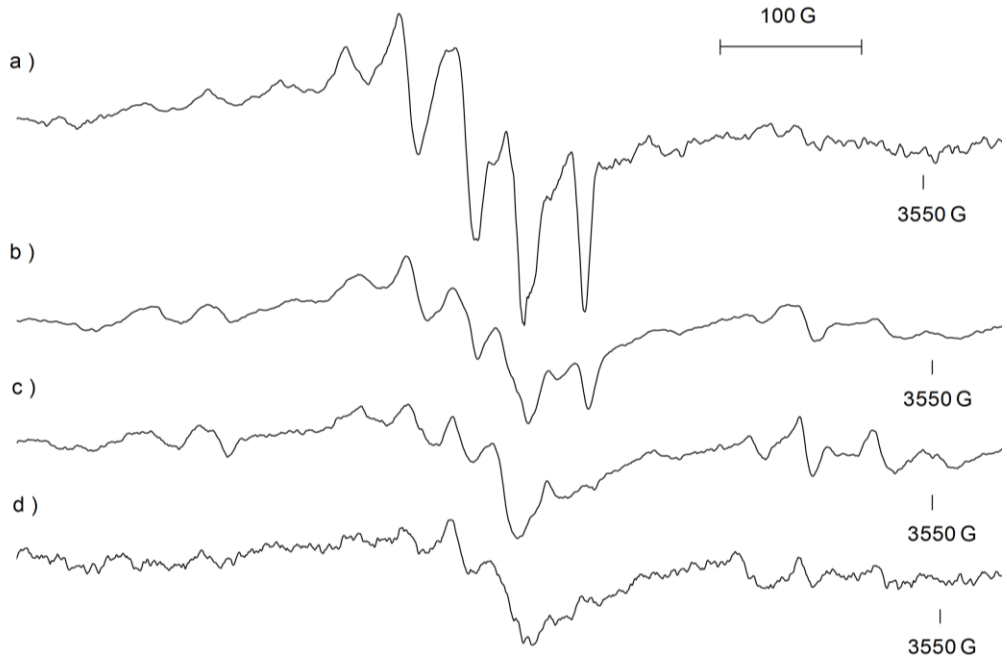

aster

Figure 28. The effect of temperature on the EPR transition lines of A-d$_4$ formed in the reaction of $^{63/65}$Cu atoms with ethylene oxide-d$_4$; a) 77 K (ν = 9088 MHz), b) 100 K (ν = 9120 MHz), c) 130 K (ν = 9120 MHz) and d) 160 K (ν = 9120 MHz). All spectra recorded with a microwave power of 2 mW.

Another sample of the $^{63/65}$Cu-ethylene oxide-d_4 reaction mixture was photoirradiated for 6 h using a Hg-Xe lamp and a band pass filter with λ_{max} of 330 nm. Interestingly, ^{63}Cu-EO-d_4-2 and ^{65}Cu-EO-d_4-2, which were first detected in the sample subjected to the annealing experiment, appear in the EPR spectrum of the photoirradiated sample. No changes occurred to the ^{63}Cu-EO-d_4-1 and ^{65}Cu-EO-d_4-1 transition lines, Figure 29. The most significant changes occur between 2850 and 3650 G of the EPR spectrum, Figure 30.

The anisotropic feature, A-d_4 is no longer the major component of the EPR spectrum at 77 K. Annealing the sample to 120 K reveals a distinct quartet pattern, A-d_4-UV, centered at g = 2.000, as observed in Figure 31a. A simulation was constructed with the ISOPLOT program assuming one Cu nucleus with a_{63Cu} = 196.4 MHz and a_{65Cu} = 210.4 MHz, Figure 31b. A-d_4-UV was no longer distinguishable in the EPR spectrum beyond 160 K.

4.1.1.3. Ethylene oxide-1,2-$^{13}C_2$

The reaction of $^{63/65}$Cu atoms (I = 3/2) with ethylene oxide-1,2-$^{13}C_2$, in an adamantane matrix at 77 K, produced a dark red-brown deposit on the drum. A sample of the deposit was collected and analyzed, at 77 K, by EPR spectroscopy. Once more, the transition lines at 1221 G (ν = 9088 MHz), 5581 G (ν = 9088 MHz), and 5705 G (ν = 9088 MHz) are the ^{63}Cu NMR transition, ^{63}Cu EPR transition, and ^{65}Cu EPR transition, respectively, of trapped $^{63/65}$Cu atoms. In addition, a large quartet labelled ^{63}Cu-EO-^{13}C-1, the m_I = -1/2 and m_I = -3/2 transitions labelled ^{65}Cu-EO-^{13}C-1 and a weak central feature (A-^{13}C) were observed, Figure 32. The magnetic parameters associated with $^{63/65}$Cu-EO-^{13}C-1 can be

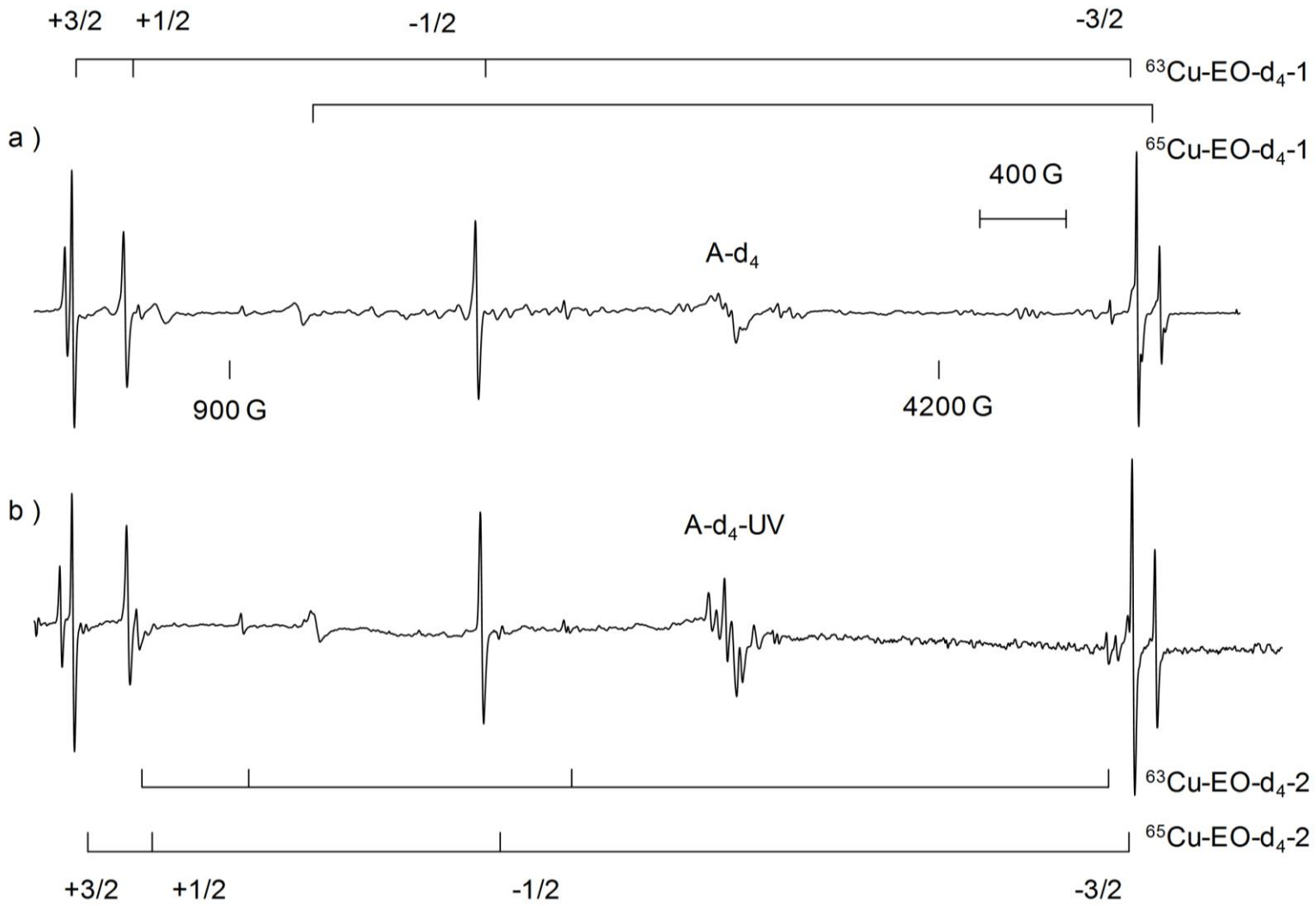

Figure 29. a) EPR spectrum of the $^{63/65}$Cu atom-ethylene oxide-d$_4$ reaction mixture annealed to 120 K (ν = 9120 MHz, m.p. = 2 mW). b) EPR spectrum of the $^{63/65}$Cu atoms and ethylene oxide-D$_4$ sample at 77 K (ν = 9086 MHz, m.p. = 2 mW) after 6 h of UV exposure with transition lines of $^{63/65}$Cu-EO-d$_4$-1 and $^{63/65}$Cu-EO-d$_4$-2 highlighted.

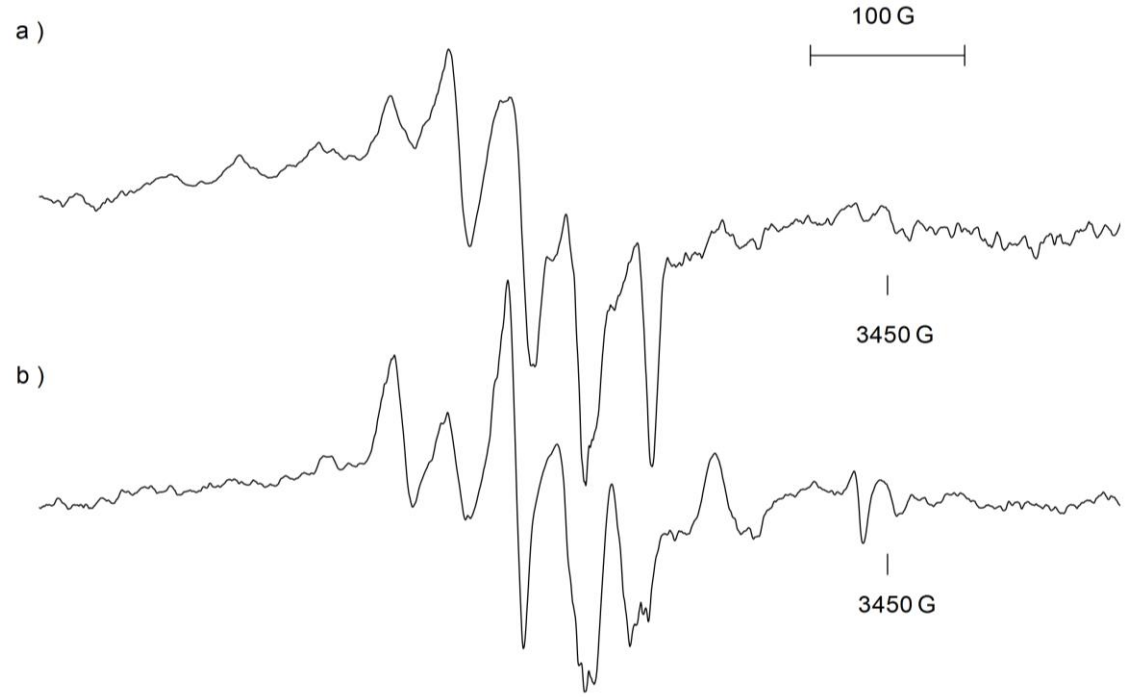

Figure 30. Comparison of EPR spectra recorded for the central region of the $^{63/65}$Cu atom-ethylene oxide-d$_4$ reaction mixture a) at 77 K (ν = 9088 MHz) and b) at 77 K after 6 h of UV exposure (ν = 9086 MHz). Both spectra were recorded with a m.p. = 2 mW.

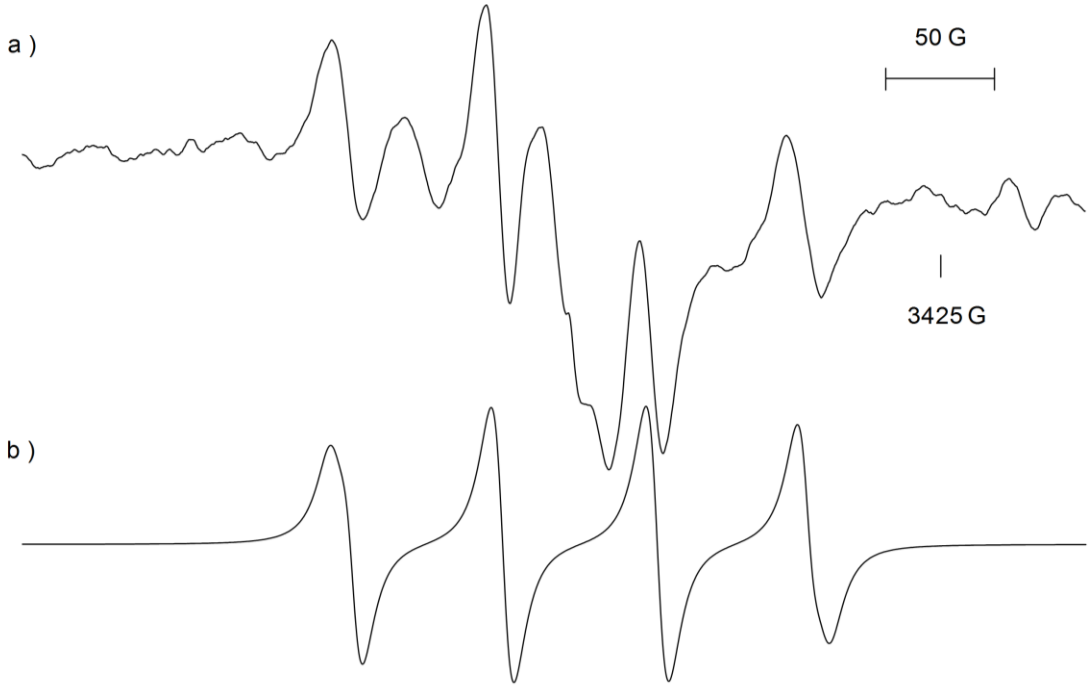

Figure 31. a) EPR spectrum of A-d$_4$-UV at 120 K over a 500 G scan range (ν = 9121 MHz, m.p. = 2 mW). b) Simulation of the experimental EPR spectrum of A-d$_4$-UV using ISOPLOT, with the parameters, g = 2.0000, $a_{^{63}Cu}$ = 196.4 MHz and $a_{^{65}Cu}$ = 210.4 MHz.

found in Table 6 (section 4.1.1.2).

Additional lines, albeit very weak, corresponding to a Cu-centered radical, ^{63}Cu-EO-^{13}C-2, appeared as the sample was warmed in the cavity of the spectrometer, Figure 33. The transition lines corresponding to the ^{65}Cu- containing isotopomer were not visible. This is explained by the fact that the transition line of the ^{65}Cu-containing radical are expected to be 0.45 times less intense than that of the ^{63}Cu radical based on the natural abundancies. An estimate of the ^{65}Cu hyperfine interaction value, based on the ratio of gyromagnetic ratios of ^{65}Cu and ^{63}Cu, is ~ 4316 MHz. The a_{Cu} and g values associated with $^{63/65}$Cu-EO-^{13}C-1 and ^{63}Cu-EO-^{13}C-2, recorded at 110 K, are also presented in Table 6. The ^{63}Cu hyperfine interaction values for ^{63}Cu-EO-^{13}C-1 and ^{63}Cu-EO-^{13}C-2, determined at 110 K differ by 340 MHz (7.8 %).

As noted for the paramagnetic products formed in reaction of $^{63/65}$Cu atoms with ethylene oxide-d_4 (section 4.1.1.2), the hyperfine interaction values of ^{63}Cu-EO-^{13}C-1 increase as a function of increasing temperature, i.e., the a_{63Cu} increases by 24 MHz (0.5 %) upon going from 77 K to 110 K. The EPR spectra of Cu-centered radicals, ^{63}Cu-EO-^{13}C-1 and ^{63}Cu-EO-^{13}C-2 were no longer visible at temperatures > 180 K.

The features at 77 K, belonging to A-^{13}C, are characteristic of an axially symmetric radical, Figure 34a. The experimental spectrum was simulated assuming $a_{\parallel}$ (^{63}Cu) = 137.7 MHz, $a_{\parallel}$ (^{65}Cu) = 147.4 MHz, $a_{\perp}$ (^{63}Cu) = 109.9 MHz, $a_{\perp}$ (^{65}Cu) = 117.6 MHz, $g_{\parallel}$ = 2.1217, and $g_{\perp}$ = 2.0075, Figure 34b. The intensity of the A-^{13}C transition lines decrease as the sample is annealed, Figure 35. Like A-d_4, A-^{13}C is no longer detectable at temperatures > 180 K.

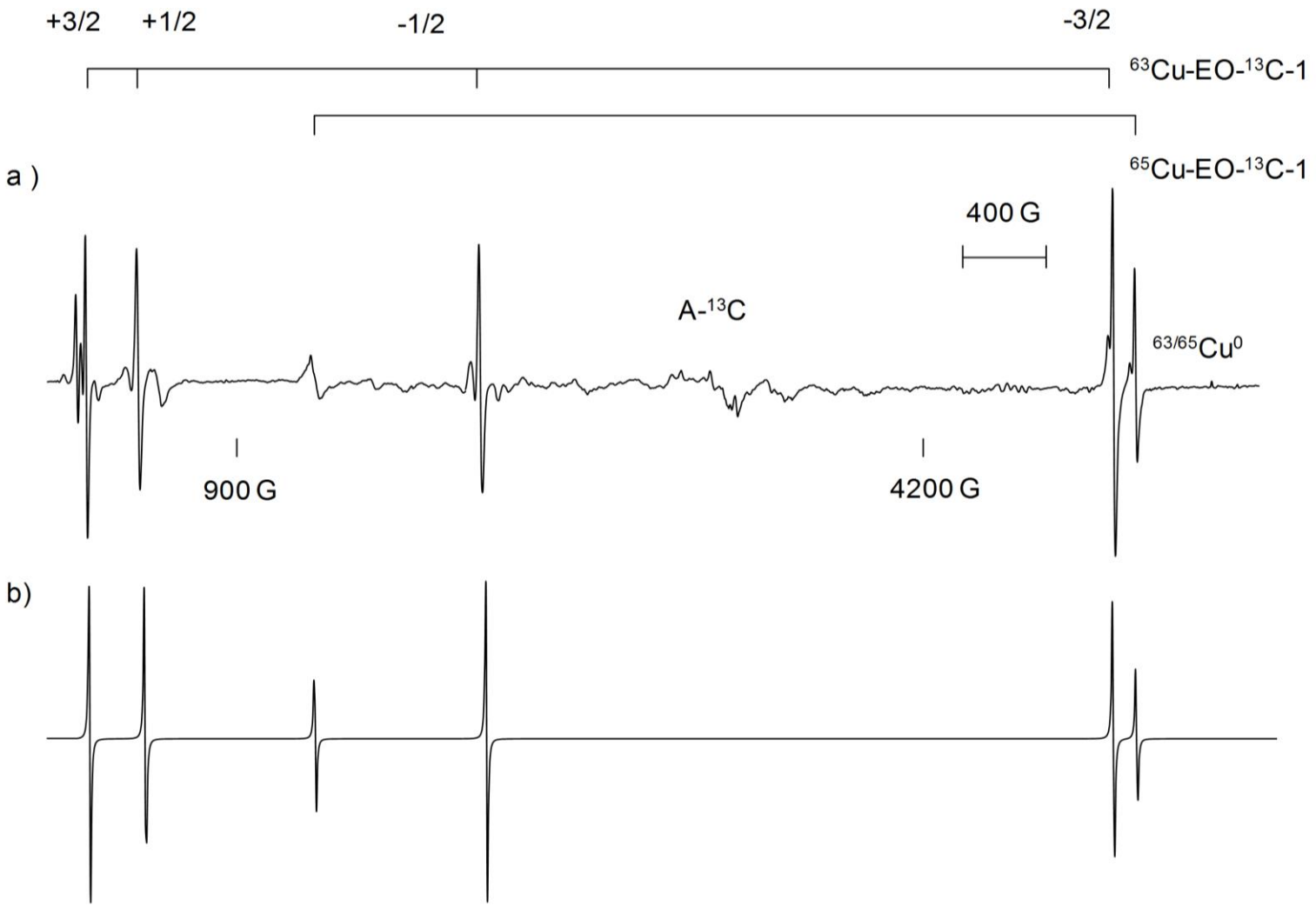

Figure 32. a) EPR spectrum recorded at 77 K (ν = 9088 MHz, m.p. = 2 mW) of the paramagnetic products, $^{63/65}$Cu-EO-^{13}C-1 and A-^{13}C, formed in the reaction of $^{63/65}$Cu atoms with ethylene oxide-1,2-$^{13}C_2$ in an adamantane matrix. b) Simulated spectra of $^{63/65}$Cu-EO-^{13}C-1 using the magnetic parameters listed in Table 6.

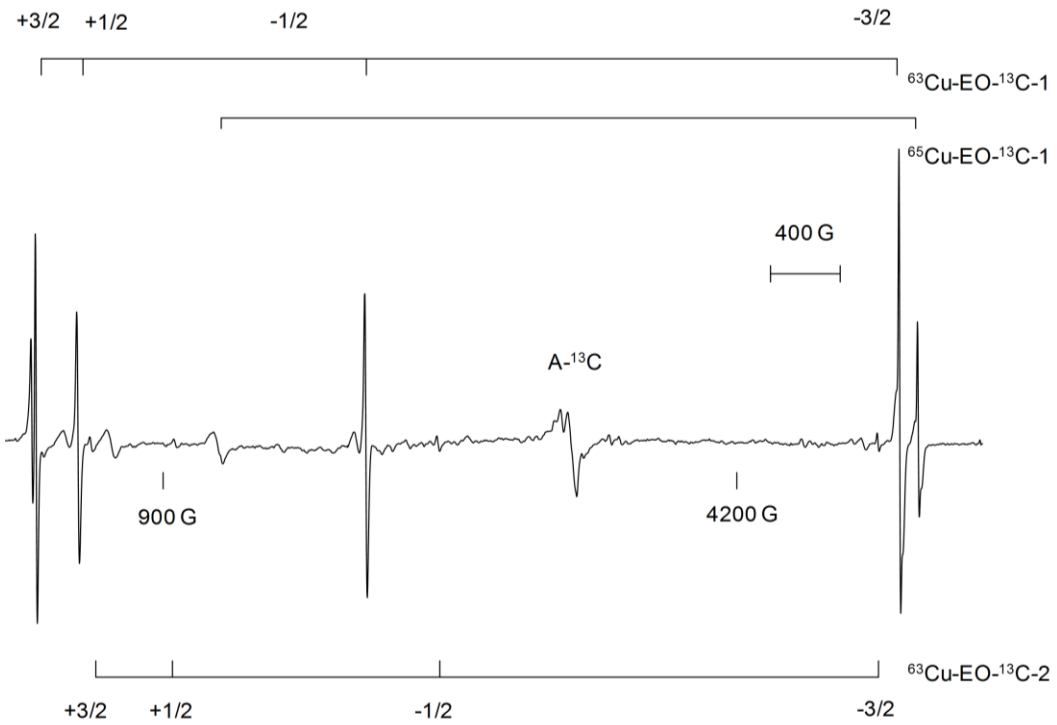

Figure 33. EPR spectrum recorded at 110 K (ν = 9120 MHz, m.p. = 2 mW) of the paramagnetic products, $^{63/65}$Cu-EO-^{13}C-1, ^{63}Cu-EO-^{13}C-2, and A-^{13}C, formed in the reaction of $^{63/65}$Cu atoms with ethylene oxide-1,2-$^{13}C_2$ in an adamantane matrix.

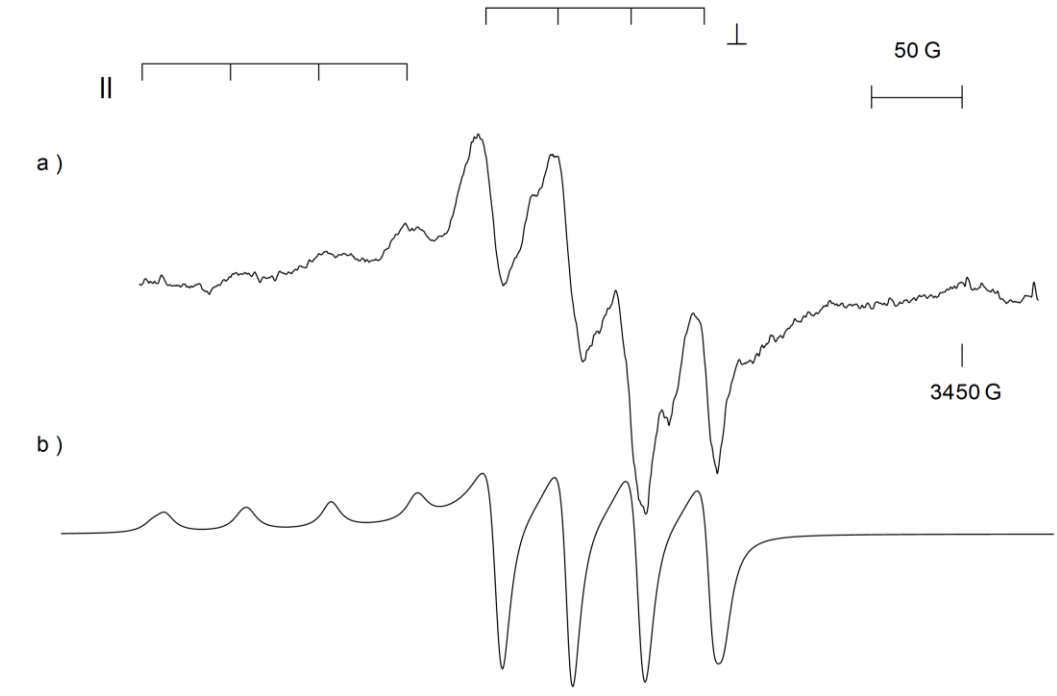

Figure 34. a) The central region, A-^{13}C, of the EPR spectrum of the $^{63/65}$Cu atom-ethylene oxide-1,2-$^{13}C_2$-adamantane reaction mixture recorded at 77 K (ν = 9139 MHz, m.p. = 2mW). b) Simulation of A-^{13}C using the parameters reported in the text (LW = 20 MHz).

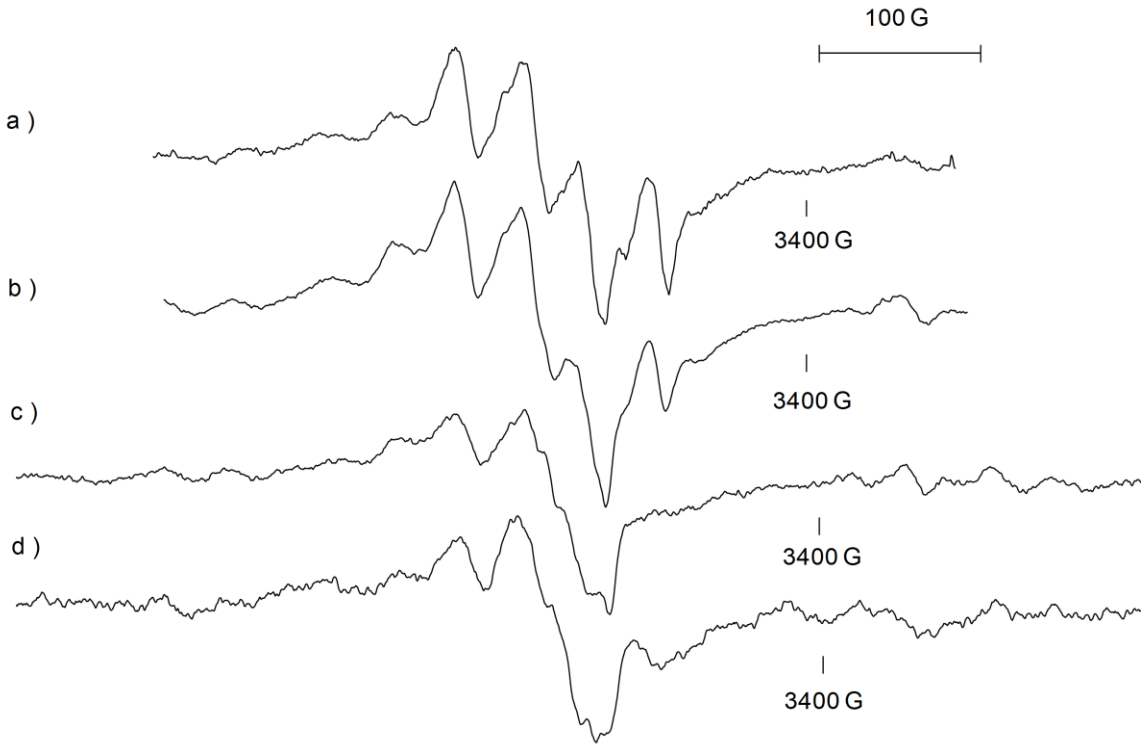

Figure 35. The effect of temperature on the EPR transition lines of A-^{13}C formed in the reaction of $^{63/65}$Cu atoms with ethylene oxide-1,2-$^{13}C_2$; a) 77 K (ν = 9139 MHz) b) 100 K (ν = 9120 MHz), c) 120 K (ν = 9120 MHz) and d) 150 K (ν = 9119 MHz). All spectra were recorded with m.p. = 2 mW.

4.1.1.4. 1,2-Epoxybutane

The reddish-brown deposit formed in the reaction of $^{63/65}$Cu atoms (I = 3/2) with 1,2-epoxybutane in an adamantane matrix at 77 K was collected and analyzed by EPR spectroscopy. Trapped $^{63/65}$Cu atoms, evident by the ^{63}Cu NMR transition at 1253 G (ν = 9089 MHz) and the $^{63/65}$Cu EPR transitions at 5581 G and 5706 G, respectively, were present in the spectrum recorded at 77 K, Figure 36a. In addition, two large quartets, ^{63}Cu-EB-1 and ^{63}Cu-EB-2, and an anisotropic central feature B were also detected. The a_{Cu} and g values, determined using the calibrated field positions of the ^{63}Cu-EB-1 and ^{63}Cu-EB-2 transition lines, are presented in Table 7. Only the m_I = -1/2 and -3/2 transition

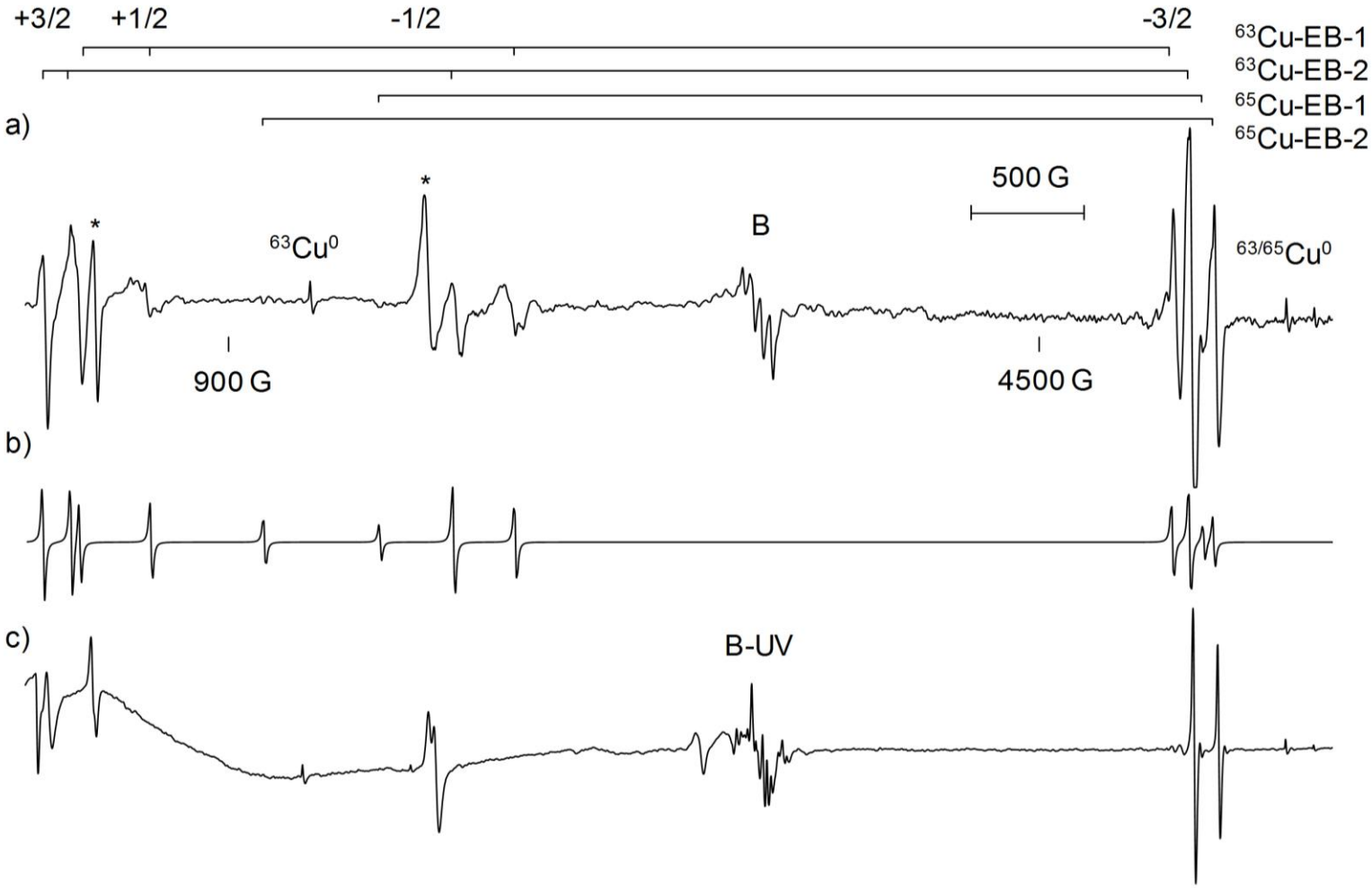

Figure 36. a) EPR spectrum recorded at 77 K (ν = 9089 MHz, m.p. = 2 mW) of the paramagnetic products, $^{63/65}$Cu-EB-1, $^{63/65}$Cu-EB-2 and B, formed in the reaction of $^{63/65}$Cu atoms with 1,2-epoxybutane in an adamantane matrix. b) Superposition of transition lines of $^{63/65}$Cu-EB-1 and $^{63/65}$Cu-EB-2 predicted by the EPR-NMR simulation program using the magnetic parameters in Table 7 and in the text. c) EPR spectrum recorded at 77 K (ν = 9085 MHz, m.p. = 2 mW) after 6 h of UV irradiation.

lines of ^{65}Cu-EB-1 were detected because the spectrometer frequency is less than the zero-field splitting, $(I+½)g\beta a$.[25] In the case of ^{65}Cu-EB-2, only the m_I = -3/2 transition line at 5265.7 G (ν = 9089 MHz) was visible. By substituting the field position of the m_I = -3/2 line, expressed in units of $\nu/g\beta$, i.e., 1.6252 where g is assumed to be 2.0043, in Equation 5 (Section 1.2.1), a_{65Cu} for ^{65}Cu-EB-2 is estimated to be 4787 MHz. This value is consistent with the value of 4786 MHz determined by multiplying a_{63Cu} for ^{63}Cu-EB-2 by the ratio of gyromagnetic ratios ($\gamma_{65Cu}/\gamma_{63Cu}$ = 1.071). A simulation of the $^{63/65}$Cu-EB-1 and $^{63/65}$Cu-EB-2 transition lines is presented in Figure 36b. The simulation for ^{65}Cu-EB-2 predicts the m_I = -1/2 transition line to be ~1055 G, although it is not visible on the experimental spectrum. It is important to note that the lines denoted by an asterisk in Figure 36a, have not yet been assigned.

Table 7. The magnetic parameters of $^{63/65}$Cu-EB-1 and ^{63}Cu-EB-2, formed in the reaction of $^{63/65}$Cu atoms with 1,2-epoxybutane in adamantane.

	a_{Cu} (MHz)	g	Temperature	ν (MHz)
^{63}Cu-EB-1	4293 ± 2.0	2.0101 ± 0.0006		
^{65}Cu-EB-1	4599	2.0066	77 K	9089
^{63}Cu-EB-2	4469 ± 7.5	2.0043 ± 0.0022		

A closer examination of the region between 2850 G and 3650 G recorded at 77 K reveals a strong anisotropic spectrum labelled B, Figure 37a. This spectrum is expected from a Cu-containing radical with axial symmetry where $g_{\|} > g_{\perp}$. An acceptable simulation of the central features, Figure 37b, was generated with the EPR parameters, $a_{\|}$ (^{63}Cu) = 130.4 MHz, $a_{\|}$ (^{65}Cu) = 139.7 MHz, $a_{\perp}$ (^{63}Cu) = 109.9 MHz, $a_{\perp}$ (^{65}Cu) = 117.6 MHz, $g_{\|}$ = 2.1143, and $g_{\perp}$ = 2.0073 taking into consideration the relative natural abundance of ^{63}Cu and ^{65}Cu.

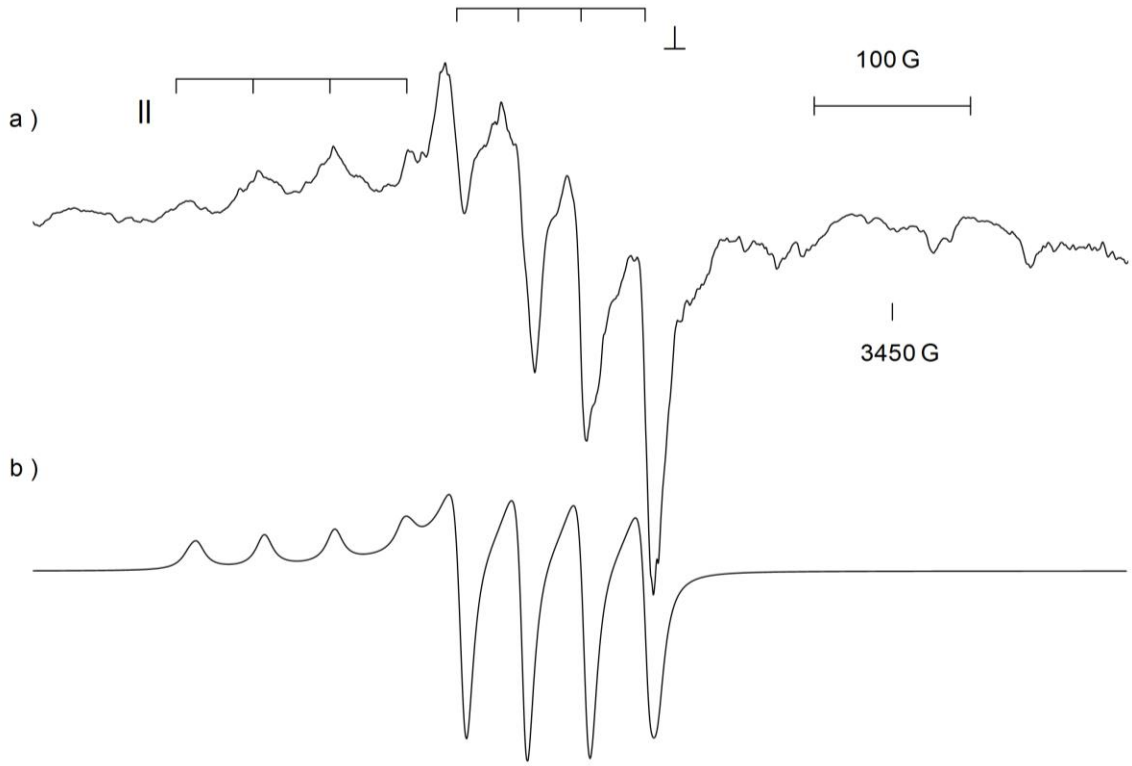

Figure 37. a) The central region, B, of the EPR spectrum of the $^{63/65}$Cu atom-1,2-epoxybutane adamantane reaction mixture recorded at 77 K (*v* = 9089 MHz, m.p. = 2 mW). b) Simulation of B using the parameters reported in the text (LW = 20 MHz).

Following initial analysis at 77 K, the $^{63/65}$Cu atoms-1,2-epoxybutane reaction mixture was photoirradiated for 6 h using a Hg-Xe high pressure lamp and a band pass filter with a λ_{max} of 330 nm. From a comparison of the EPR spectra recorded at 77 K before and after photoirradiation, it is noted that the transition lines of $^{63/65}$Cu-EB-1 (barely visible), $^{63/65}$Cu-EB-2, and $^{63}Cu^0$ diminished in intensity, Figure 36c. Additionally, the features between 3000 and 3500 G have underwent considerable changes upon photoirradiation of the sample, Figure 37a and Figure 31a.

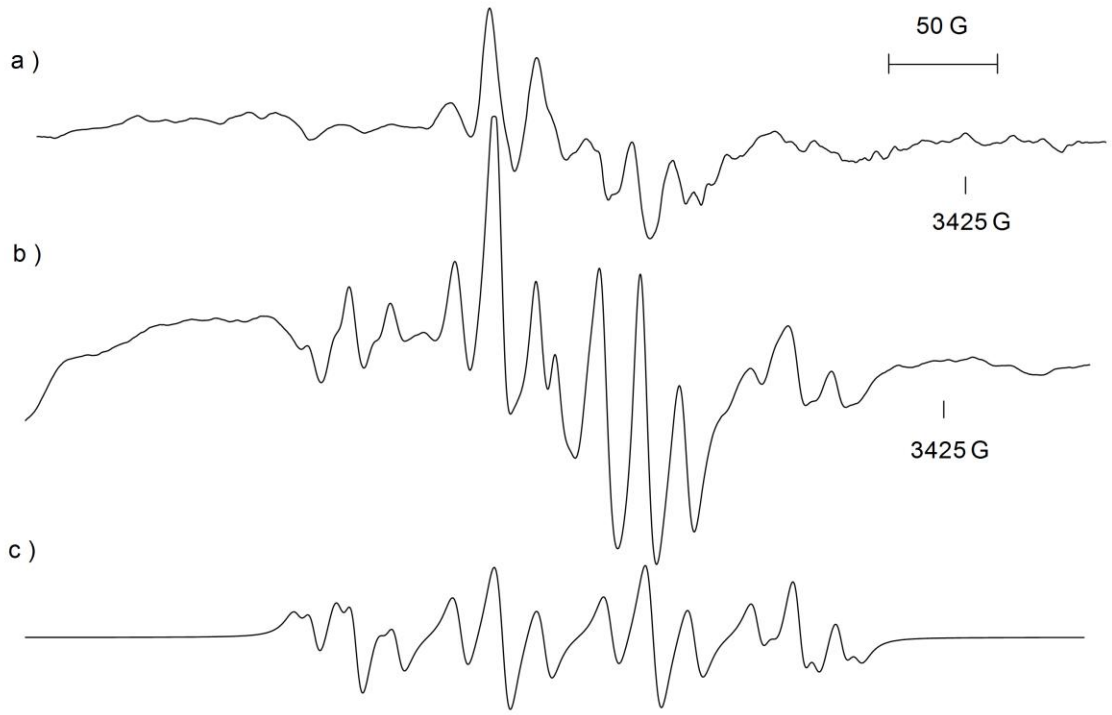

Figure 38. a) The EPR spectrum of the $^{63/65}$Cu atom-1,2-epoxybutane reaction mixture recorded between 3000 and 3500 G after 6 h of UV exposure (λ_{max} = 330 nm). a) 77 K (ν = 9086 MHz, m.p. = 2 mW). b) 130 K (ν = 9120 MHz, m.p. = 2 mW). c) Spectral simulation of B-UV at 130 K constructed assuming two overlapping spectra with a_{63Cu} = 191.6 MHz, a_{65Cu} = 205.1 MHz, a_H (2) = 54.1 MHz, g = 2.0009 (LW = 20 MHz).

As the sample was annealed to 130 K in the cavity of the spectrometer the central feature resolved to give a quartet of triplets, B-UV, presumably from the interaction of the unpaired electron with one Cu and two equivalent hydrogen nuclei, Figure 38b. A spectral simulation, Figure 38c, was constructed assuming that a ^{63}Cu-containing radical as well as its ^{65}Cu isotopomer contributes in the ratio of 1:0.45 to the EPR spectrum observed between 3000 to 3500 G. The magnetic parameters used to simulate the spectrum are a_{63Cu} = 191.6 MHz, a_{65Cu} 205.1 MHz, a_H(2) = 54.1 MHz and g = 2.0009.

Further changes in the central region of the EPR spectrum occurred in annealing the sample from 130 to 220 K, Figure 39. At 180 K, an intense quartet with line spacings of 101.7 MHz and g = 2.0293 developed while at 220 K the quartet spacing increased to 129.1 MHz.

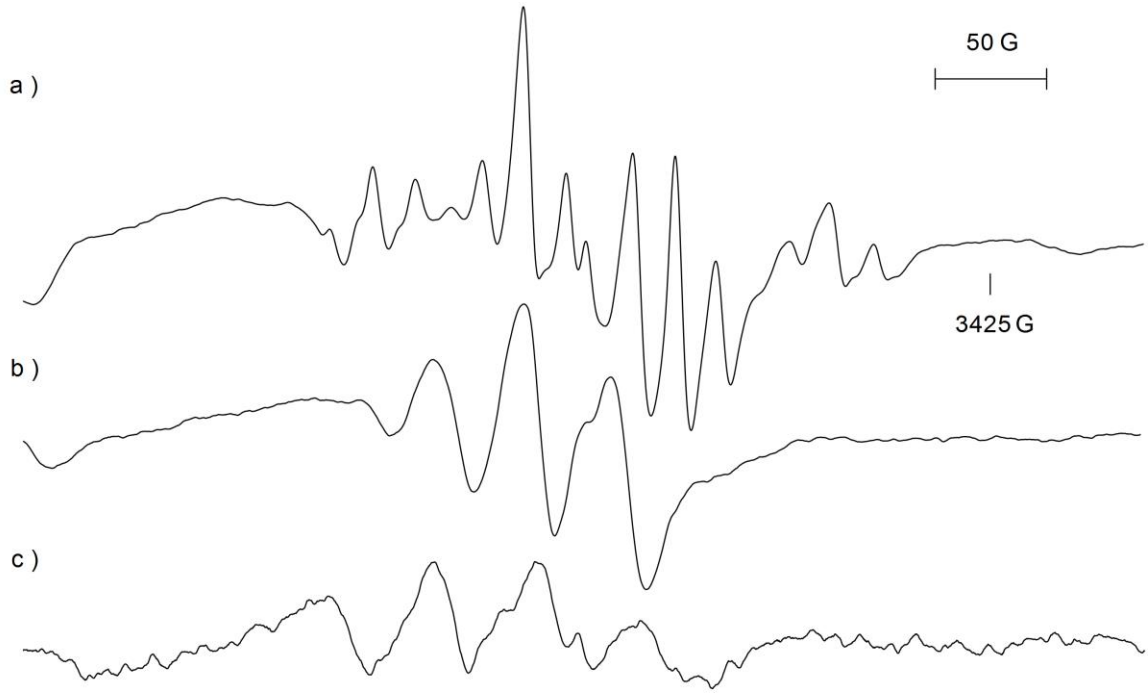

Figure 39. The effect of temperature on the EPR transition lines of B-UV formed in the reaction of $^{63/65}$Cu atoms and 1,2-epoxybutane a) 140 K, b) 180 K and c) 220 K. All spectra recorded with ν = 9119 MHz and m.p. = 2 mW.

4.1.1.5. Styrene oxide

The reaction of $^{63/65}$Cu atoms (I = 3/2) with styrene oxide in an adamantane matrix at 77 K yielded an orange-brown deposit. A sample of the deposit was collected in a quartz tube for analysis by EPR spectroscopy. At 77 K, Figure 40, lines at 1230 G, 5602 G and 5727 G are the ^{63}Cu NMR and $^{63/65}$Cu EPR transition lines of trapped $^{63/65}$Cu atoms. However, the spectrum is dominated by the central feature, C.

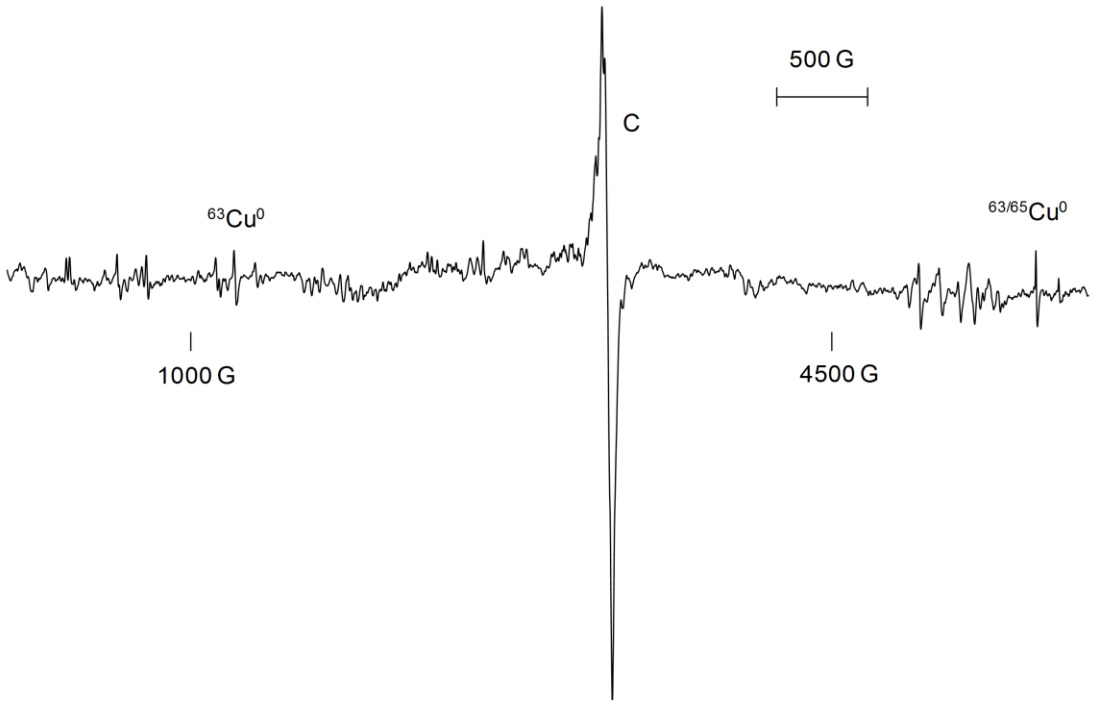

Figure 40. EPR spectrum recorded at 77 K (ν = 9137 MHz, m.p = 2 mW) of the paramagnetic products formed in the reaction of $^{63/65}$Cu atoms with styrene oxide in an adamantane matrix.

As the sample was annealed in the cavity of the spectrometer, the spectral resolution improved, Figure 41a, and four quartets, ^{63}Cu-SO-1, ^{65}Cu-SO-1, ^{63}Cu-SO-2 and ^{65}Cu-SO-2 were observed. The magnetic field positions used to determine the a_{Cu} and g values of the Cu-containing radicals are presented in Table 8. A spectral simulation was constructed using these parameters with EPR-NMR, Figure 41b. The hyperfine interaction values of ^{63}Cu-SO-1 and ^{63}Cu-SO-2 differ by 180 MHz (4.8 %) while the ^{65}Cu-SO-1 and ^{65}Cu-SO-2 hyperfine interaction values differ by 202 MHz (5.0 %). Both Cu-centered radicals were no longer visible on the EPR at temperatures > 190 K.

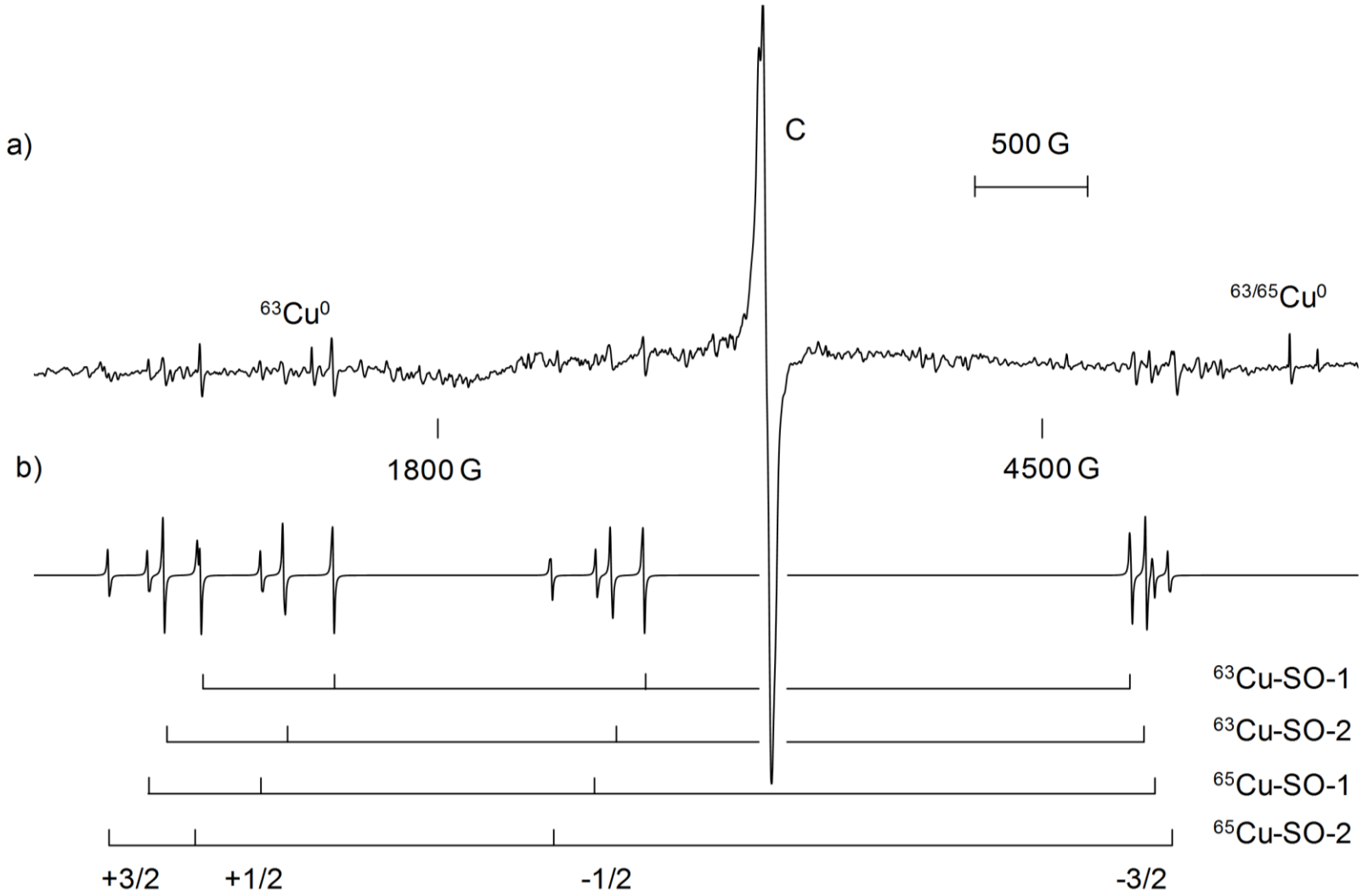

Figure 41. a) EPR spectrum recorded at 120 K (ν = 9116 MHz, m.p. = 2 mW), of the paramagnetic products, $^{63/65}$Cu-SO-1, $^{63/65}$Cu-SO-2 and C, formed in the reaction of $^{63/65}$Cu atoms with styrene oxide in an adamantane matrix. b) Simulated spectra of $^{63/65}$Cu-SO-1 and $^{63/65}$Cu-SO-2 using the parameters listed in Table 8.

Table 8. The magnetic parameters of $^{63/65}$Cu-SO-1 and $^{63/65}$Cu-SO-2, formed in the reaction of $^{63/65}$Cu atoms with styrene oxide in adamantane.

	a_{Cu} (MHz)	g	Temperature	ν (MHz)
^{63}Cu-SO-1	3740 ± 2.3	2.0099 ± 0.0006	77 K	9117
^{65}Cu-SO-1	4000 ± 0.6	2.0092 ± 0.0002		
^{63}Cu-SO-2	3920 ± 2.2	2.0011 ± 0.0006		
^{65}Cu-SO-2	4202 ± 2.7	2.0050 ± 0.0008		

The EPR spectrum of C, centered g = 2.0018, is well resolved at 160 K, Figure 42a. The signal C is thought to be a doublet of triplets arising from the interaction of the unpaired electron with a hydrogen nucleus where $a_H(1)$ = 68.9 MHz and two hydrogen nuclei where $a_H(2)$ = 56.0 MHz. The simulation constructed with these parameters and the FORTRAN program ISOPLOT is presented below the experimental spectrum for comparison, Figure 42b. The thermal stability of C is greater than that of $^{63/65}$Cu-SO-1 and $^{63/65}$Cu-SO-2 and persisted at temperatures greater than 220 K.

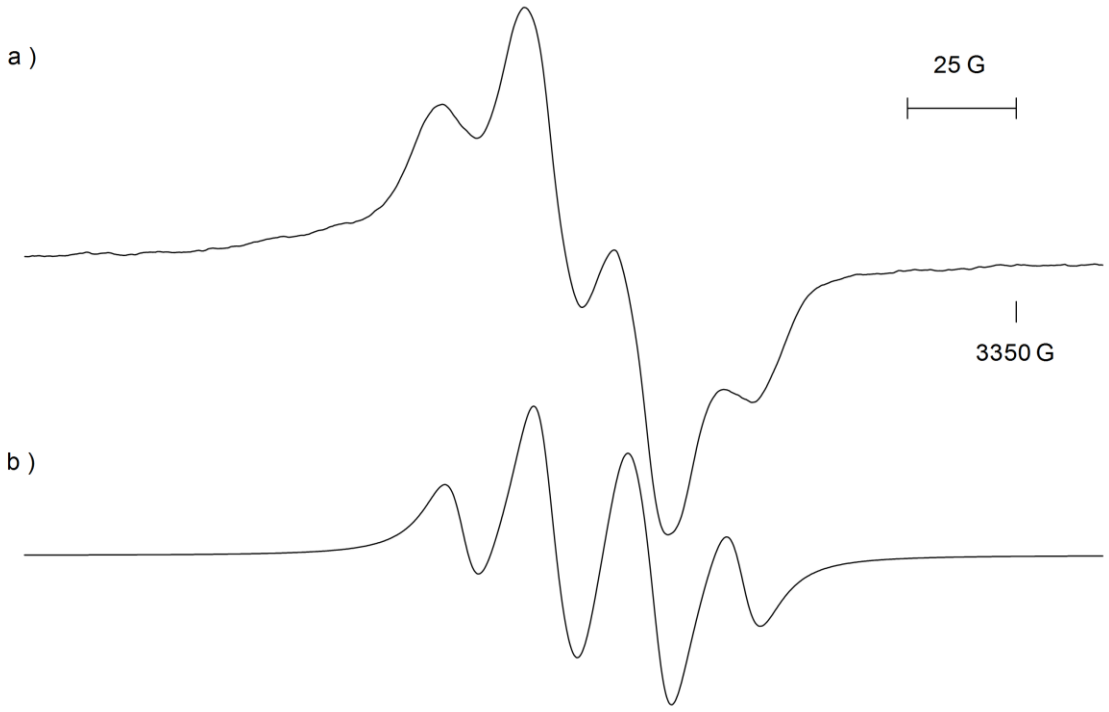

Figure 42. a) EPR spectrum of C at 160 K over a 250 G scan range (ν = 9118 MHz, m.p. = 2 mW). b) Simulation of the experimental EPR spectrum of C using the FORTRAN program ISOPLOT, assuming 1 H with a_H = 68.9 MHz and 2 H with a_H = 56.0 MHz.

4.1.2. Ethylene sulfide

The $^{63/65}$Cu atoms (I = 3/2) and ethylene sulfide were co-deposited in an adamantane matrix on a rotating cryostat at 77 K. The dark brown-black deposit was collected under vacuum at 77 K in a quartz, EPR tube. The sample tube was placed in the cavity of the EPR spectrometer at 77 K and a spectrum of the paramagnetic products was recorded, Figure 43a. The EPR spectrum reveals the successful deposition of Cu atoms, evident by the transitions at 1232 G and 5607 G, consistent with the NMR and EPR transitions of the ^{63}Cu atom, and the transition at 5728 G consistent with EPR transition of the ^{65}Cu atom.[36] In addition, two new sets of four lines, attributed to the transitions of a ^{63}Cu- and ^{65}Cu- centered radical, labelled ^{63}Cu-ES-1 and ^{65}Cu-ES-1, respectively, as well as an intense central feature were observed. The magnetic parameters, a_{Cu} and g-value, corresponding to ^{63}Cu-ES and ^{65}Cu-ES were obtained by entering the field position of the respective transition lines and the microwave frequency into the ESRLSQ computer program, Table 9. The ratio of the hyperfine interaction in ^{65}Cu-ES-1 and ^{63}Cu-ES-1, i.e., a_{65Cu}/a_{63Cu} is equal to 1.071, matching the ratio of the gyromagnetic ratios of ^{65}Cu and ^{63}Cu atoms. The spectral simulation shown in Figure 43b was generated using the EPR-NMR program, the magnetic parameters in Table 9, and assuming the natural abundance of ^{63}Cu and ^{65}Cu were 69.09 and 30.91 %, respectively.[24]

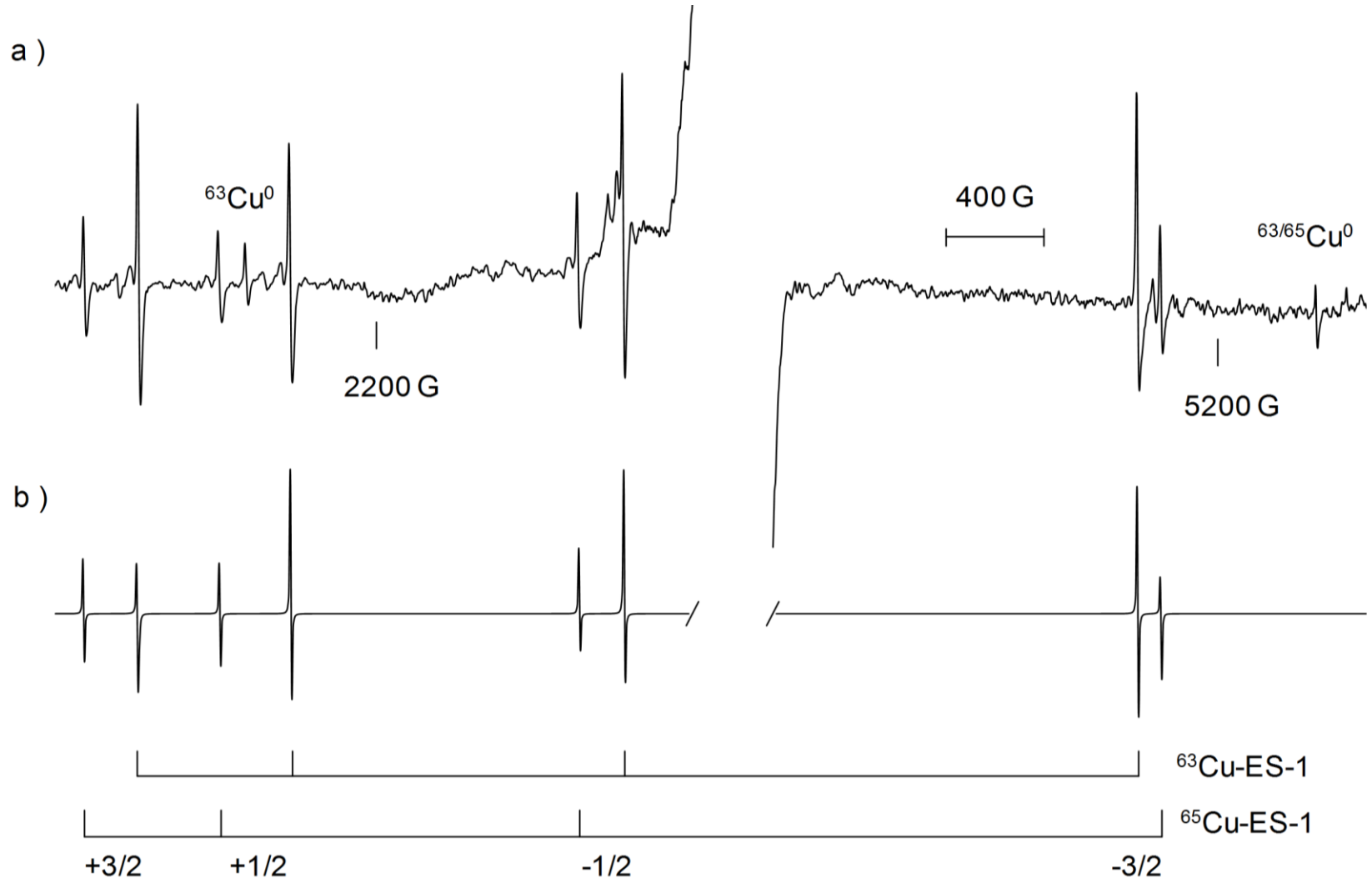

Figure 43. a) EPR Spectrum recorded at 77 K (ν = 9092 MHz, m.p. = 2 mW), of the paramagnetic products, ^{63}Cu-ES-1 and ^{63}Cu-ES-1, formed in the reaction of $^{63/65}$Cu atoms with ethylene sulfide in an adamantane matrix. b) Simulated spectra of $^{63/65}$Cu-ES-1 using the magnetic parameters listed in Table 9. The center of the spectrum is omitted.

Table 9. The magnetic parameters of $^{63/65}$Cu-ES-1 and $^{63/65}$Cu-ES-2, formed in the reaction of $^{63/65}$Cu atoms and ethylene sulfide in adamantane.

	a_{Cu} (MHz)	g	Temperature	ν (MHz)
^{63}Cu-ES-1	3625 ± 3.9	2.0082 ± 0.0011	77 K	9092
^{65}Cu-ES-1	3885 ± 4.2	2.0082 ± 0.0011		
^{63}Cu-ES-2	439 ± 0.9	1.9993 ± 0.0002	100 K	9120
^{65}Cu-ES-2	467 ± 0.5	2.0001 ± 0.0002		

Interestingly the transition lines for $^{63/65}$Cu-ES-1 were short lived not persisting at temperatures > 77 K. However, in annealing the sample to 100 K a second pair of quartets corresponding to paramagnetic Cu-containing species, labelled ^{63}Cu-ES-2 and ^{65}Cu-ES-2, was detected, Figure 44a. The program ESRLSQ was used to determine the magnetic parameters of $^{63/65}$Cu-ES-2 (Table 9) giving as input the magnetic field

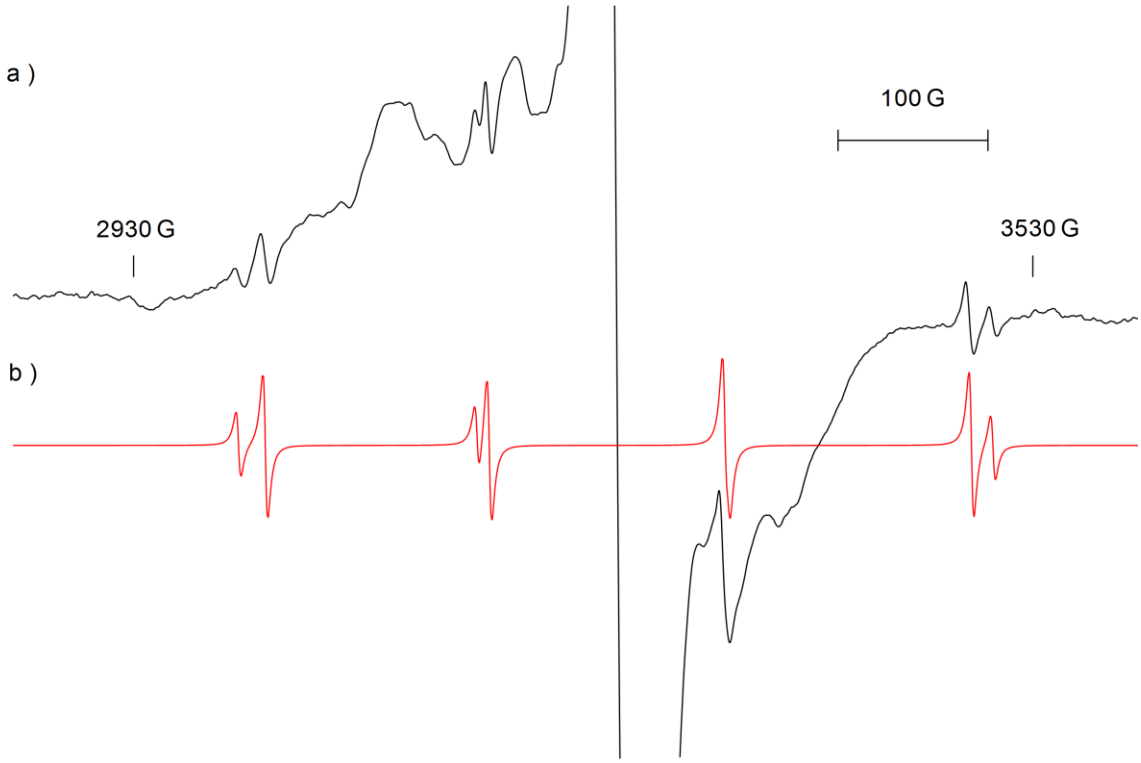

Figure 44. a) EPR spectrum recorded at 100 K (ν = 9120 MHz, m.p. = 2 mW) of ^{63}Cu-ES-2 and ^{65}Cu-ES-2 formed in the reaction of $^{63/65}$Cu atoms with ethylene sulfide. b) Simulated spectrum using the magnetic parameters listed in Table 9 and the EPR-NMR computer program.

positions along with the corresponding microwave frequency at which they were recorded. These parameters were used in conjunction with EPR-NMR to produce a simulated spectrum, Figure 44b. $^{63/65}$Cu-ES-2 was no longer present when the sample was warmed beyond 120 K.

The central region of the EPR spectrum, between 3050 and 3450 G consists of several transition lines centered at g ~ 2.0045, Figure 45a. One can see that the features change slightly when the sample is annealed between 77 K and 160 K, Figure 45b and c, with the central line remaining prominent until 210 K, when the signal is very weak, Figure 45d. Unfortunately, at this time no assignment can be made without additional information.

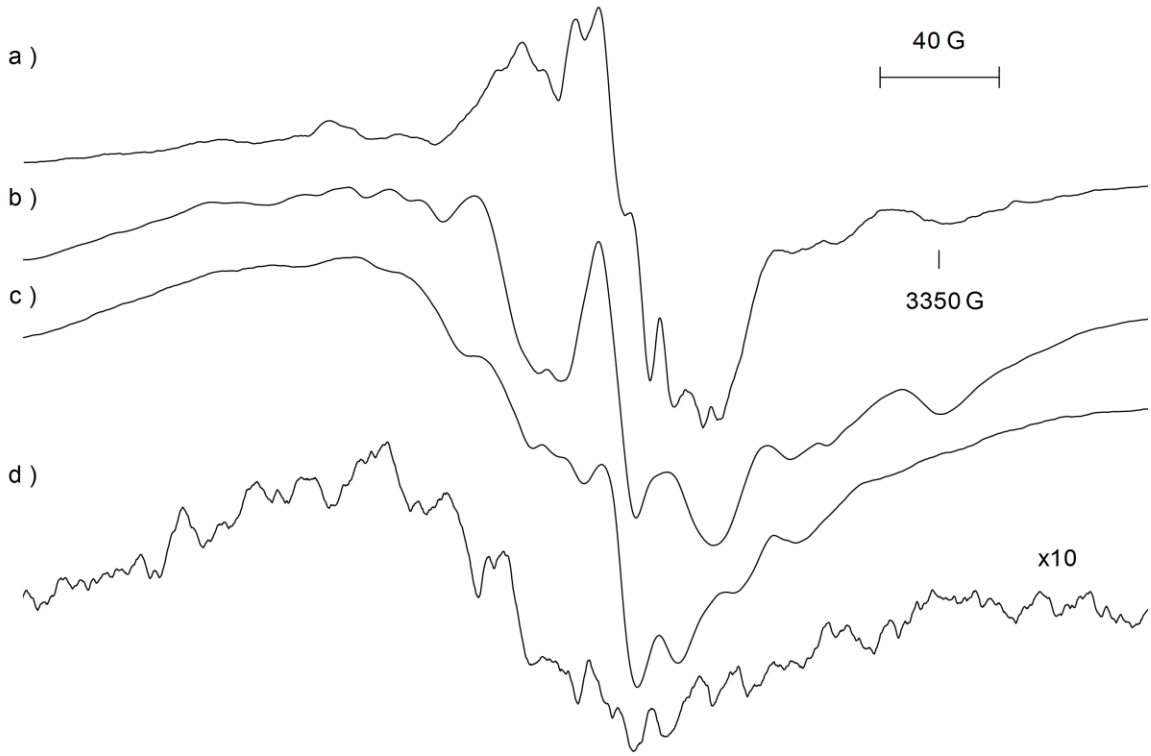

Figure 45. The effect of temperature on the central region of the EPR spectrum of the $^{63/65}$Cu atoms- ethylene sulfide reaction mixture a) 77 K, b) 120 K, c) 160 K and d) 210 K. All spectra recorded at ν = 9089 MHz with a m.p. of 2 mW.

4.1.3. Aziridine

4.1.3.1. Aziridine-^{14}N

The $^{63/65}$Cu atoms and aziridine were co-deposited in an adamantane matrix on a rotating cryostat at 77 K. A dark reddish-brown deposit formed on the drum during the reaction. The sample was collected in a quartz tube and placed in the cavity of the EPR spectrometer. Spectra were recorded from 77 to 240 K at 10 K intervals. The EPR spectrum recorded at 77 K has a number of multiline transitions, labelled ^{63}Cu-Az-1 and ^{65}Cu-Az-1, a central feature, D, centered at g = 2.0012 and transitions at 5584 G and 5708 G which correspond to the EPR transitions of ^{63}Cu and ^{65}Cu atoms, respectively Figure 46a. At 100 K, the multiline transitions of ^{63}Cu-Az-1 and ^{65}Cu-Az-1 resolve to triplets, Figure 46b, suggesting that the magnetic moment of the unpaired electron interacts with both a nitrogen nucleus (I = 1) and the ^{63}Cu or ^{65}Cu nuclei (I = 3/2). The a_{Cu}, a_{14N} and g values for ^{63}Cu-Az-1 and ^{65}Cu-Az-1, are found in Table 10. The ratio of the hyperfine interaction values for ^{65}Cu-Az-1 and ^{63}Cu-Az-1, i.e. a_{65Cu}/a_{63Cu} is equal to 1.071, matching the ratio of the gyromagnetic ratios of ^{65}Cu and ^{63}Cu atoms. The spectral simulation in Figure 46c was generated with the EPR-NMR program using the magnetic parameters in Table 10 taking into account the natural abundance of the Cu isotopes, i.e., ^{63}Cu = 69.09 % and ^{65}Cu = 30.91 %.

There is only a slight increase (0.17 – 0.25 %) in the a_{Cu} values as the temperature is increased from 77 – 100 K while the a_{14N} values remain unchanged. Upon expanding the region of the spectrum between 800 and 2200 G, a pair of very weak quartet of triplets become visible, ^{63}Cu-Az-2 and ^{65}Cu-Az-2, Figure 47a. The magnetic field

positions of $^{63/65}$Cu-Az-2 measured at microwave frequency of 9119 MHz were given as input to the ESRLSQ FORTRAN program yielding the parameters listed in Table 10. The second Cu-containing species is 1/10 the intensity of $^{63/65}$Cu-Az-1 and its a_{Cu} value is 3% less. The EPR-NMR simulation of the m_I = +3/2 and +1/2 transitions of $^{63/65}$Cu-Az-1 and $^{63/65}$Cu-Az-2 are shown in Figure 47b. Althought the m_I = -1/2 and -3/2 transitions of $^{63/65}$Cu-Az-2 were partially obscured by $^{63/65}$Cu-Az-1 transitions, however we were still able to obtain accurate values for the magnetic parameters.

Table 10. The magnetic parameters of $^{63/65}$Cu-Az-1, $^{63/65}$Cu-Az-2, $^{63/65}$Cu-Az^{15}N-1, and $^{63/65}$Cu-Az^{15}N-2, formed in the reactions of $^{63/65}$Cu atoms with aziridine or its isotopomer, aziridine-^{15}N in adamantane.

Aziridine	a_{Cu} (MHz)	a_{14N} (MHz)	g	Temp.	ν (MHz)
^{63}Cu-Az-1	3216 ± 0.7	70 ± 0.9	2.0097 ± 0.0002	77 K	9088
^{65}Cu-Az-1	3447 ± 1.7	70 ± 2.0	2.0076 ± 0.0005		
^{63}Cu-Az-1	3224 ± 0.5	69 ± 0.6	2.0094 ± 0.0001	100 K	9119
^{65}Cu-Az-1	3454 ± 0.5	70 ± 0.7	2.0087 ± 0.0001		
^{63}Cu-Az-2	3122 ± 0.9	65 ± 1.1	2.0083 ± 0.0002		
^{65}Cu-Az-2	3343 ± 2.4	66 ± 2.9	2.0099 ± 0.0007		
Aziridine-^{15}N	a_{Cu} (MHz)	a_{15N} (MHz)	g	Temp.	ν (MHz)
^{63}Cu-Az^{15}N-1	3210 ± 0.7	103 ± 1.5	2.0098 ± 0.0002	77 K	9089
^{65}Cu-Az^{15}N-1	3441 ± 1.2	103 ± 2.3	2.0090 ± 0.0003		
^{63}Cu-Az^{15}N-1	3221 ± 0.8	103 ± 1.5	2.0096 ± 0.0002	100 K	9121
^{65}Cu-Az^{15}N-1	3451 ± 0.7	103 ± 1.4	2.0098 ± 0.0002		
^{63}Cu-Az^{15}N-2	3122 ± 0.7	93 ± 1.5	2.0074 ± 0.0002		
^{65}Cu-Az^{15}N-2	3337 ± 0.4	95 ± 1.7	2.0096 ± 0.0001		
^{63}Cu-Az^{15}N-1	3209 ± 0.5	103 ± 1.0	2.0097± 0.0001	Recooled (77 K)	9087
^{65}Cu-Az^{15}N-1	3440 ± 0.8	103 ± 1.6	2.0091± 0.0002		

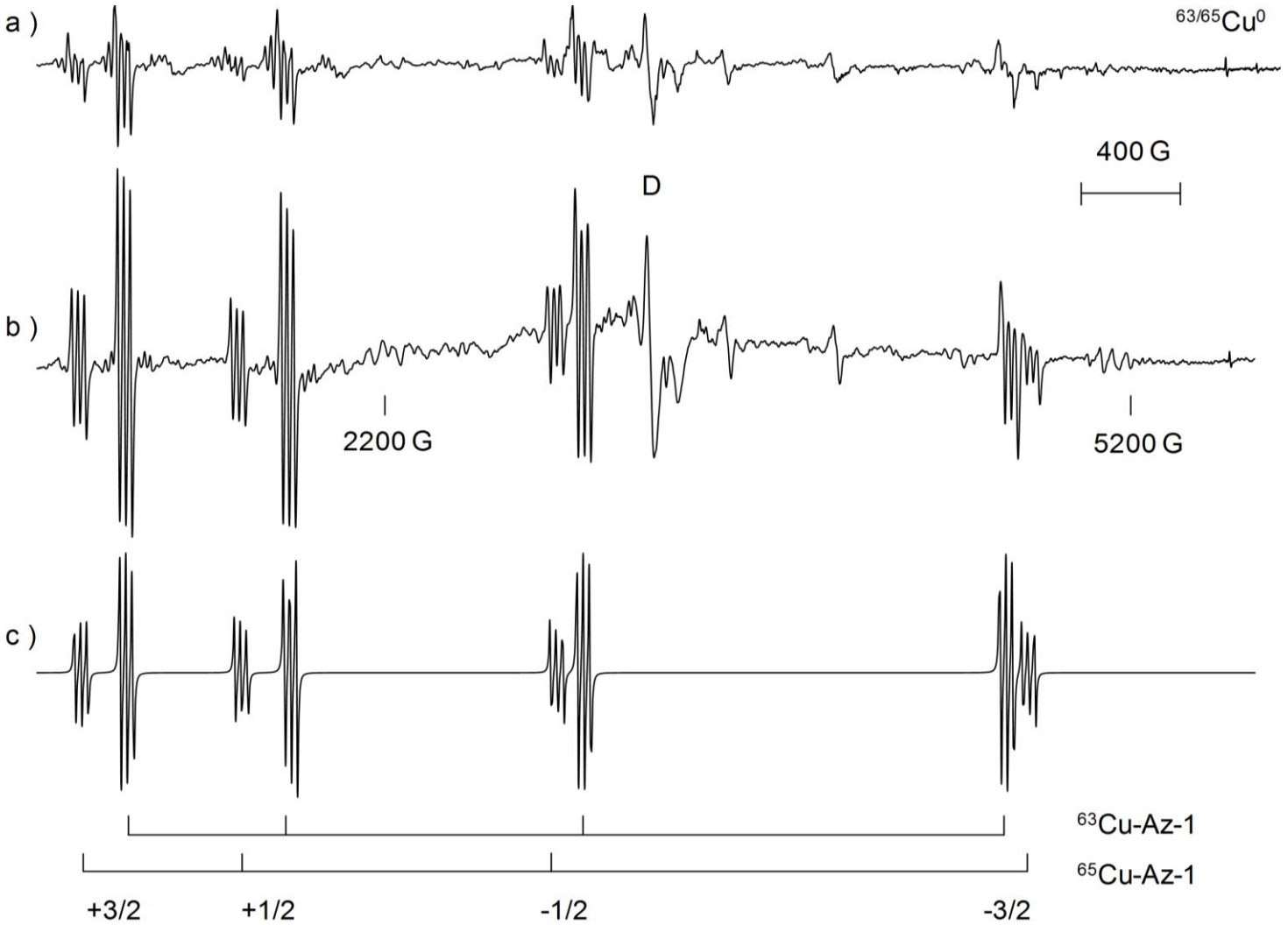

Figure 46. a) EPR Spectrum recorded at 77 K (ν = 9087 MHz, m.p. = 2 mW), of the paramagnetic products, $^{63/65}$Cu-Az-1 and D, formed in the reaction of $^{63/65}$Cu atoms with aziridine in an adamantane matrix. b) Annealed to 100 K (ν = 9118 MHz, m.p. = 2 mW). c) Simulated spectra of $^{63/65}$Cu-Az-1 at 100 K using the magnetic parameters listed in Table 10.

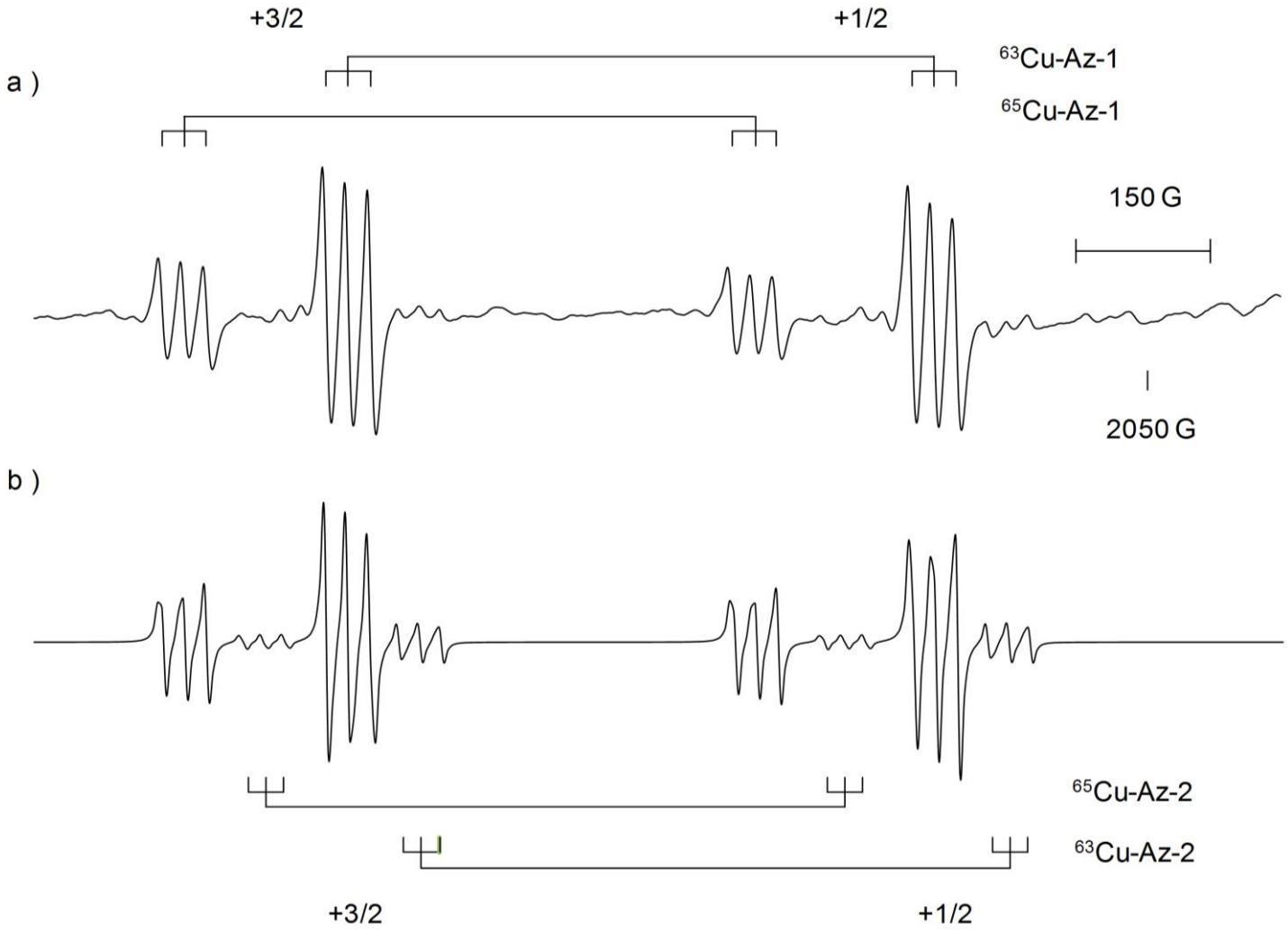

Figure 47. a) Experimental EPR spectrum of the m_I = +3/2 and +1/2 transitions of $^{63/65}$Cu-Az-1 and $^{63/65}$Cu-Az-2 recorded at 100 K (v = 9118 MHz, m.p. =2 mW). b) Simulated spectra of the m_I = +3/2 and +1/2 transitions of $^{63/65}$Cu-Az-1 and $^{63/65}$Cu-Az-2 using the magnetic parameters listed in Table 10.

As the temperature was increased beyond 100 K, the transition lines corresponding to ^{63}Cu-Az-1, ^{65}Cu-Az-1, ^{63}Cu-Az-2, and ^{65}Cu-Az-2 began to decay. Those belonging to $^{63/65}$Cu-Az-2 were no longer distinguishable from the background at 200 K, while those of $^{63/65}$Cu-Az-1 persisted to temperatures > 240 K.

The weak central feature, D, resolved at 120-160 K to give a quartet with a spacing of 24.4 MHz centered at g = 2.0023, Figure 48. The quality of the spectrum did not improve at temperatures > 160 K.

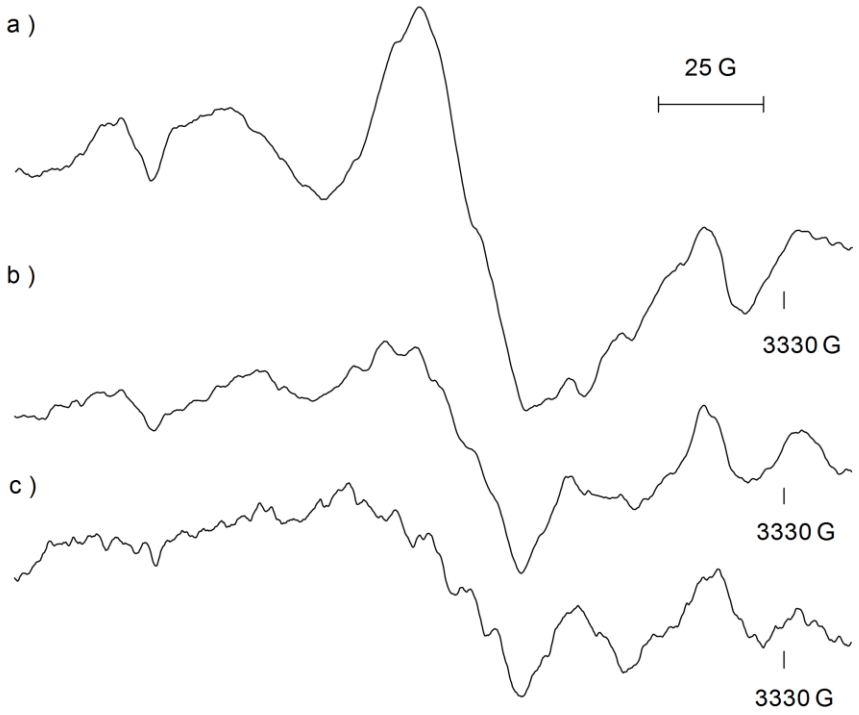

Figure 48. The effect of temperature on the EPR transition lines of D formed in the reaction of $^{63/65}$Cu atoms with aziridine recorded over 200 G at a) 100 K (ν = 9119 MHz, m.p. = 10 mW), b) 120 K (ν = 9119 MHz, m.p. = 10 mW) and c) 160 K (ν = 9120 MHz, m.p. = 20 mW).

4.1.3.2. Aziridine-^{15}N

The $^{63/65}$Cu atom reaction was repeated with aziridine-^{15}N. Once again evidence for the deposition of Cu atoms comes from the weak EPR transitions, $\Delta m_s = \pm 1$, m_I = -3/2 of ^{63}Cu and ^{65}Cu atoms at 5592 and 5717 G, respectively, Figure 49a. In addition, two quartets, ^{63}Cu-Az^{15}N-1 and ^{65}Cu-Az^{15}N-1, with a_{63Cu} and a_{65Cu} values similar to those of ^{63}Cu-Az-1 and ^{65}Cu-Az-1 were observed. The transition lines of $^{63/65}$Cu-Az^{15}N-1 are further split into doublets, expected from the interaction of the ^{15}N nuclei (I = 1/2) with the magnetic moment of the unpaired electron. The a_{Cu}, a_{15N}, and g values with their corresponding error limits, Table 10, were calculated using the ESRLSQ computer program and the field positions of the transition lines.

Raising the temperature of the sample to 240 K by 10 K intervals, in the cavity of the spectrometer, resulted in improved spectral resolution. For example, at 100 K, weak signals, most probably due to radicals in different adamantane trapping sites, have decayed and the transition lines for $^{63/65}$Cu-Az^{15}N-1 are nearly isotropic, Figure 49b. There is a slight increase (0.3 %) in the Cu hyperfine interaction value for both the ^{63}Cu-Az^{15}N-1 and ^{65}Cu-Az^{15}N-1 species. The magnetic parameters determined at 100 K, Table 10, were used to simulate the EPR spectrum taking into account the relative ratio of the natural abundancies of the ^{63}Cu and ^{65}Cu isotopes, i.e., ^{63}Cu = 69.09 % and ^{65}Cu = 30.91 %, Figure 49c. At low field, Figure 50a, transition lines corresponding to additional Cu-containing species, ^{63}Cu-Az^{15}N-2 and ^{65}Cu-Az^{15}N-2, were detected at 100 K. The relative intensity of the $^{63/65}$Cu-Az^{15}N-1 to $^{63/65}$Cu-Az^{15}N-2 transition lines is 6:1. The a_{Cu} values of $^{63/65}$Cu-Az^{15}N-2 are ~3 % smaller than those of the corresponding

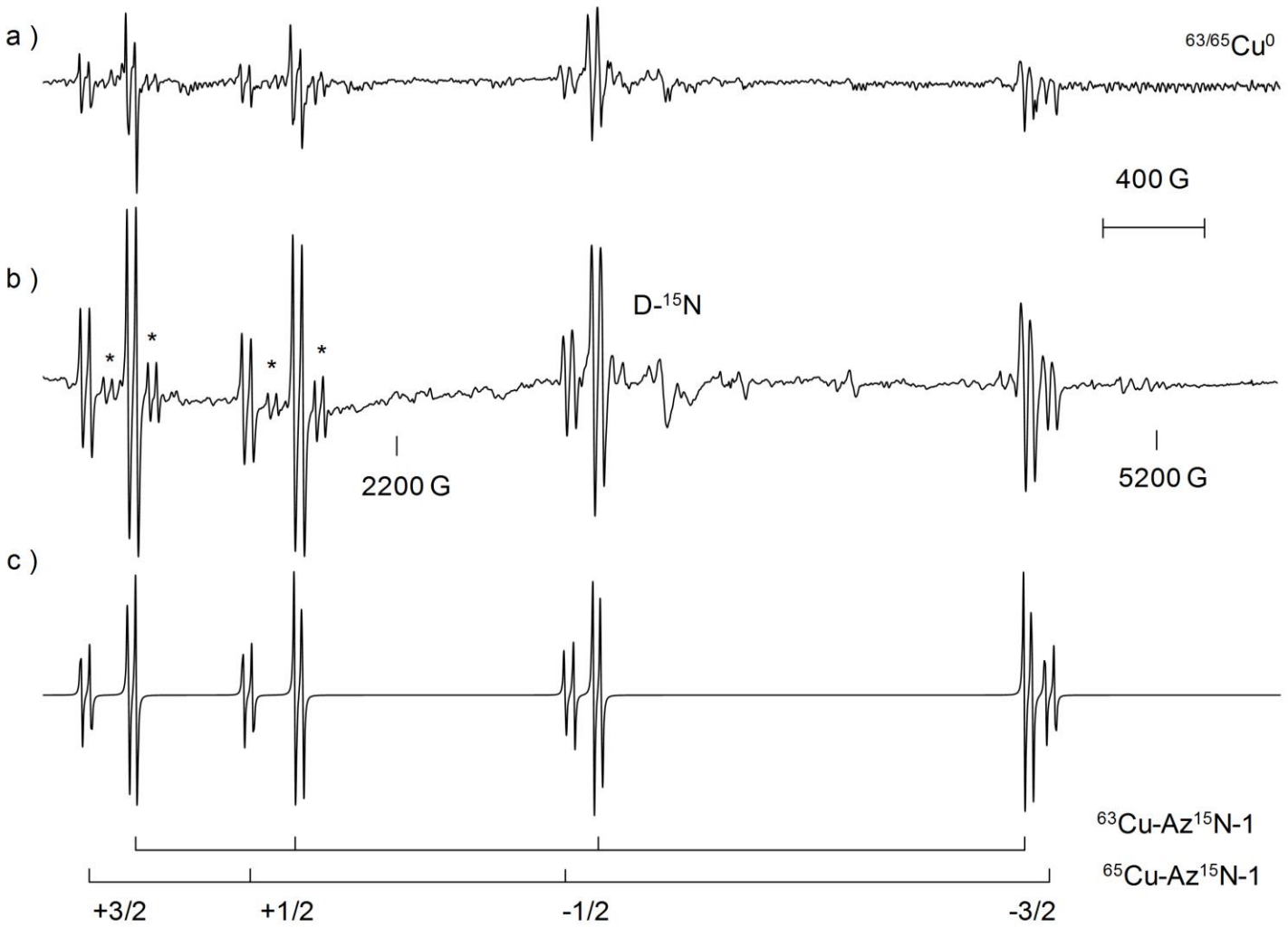

Figure 49. a) EPR Spectrum recorded at 77 K (ν = 9088 MHz, m.p. = 2 mW), of the paramagnetic products, $^{63/65}$Cu-Az^{15}N-1 and D-^{15}N, formed in the reaction of $^{63/65}$Cu atoms with aziridine-^{15}N in an adamantane matrix. b) Annealed to 100 K (ν = 9121 MHz, m.p. = 2 mW). c) Simulated spectra of $^{63/65}$Cu-Az^{15}N-1 at 100 K using the magnetic parameters listed in Table 10. *Transition lines corresponding to $^{63/65}$Cu-Az^{15}N-2.

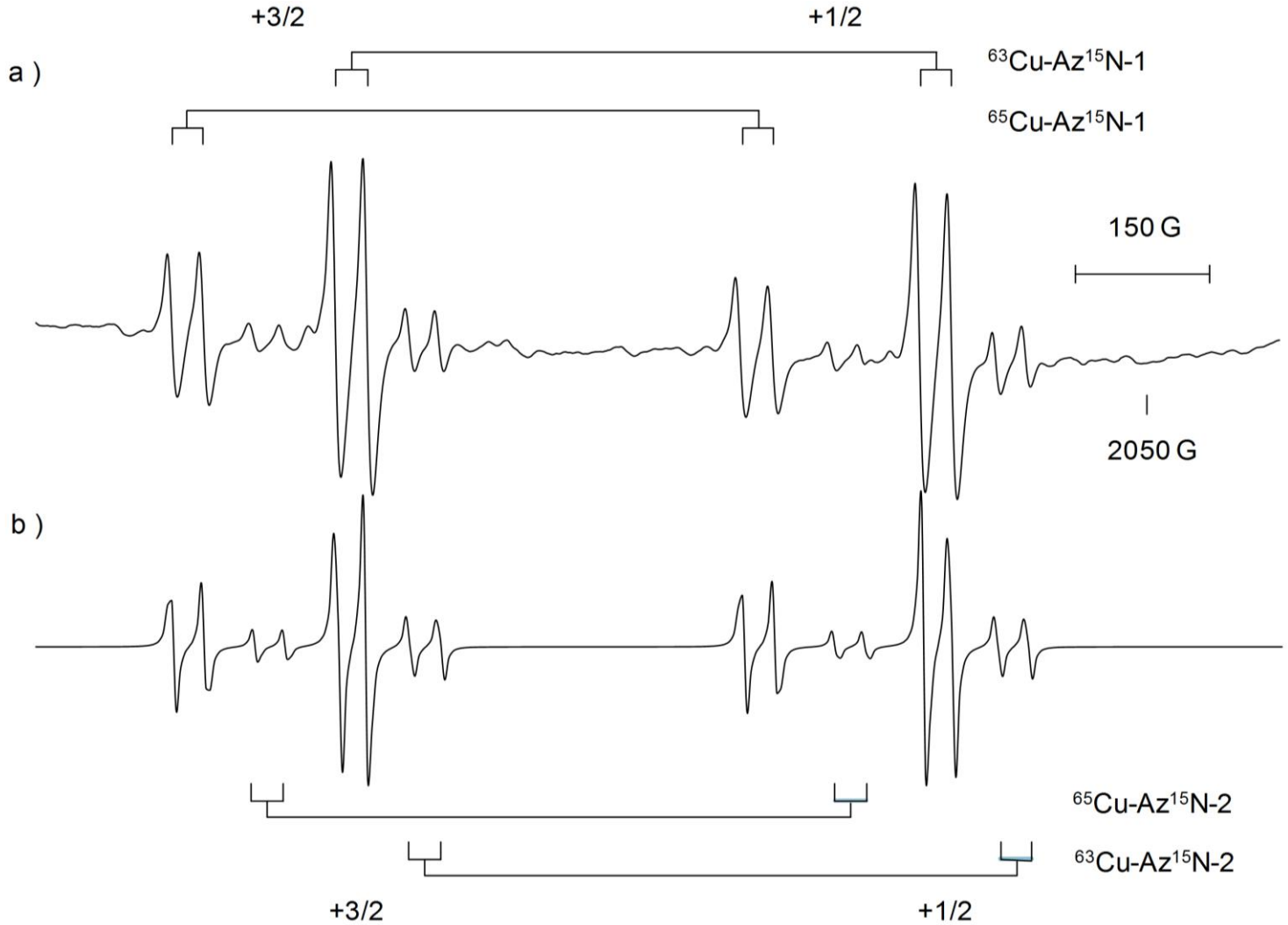

Figure 50. a) Experimental EPR spectrum of the m_I = +3/2 and +1/2 transitions of $^{63/65}$Cu-Az^{15}N-1 and $^{63/65}$Cu-Az^{15}N-2 recorded at 100 K (v = 9121 MHz, m.p. =2 mW). b) Simulated spectra of the m_I = +3/2 and +1/2 transitions of $^{63/65}$Cu-Az^{15}N-1 and $^{63/65}$Cu-Az^{15}N-2 using the magnetic parameters listed in Table 10.

$^{63/65}$Cu-Az^{15}N-1 species while the a_{15N} values differ by 7 to 10 %. Figure 50b shows the simulation of the m_I = +3/2 and +1/2 transition lines of all four Cu-centered radicals present at 100 K generated using the values of a_{Cu}, a_{15N}, and g values reported in Table 10.

The transition lines corresponding to ^{63}Cu-Az^{15}N-1, ^{65}Cu-Az^{15}N-1, ^{63}Cu-Az^{15}N-2, and ^{65}Cu-Az^{15}N-2 began to decay with increasing temperature. The transition lines of $^{63/65}$Cu-Az^{15}N-2 were not visible beyond 180 K. The sample annealed to 200 K was recooled to 77 K. Only the ^{63}Cu-Az^{15}N-1 and ^{65}Cu-Az^{15}N-1 species were visible in the EPR spectrum. The a_{Cu} values, Table 10, were recalculated and found to be the same as those initially determined at 77 K. The transition lines for $^{63/65}$Cu-Az^{15}N-1 persisted to temperatures > 240 K.

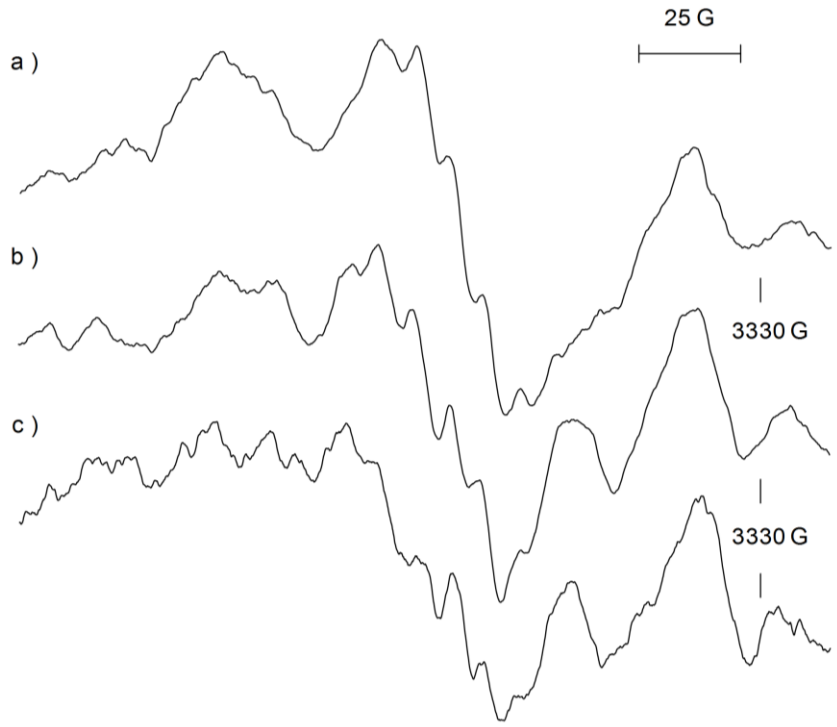

Figure 51. The effect of temperature on the EPR transition lines of D-^{15}N formed in the reaction of $^{63/65}$Cu atoms with aziridine-^{15}N recorded over 200 G at a) 100 K (ν = 9121 MHz, m.p. = 10 mW), b) 120 K (ν = 9120 MHz, m.p. = 10 mW) and c) 160 K (ν = 9121 MHz, m.p. = 20 mW).

4.2. Reaction of Silver Atoms with Three-Membered Heterocyclic Compounds

4.2.1. Oxiranes

4.2.1.1. Ethylene oxide

The reaction of $^{107/109}$Ag atoms (I = 1/2) with ethylene oxide in an adamantane matrix at 77 K, yielded a yellow-green deposit. The EPR spectrum of the resulting paramagnetic products, recorded at 77 K, Figure 52, consisted of (1) four doublets,^{107}Ag^0-1, ^{109}Ag^0-1, ^{107}Ag^0-2 and ^{109}Ag^0-2 assigned to trapped Ag atoms in two distinct sites,[36] (2) two doublets, ^{107}Ag-EO and ^{109}Ag-EO, and (3) an anisotropic feature, E, with $g_{\|}$ = 2.0264 and $g_{\perp}$ = 2.0088. The Ag hyperfine interaction and g values for^{107}Ag-EO, ^{109}Ag-EO, and the trapped atoms, Table 11, were determined using the calibrated magnetic field positions of their respective transition lines, Figure 53. The a_{Ag} values of ^{107}Ag-EO and ^{109}Ag-EO are 3.7 % smaller than the values found for ^{107}Ag^0-1 and ^{109}Ag^0-1, respectively. The ratio of a_{Ag} for ^{107}Ag-EO and ^{109}Ag-EO, i.e., $a_{109Ag}/_{107Ag}$ matches the ratio of the gyromagnetic ratio for ^{107}Ag and ^{109}Ag isotopes ($\gamma_{109Ag}/\gamma_{107Ag}$ = 1.150).

Table 11. The magnetic parameters of $^{107/109}$Ag^0-1, $^{107/109}$Ag^0-2, and $^{107/109}$Ag-EO, formed in the reaction of $^{107/109}$Ag atoms with ethylene oxide in adamantane.

	Site	a_{Ag} (MHz)	g	Temperature	ν (MHz)
^{107}Ag^0	1	1676	2.0018	77 K	9137
	2	1762	2.0016		
^{109}Ag^0	1	1940	2.0016		
	2	2049	2.0010		
^{107}Ag-EO		1619	2.0016		
^{109}Ag-EO		1650	2.0017		
^{107}Ag-EO		1867	2.0017	200 K	9118
^{109}Ag-EO		1907	2.0018		

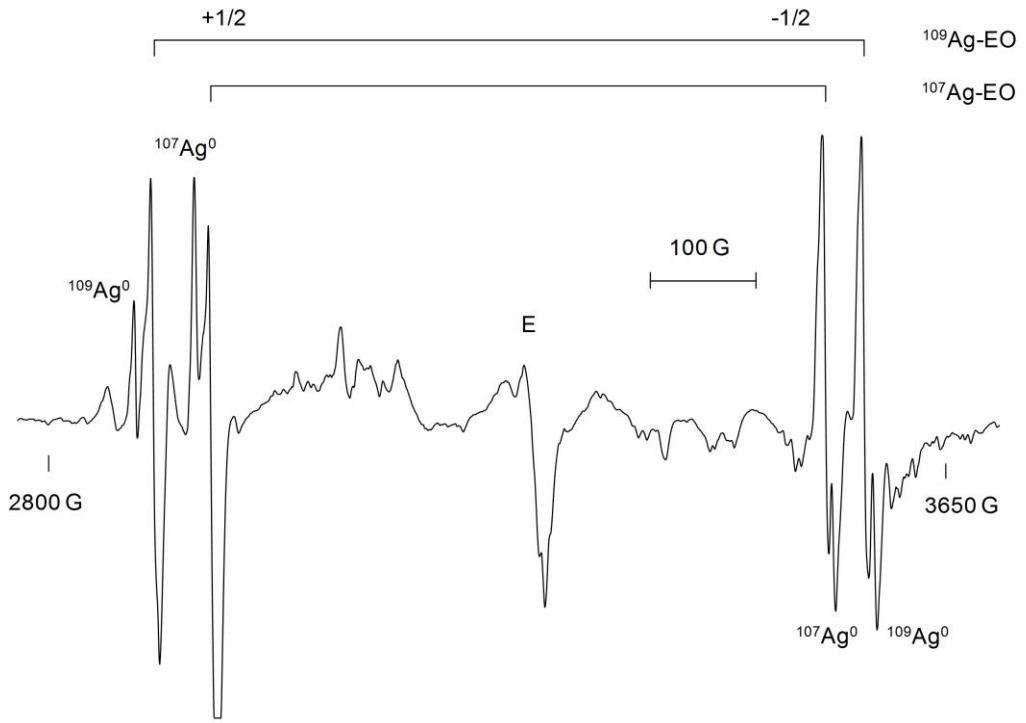

Figure 52. EPR spectrum recorded at 77 K (ν = 9139 MHz, m.p. = 2 mW), of the paramagnetic products, $^{107/109}Ag^0$-1, $^{107/109}Ag^0$-2, $^{107/109}$Ag-EO, and E, formed in the reaction of $^{107/109}$Ag atoms with ethylene oxide in an adamantane matrix.

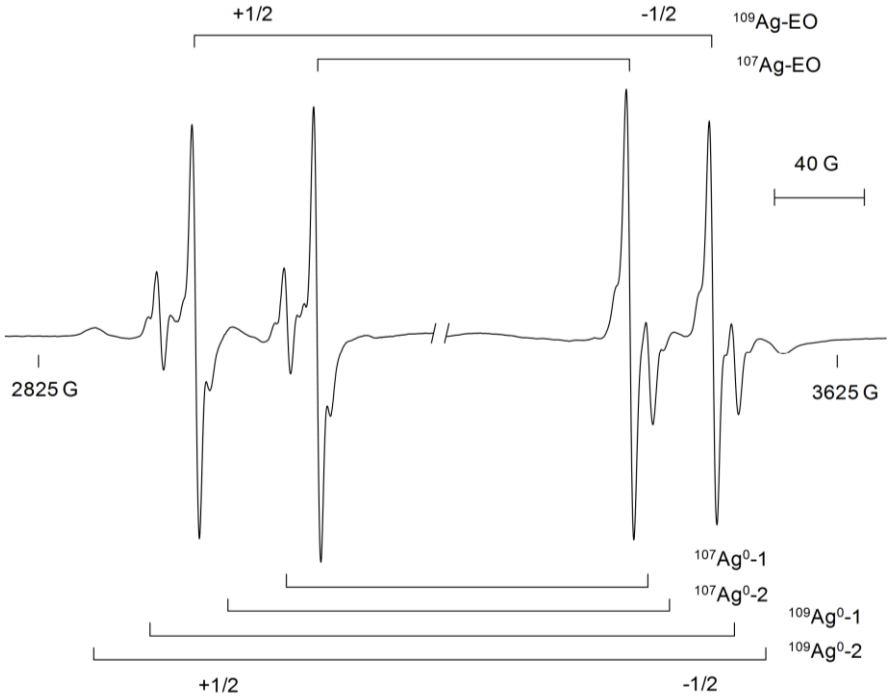

Figure 53. Calibrated EPR spectra of the m_I = +1/2 and -1/2 transition lines of $^{107/109}Ag^0$-1, $^{107/109}Ag^0$-2, and $^{107/109}$Ag-EO over a 200 G scan range at 77 K (ν = 9137 MHz, m.p.= 2mW).

The m_I = +1/2 and -1/2 transitions of $^{107/109}Ag^0$-1 and $^{107/109}$Ag-EO exhibit forbidden proton spin-flipping satellites of ~15 MHz from the central line giving the appearance of a triplet. This was confirmed by observing the effect of increasing microwave power from 0.1 to 20 mW on the $^{107/109}Ag^0$-1 and $^{107/109}$Ag-EO transition lines, Figure 54. Increasing the power between 0.1 to 5 mW caused the intensity of the transition lines and associated satellite peaks to increase. Power saturation > 5 mW caused the $^{107/109}Ag^0$-1 and $^{107/109}$Ag-EO transition line intensity to decrease and the satellite peaks to further increase.

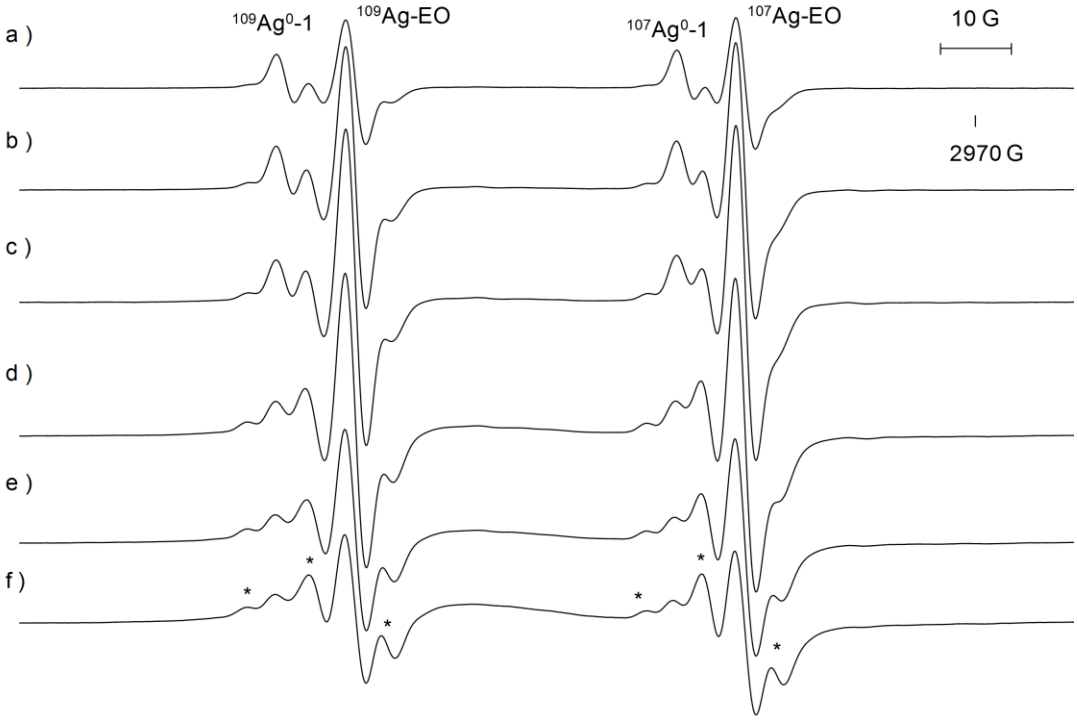

Figure 54. EPR power study on the m_I = +1/2 transition lines of $^{107/109}Ag^0$-1 and $^{107/109}$Ag-EO (v = 9115 MHz) with spectra recorded at a) 0.1 mW, b) 0.5 mW, c) 1 mW, d) 5 mW, e) 10 mW and f) 20 mW. *Proton spin-flips.

The a_{Ag} values associated with $^{107/109}$Ag-EO increase with temperature while the a_{Ag} values for trapped $^{107/109}Ag^0$ remain constant. Comparing the values determined at 200 K presented in Table 11 for $^{107/109}$Ag-EO to those recorded at 77 K, we can see that

the a_{Ag} value of ^{107}Ag-EO increased by 31.0 MHz (1.9 %) and that of ^{109}Ag-EO by 39.9 MHz (2.1 %). The transition lines of $^{107/109}$Ag-EO persisted to temperatures > 210 K.

The broad peak in the central region of the EPR spectrum does not change significantly with temperature, Figure 55. The anisotropic feature, E, began to decay as the temperature increased from 100 – 210 K, and is presumed to belong to microcrystalite particles of Ag.[36] When the sample was recooled to 117 K, $^{107/109}$Ag-EO was no longer visible in the spectrum but another intense feature emerged. This feature shown in Figure 56 is an anisotropic triplet, arising from two equivalent Ag nuclei. The $a_{||}$ = 594.5 MHz, $a_{\perp}$ = 587.5 MHz, $g_{||}$ = 2.0020 and $g_{\perp}$ = 2.0851 values are consistent with those reported by Howard et al[103] for Ag_5 with a distorted trigonal-bipyramidal structure, formed spontaneously upon recooling the annealed ^{107}Ag atom-adamantane reaction mixture.

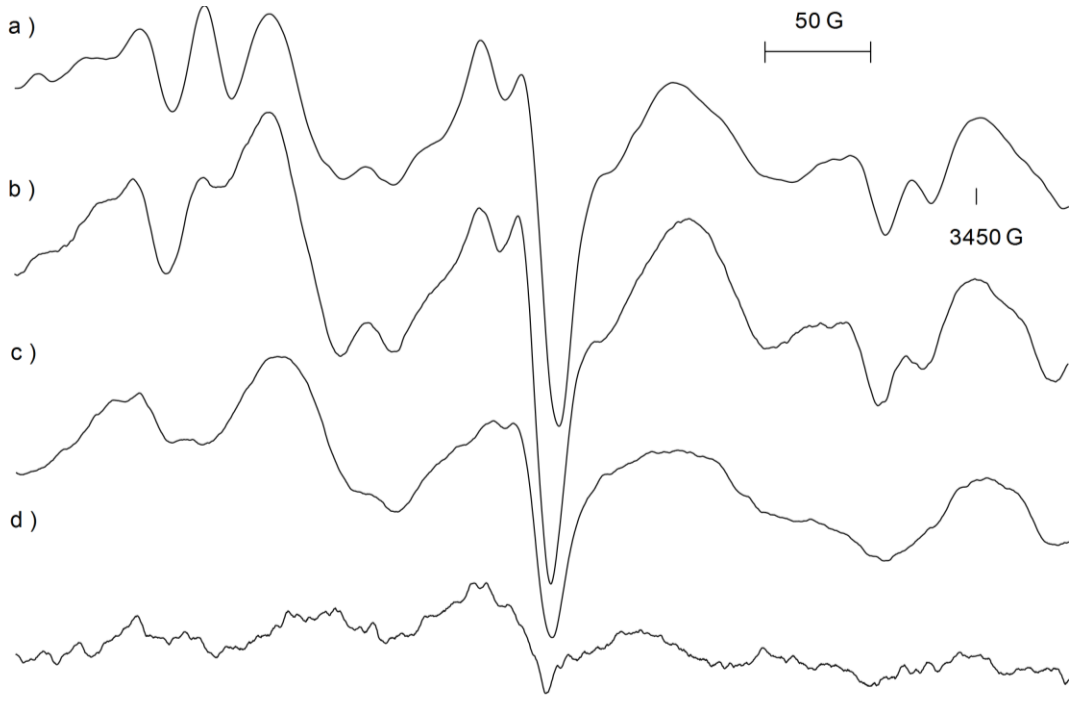

Figure 55. The effect of temperature on the central feature, E, formed in the reaction of $^{107/109}$Ag atoms with ethylene oxide recorded over 400 G at a) 100 K (ν = 9113 MHz), b) 140 K (ν = 9114 MHz), c) 180 K (ν = 9118 MHz) and d) 210 K (ν = 9118 MHz). All spectra recorded at m.p. = 2 mW.

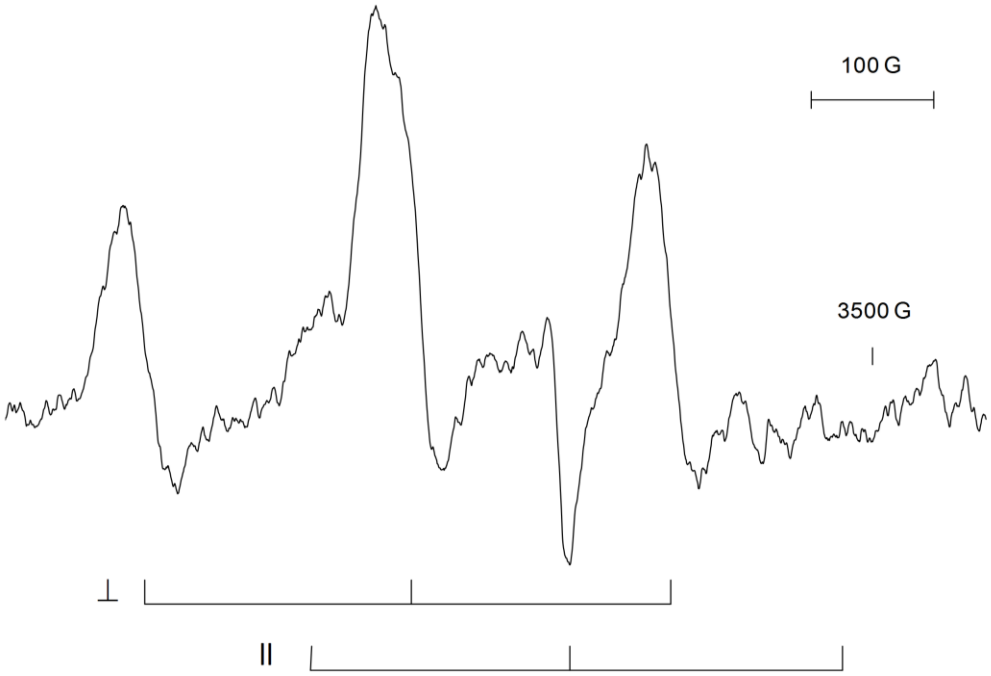

Figure 56. EPR spectrum of Ag_5 recorded at 117 K (ν = 9118 MHz, m.p = 2 mW) formed upon recooling the annealed sample collected from the reaction of $^{107/109}$Ag atoms and ethylene oxide.

4.2.1.2. Styrene oxide

The reaction of $^{107/109}$Ag atoms (I = 1/2) with styrene oxide in an adamantane matrix at 77 K resulted in a green deposit. The EPR spectrum of the reaction mixture, Figure 57, consisted of several overlapping doublets labelled $^{107}Ag^0$, $^{109}Ag^0$, ^{107}Ag-SO-1, ^{107}Ag-SO-2, ^{107}Ag-SO-3, ^{109}Ag-SO-1 and ^{109}Ag-SO-3, F, as well as a large isotropic central feature, G centered at at g = 2.0066. Upon closer examination, the transitions labelled $^{107}Ag^0$ and $^{109}Ag^0$ revealed 4 doublets assigned to trapped Ag atoms in two distinct sites.[36] In addition, the m_I = +1/2 and -1/2 transitions of the primary trapping site for $^{107/109}Ag^0$ atoms exhibit forbidden proton spin-flipping satellites ~ 13.6 MHz from the central line giving the appearance of a triplet. The field positions used to determine the a_{Ag} and g values of $^{107/109}Ag^0$, $^{107/109}$Ag-SO-1, ^{107}Ag-SO-2, $^{107/109}$Ag-SO-3 are presented in Table 12.

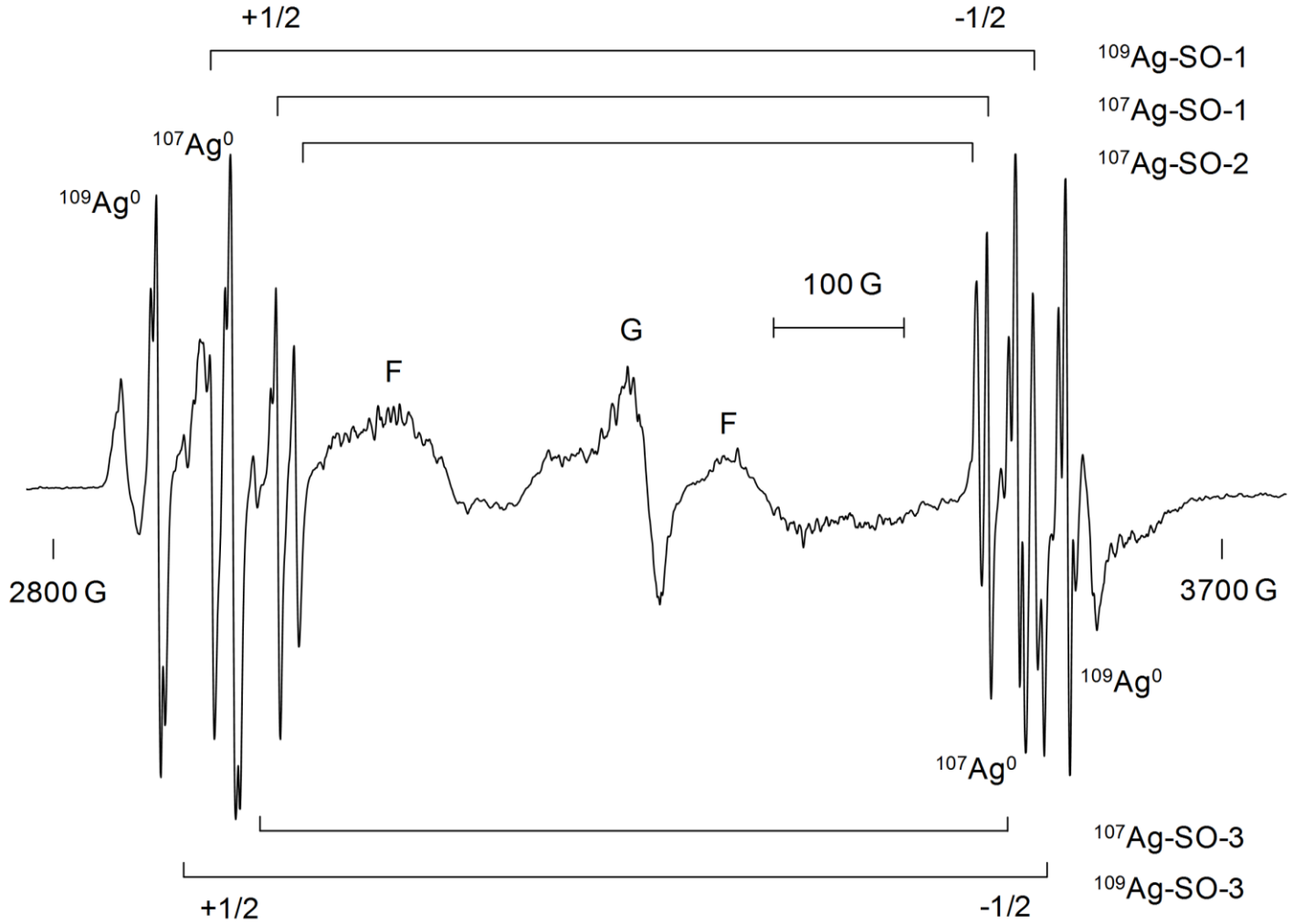

Figure 57. EPR spectrum recorded at 77 K (ν = 9138 MHz, m.p. = 2 mW), of the paramagnetic products, $^{107/109}Ag^0$, $^{107/109}Ag$-SO-1, ^{107}Ag-SO-2, $^{107/109}Ag$-SO-3, F, and G, formed in the reaction of $^{107/109}Ag$ atoms with styrene oxide in an adamantane matrix.

Table 12. The magnetic parameters of $^{107/109}Ag^0$, $^{107/109}Ag$-SO-1, $^{107/109}Ag$-SO-2 and $^{107/109}Ag$-SO-3, formed in the reaction of $^{107/109}Ag$ atoms with styrene oxide in adamantane.

	Site	a_{Ag} (MHz)	g	Temperature	ν (MHz)
$^{107}Ag^0$	1	1679	2.0019		
	2	1791	2.0006		
$^{109}Ag^0$	1	1939	2.0020		
	2	2053	2.0015		
^{107}Ag-SO-1		1524	2.0009	77 K	9139
^{107}Ag-SO-2		1462	2.0001		
^{107}Ag-SO-3		1601	2.0018		
^{109}Ag-SO-1		1757	2.0010		
^{109}Ag-SO-2		1681[a]	-		
^{109}Ag-SO-3		1849	2.0016		
^{107}Ag-SO-1		1550	2.0008		
^{107}Ag-SO-2		1485	2.0003		
^{107}Ag-SO-3		1619	2.0018	140 K	9120
^{109}Ag-SO-1		1783	2.0009		
^{109}Ag-SO-2		1713	1.9999		
^{109}Ag-SO-3		1869	2.0022		

[a]Value estimated using, $a_{107Ag\text{-}SO\text{-}2} \times \gamma_{109Ag}/\gamma_{107Ag} = 1462 \times 1.15 = 1681$.

The m_I = -1/2 transition of ^{109}Ag-SO-2 transition is masked by the m_I = -1/2 transition of $^{107}Ag^0$. Therefore, the hyperfine interaction at 77 K was estimated by multiplying the a_{107Ag} of ^{107}Ag-SO-2 by the ratio of gyromagnetic ratios of ^{109}Ag and ^{107}Ag, i.e., 1462 MHz x $\gamma_{109Ag}/\gamma_{107Ag}$ ~1681 MHz. It is interesting to note that based on the intensity of the transition lines, we find [$^{107/109}Ag^0$] > [$^{107/109}$Ag-SO-1] > [$^{107/109}$Ag-SO-2] >> [$^{107/109}$Ag-SO-3].

As the sample was annealed in the cavity of the spectrometer the transition lines corresponding to $^{107/109}$Ag-SO-1, $^{107/109}$Ag-SO-2, and $^{107/109}$Ag-SO-3 shifted while the lines of $^{107/109}Ag^0$ remained in the same position. As a result, at 140 K, the transitions of the ^{109}Ag-SO-2, masked at 77 K, are clearly visible since the peaks have shifted away

from the transition lines of $^{107}Ag^0$. The EPR parameters, determined at 140 K for ^{109}Ag-SO-2, are presented in Table 12 along with those of the other Ag species. Comparing the values recorded at 77 and 140 K, there is a 25 MHz, 23 MHz and 17 MHz increase in the a_{Ag} of ^{107}Ag-SO-1, ^{107}Ag-SO-2, and ^{107}Ag-SO-3, respectively. The a_{Ag} values continued to increase with increasing temperature until $^{107/109}$Ag-SO-1, $^{107/109}$Ag-SO-2, and $^{107/109}$Ag-SO-3 were no longer visible at temperatures > 210 K.

The features in the central region of the EPR spectrum, F and G, resolved as the temperature increased, Figure 58. At 120 K, F is considered to be anisotropic with $a_{\|}$ = 766 MHz, $a_{\perp}$ = 692 MHz, $g_{\|}$ = 1.9857, and $g_{\perp}$ = 2.0291. The calculated a_{iso} and g_{iso} are 716.6 and 2.0146, respectively. At 170 K, the m_I = +1/2 transition has resolved superhyperfine splitting; five lines equally spaced by 54.4 MHz. The signal G, centered at g = 2.0030, is thought to be a doublet of triplets arising from the interaction of the unpaired electron with a hydrogen nucleus where $a_H(1)$ = 68.9 MHz and two hydrogen nuclei where $a_H(2)$ = 56.0 MHz, Figure 59a. The simulation constructed with these parameters and the FORTRAN program ISOPLOT is presented below the experimental spectrum recorded at 160 K for comparison, Figure 59b. The signal G persists on the EPR at temperatures > 240 K.

Similar to the reaction of $^{107/109}$Ag and ethylene oxide, when the sample was recooled to 77 K, signals from Ag_5 clusters were visible in the EPR spectrum but no transitions from $^{107/109}$Ag-SO-1, $^{107/109}$Ag-SO-2 or $^{107/109}$Ag-SO-3 were present, Figure 60.

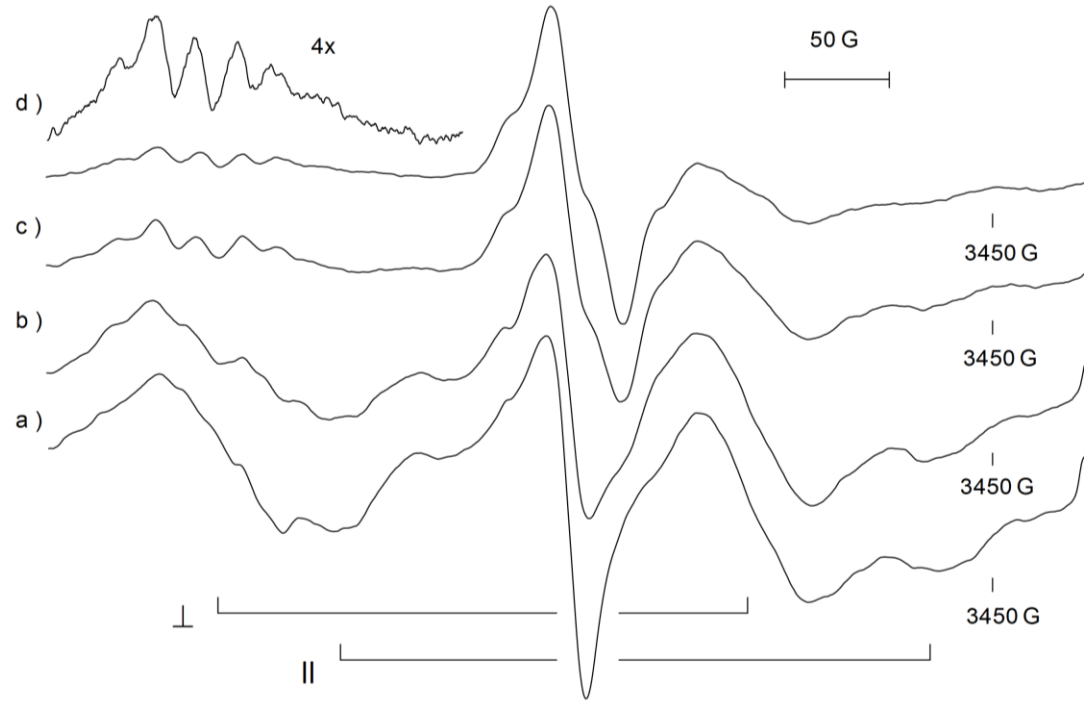

Figure 58. The effect of temperature on the central features, F and G, formed in the reaction of $^{107/109}$Ag atoms with styrene oxide recorded over 400 G a) 100 K (ν =9119 MHz), b) 120 K (ν = 9120 MHz), c) 150 K (ν = 9120 MHz) and d) 170 K (ν = 9119 MHz). All spectra recorded with m.p. = 2 mW.

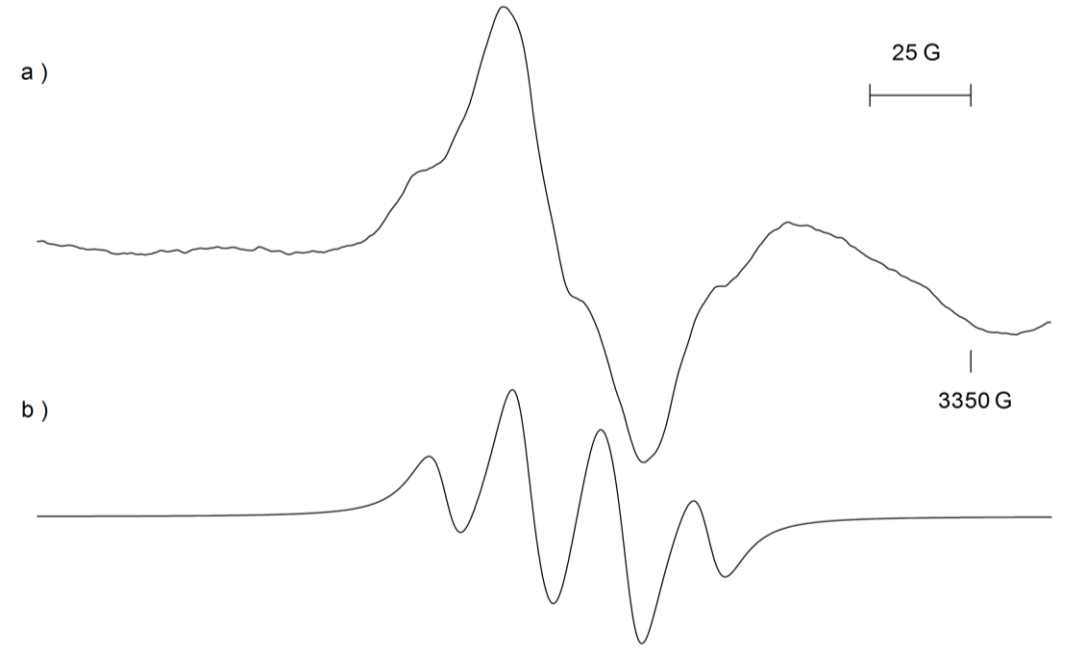

Figure 59. a) EPR spectrum of G at 160 K over a 250 G scan range (ν = 9119 MHz, m.p. = 2 mW). b) Simulation of the experimental EPR spectrum of G using the FORTRAN program ISOPLOT, assuming 1 H with $a_H(1)$ = 68.9 MHz and 2 H with $a_H(2)$ = 56.0 MHz.

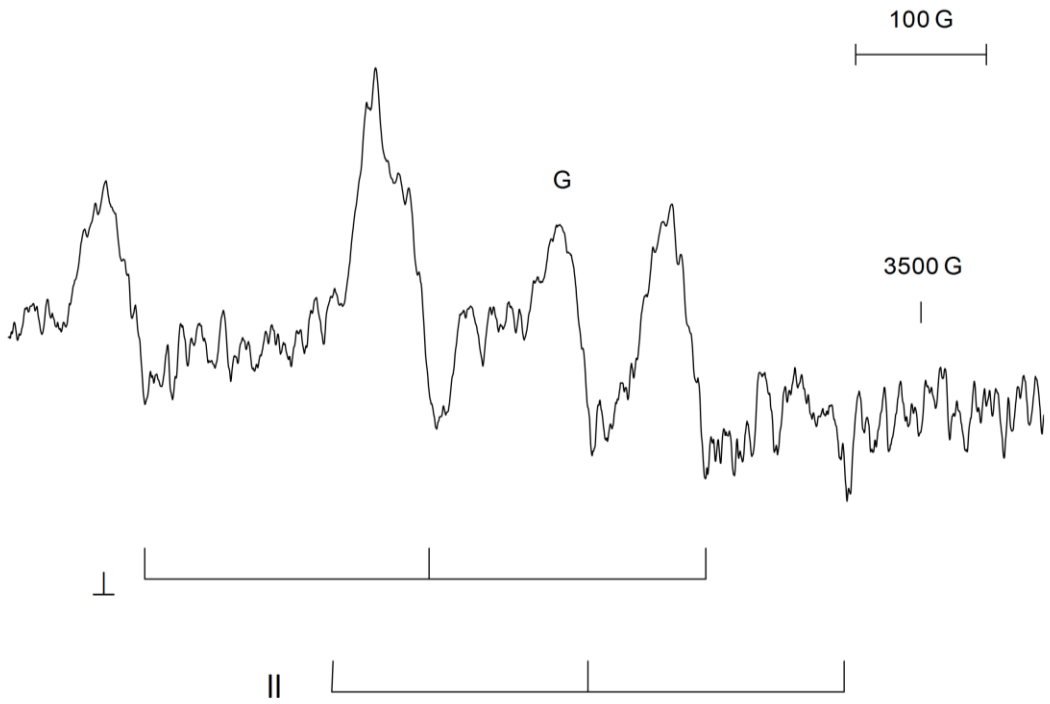

Figure 60. EPR spectrum of Ag_5, recorded at 77 K (ν = 9088 MHz, m.p. = 2 mW), formed upon recooling the annealed sample collected from the reaction of $^{107/109}$Ag atoms and styrene oxide.

4.2.2. Thiiranes

4.2.2.1. Ethylene sulfide

The $^{107/109}$Ag atoms were co-deposited with ethylene sulfide in an adamantane matrix at 77 K on a rotating cryostat. The redish brown deposit was collected in a quartz EPR sample tube. The EPR spectrum of the paramagnetic species, recorded at 77 K, Figure 61, consists of at least 4 doublets labelled $^{107}Ag^0$, $^{109}Ag^0$, ^{107}Ag-ES-1, ^{109}Ag-ES-1, and a strong central feature labelled H. The magnetic parameters, a_{Ag} and g-values for $^{107/109}Ag^0$ and $^{107/109}$Ag-ES-1, Table 13, were determined from the magnetic field positions of the transition lines extracted from calibrated EPR spectra. The magnetic parameters for $^{107/109}Ag^0$ are consistent with those reported for trapped Ag atoms in adamantane (a_{107Ag} = 1682 MHz and a_{109Ag} = 1938 MHz).[36]

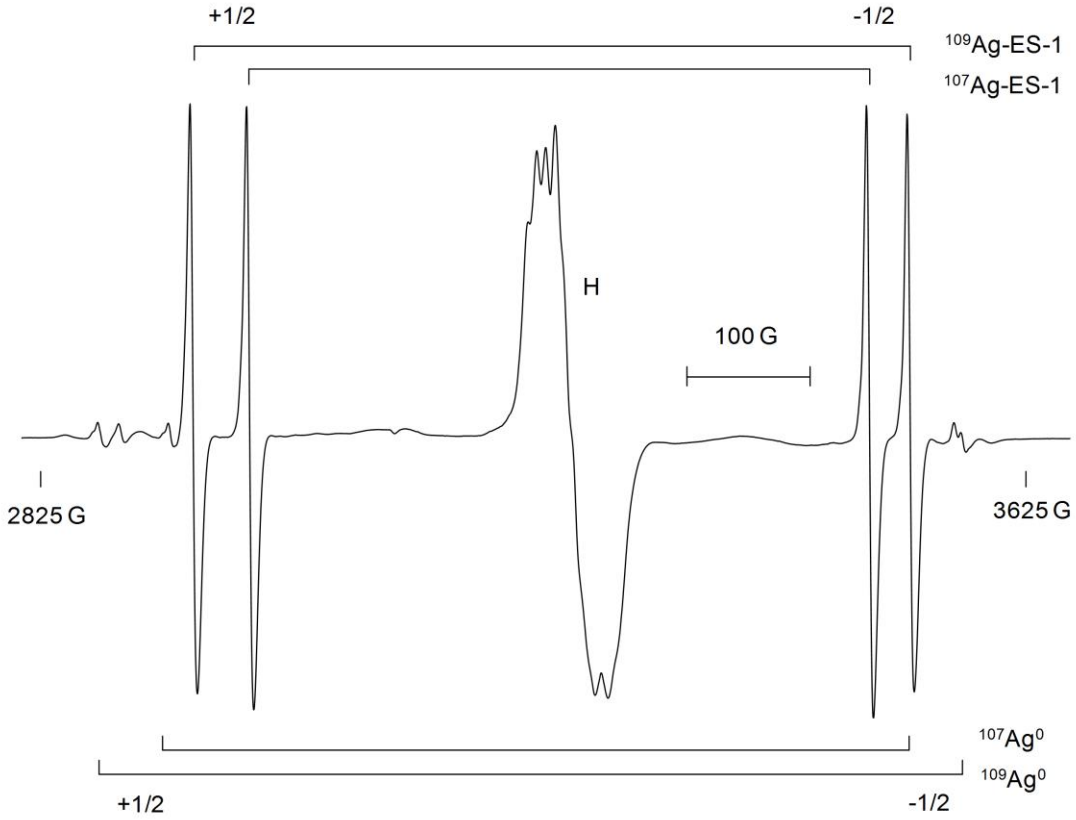

Figure 61. EPR spectrum recorded at 77 K (ν = 9111 MHz, m.p. = 2 mW) of the paramagnetic products, $^{107/109}Ag^0$, $^{107/109}$Ag-ES-1 and H, formed in the reaction of $^{107/109}$Ag atoms with ethylene sulfide in an adamantane matrix.

The $^{107/109}$Ag-ES-1 transition lines decayed quickly when the sample was annealed in the cavity of the spectrometer and were no longer visible at temperatures over 130 K, Figure 62. However, the disappearance of the intense transitions assigned to $^{107/109}$Ag-ES-1 revealed the m_I = +1/2 transition of a second $^{107/109}$Ag-containing species lablelled $^{107/109}$Ag-ES-2 and forbidden proton spin-flipping satellites of ~15 MHz from the central line of $^{107/109}Ag^0$, giving the appearance of a triplet, Figure 62c. Upon reexamining the 77 K spectrum, ^{109}Ag-ES-2 was detected indicating that the species was formed at the same time as $^{107/109}$Ag-ES-1 albeit in very small amounts. The ^{107}Ag-ES-2 transition was masked by that of ^{109}Ag-ES-1 at 77 K. The magnetic parameters for ^{107}Ag-ES-2 and ^{109}Ag-ES-2 were calculated with the aid of ESRLSQ using the magnetic field

positions of the transitions recorded at 140 K and spectrometer operating frequency, ν = 9122 MHz, Table 20. It is interesting to note, at this point, that the line positions of both ^{107}Ag-ES-2 and ^{109}Ag-ES-2 shift as the temperature of the sample is raised, giving slightly larger a_{Ag} values while a_{Ag} for the trapped atoms remains constant.

Table 13. The magnetic parameters of $^{107/109}$Ag^0, $^{107/109}$Ag-ES-1, $^{107/109}$Ag-ES-2, $^{107/109}$Ag-ES-3, $^{107/109}$Ag-ES-d$_4$-1, and $^{107/109}$Ag-ES-d$_4$-2, formed in the reactions of $^{107/109}$Ag atoms with ethylene sulfide or its isotopomer, ethylene sulfide-d$_4$ in adamantane.

Ethylene sulfide	a_{Ag} (MHz)	g	Temperature	ν (MHz)
^{107}Ag^0	1675	2.0016	140 K	9122
^{109}Ag^0	1937	2.0016		
^{107}Ag-ES-1	1401	1.9988	77 K	9111
^{107}Ag-ES-1	1618	1.9987		
^{107}Ag-ES-2	1634	2.0001	140 K	9122
^{107}Ag-ES-2	1884	1.9999		
^{107}Ag-ES-3	1376	1.9974	200 K	9122
^{107}Ag-ES-3	1585	1.9977		
Ethylene sulfide-d$_4$	a_{Ag} (MHz)	g	Temperature	ν (MHz)
^{107}Ag^0	1677	2.0014	140 K	9120
^{109}Ag^0	1936	2.0014		
^{107}Ag-ES-1	1400	1.9991	77 K	9086
^{107}Ag-ES-1	1616	1.9988		
^{107}Ag-ES-d$_4$-2	1374	1.9974	200 K	9119
^{107}Ag-ES-d$_4$-2	1587	1.9973		

Another pair of doublets appeared at 180 K, ^{107}Ag-ES-3 and ^{109}Ag-ES-3, which persisted to 210 K. The positions of the transition lines taken from the EPR spectrum recorded at 200 K, Figure 63, was used with the aid of the ESRLSQ program to generate the magnetic parameters, a_{Ag} and g, Table 13. The a_{Ag} values of $^{107/109}$Ag-ES-3 respect the ratio of gyromagnetic ratios for ^{107}Ag and ^{109}Ag nuclei, i.e. $a_{107\text{Ag-ES-3}}/a_{109\text{Ag-ES-3}}$ equals 1.15 and are 2% smaller than those of $^{107/109}$Ag-ES-1.

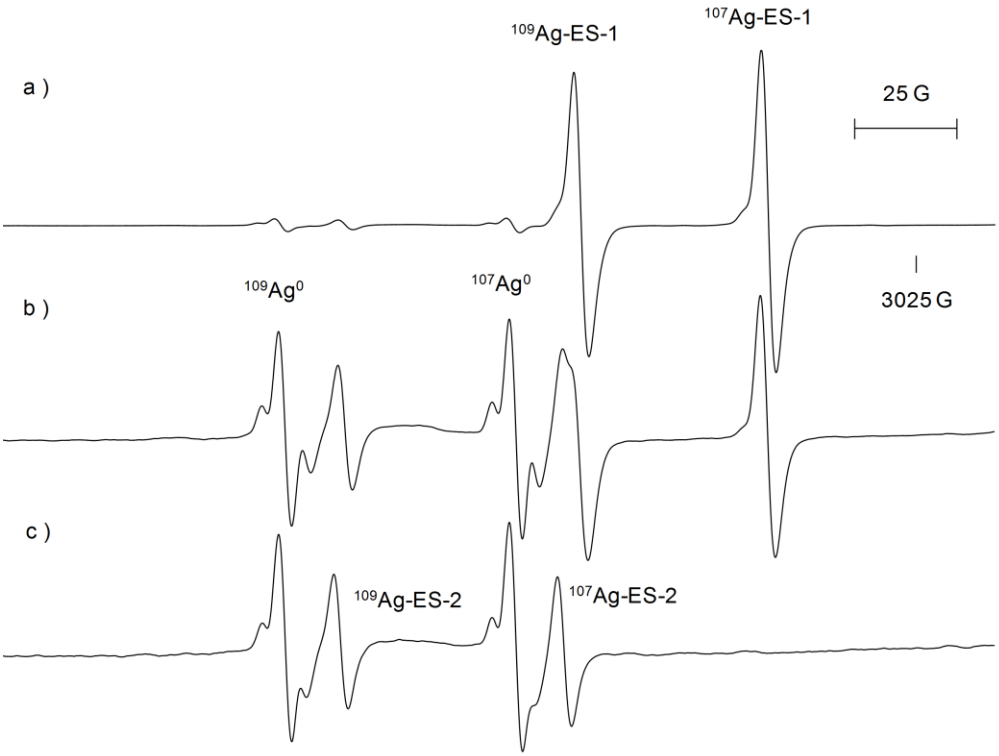

Figure 62. The m_I = +1/2 EPR transitions of $^{107/109}$Ag^{0}, $^{107/109}$Ag-ES-1 and $^{107/109}$Ag-ES-2, formed in the reaction of $^{107/109}$Ag atoms with ethylene sulfide in an adamantane matrix recorded at a) 100 K, b) 120 K and c) 140 K. All spectra recorded at a frequency, ν = 9122 MHz and m.p. = 2 mW.

The feature H, centered at g = 2.0054, in the EPR spectrum recorded over a 200 G scan range at 77 K, Figure 64a, showed a well-resolved hyperfine splitting of 21.7 MHz. At 100 K, Figure 64b, the spectral resolution improved further and a simulation of H was obtained using the FORTRAN program ISOPLOT, assuming the following magnetic parameters, a_{107Ag} = 53.6 MHz, a_{109Ag} = 61.7 MHz and eight hydrogen nuclei where $a_H(8)$ = 21.7 MHz, Figure 64c. At temperatures > 140 K, Figure 65a-c, a 4-line spectrum developed as the transitions, initially visible at 77 K, decayed. At 220 K, the quartet centered at g = 2.0187 has a spacing of 32.4 MHz. Following the annealing experiment, the sample was recooled to 77 K and an anisotropic spectrum with magnetic parameters $g_{\|}$ = 2.0019 and $g_{\perp}$ = 2.0297 was obtained, Figure 65d.

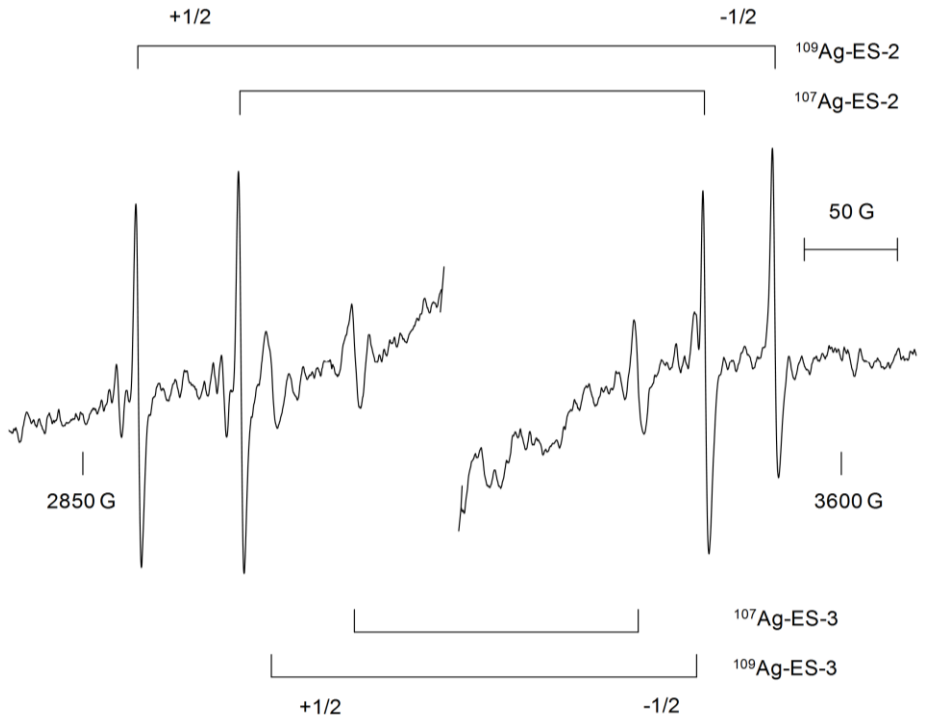

Figure 63. EPR spectrum recorded at 200 K (ν = 9121 MHz, m.p. = 20 mW), of the paramagnetic products, $^{107/109}$Ag-ES-2 and $^{107/109}$Ag-E3-3 formed, in the reaction of $^{107/109}$Ag atoms with ethylene sulfide in an adamantane matrix.

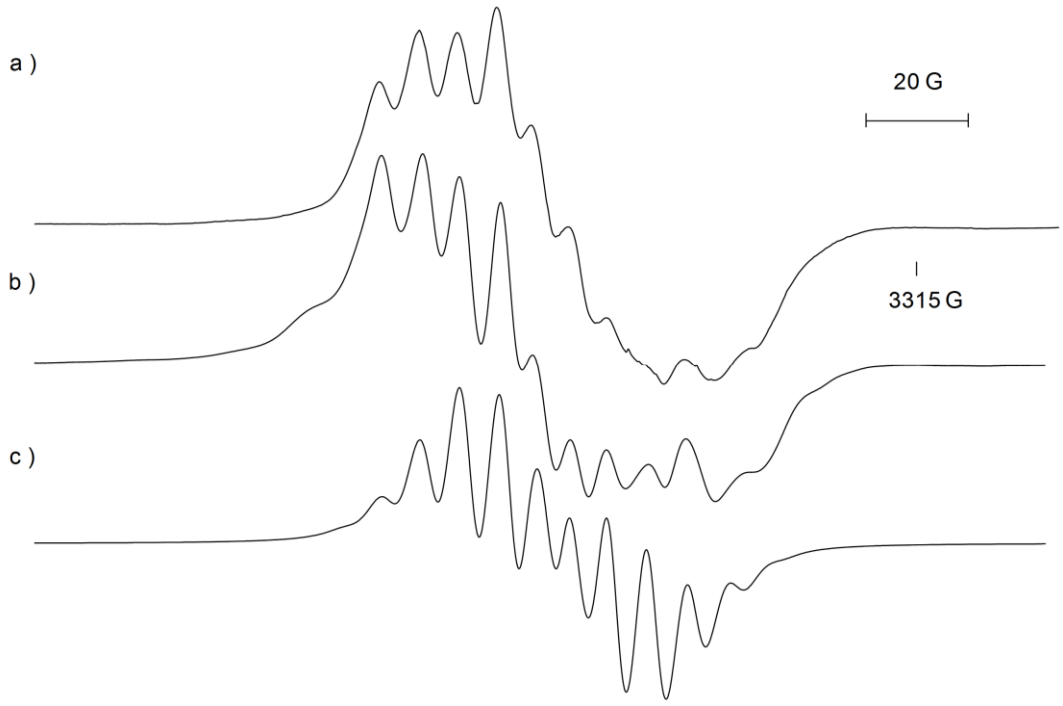

Figure 64. a) EPR spectrum of H a) at 77 K over a 200 G scan range (ν = 9111 MHz, m.p. = 2 mW); b) 100 K (9123 MHz, m.p. = 2 mW). c) Simulation of the experimental EPR spectrum of H using the FORTRAN program ISOPLOT, assuming two isotopes of Ag, $a_{^{107}Ag}$ = 53.6 MHz, $a_{^{107}Ag}$ = 61.7 MHz and 8 hydrogen nuclei with $a_H(8)$ = 21.7 MHz.

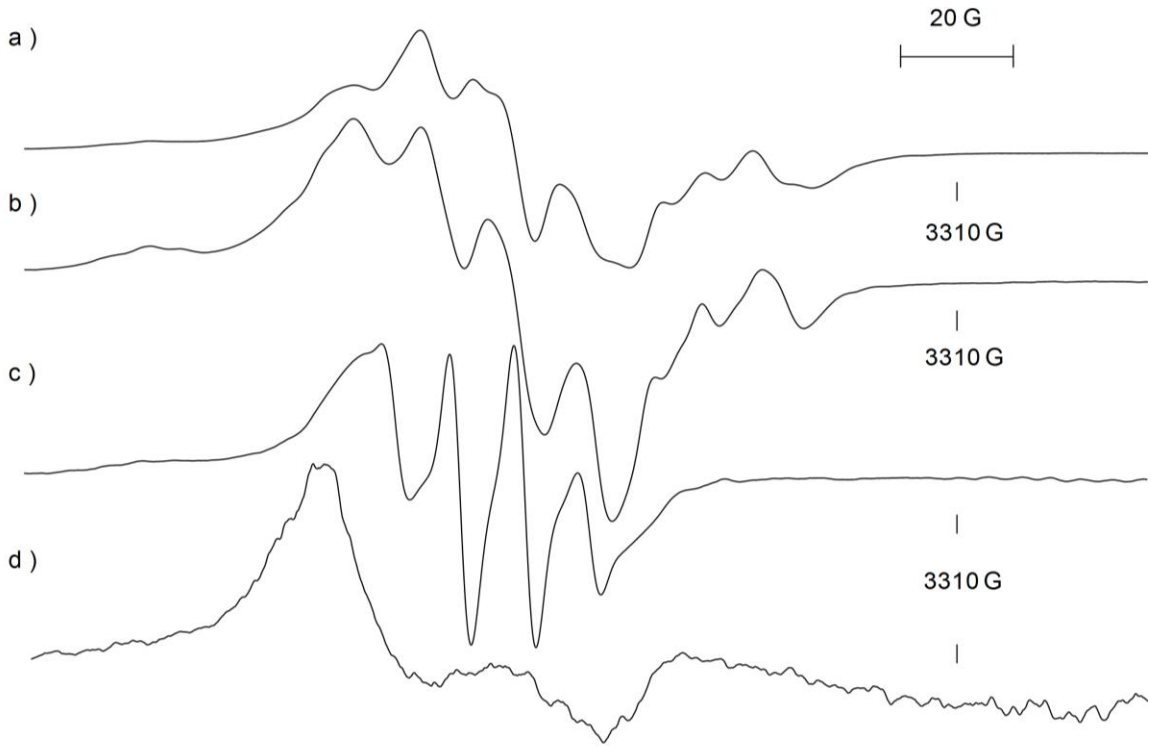

Figure 65. The effect of temperature on the central region of the EPR spectrum, recorded over a 200 G scan range, for the sample collected from the reaction of $^{107/109}$Ag atoms with ethylene sulfide at a) 140 K (ν = 9122 MHz, m.p. = 2 mW), b) 180 K (ν = 9122 MHz, m.p. = 2 mW), c) 220 K (ν = 9121 MHz, m.p. = 10 mW) and d) recooled to 77 K (ν = 9102 MHz, m.p. = 10 mW).

4.2.2.2. Ethylene sulfide-d_4

The reaction of $^{107/109}$Ag atoms (I = 1/2) with ethylene sulfide-d_4 in an adamantane matrix at 77 K yielded a yellowish tan-brown deposit on the drum. The EPR spectrum recorded at 77 K consisted of at least four overlapping doublets, labelled $^{107}Ag^0$, $^{109}Ag^0$, ^{107}Ag-ES-d_4-1, and ^{109}Ag-ES-d_4-1, respectively, as well as an intense central feature, H-d_4, Figure 66. The g and Ag hyperfine interaction values for the Ag-containing radicals are recorded in Table 13. The magnetic parameters for $^{107}Ag^0$ and $^{109}Ag^0$ are consistent with those previously reported for trapped atoms in adamantane.[36]

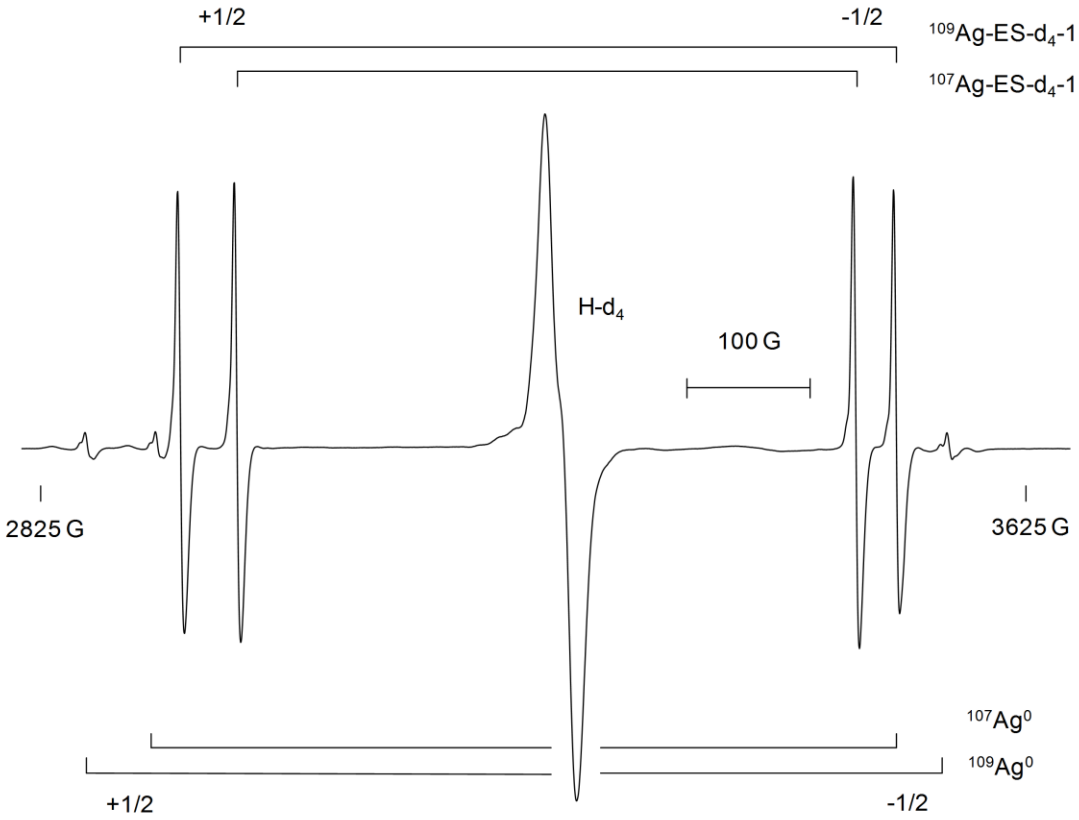

Figure 66. EPR spectrum recorded at 77 K (ν = 9085 MHz, m.p. = 2 mW), of the paramagnetic products, $^{107/109}$Ag^0, $^{107/109}$Ag-ES-d$_4$-1 and H-d$_4$, formed in the reaction of $^{107/109}$Ag atoms with ethylene sulfide-d$_4$ in an adamantane matrix.

$^{107/109}$Ag-ES-1 decayed when annealed in the cavity of the spectrometer and was no longer present in the spectrum past 120 K. When the sample was warmed to 200 K, two additional doublets, ^{107}Ag-ES-d$_4$-2 and ^{109}Ag-ES-d$_4$-2, appeared in the spectrum and persisted to 220 K. As seen in the EPR spectrum recorded at 200 K, Figure 67, the $^{107/109}$Ag-ES-d$_4$-2 transition lines are less intense than those of isolated $^{107/109}$Ag^0 atoms. In addition, the hyperfine interaction values of ^{107}Ag-ES-d$_4$-2 and ^{109}Ag-ES-d$_4$-2 differ from those of ^{107}Ag-ES-d$_4$-1 and ^{109}Ag-ES-d$_4$-2 by 26 MHz (1.9 %) and 29 MHz (1.9 %), respectively.

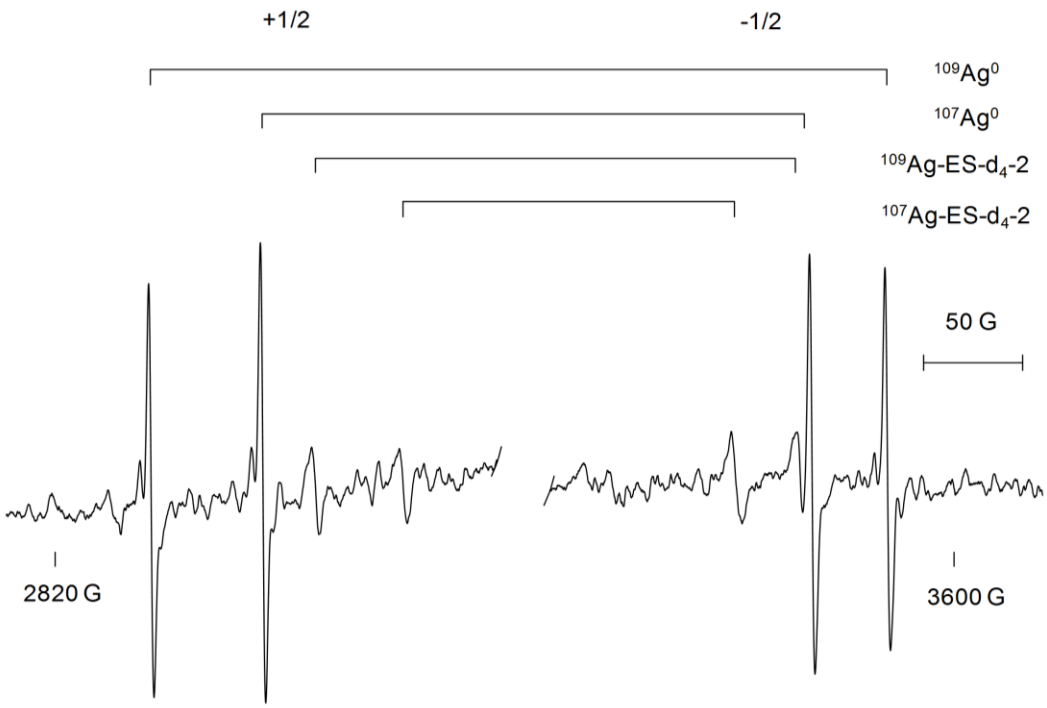

Figure 67. EPR spectrum recorded at 200 K (ν = 9119 MHz, m.p. = 2 mW) of the paramagnetic products, $^{107/109}$Ag-ES-d_4-2 and $^{107/109}Ag^0$, formed in the reaction of $^{107/109}$Ag atoms with ethylene sulfide-d_4 in an adamantane matrix.

The spectrum of the central feature H-d_4, Figure 68a, recorded at 77 K over a 200 G scan range, is thought to be a doublet due to the interaction of an unpaired electron with a Ag nucleus (I = 1/2). The center was simulated by superimposing the spectra of two species with the parameters, a_{107Ag} = 53.6 MHz, a_D (8) = 3.3 MHz, g = 2.0054 and a_{109Ag} = 61.7 MHz, a_D (8) = 3.3 MHz, g = 2.0054 in the ratio of 1:1, Figure 68b. The central feature changes as the sample was annealed from 77 K to 220 K, Figure 69a-d. More specifically, several new transitions centered at a higher g-value developed as the initial doublet disappeared. At 220 K, an intense quartet at g = 2.0189 with a spacing of 32.6 MHz was observed. The quartet persisted at temperatures > 280 K indicating the stability of the radical.

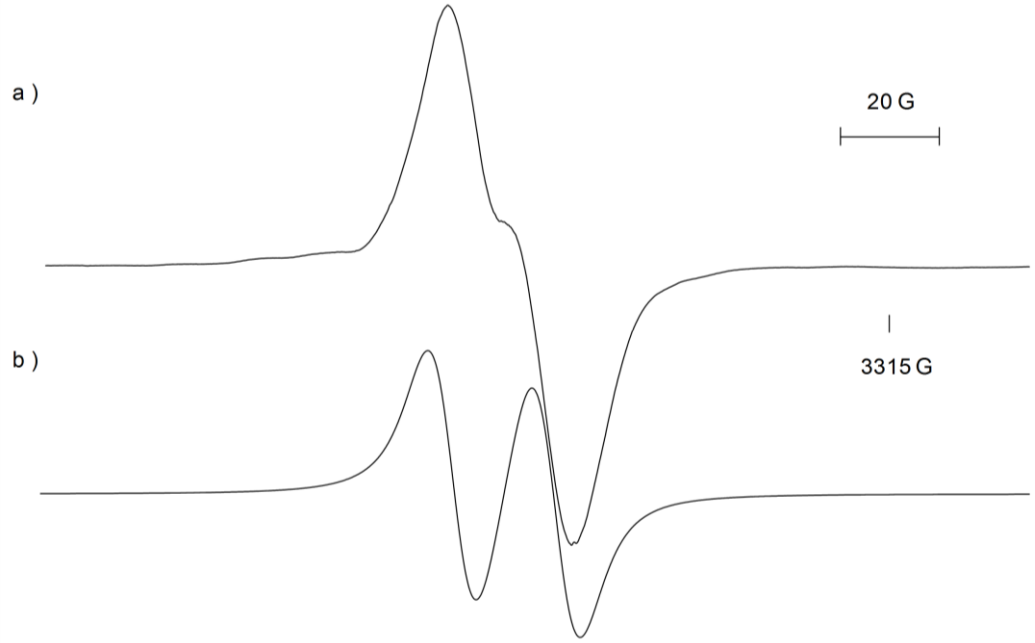

Figure 68. a) EPR spectrum of H-d_4 at 77 K over a 200 G scan range (ν = 9086 MHz, m.p. = 2 mW). b) Simulation of the experimental EPR spectrum of H-d_4 using the FORTRAN program ISOPLOT, assuming two isotopes of Ag, $a_{^{107}Ag}$ = 53.6 MHz, $a_{^{107}Ag}$ = 61.7 MHz, 8 D with $a_D(8)$ = 3.3 MHz and g = 2.0054.

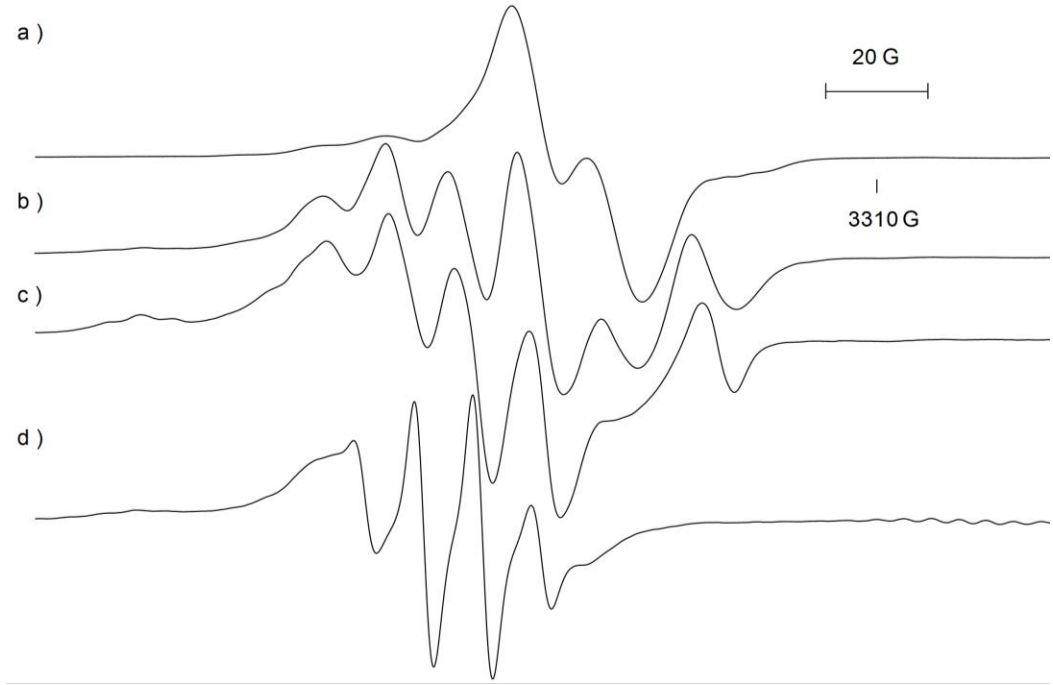

Figure 69. The effect of temperature on the central region of the EPR spectrum, recorded over a 200 G scan range, for the sample collected from the reaction of $^{107/109}$Ag atoms with ethylene sulfide-d_4 at a) 100 K, b) 140 K, c) 180 K and d) 220 K. All spectra recorded with ν = 9120 MHz and m.p. = 2 mW.

When the sample that had been annealed to 280 K was cooled to 100 K the intense quartet was replaced by a large anisotropic feature with $g_{\|} = 2.0019$ and $g_{\perp} = 2.0297$. The intense quartet reappeared upon warming the sample back to 220 K, suggesting a radical undergoing a conformational change as a function of temperature. Figure 70 compares the quartet observed at high temperatures with the anisotropic feature present at low temperatures.

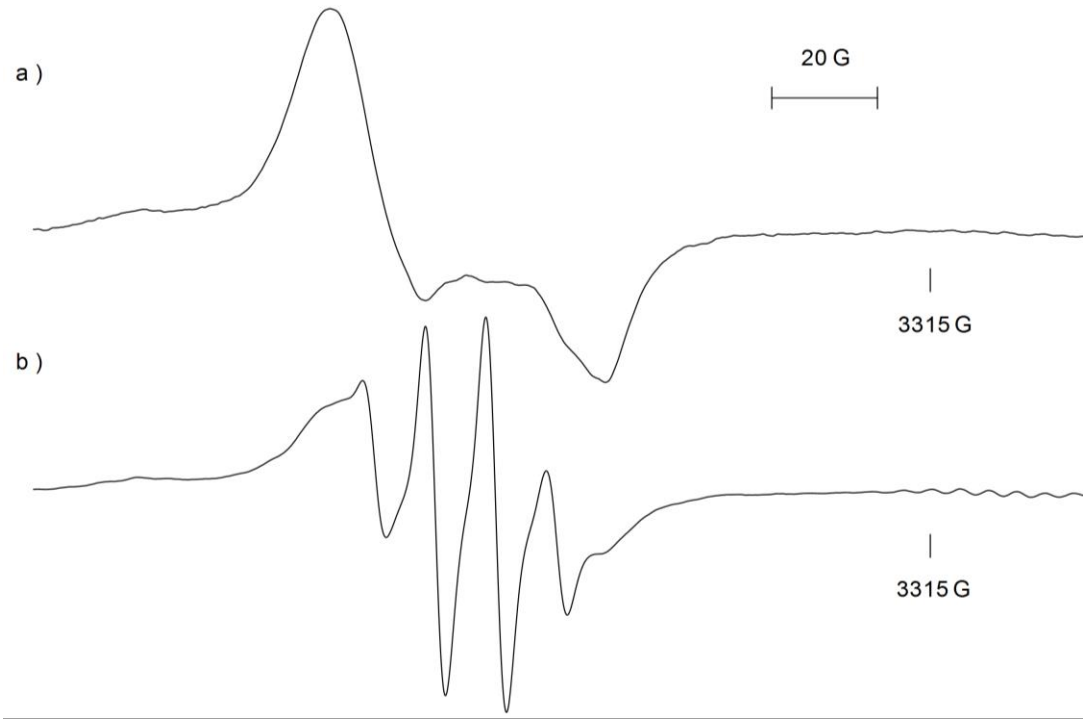

Figure 70. Central region of the EPR spectrum for the annealed $^{107/109}$Ag atom-ethylene sulfide-d_4 reaction mixture a) recooled and recorded at 100 K and b) recorded at 220 K. Both spectra recorded with ν = 9119 MHz and m.p. = 2 mW.

4.2.3. Aziridines

4.2.3.1. Aziridine-^{14}N

The reaction of $^{107/109}$Ag atoms (I = 1/2) with aziridine in an adamantane matrix at 77 K, yielded a yellow-green deposit. At 77 K, four overlapping doublets, Figure 71, as well as ^{107}Ag^0 and ^{109}Ag^0, with a_{Ag} values consistent with those of Ag atoms in two distinct sites were observed, Table 14.[36] Interestingly, the atom lines in site 1 are complicated by forbidden proton-spin flipping. Four doublets of triplets, ^{107}Ag-Az-1, ^{109}Ag-Az-1, ^{107}Ag-Az-2, and ^{109}Ag-Az-2, and finally a weak anisotropic feature, I, centered at g = 2.0066 were also visible. The a_{Ag} and g values of the ^{107}Ag-Az-1, ^{109}Ag-Az-1, ^{107}Ag-Az-2, and ^{109}Ag-Az-2 species were obtained using the magnetic field position of the transition lines from calibrated spectra, Table 23. Unfortunately, an accurate g-value for ^{109}Ag-Az-2 could not be calculated at low temperatures because the m_I = +1/2 transition line was obscured by those of the other products. All four products have a similar triplet splitting of ~57 MHz (within experimental error) which is thought to arise from the interaction of the nitrogen nucleus (I = 1) in the aziridine ring with the unpaired electron.

Increasing the temperature of the sample to 220 K in the spectrometer cavity caused the peaks belonging to $^{107/109}$Ag-Az-1 and $^{107/109}$Ag-Az-2 to sharpen, Figure 72a. The spectrum was simulated, Figure 72b, using the magnetic parameters determined for ^{107}Ag-Az-1, ^{109}Ag-Az-1, ^{107}Ag-Az-2, and ^{109}Ag-Az-2 at 220 K. Based on the intensity of the spectral lines the ratio of [$^{107/109}$Ag-Az-1]:[$^{107/109}$Ag-Az-2] is 3. The a_{Ag} values of ^{107}Ag-Az-1, ^{109}Ag-Az-1, and ^{107}Ag-Az-2 increased by 22.4 MHz (1.7%), 22.8 MHz (1.8%), and of 24.4 MHz (1.6 %), respectively, as the temperature was increased

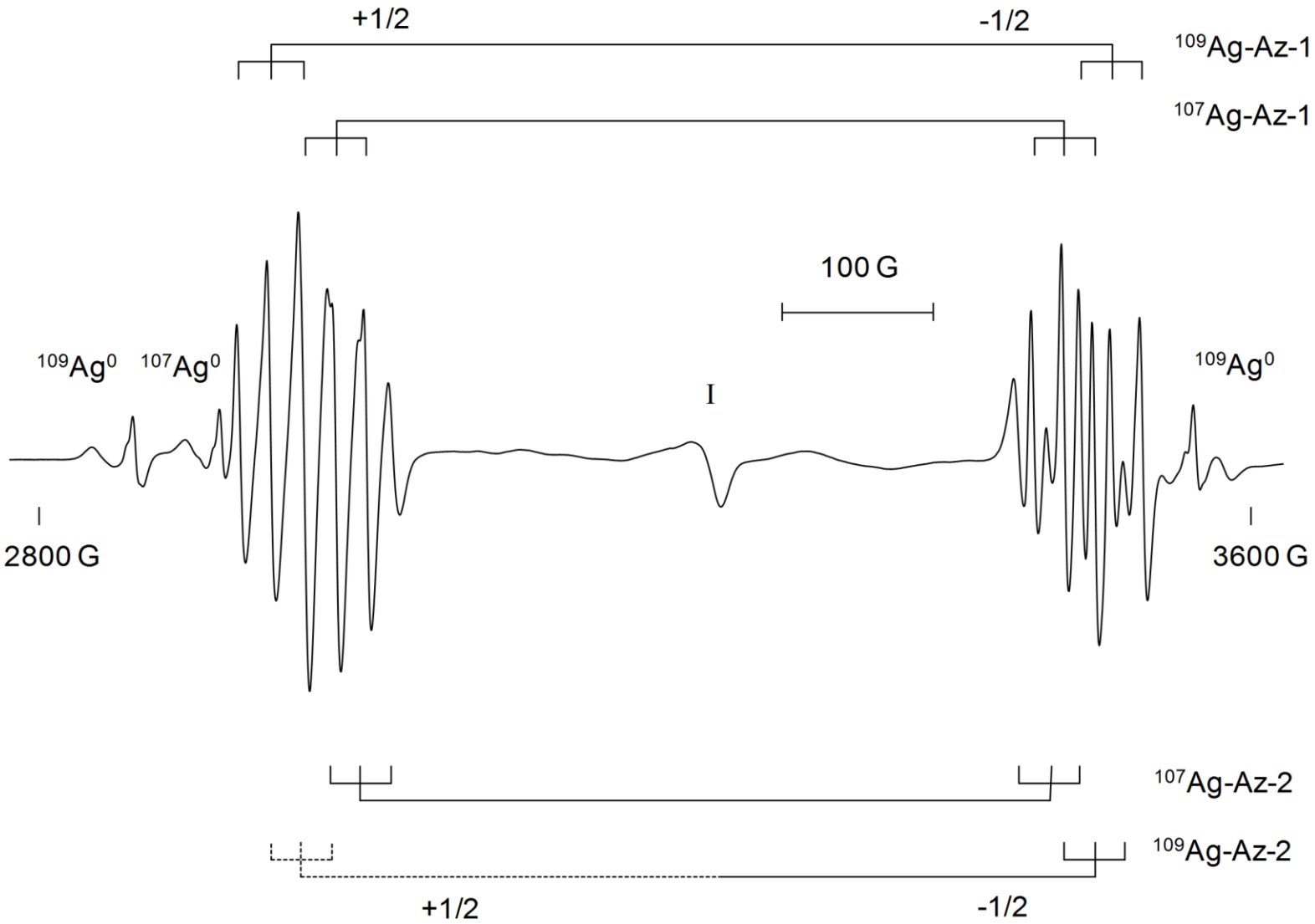

Figure 71. EPR spectrum recorded at 77 K (ν = 9087 MHz, m.p. = 2 mW), of the paramagnetic products, $^{107/109}$Ag^{0}, $^{107/109}$Ag-Az-1, $^{107/109}$Ag-Az-2, and I, formed in the reaction of $^{107/109}$Ag atoms with aziridine in an adamantane matrix.

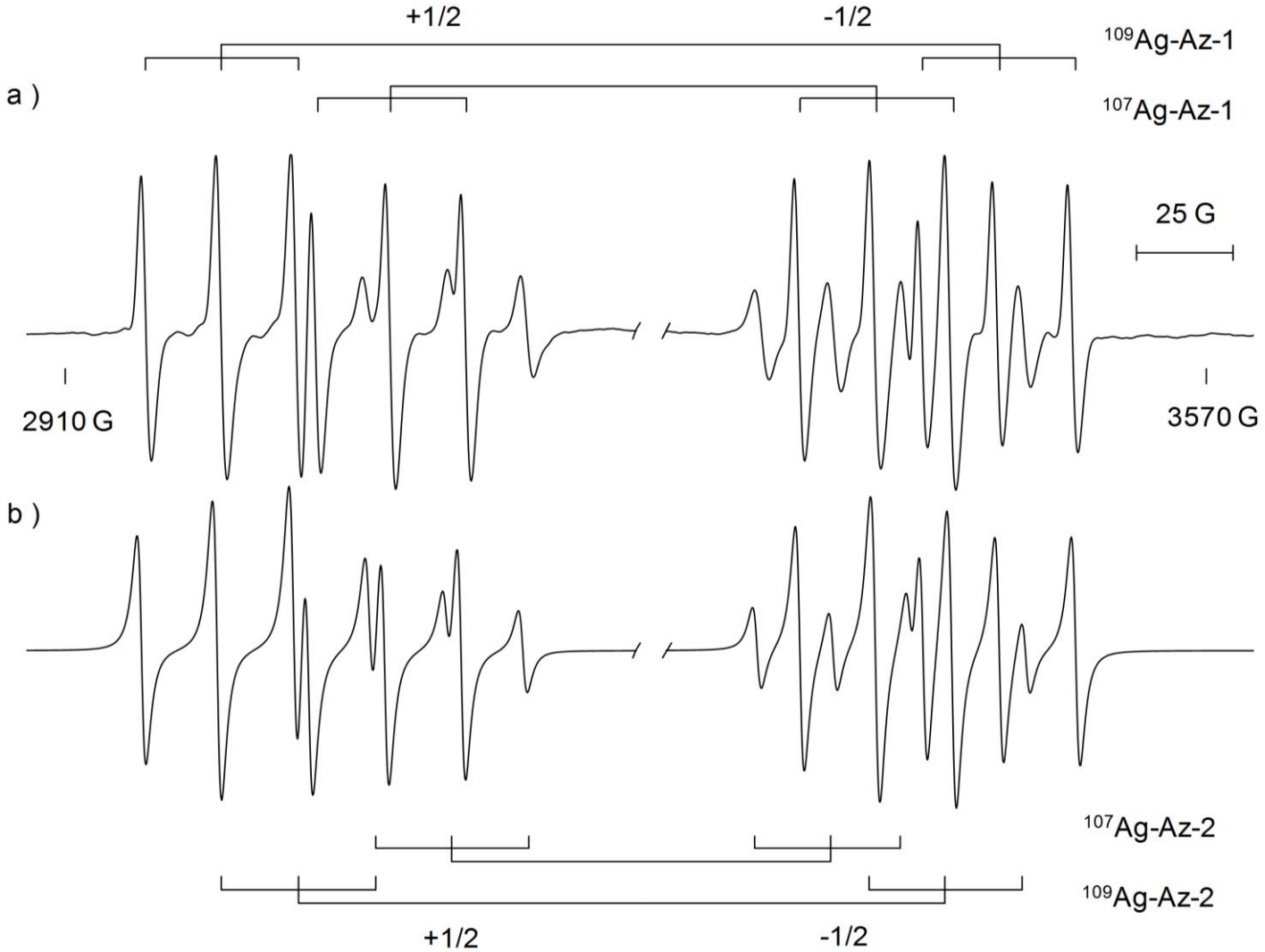

Figure 72. a) EPR spectrum recorded at 220 K, of the m_I = +1/2 and -1/2 transitions of $^{107/109}$Ag-Az-1 and $^{107/109}$Ag-Az-2 (ν = 9120 MHz, m.p = 2 mW). b) Simulated spectra of the m_I = +1/2 and -1/2 transitions of $^{107/109}$Ag-Az-1 and $^{107/109}$Ag-Az-2 using the magnetic parameters listed in Table 14.

Table 14. The magnetic parameters of $^{107/109}Ag^0$, $^{107/109}Ag$-Az-1, $^{107/109}Ag$-Az-2, $^{107/109}Ag$-Az^{15}N-1, and $^{107/109}Ag$-Az^{15}N-1, formed in the reactions of $^{107/109}Ag$ atoms with aziridine or its isotopomer aziridine-^{15}N in adamantane.

Aziridine	Site	a_{Ag} (MHz)	a_{14N} (MHz)	g	Temp.	ν (MHz)
$^{107}Ag^0$	1	1681	-	2.0016	77 K	9087
	2	1777	-	2.0011		
$^{109}Ag^0$	1	1950	-	2.0025		
	2	2054	-	2.0009		
^{107}Ag-Az-1		1340	57 ± 1.7	2.0002		
^{109}Ag-Az-1		1547	56 ± 1.6	2.0000		
^{107}Ag-Az-2		1268	58 ± 2.5	1.9997		
^{109}Ag-Az-2		1458[a]	57 ± 3.1	-		
^{107}Ag-Az-1		1362	55 ± 1.0	2.0000	220 K	9120
^{109}Ag-Az-1		1571	55 ± 1.0	1.9996		
^{107}Ag-Az-2		1291	55 ± 1.7	1.9995		
^{109}Ag-Az-2		1486	53 ± 1.7	1.9992		
Aziridine-^{15}N	Site	a_{Ag} (MHz)	a_{15N} (MHz)	g	Temp.	ν (MHz)
$^{107}Ag^0$	1	1682	-	2.0014	77 K	9088
	2	1778	-	2.0011		
$^{109}Ag^0$	1	1941	-	2.0017		
	2	2052	-	2.0012		
^{107}Ag-Az^{15}N-1		1336	78	1.9999		
^{109}Ag-Az^{15}N-1		1543	78	2.0000		
^{107}Ag-Az^{15}N-2		1259	78	1.9992		
^{109}Ag-Az^{15}N-2		1460	78	1.9997		
^{107}Ag-Az^{15}N-1		1360	78	1.9999	220 K	9119
^{109}Ag-Az^{15}N-1		1571	78	1.9995		
^{107}Ag-Az^{15}N-2		1290	78	1.9992		
^{109}Ag-Az^{15}N-2		1487	78	1.9985		
^{107}Ag-Az^{15}N-1		1338	80	1.9999	Recooled (77 K)	9088
^{109}Ag-Az^{15}N-1		1543	80	2.0003		

[a]Value estimated using $a_{109Ag\text{-}Az\text{-}2}$ x $\gamma_{109Ag}/\gamma_{107Ag}$ = 1268 x 1.15 = 1458 MHz.

from 77 to 220 K. An increase in the a_{Ag} value for ^{109}Ag-Az-2 of 28 MHz (1.9 %) at 220 K falls within close range to the values obtained for the other Ag-species, albeit slightly higher since the a_{Ag} value of 1452 MHz obtained at 77 K was estimated based on the ratio of gyromagnetic ratios of ^{109}Ag and ^{107}Ag, $\gamma_{109Ag}/\gamma_{107Ag}$ = 1.150. The transition lines

of species $^{107/109}$Ag-Az-1 and $^{107/109}$Ag-Az-2 began to decay at temperatures > 220 K and were no longer visible at temperatures > 240 K.

The effect of temperature in the small feature, I, centered at g = 2.0066, is shown in Figure 73. When the temperature reached 180 K there appeared to be small additional hyperfine interaction. Further annealing of the sample resulted in a single peak at g = 2.0042 that persisted to temperatures > 240 K.

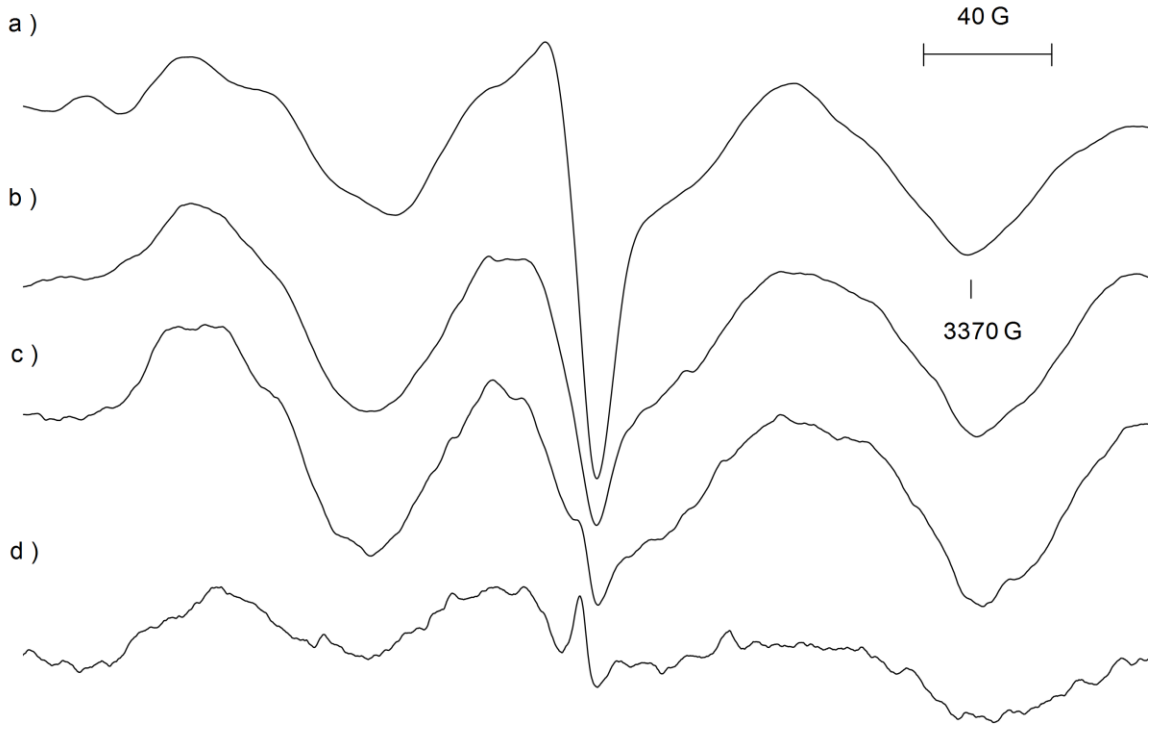

Figure 73. The effect of temperature on the central region of the $^{107/109}$Ag-aziridine EPR spectrum, I, recorded over 400 G a) 100 K (ν = 9121 MHz, m.p. = 2 mW), b) 140 K (ν = 9121 MHz, m.p. = 2 mW), c) 180 K (ν = 9120 MHz, m.p. = 2 mW), and d) 220 K (ν = 9119 MHz, m.p. = 10 mW).

4.2.3.2. Aziridine-^{15}N

Repeating the $^{107/109}$Ag atom reaction with aziridine-^{15}N also resulted in the formation of a yellow-green deposit. The EPR spectrum, recorded at 77 K, consisted of eight doublets

and a weak anisotropic feature, I-^{15}N, Figure 74. The doublets labelled $^{107}Ag^0$ and $^{109}Ag^0$, are assigned to trapped Ag atoms in two distinct sites based on the magnetic parameters determined from the magnetic field positions of the transition lines, Table 14 and visible proton spin-flipping at site 1. The EPR parameters, a_{Ag} and g-values, of the additional four doublets, ^{107}Ag-Az^{15}N-1, ^{109}Ag-Az^{15}N-1, ^{107}Ag-Az^{15}N-2, and ^{109}Ag-Az^{15}N-2, are also found in Table 14. Closer examination of the transition lines for $^{107/109}$Ag-Az^{15}N-1 and $^{107/109}$Ag-Az^{15}N-2 revealed additional hyperfine splitting. More specifically, the transition lines were doublets with a spacing of 78 MHz, which could arise from the interaction of the isotopically enriched nitrogen nucleus (I = 1/2) in the aziridine-^{15}N ring with the unpaired electron on Ag.

As the temperature of the sample increased, the peaks belonging to $^{107/109}$Ag-Az^{15}N-1 and $^{107/109}$Ag-Az^{15}N-2 sharpened. At 220 K, Figure 75a, the transition lines became clearer allowing for their assignment. A simulation of the EPR spectrum, Figure 75b, was generated using the a_{Ag}, a_{15N} and g values, Table 14, of ^{107}Ag-Az^{15}N-1, ^{109}Ag-Az^{15}N-1, ^{107}Ag-Az^{15}N-2 and ^{109}Ag-Az^{15}N-2 determined at 220 K. Based on the intensity of the transition lines, the ratio of [$^{107/109}$Ag-Az^{15}N-1] and [$^{107/109}$Ag-Az^{15}N-2] was found to be 10. The nitrogen splitting of 78 MHz remained the same at 220 K for all four species. The a_{Ag} values of ^{107}Ag-Az^{15}N-1, ^{109}Ag-Az^{15}N-1, ^{107}Ag-Az^{15}N-2, and ^{109}Ag-Az^{15}N-2 increased by 24.5 MHz (1.8%), 27.5 MHz (1.8%), 31.3 MHz (2.5 %), and 27.6 MHz (1.9 %), respectively, as the temperature was increased from 77 to 220 K.

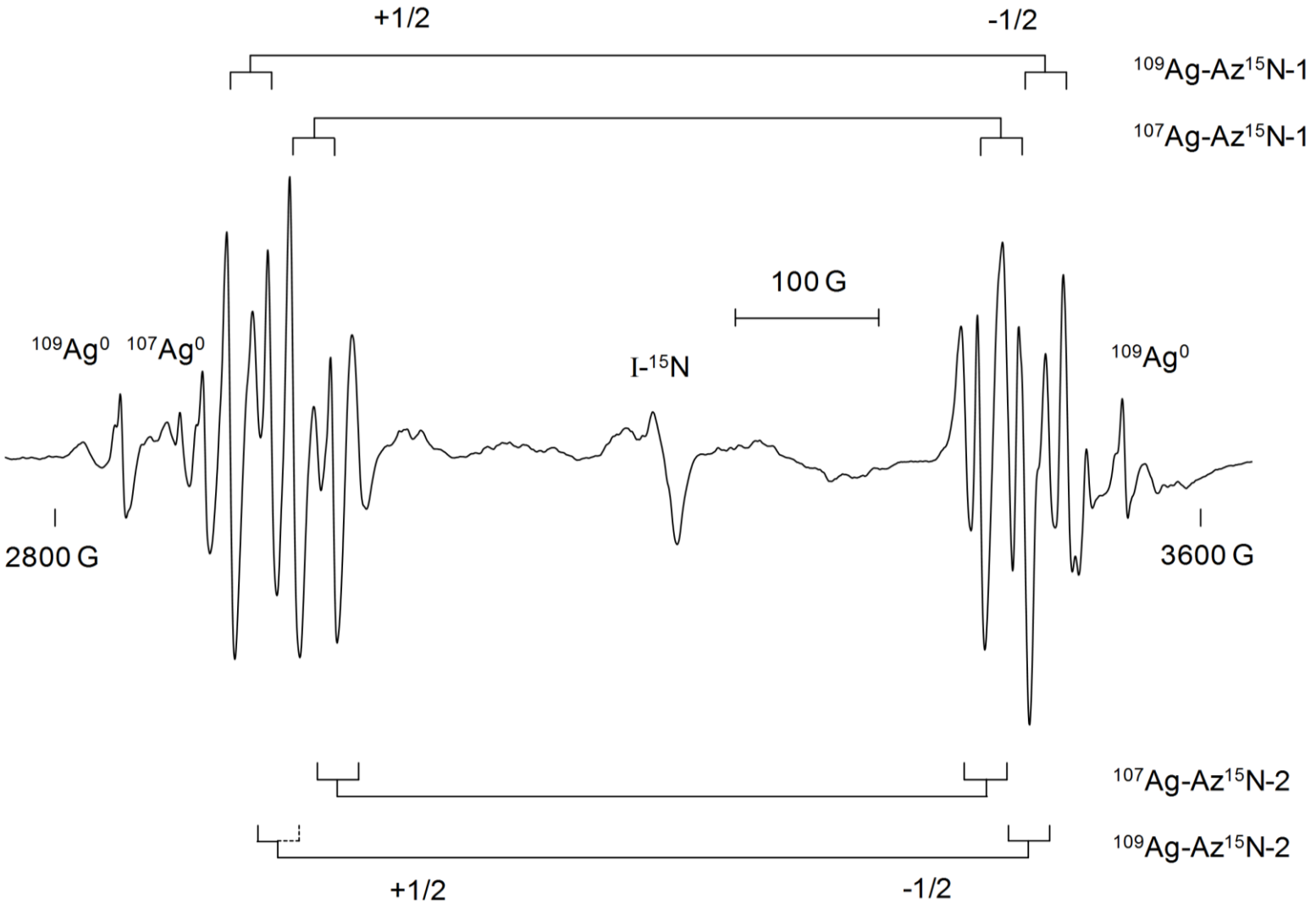

Figure 74. EPR spectrum recorded at 77 K (ν = 9088 MHz, m.p. = 2 mW), of the paramagnetic products, $^{107/109}$Ag^{0}, $^{107/109}$Ag-Az^{15}N-1, $^{107/109}$Ag-Az^{15}N-2, and I-^{15}N, formed in the reaction of $^{107/109}$Ag atoms with aziridine-^{15}N in an adamantane matrix.

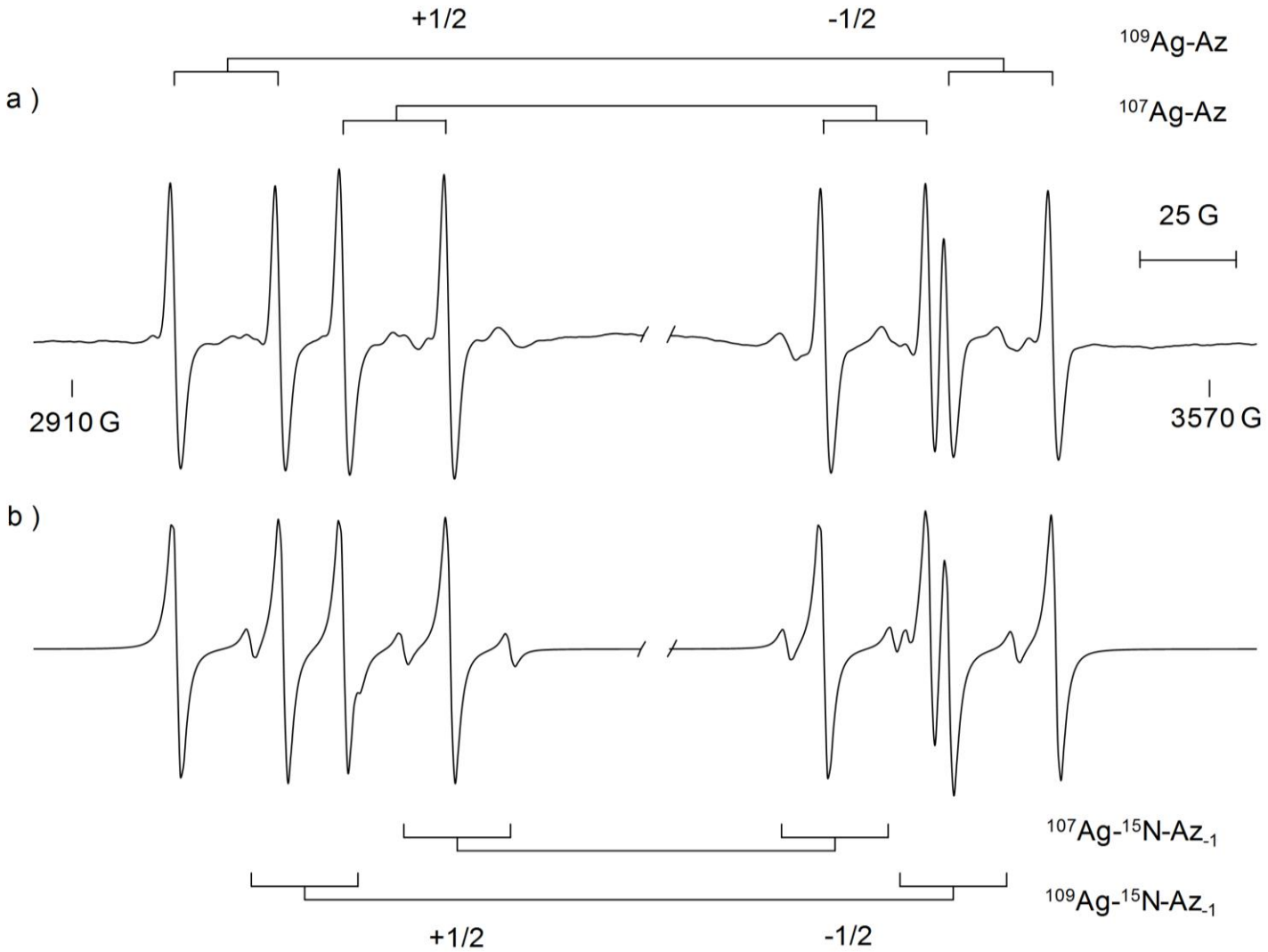

Figure 75. a) EPR spectrum recorded at 220 K, of the m_I = +1/2 and -1/2 transitions of $^{107/109}$Ag-Az^{15}N-1 and $^{107/109}$Ag-Az^{15}N-2 (ν = 9119 MHz, m.p = 2 mW). b) Simulation of the m_I = +1/2 and -1/2 transitions of $^{107/109}$Ag-Az^{15}N-1 and $^{107/109}$Ag-Az^{15}N-2, using the magnetic parameters listed in Table 14.

After the temperature in the spectrometer cavity reached 220 K, the sample was recooled to 77 K. The $^{107/109}$Ag-Az^{15}N-1 transition lines shifted back to the positions originally observed at 77 K, while those of $^{107/109}$Ag-Az^{15}N-2 were too weak to observe. This, of course, resulted in the same a_{Ag} and g values, within experimental error, as those summarized in Table 14. In addition, satellite lines, 13.6 MHz on either side of the $^{107/109}$Ag-Az^{15}N-1 transition lines, were observed. This is thought to arise from forbidden proton-spin flipping within the adamantane matrix.

The small feature, I-^{15}N, present at 77 K and centered, g = 2.0062, was monitored as the temperature was increased from 77 to 220 K, Figure 76. When the temperature reached 180 K, there appeared to be an additional hyperfine interaction. At 210 K, the spectrum appears to have resolved into a quintet of doublets superimposed upon a broad underlying feature, Figure 77a. The quintet spacing is 85.2 MHz from four equivalent hydrogen nuclei (I = 1/2) and the 47.7 MHz doublet spacing from the isotopically enriched ^{15}N nitrogen nucleus (I = 1/2). These parameters match those of the aziridino radical[104] if we take into account that a_{15N} should be 5 MHz larger than a_{14N}, based on the ratio of gyromagnetic ratios of ^{15}N and ^{14}N, i.e. $\gamma_{15N}/\gamma_{14N}$ = 1.402. A simulation of the aziridino-^{15}N radical was generated using the FORTRAN program ISOPLOT, Figure 77b. Further annealing of the sample resulted in a single peak at g = 2.0052 that persisted at temperatures > 240 K.

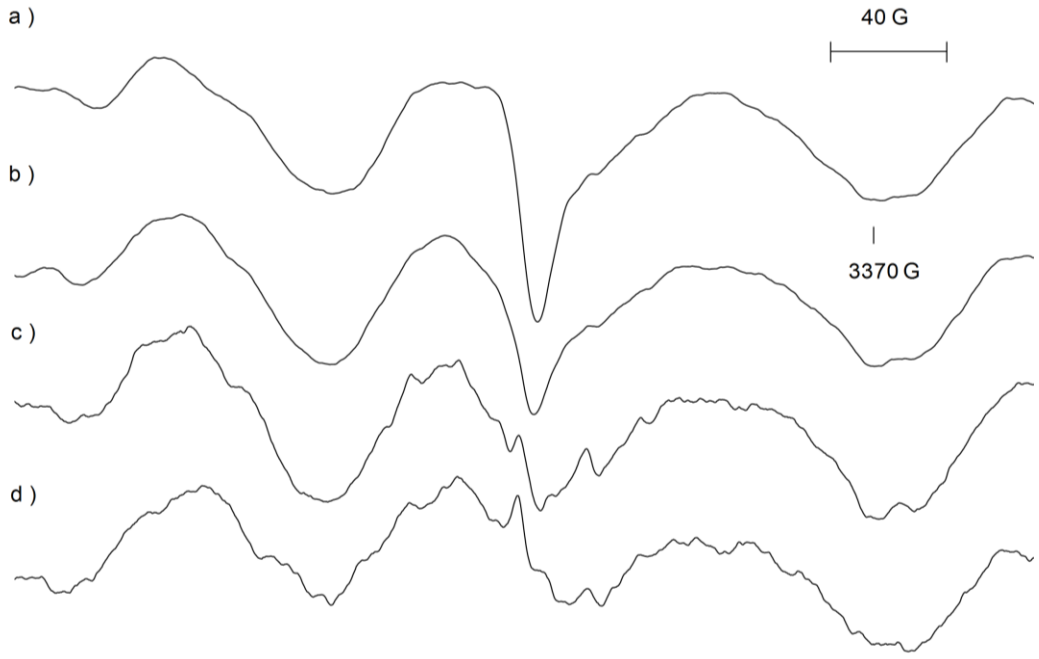

Figure 76. The effect of temperature on the central region of the $^{107/109}$Ag-aziridine-^{15}N EPR spectrum, I-^{15}N, recorded over 400 G a) 100 K (ν = 9121 MHz, m.p. = 2 mW), b) 140 K (ν = 9120 MHz, m.p. = 2 mW), c) 180 K (ν = 9120 MHz, m.p. = 2 mW) and d) 220 K (ν = 9119 MHz, m.p. = 20 mW).

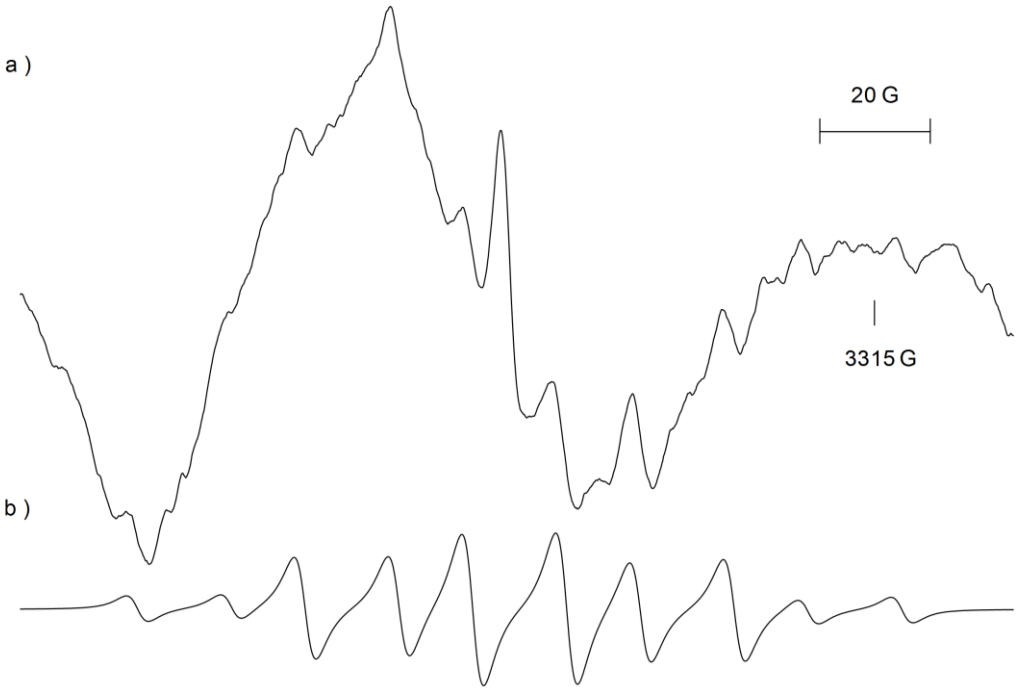

Figure 77. a) Central region of the EPR spectrum of the $^{107/109}$Ag atom-aziridine-^{15}N reaction mixture over 200 G (v = 9119 MHz, m.p. = 20 mW), at 210 K. b) Simulation of the experimental EPR spectrum using the FORTRAN program ISOPLOT, and assuming, a_{H}(4) = 85.2 MHz, a_{15N} = 47.7 MHz, and g = 2.0044 (LW = 11 MHz).

4.3. Reaction of Gold Atoms with Three-Membered Heterocyclic Compounds

4.3.1. Oxiranes

4.3.1.1. Ethylene oxide

The ^{197}Au atoms (I = 3/2) were reacted with ethylene oxide in an adamantane matrix at 77 K on the cryostat. The EPR spectrum given by the resulting white deposit at 77 K, Figure 78, consisted of four quartets, namely, ^{197}Au^{0}-1, ^{197}Au^{0}-2, and ^{197}Au^{0}-3, (assigned to ^{197}Au atoms isolated in adamantane in three distinct trapping sites)[36] and ^{197}Au-EO-1. The Au hyperfine interaction and g values, Table 15, were determined using the magnetic field positions of ^{197}Au^{0}-1, ^{197}Au ^{0}-2, ^{197}Au^{0}-3, and ^{197}Au-EO-1. In addition, an anisotropic feature, J, centered at g = 2.0069 (attributed to Au aggregates and microcrystallites) were observed.[36]

When the sample was annealed to 100 K in the cavity of the spectrometer a fifth quartet, ^{197}Au-EO-2, appeared, Figure 79. The a_{Au} and g values of both ^{197}Au-EO-1 and ^{197}Au-EO-2, recorded at 100 K, are presented in Table 15. It is interesting to note that the m_I = +1/2 transition line of ^{197}Au-EO-2 was narrower than that of ^{197}Au-EO-1, i.e., a line width of 81 MHz (^{197}Au-EO-2) versus 163 MHz (^{197}Au-EO-1). At 140 K, the position of the transition lines for the ^{197}Au-EO-1 and ^{197}Au-EO-2 species shift. As a result, the value of the Au hyperfine interaction for ^{197}Au-EO-1 increased from 2652 MHz at 100 K to 2710 MHz at 140 K, i.e., 2 %. In the case of ^{197}Au-EO-2, the Au hyperfine interaction increases by 0.4 % in going from 100 to 140 K, i.e., 2794 to 2806 MHz. As the temperature was raised above 140 K, the transition lines of both ^{197}Au-EO-1 and ^{197}Au-EO-2 decayed and were no longer visible at temperatures > 160 K.

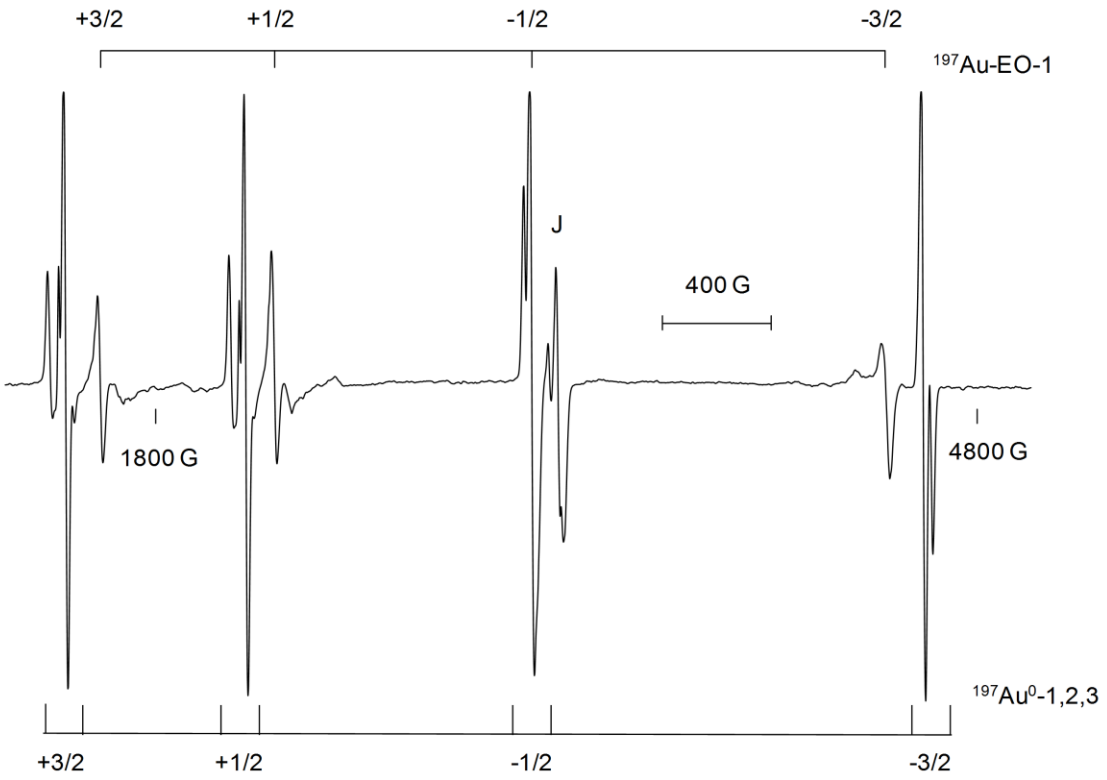

Figure 78. EPR spectrum recorded at 77 K (ν = 9138 MHz, m.p. = 2 mW), of the paramagnetic products, $^{197}Au^0$-1, $^{197}Au^0$-2, $^{197}Au^0$-3, ^{197}Au-EO-1, and J, formed in the reaction of ^{197}Au atoms with ethylene oxide in an adamantane matrix.

Table 15. The magnetic parameters of $^{197}Au^0$-1, $^{197}Au^0$-2, $^{197}Au^0$-3, ^{197}Au-EO-1, and ^{197}Au-EO-2, formed in the reaction of ^{197}Au atoms with ethylene oxide in adamantane.

	a_{Au} (MHz)	g	Temperature	ν (MHz)
$^{197}Au^0$-1	2932 ± 0.7	1.9999 ± 0.0002	77 K	9140
$^{197}Au^0$-2	2882 ± 0.8	2.0008 ± 0.0002		
$^{197}Au^0$-3	2857 ± 0.2	1.9997 ± 0.0001		
^{197}Au-EO-1	2627 ± 1.0	2.0252 ± 0.0003		
^{197}Au-EO-1	2652 ± 0.5	2.0232 ± 0.0001	100 K	9122
^{197}Au-EO-2	2794 ± 2.2	2.0096 ± 0.0002		
^{197}Au-EO-1	2710 ± 3.9	2.0201 ± 0.0010	140 K	9122
^{197}Au-EO-2	2806 ± 0.4	2.0085 ± 0.0001		

The central feature, J, did not change significantly as the sample temperature was increased and persisted in the EPR spectrum at temperatures > 180 K.

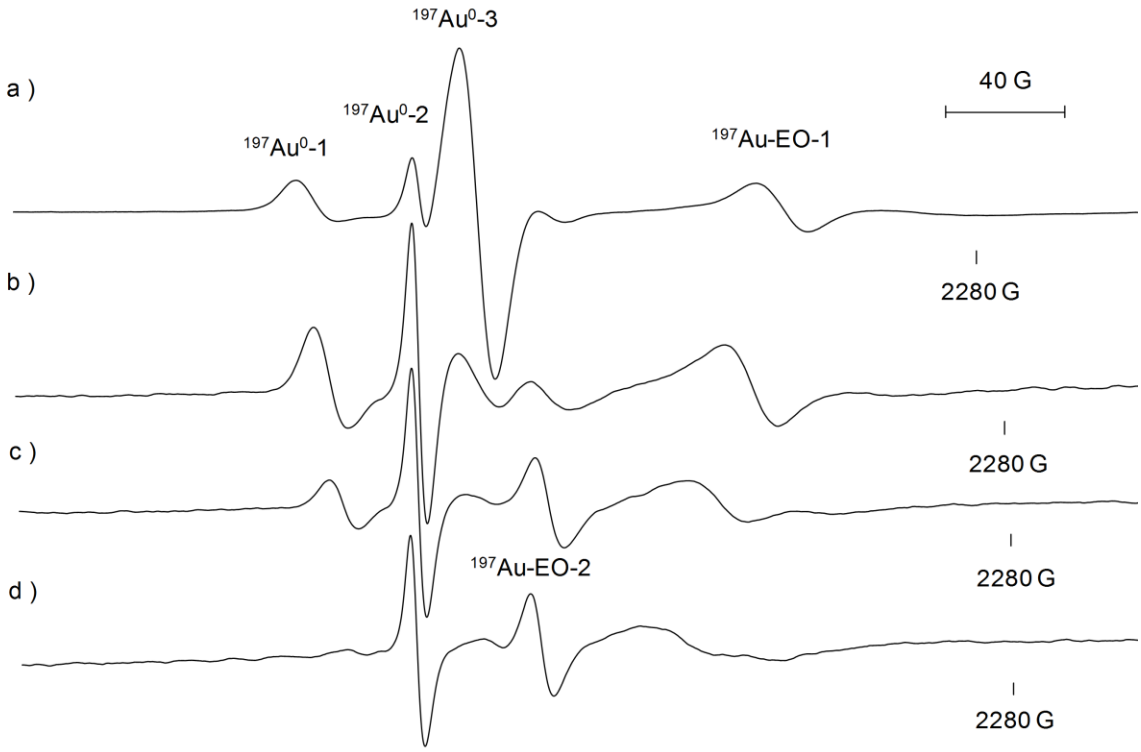

Figure 79. Comparison of a section of the EPR spectrum of the ^{197}Au atom-ethylene oxide reaction mixture recorded at a) 77 K (ν = 9140 MHz), b) 100 K (ν = 9122 MHz), c) 120 K (ν = 9122 MHz), and d) 140 K (ν = 9122 MHz), showing a shift in the m_I = +1/2 transition lines of ^{197}Au-EO-1 and ^{197}Au-EO-2. All spectra recorded at m.p. = 2 mW.

4.3.1.2. Styrene oxide

The ^{197}Au atoms (I = 3/2) were reacted with styrene oxide in an adamantane matrix at 77 K on the cryostat. The EPR spectrum given by the resulting white deposit, Figure 80, consisted of three quartets, ^{197}Au^0-1, ^{197}Au^0-2, and ^{197}Au^0-3, assigned to ^{197}Au atoms isolated in adamantane in three distinct trapping sites,[36] and an anisotropic feature, K, centered at g = 2.0080 (attributed to Au aggregates and microcrystallites). The magnetic parameters, a_{Au} and g values, of ^{197}Au^0-1, ^{197}Au^0-2 and ^{197}Au^0-3 are listed in Table 16. No signals with large hyperfine interaction were observed, as seen in other cases above.

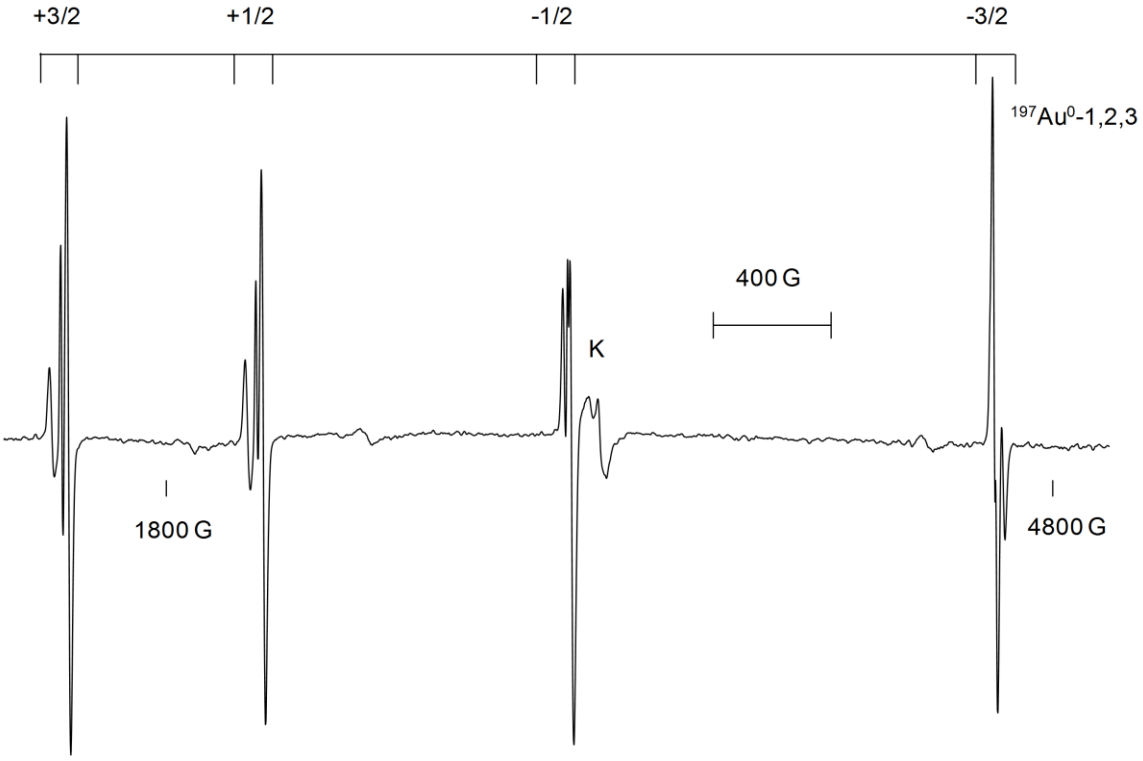

Figure 80. EPR spectrum recorded at 77 K (ν = 9139 MHz, m.p. = 2 mW) of the paramagnetic products, $^{197}Au^0$-1, $^{197}Au^0$-2, $^{197}Au^0$-3, and K, formed in the reaction of ^{197}Au atoms with styrene oxide in an adamantane matrix.

Table 16. The magnetic parameters of $^{197}Au^0$-1, $^{197}Au^0$-2 and $^{197}Au^0$-3, formed in the reaction of ^{197}Au atoms with styrene oxide in adamantane.

	a_{Au} (MHz)	g	Temperature	ν (MHz)
$^{197}Au^0$-1	2932 ± 0.5	2.0004 ± 0.0001		
$^{197}Au^0$-2	2881 ± 0.7	2.0010 ± 0.0002	77 K	9140
$^{197}Au^0$-3	2854 ± 0.7	2.0007 ± 0.0002		

4.3.2. Ethylene sulfide

The ^{197}Au atoms (I = 3/2) and ethylene sulfide were co-deposited in an adamantane matrix on a rotating cryostat at 77 K. The yellow deposit was collected in a quartz EPR sample tube. The EPR spectrum of the paramagnetic species, recorded at 77 K, Figure 81, reveals the presence of several paramagnetic species. The transition lines marked, ^{197}Au^0-1, ^{197}Au^0-2, and ^{197}Au^0-3, can be assigned to ^{197}Au atoms isolated in adamantane in three different trapping sites.[36] The magnetic parameters, a_{Au} and g values, Table 17, were determined with the aid of ESRLSQ. In addition, an intense quartet labelled, ^{197}Au-ES, and a central feature, L, were detected. The ^{197}Au-ES species, has a g-value and isotropic hyperfine interaction of 1.9862 ± 0.0001 and 1542 ± 0.4 MHz, respectively, Table 17. The intensity of the ^{197}Au-ES spectrum decreased as the sample was subjected to higher temperatures and was no longer visible at temperatures > 130 K.

The EPR spectrum of the central feature, L, centered at g = 2.0080 and recorded over a 200 G scan range, shows unresolved hyperfine interaction, Figure 82a. A simulation of the spectrum was constructed, Figure 81b, with the FORTRAN program ISOPLOT, assuming the interaction of the unpaired electron with one gold and eight hydrogen nuclei where, a_{Au} = 47.6 MHz, $a_H(8)$ = 21.7 MHz, and g = 2.0080. The EPR spectrum of the central region looked quite different when the sample was annealed, Figure 83. At 140 K there were new broad lines in the spectrum at g values larger than 2.0023 that decayed as the temperature was increased to 220 K. On closer examination of the EPR spectrum recorded at 180 K, Figure 84, two quartets were observed (highlighted with dashed lines); the quartet at g = 2.0134 had a spacing of 14 MHz while that at g = 1.9953 had a spacing of 17 MHz.

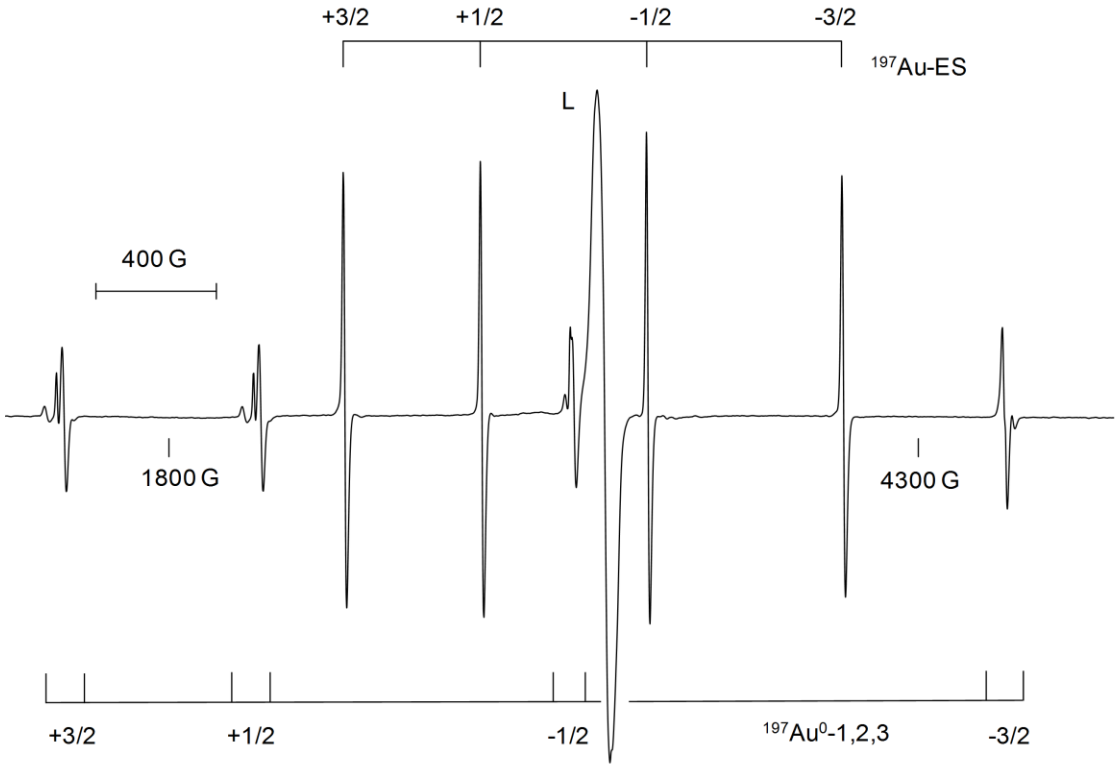

Figure 81. EPR spectrum recorded at 77 K (ν = 9086 MHz, m.p. = 2 mW), of the paramagnetic products, $^{197}Au^0$-1, $^{197}Au^0$-2, $^{197}Au^0$-3, ^{197}Au-ES, and L, formed in the reaction of ^{197}Au atoms with ethylene sulfide in an adamantane matrix.

Table 17. The magnetic parameters of $^{197}Au^0$-1, $^{197}Au^0$-2, $^{197}Au^0$-3, and ^{197}Au-ES, formed in the reaction of ^{197}Au atoms with ethylene sulfide in adamantane.

	a_{Au} (MHz)	g	Temperature	ν (MHz)
$^{197}Au^0$-1	2933 ± 0.7	2.0008 ± 0.0002	77 K	9086
$^{197}Au^0$-2	2881 ± 0.9	2.0015 ± 0.0002		
$^{197}Au^0$-3	2855 ± 1.3	2.0008 ± 0.0004		
^{197}Au-ES-1	1542 ± 0.4	1.9862 ± 0.0001		

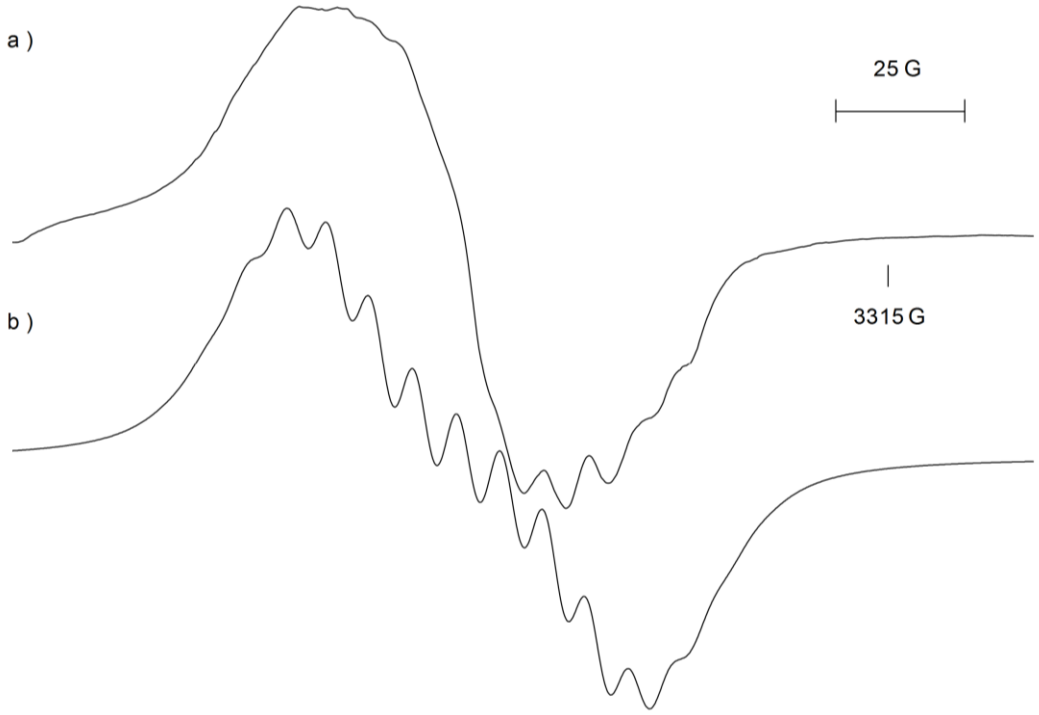

Figure 82. a) EPR spectrum of L at 77 K over a 200 G scan range (ν = 9086 MHz, m.p. = 2 mW). b) Simulation of the experimental EPR spectrum of L, using the FORTRAN program ISOPLOT, assuming, a_{Au} = 47.6 MHz, a_H(8) = 21.7 MHz, and g = 2.0080.

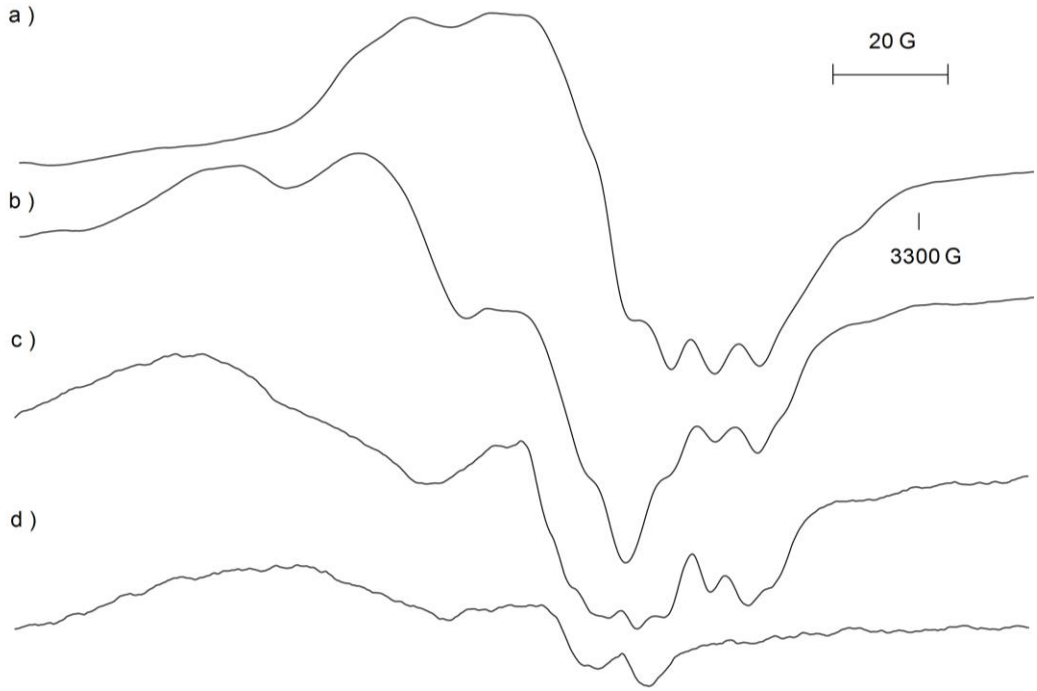

Figure 83. The effect of temperature on the central region of the ^{197}Au atom-ethylene sulfide EPR spectrum, L, recorded over 200 G at a) 100 K, b) 140 K, c) 180 K and d) 220 K. All spectra recorded at ν = 9120 MHz and m.p. = 2 mW.

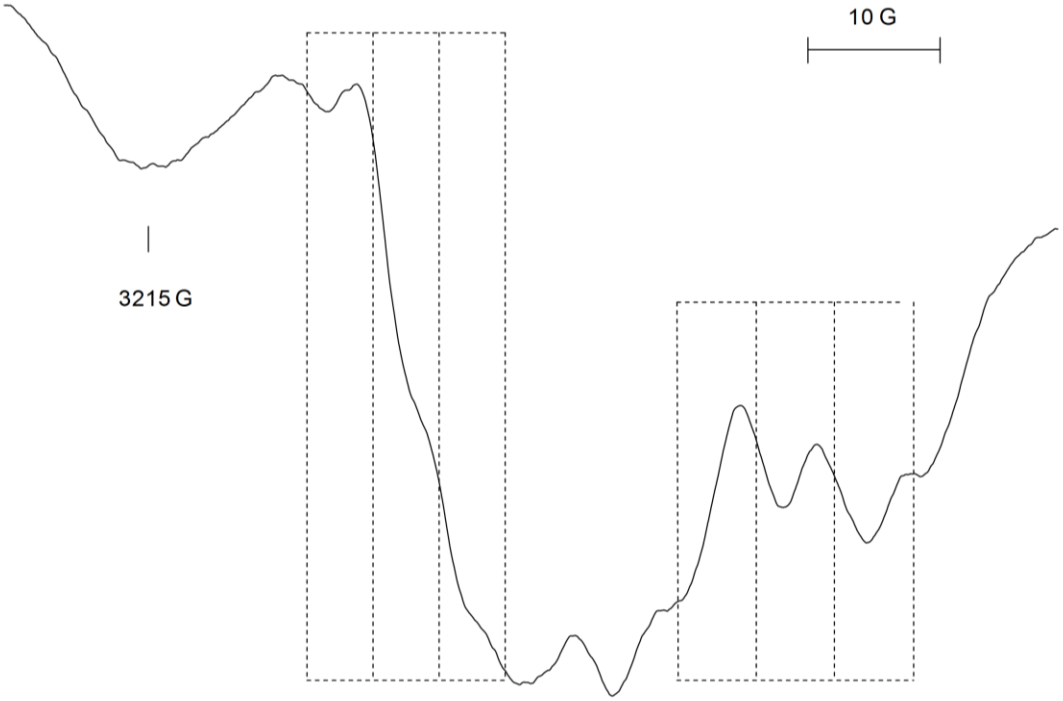

Figure 84. Central portion of the EPR spectrum of the ^{197}Au atom-ethylene sulfide reaction mixture at 180 K over an 80 G scan range (ν = 9086 MHz, m.p. = 2 mW). The dashed lines represent the position of transition lines of the two quartets described in the text.

4.3.3. Aziridines

4.3.3.1. Aziridine-^{14}N

The ^{197}Au atoms (I= 3/2) were reacted with aziridine in an adamantane matrix at 77 K using the rotating cryostat. The EPR spectrum given by the resulting light pink deposit at 77 K, Figure 85, consisted of four quartets, ^{197}Au^0-1, ^{197}Au^0-2, ^{197}Au^0-3, and ^{197}Au-Az-1. The transition lines marked, ^{197}Au^0-1, ^{197}Au^0-2, and ^{197}Au^0-3, can be assigned to ^{197}Au atoms isolated in adamantane in three different trapping sites.[36] The magnetic parameters, a_{Au} and g values, Table 18, were determined with the aid of ESRLSQ. Upon closer examination, the transitions of ^{197}Au-Az-1 are split into triplets, suggesting that the magnetic moment of the unpaired electron interacts with both a N nucleus (I = 1)

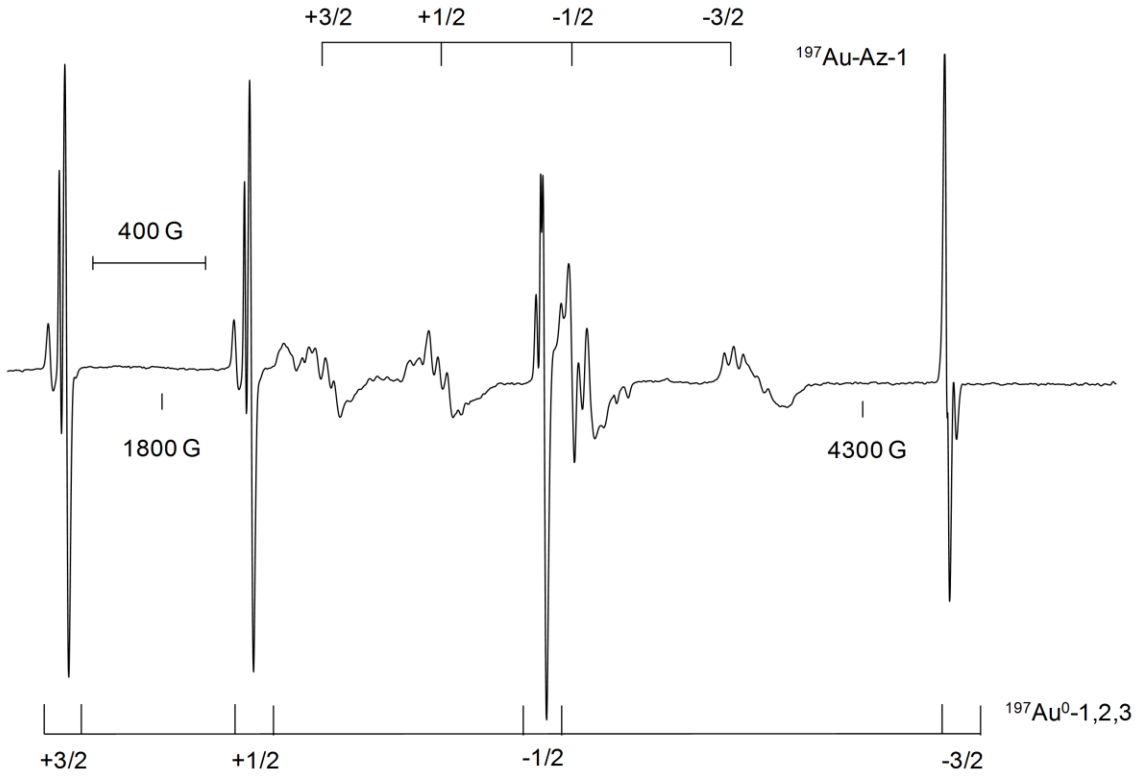

Figure 85. EPR spectrum recorded at 77 K (ν = 9121 MHz, m.p. = 2 mW), of the paramagnetic products, $^{197}Au^0$-1, $^{197}Au^0$-2, $^{197}Au^0$-3, and ^{197}Au-Az-1, formed in the reaction of ^{197}Au atoms with aziridine in an adamantane matrix.

Table 18. The magnetic parameters of $^{197}Au^0$-1, $^{197}Au^0$-2, $^{197}Au^0$-3, ^{197}Au-Az-1, ^{197}Au-Az-2, ^{197}Au-Az^{15}N-1, and ^{197}Au-Az^{15}N-2, formed in the reactions of ^{197}Au atoms with aziridine or its isotopomer, aziridine-^{15}N in adamantane.

Aziridine	a_{Au} (MHz)	a_{14N} (MHz)	g	Temp.	ν (MHz)
$^{197}Au^0$-1	2932 ± 0.3	-	2.0011 ± 0.0001		
$^{197}Au^0$-2	2881 ± 0.9	-	2.0016 ± 0.0002	77 K	9121
$^{197}Au^0$-3	2856 ± 0.7	-	2.0004 ± 0.0002		
^{197}Au-Az-1 (‖)	1417 ± 2.5	114	1.9867 ± 0.0017	100 K	9121
^{197}Au-Az-1 (⊥)	1352 ± 6.2	92	2.0633 ± 0.0038		
^{197}Au-Az-2	1474 ± 0.4	101 ± 0.5	2.0332 ± 0.0001	200 K	9120
Aziridine-^{15}N	a_{Cu} (MHz)	a_{15N} (MHz)	g	Temp.	ν (MHz)
$^{197}Au^0$-1	2920 ± 0.7	-	2.0007 ± 0.0002		
$^{197}Au^0$-2	2881 ± 0.9	-	2.0013 ± 0.0002		
$^{197}Au^0$-3	2855 ± 0.7	-	2.0001 ± 0.0002	77 K	9086
^{197}Au-Az^{15}N-1 (‖)	1419 ± 3.3	159	1.9865 ± 0.0014		
^{197}Au-Az^{15}N-1 (⊥)	1351± 5.0	129	2.0634 ± 0.0003		
^{197}Au-Az^{15}N-2	1476 ± 0.5	142 ± 1.2	2.0328 ± 0.0001	200 K	9118

and the ^{197}Au (I = 3/2) nucleus. When the sample was annealed to 100 K, Figure 86a, it became evident that the spectrum was anisotropic with the ^{197}Au and ^{14}N transitions split into parallel and perpendicular components. In addition, the interesting features, labelled Q (halfway between the first two transitions and last two transitions) with a triplet spacing of ~ 104 MHz, are assigned to forbidden transitions caused by nuclear quadrupole interaction.[72] The a_{Au}, a_{14N}, and the g-values, were determined using the magnetic field positions of the parallel and perpendicular transition lines and the ANISO program, Table 18. A simulation of the EPR spectrum was constructed, Figure 86b, with the EPR-NMR program using the magnetic parameters in Table 18, assuming the presence of quadrupole (P) interaction from the Au nucleus, i.e., $P_{\|}$ = 98 MHz and $P_{\perp}$= - $P_{\|}$/2. The magnitude of $P_{\|}$ was determined to be 98 ± 14 MHz based on the simulation of the experimental spectrum. Generally speaking, the inclusion of quadrupole interactions in the simulations results in slight changes in the line shape and position of the spectral lines, with the m_I = +3/2 and m_I = -3/2 transitions shifting downfield and upfield, respectively. However, inclusion of $P_{\|} \geq$ 45 MHz in the simulation caused the transition lines associated with the parallel components of ^{197}Au-Az-1 to vanish.

Warming the sample in the cavity of the spectrometer above 170 K, revealed the presence of a second Au-containing species, ^{197}Au-Az-2. The EPR spectrum of ^{197}Au-Az-2, recorded at 200 K, is isotropic, Figure 87a. The magnetic parameters, calculated with the ESRLSQ program from the magnetic field positions of the transition lines, are listed in Table 18, alongside those of ^{197}Au-Az-1. A simulation of the experimental spectrum, Figure 87b, was constructed using the a_{Au}, a_{14N}, and g values of ^{197}Au-Az-2. Upon reexamining the EPR spectrum recorded at 100 K, it was concluded that ^{197}Au-Az-2 was

in fact present. Its transition lines were, however, obscured by those of ^{197}Au-Az-1, Figure 86a. As was the case with ^{197}Au-Az-1, the low temperature spectrum for ^{197}Au-Az-2 displays axial symmetry and the magnetic parameters of ^{197}Au-Az-2, $a_{Au\perp}$ = 1452 MHz, $a_{Au\parallel}$ = 1527 MHz, $a_{N\perp}$ = 104 MHz, $a_{N\parallel}$ = 97 MHz, $g_{\perp}$ = 2.0191, and $g_{\parallel}$ = 2.0585, were obtained by simulating the experimental spectrum with EPR-NMR, Figure 86c. By combining the EPR-NMR simulations of ^{197}Au-Az-1 and ^{197}Au-Az-2 in a 1.6:1 ratio, Figure 86d, a better simulation of the experimental EPR spectrum was achieved.

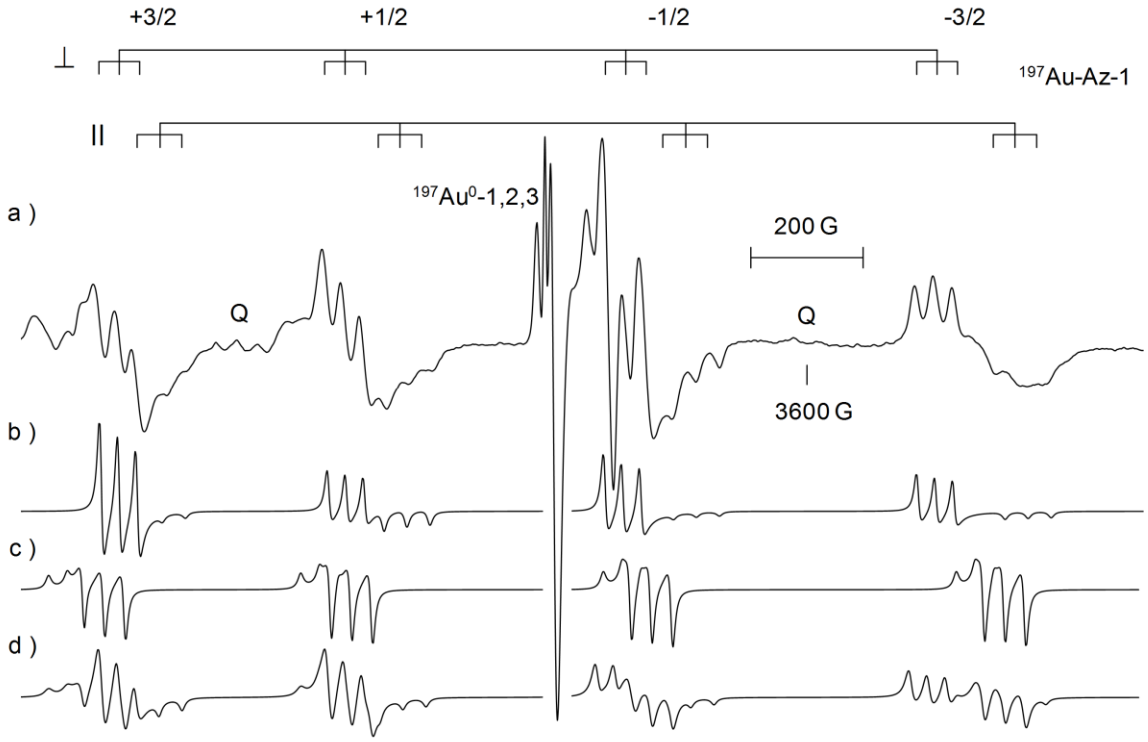

Figure 86. a) Anisotropic EPR spectrum recorded at 100 K (v = 9120 MHz, m.p. = 2 mW), of ^{197}Au-Az-1 formed in the reaction of ^{197}Au atoms and aziridine (forbidden transitions labeled Q). b) Simulated spectrum of ^{197}Au-Az-1 using the magnetic parameters in Table 18. c) Simulated spectrum of ^{197}Au-Az-2 using the anisotropic parameters in the text. d) Simulations of ^{197}Au-Az-1 and ^{197}Au-Az-2 combined assuming a ratio of 1.6:1, respectively.

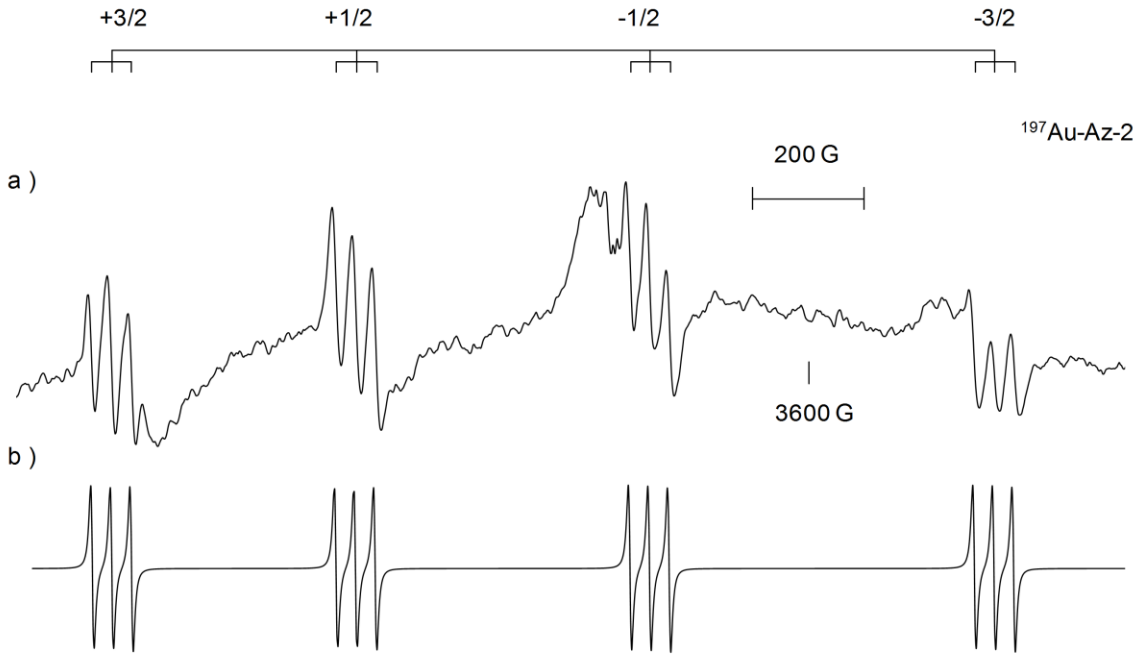

Figure 87. EPR spectrum recorded at 200 K (ν = 9120 MHz, m.p. = 2 mW) of ^{197}Au-Az-2 formed in the reaction of ^{197}Au atoms with aziridine in an adamantane matrix. b) Simulated spectra of ^{197}Au-Az-2 using the magnetic parameters listed in Table 18.

At low temperatures, the central region of the EPR spectrum, ~3250 G, was dominated by the m_I = -1/2 transitions of ^{197}Au-Az^{15}N-1 and ^{197}Au-Az^{15}N-2. However, when the sample was annealed above 180 K, additional lines were visible. At 220 K, an intense quintet of triplets was observed, Figure 88a. This spectrum, centered at g = 2.0041, involves the interaction of an unpaired electron with four equivalent H nuclei (I = 1/2) with $a_H(4)$ = 86 MHz and one ^{14}N nuclei (I = 1) with a_{14N} = 35 MHz, attributed to the aziridino-^{14}N radical.[104] The experimental EPR spectrum was simulated with the FORTRAN program ISOPLOT and the magnetic parameters mentioned above, Figure 88b.

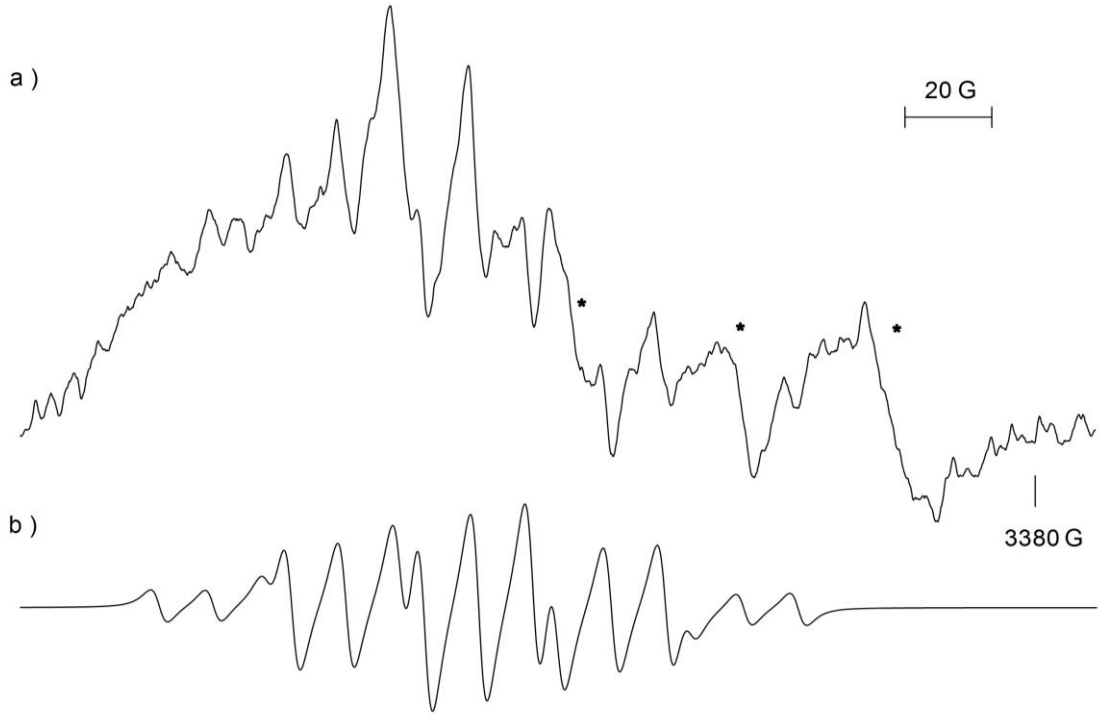

Figure 88. a) Central portion of the EPR spectrum recorded at 220 K (v = 9120 MHz, m.p. = 20 mW), of the ^{197}Au atom-aziridine reaction mixture over a 200 G range. b) Simulated spectrum of the aziridino radical using ISOPLOT, with $a_H(4)$ = 86 MHz and a_{14N} = 35 MHz, and g = 2.0041 (LW = 11 MHz). *m_I = -1/2 transition of ^{197}Au-Az-2.

4.3.3.2. Aziridine-^{15}N

Repeating the ^{197}Au atom reaction with aziridine-^{15}N also resulted in the formation of a light pink deposit. The EPR spectrum recorded at 77 K consisted of four quartets, Figure 89. The quartets labelled $^{197}Au^0$-1, $^{197}Au^0$-2, and $^{197}Au^0$-3, are assigned to trapped Au atoms in three distinct sites based on the magnetic parameters determined from the magnetic field positions of the transition lines,[36] Table 18. The transition lines of the fourth quartet, ^{197}Au-Az^{15}N-1, are further split into doublets, from the interaction of the isotopically enriched nitrogen nucleus, ^{15}N (I = 1/2) with the magnetic moment of the unpaired electron. The parallel and perpendicular components of ^{197}Au-Az^{15}N-1, as well

as the forbidden transitions with a doublet spacing of ~146 MHz (Q), are evident in Figure 90a. The EPR parameters of ^{197}Au-Az^{15}N-1, Table 18, were determined using the magnetic field positions of the transitions recorded from calibrated spectra and the computer program ANISO. A simulated spectrum of ^{197}Au-Az^{15}N-1, Figure 90b, was constructed with the magnetic parameters in Table 18, assuming $P_{\|}$ = 98 MHz and $P_{\perp} = -P_{\|}/2$.

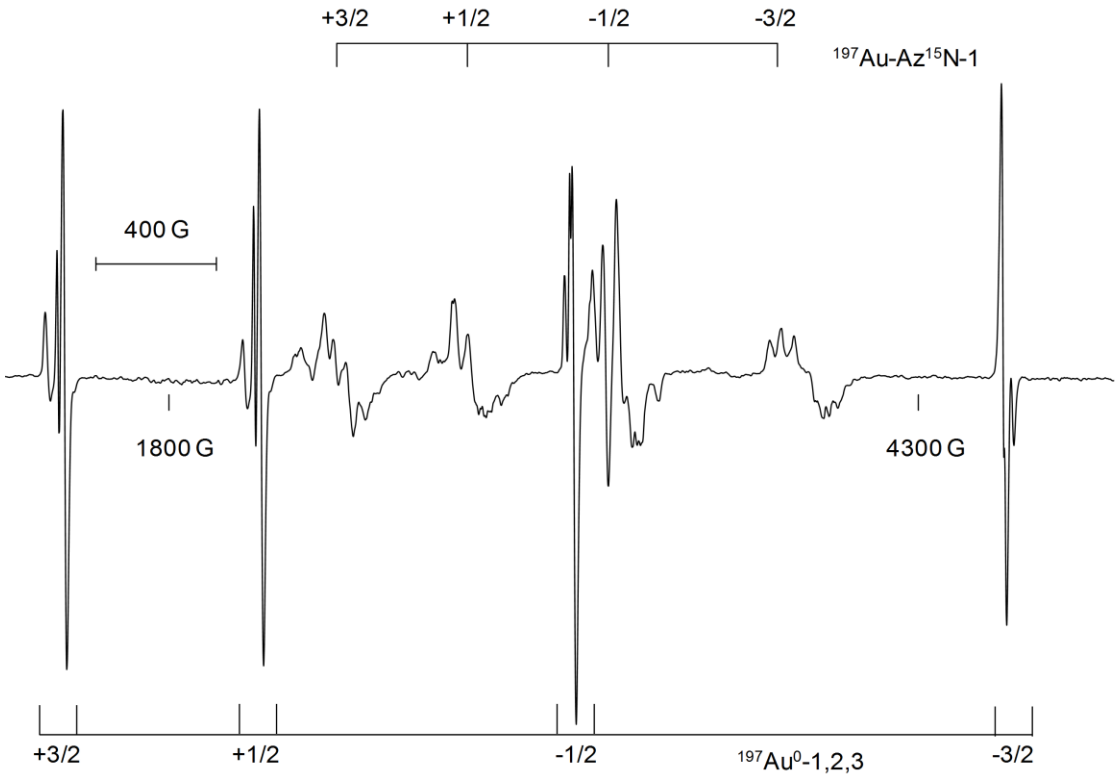

Figure 89. EPR spectrum recorded at 77 K (v = 9086 MHz, m.p = 2 mW), of the paramagnetic products, ^{197}Au^{0}-1, ^{197}Au^{0}-2, ^{197}Au^{0}-3, and ^{197}Au-Az^{15}N-1 formed in the reaction of ^{197}Au atoms with aziridine-^{15}N in an adamantane matrix.

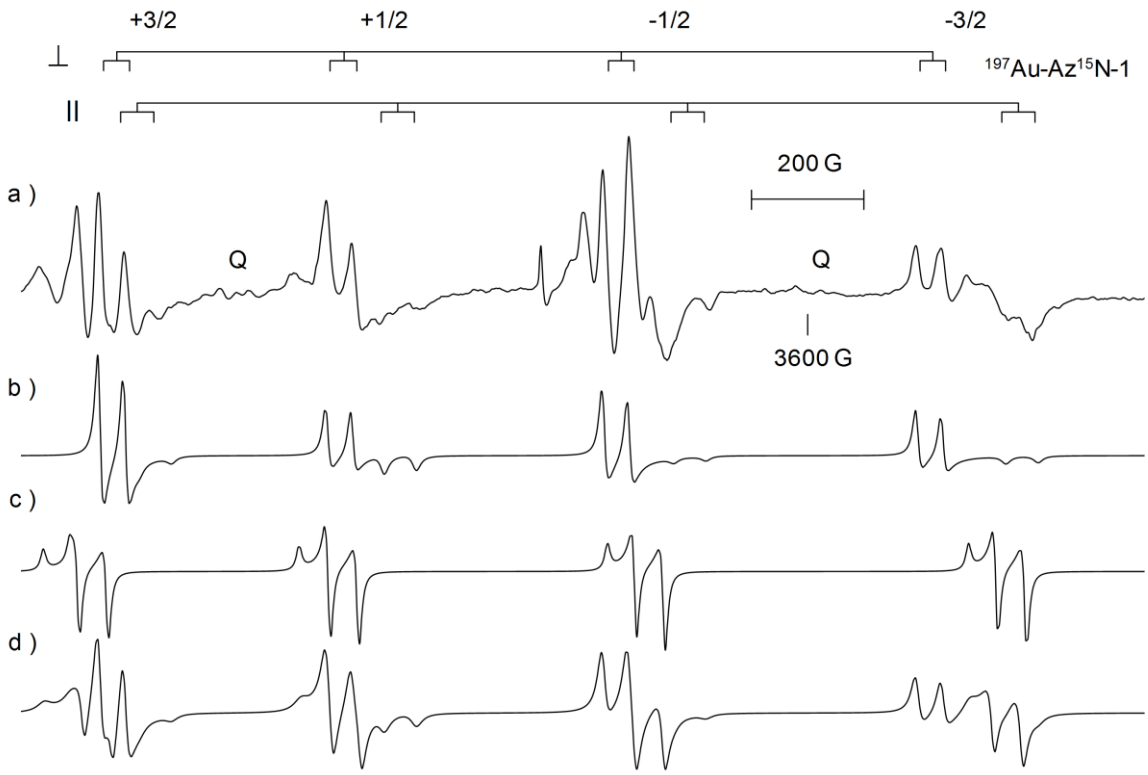

Figure 90. a) Anisotropic EPR spectrum recorded at 77 K (v = 9086 MHz, m.p. = 2 mW), of ^{197}Au-Az^{15}N-1 formed in the reaction of ^{197}Au atoms and aziridine-^{15}N with forbidden transitions labeled, Q. b) Simulated spectrum of ^{197}Au-Az^{15}N-1 using the magnetic parameters in Table 18. c) Simulated spectrum of ^{197}Au-Az^{15}N-2 using the anisotropic parameters in the text. d) Simulations of ^{197}Au-Az^{15}N-1 and ^{197}Au-Az^{15}N-2 combined.

A second Au-containing species, ^{197}Au-Az^{15}N-2, concealed at lower temperatures by overlapping peaks of ^{197}Au-Az^{15}N-1, developed into an isotropic quartet of doublets when the sample was annealed to 220 K in the cavity of the spectrometer, Figure 91a. The experimental spectrum, Figure 91b, was simulated using the a_{Au}, a_{15N} and g-values, Table 18, for ^{197}Au-Az^{15}N-2. ^{197}Au-Az^{15}N-2 is believed to be anisotropic just like ^{197}Au-Az^{15}N-1 at 77 K and becomes isotropic through rotational motion at 200 K. The anisotropic parameters, $a_{Au_\perp}$ = 1452 MHz, $a_{Au_\parallel}$ = 1527 MHz, $a_{15N_\perp}$ = 145 MHz, $a_{15N_\parallel}$ = 135 MHz, $g_\perp$ = 2.0191, and $g_\parallel$ = 2.0585, of ^{197}Au-Az^{15}N-2 were determined through simulation, Figure 90c. A better representation of the experimental spectrum

observed at 77 K, Figure 90a, was achieved by combining simulations of both ^{197}Au-Az^{15}N-1 and ^{197}Au-Az^{15}N-2 in a 1.6:1 ratio, respectively, Figure 90d.

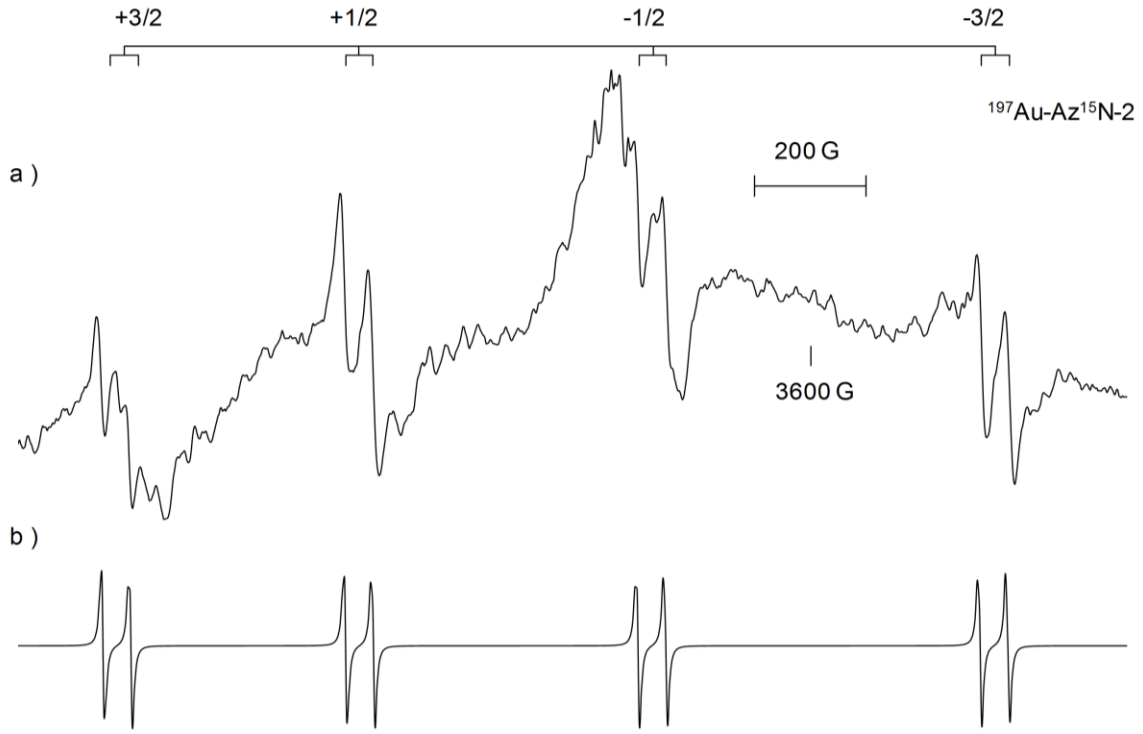

Figure 91. EPR spectrum recorded at 220 K (ν = 9120 MHz, m.p. = 2 mW), of ^{197}Au-Az^{15}N-2 formed in the reaction of ^{197}Au atoms with aziridine in an adamantane matrix. b) Simulated spectra of ^{197}Au-Az^{15}N-2 using the magnetic parameters listed in Table 18.

The effect of temperature on the EPR spectrum of the ^{197}Au atom-aziridine-^{15}N reaction mixture is shown in Figure 92. Both ^{197}Au-Az^{15}N-1 and ^{197}Au-Az^{15}N-2 were anisotropic at 77 K. As the sample was annealed to 220 K, the signals of ^{197}Au-Az^{15}N-2 became isotropic and dominated the spectrum, whereas the transitions of ^{197}Au-Az^{15}N-1 were barely visible. When the sample was recooled to 77 K, a spectrum identical to that observed before warming was observed, with the exception of transitions belonging to isolated ^{197}Au atoms, Figure 92d. ^{197}Au-Az^{15}N-2 reverted back to a characteristic

anisotropic pattern and was a minor species compared to the intense lines of ^{197}Au-Az^{15}N-1.

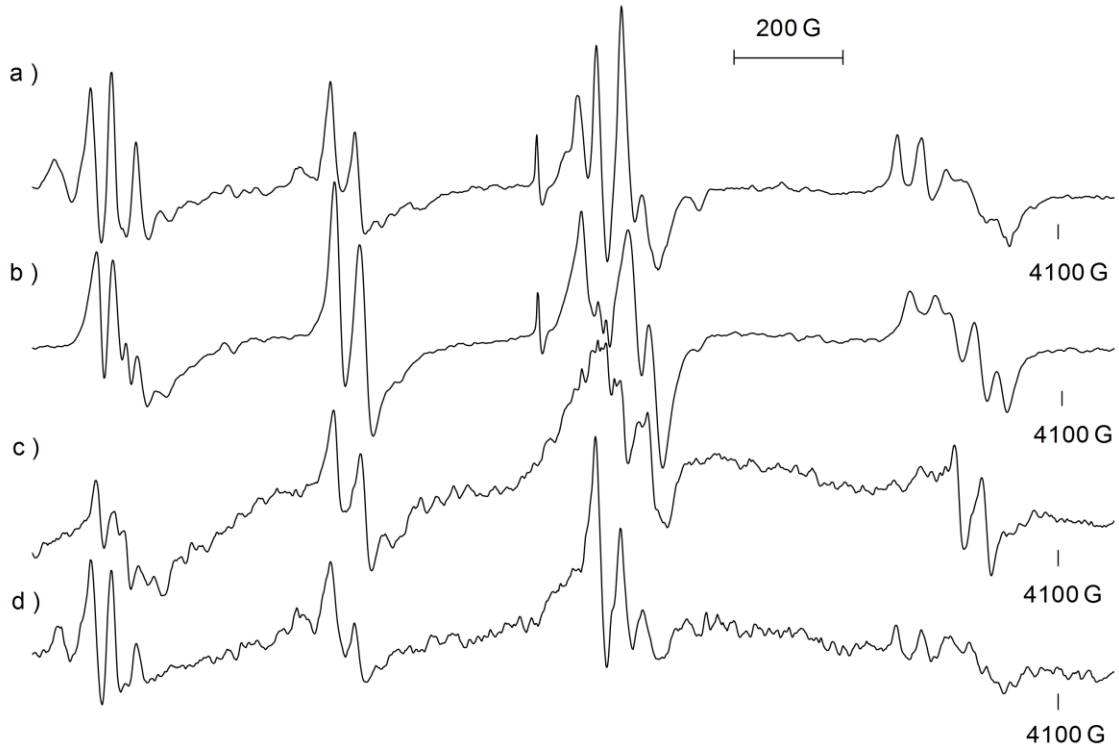

Figure 92. The effect of temperature on the EPR spectrum recorded for the ^{197}Au atom-aziridine-^{15}N reaction mixture at a) 77 K (ν = 9086 MHz, m.p. = 2 mW), b) 170 K (ν = 9119 MHz, m.p. = 10 mW), c) 220 K (ν = 9118 MHz, m.p. = 20 mW) and d) recooled to 77 K (ν = 9086 MHz, m.p. = 10 mW).

The central region of the EPR spectrum, ~3250 G, was dominated by the m_I = -1/2 transitions of the ^{197}Au-Az^{15}N-1 and ^{197}Au-Az^{15}N-2 at 77 K. However, when the sample was annealed above 180 K, additional lines were visible. At 210 K, an intense quintet of doublets was observed, Figure 93a. This spectrum centered at g = 2.0046 involves the interaction of an unpaired electron with four equivalent H nuclei with a_H(4) = 85 MHz and one ^{15}N nuclei (I = 1/2) with a_{15N} = 49 MHz, attributed to the aziridino-^{15}N radical, observed previously in the reaction of $^{107/109}$Ag atoms with aziridine-^{15}N. A

simulation of the aziridino-^{15}N radical, Figure 93b, was constructed using ISOPLOT and the magnetic parameters mentioned above. The aziridino-^{15}N radical persisted to temperatures > 220 K and also upon recooling to 77 K.

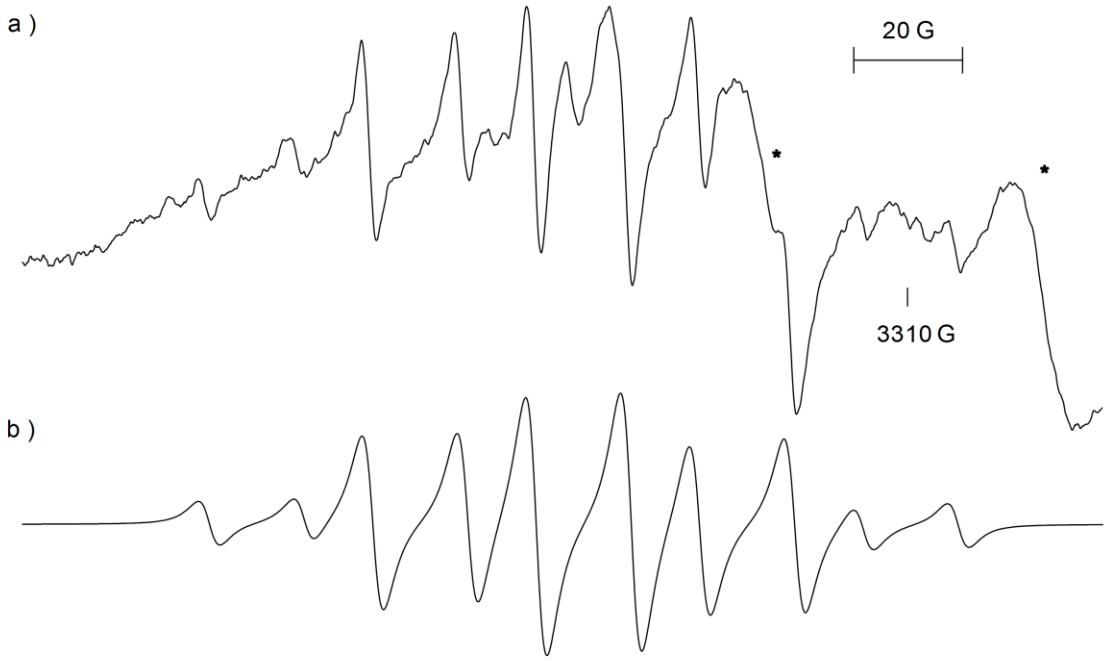

Figure 93. a) Central region of the EPR spectrum, recorded at 210 K (v = 9118 MHz, m.p. = 50 mW) of the ^{197}Au atom-aziridine-^{15}N reaction mixture over a 200 G range. B) Simulated spectrum of the aziridino-^{15}N radical using ISOPLOT, with $a_{H}(4)$ = 84.8 MHz, a_{15N} = 49.2, and g = 2.0046 (LW = 11 MHz). *m_I = -1/2 transition of ^{197}Au-Az^{15}N-2.

4.4. Temperature effects on a_M

Species with large metal-hyperfine interactions were observed in many of the Group 11 metal atom-heterocyclic compound reactions described above. When the samples collected from the reactions of $^{63/65}$Cu or $^{107/109}$Ag atoms with ethylene oxide, ethylene oxide-d_4, aziridine-^{15}N, and styrene oxide were annealed in the cavity of the EPR spectrometer, an increase in the a_M values was observed as the temperature increased while the *g*-value remained relatively constant, Tables 19 and 20. The paramagnetic products formed in reactions of the Group 11 metal atoms and ethylene sulfide, yielded species with large a_M values but they did not exist beyond 130 K, restricting the temperature study. In reactions of ^{197}Au atoms and ethylene oxide or $^{63/65}$Cu atoms and styrene oxide the same phenomenon was observed but accurate data could not be obtained since the products were formed in relatively low concentrations. However, the m_I = +3/2 and ± 1/2 transition lines of the Cu-centered radicals shifted to lower field while the m_I = -3/2 transition shifted to higher field as the temperature of the sample was raised. Similarly, for Ag radicals the m_I = +1/2 and -1/2 transition lines were shifted to lower and higher field, respectively, as the temperature was increased. The change in a_M observed between 77 and 200 K, Table 21, varied from 1.4 – 3.3 %. The % change for ^{63}Cu-EO-d_4-1 was determined between 77 and 200 K, as the EPR signals did not persist beyond 160 K. Interestingly, for reactions with ^{197}Au atoms, the transition lines of ^{197}Au-ES or ^{197}Au-Az-1 did not shift as a function of increasing temperature.

The a_M values of ^{63}Cu-EO-1, ^{63}Cu-Az^{15}N-1, ^{109}Ag-Az^{15}N-1, ^{109}Ag-EO, ^{109}Ag-SO-1, and ^{109}Ag-ES-2, were plotted as a function of temperature, Figures 93-94. The data

was fitted using a second order polynomial, Table 22. Error bars have been included when possible, i.e., the standard deviation of the a_M values provided ESRLSQ. Generally speaking, all the plots have positive trends while ^{109}Ag-EO, ^{63}Cu-Az^{15}N-1, and ^{109}Ag-Az^{15}N-1 are concave up and ^{63}Cu-EO-1 and ^{109}Ag-SO-1 are both concave down.

Table 19. EPR parameters of some Ag-containing species at various temperatures.

Species	Temperature (K)	ν (MHz)	g_{107Ag}	a_{107Ag} (MHz)	g_{109Ag}	a_{109Ag} (MHz)
Ag-EO	77	9138	2.0016	1619	2.0017	1867
	100	9113	2.0014	1627	2.0012	1881
	110	9112	2.0015	1630	2.0016	1883
	120	9112	2.0015	1633	2.0013	1886
	130	9113	2.0014	1635	2.0013	1889
	140	9114	2.0019	1638	2.0016	1892
	150	9115	2.0017	1641	2.0016	1894
	160	9116	2.0014	1642	2.0015	1897
	200	9118	2.0017	1650	2.0018	1907
Ag-Az^{15}N-1	77	9088	1.9999	1336	2.0000	1543
	100	9121	1.9999	1337	1.9996	1548
	120	9120	1.9998	1342	1.9994	1553
	140	9120	1.9999	1347	1.9996	1555
	160	9120	1.9998	1349	1.9995	1560
	180	9120	1.9999	1355	1.9996	1565
	200	9120	1.9998	1357	1.9994	1567
	220	9119	1.9999	1360	1.9995	1571
	77[a]	9088	1.9999	1338	2.0003	1543
Ag-SO-1	77	9139	2.0009	1524	2.0010	1757
	100	9119	2.0010	1528	2.0008	1765
	110	9119	2.0008	1533	2.0008	1769
	120	9120	2.0012	1538	2.0009	1774
	130	9120	2.0009	1542	2.0008	1780
	140	9120	2.0008	1550	2.0009	1783
	150	9120	2.0010	1549	2.0008	1787
	160	9119	2.0010	1555	2.0010	1795
	170	9119	2.0011	1557	2.0011	1799
	180	9119	2.0010	1562	2.0008	1806
	200	9119	2.0011	1574	2.0013	1815

[a]Recooled after annealed to 220 K.

Table 20. EPR parameters of some Cu-containing species at various temperatures.

Species	Temperature (K)	ν (MHz)	g	a_{Cu} (MHz)
^{63}Cu-EO-d$_4$-1	77	9087	2.0098 ± 0.0014	4337 ± 4.7
	100	9122	2.0096 ± 0.0019	4349 ± 6.5
	110	9121	2.0108 ± 0.0010	4363 ± 4.9
	120	9121	2.0110 ± 0.0010	4371 ± 3.5
	130	9121	2.0099 ± 0.0014	4389 ± 5.0
	140	9120	2.0094 ± 0.0014	4401 ± 4.8
	150	9120	2.0098 ± 0.0010	4408 ± 3.4
^{63}Cu-Az^{15}N-1	77	9087	2.0098 ± 0.0002	3210 ± 0.7
	100	9121	2.0096 ± 0.0002	3221 ± 0.8
	120	9120	2.0096 ± 0.0001	3229 ± 0.3
	140	9120	2.0093 ± 0.0001	3239 ± 0.6
	160	9121	2.0089 ± 0.0002	3248 ± 0.9
	180	9120	2.0098 ± 0.0003	3254 ± 0.9
	200	9121	2.0102 ± 0.0002	3258 ± 0.7
	220	9121	2.0097 ± 0.0001	3264 ± 0.4
	77[a]	9087	2.0097± 0.0001	3209 ± 0.5
^{65}Cu-Az^{15}N-1	77	9087	2.0090 ± 0.0003	3441 ± 1.2
	100	9121	2.0098 ± 0.0002	3451 ± 0.7
	120	9120	2.0096 ± 0.0002	3460 ± 0.9
	140	9120	2.0094 ± 0.0002	3469 ± 0.9
	160	9121	2.0095 ± 0.0002	3478 ± 0.7
	180	9120	2.0102 ± 0.0001	3486 ± 0.2
	200	9121	2.0102 ± 0.0001	3489 ± 0.4
	220	9121	2.0107 ± 0.0002	3498 ± 0.8
	77[a]	9087	2.0091 ± 0.0002	3440 ± 0.8

[a]Recooled after annealed to 220 K.

Table 21. Increase in the metal hyperfine interaction (a_M) at 200 K relative to that determined at 77 K.

Species	Increase in a_M (MHz)	Increase in a_M (%)
^{63}Cu-EO-d$_4$-1	72[a]	1.7[a]
^{107}Ag-EO	31	1.9
^{109}Ag-EO	40	2.1
^{63}Cu-Az^{15}N-1	48	1.5
^{65}Cu-Az^{15}N-1	48	1.4
^{107}Ag-Az^{15}N-1	21	1.6
^{109}Ag-Az^{15}N-1	24	1.6
^{107}Ag-SO-1	50	3.3
^{109}Ag-SO-1	58	3.3

[a]Difference between 77 and 150 K.

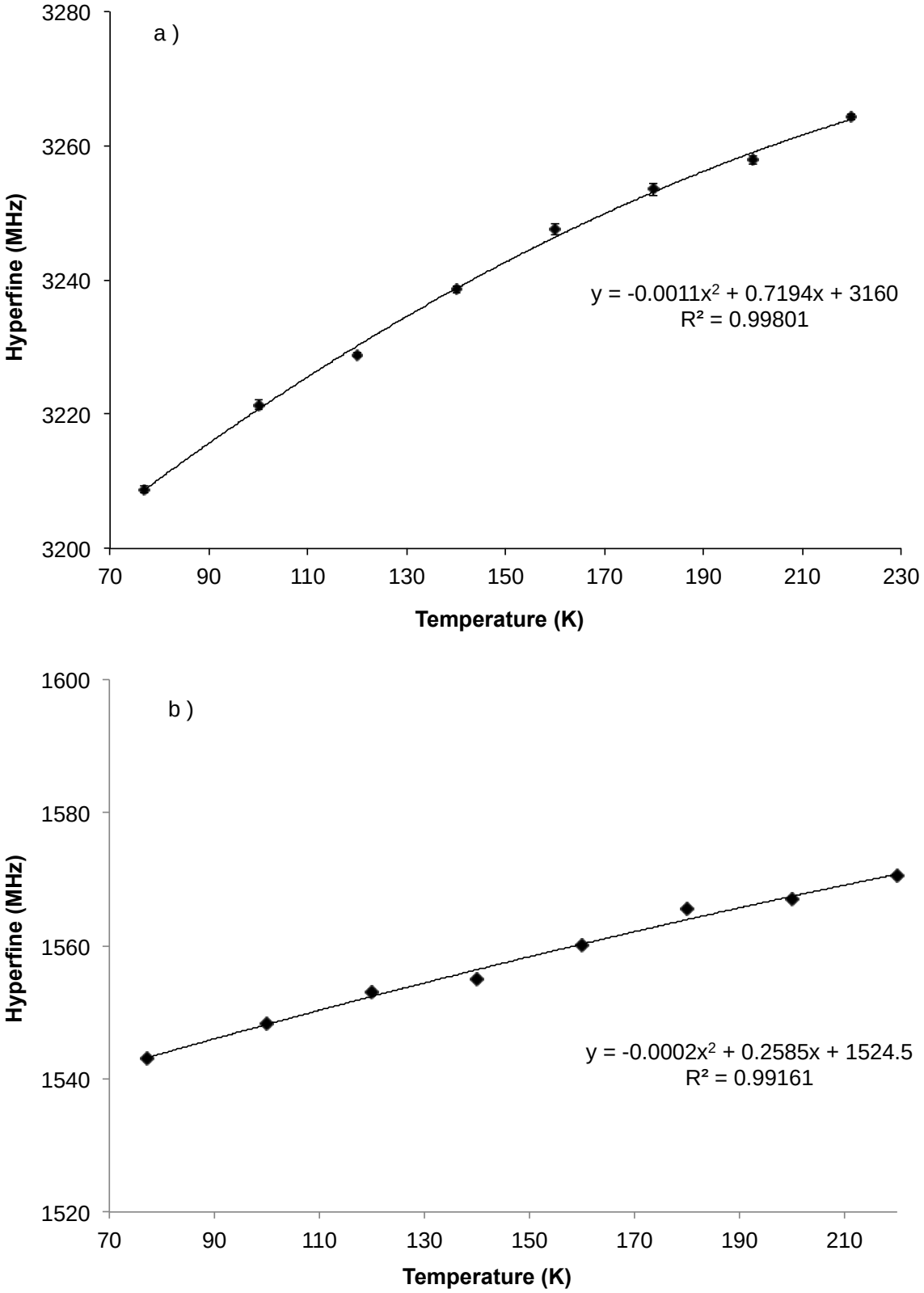

Figure 94. Plots of the hyperfine interaction values (a_M) as a function of temperature for a) ^{63}Cu-Az^{15}N-1 and b) ^{109}Ag-Az^{15}N-1.

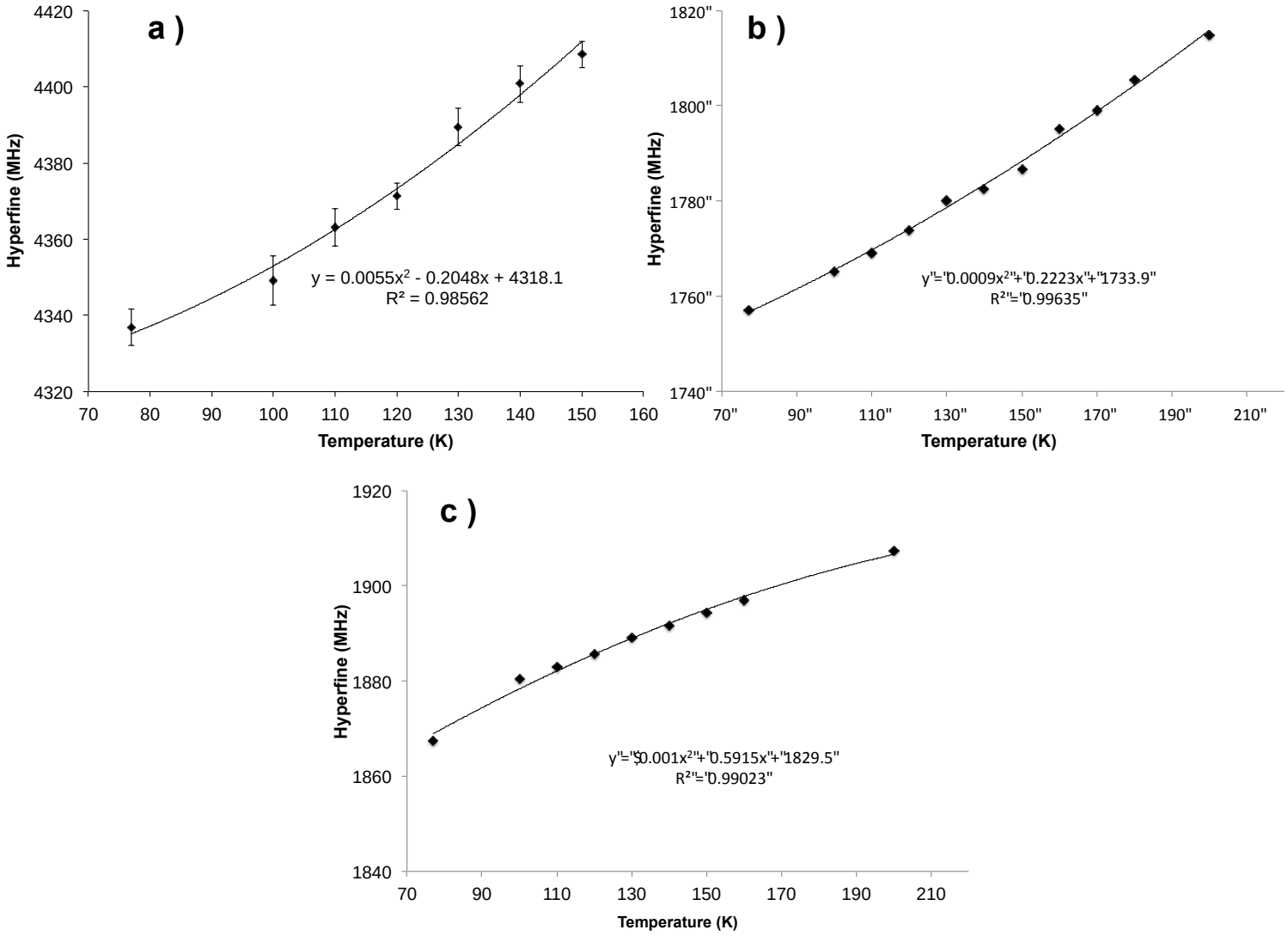

Figure 95. Plots of the hyperfine interaction values (a_M) as a function of temperature for a) ^{63}Cu-EO-d$_4$, b) ^{109}Ag-SO-1 and c) ^{109}Ag-EO.

Table 22. Equations of the trend lines and associated R^2-value of plots in Figures 94 and 95.

Species	Equation of the line	R^2 value
^{63}Cu-EO-d_4-1	$y = 0.0055x^2 - 0.2048x + 4318.1$	0.98562
^{63}Cu-Az^{15}N-1	$y = -0.0011x^2 + 0.7194x + 3160$	0.99801
^{109}Ag-EO	$y = -0.001x^2 + 0.5915x + 1829.5$	0.99023
^{109}Ag-SO-1	$y = 0.0009x^2 + 0.2223x + 1733.9$	0.99635
^{109}Ag-Az^{15}N-1	$y = -0.0002x^2 + 0.2585x + 1524.5$	0.99161

It is important to note that in the cases of $^{63/65}$Cu-Az^{15}N-1 and $^{107/109}$Az^{15}N-1, when the sample was recooled to 77 K after being annealed to 220 K, the transition lines reverted back to their original field positions, revealing a reversible phenomenon. Another interesting feature was that while the hyperfine interaction of the metal centers (a_M) increased as a function of temperature, the value of a_{15N} from the ligand interaction did not change.

4.5. DFT Calculations

4.5.1. Predictions of known a_{Nu} values

Theoretical calculations of nuclear hyperfine interaction values have been used in combination with experimental data to support the structural assignments of matrix-isolated paramagnetic molecules.[21] When it comes to Group 11 metal atom complexes and molecules, many researchers have used DFT to compare predicted and observed IR vibrations.[77,105] To our knowledge there is yet to be a published study involving the use of DFT to predict the hyperfine values of Cu(0)-containing molecules. Thus we decided to test the efficacy of several DFT methods at predicting the a_{63Cu} for known paramagnetic Cu(0) complexes before progressing onto new structures proposed in the present study. That being said we chose to use the functionals, B3LYP, frequently used as a standard in

many calculations, M06, cited to work well for long-range and dispersion interactions with transition metals,[106] and the hybrid functional, BHandHLYP. Each functional was used in conjunction with a number of basis sets, namely 6-311G, 6-311+G, 6-311+G(d), EPR-III, and 6-31++G(d,p). All optimized geometry information (bond lengths, angles and dihedral angles) can be found in the Appendix section (see sections 8.1.1 and 8.1.2).

Tables 23 and 24 contain the predicted Cu nuclear hyperfine interaction values, a_{63Cu}, of $^{63}Cu^0$, σ-bonded ($^{63}CuCO$, $^{63}Cu(CO)_3$, $^{63}CuSiO$ and $^{63}CuNH_3$) and π-bonded ($^{63}CuC_2H_4$, $^{63}Cu(C_2H_4)_2$, $^{63}Cu(C_2H_2)_2$, and $^{63}CuHCN$) complexes. The corresponding % deviation from the experimental values is recorded in brackets. In general, poor agreement was found between the experimental a_{63Cu} and values predicted by all functionals when the 6-311G basis set was used. Experimental values of a_{63Cu} adhere to the following trend, $^{63}Cu^0 >> {}^{63}CuSiO > {}^{63}CuCO > {}^{63}CuNH_3 >> {}^{63}Cu(CO)_3$. All the calculated a_{63Cu} values follow the same trend with the exception of the a_{63Cu} values calculated at the BHandHLYP/6-311+G and B3LYP/6-31++G(d,p) level of theory. The experimental a_{63Cu} value of the π-bonded Cu complexes follow the trend, $^{63}Cu[HCN] > {}^{63}Cu[C_2H_4] >> {}^{63}Cu[C_2H_4]_2 \approx {}^{63}Cu[C_2H_2]_2$. Only the M06 calculation predicts the relative order of the a_{63Cu} for $^{63}Cu[HCN]$ and $^{63}Cu[C_2H_4]$. All calculations predict that the a_{63Cu} value of $^{63}Cu[C_2H_4]_2$ is greater than that of $^{63}Cu[C_2H_2]_2$, when in fact the experimental values are virtually identical. In spite of this, all calculations correctly predict that the a_{63Cu} values for $^{63}Cu[C_2H_4]_2$ and $^{63}Cu[C_2H_2]_2$ are much smaller than those for $^{63}Cu[HCN]$ and $^{63}Cu[C_2H_4]$.

Table 23. Predicted ^{63}Cu nuclear hyperfine interaction,[a] a_{63Cu}, of σ-bonded mononuclear-Cu complexes. (The values in parentheses are the % difference between the calculated and experimental hyperfine interaction values.)[b]

Functional	Basis Set	$^{63}Cu^0$	σ - Bonded Complexes			
			$^{63}CuCO$	$^{63}Cu(CO)_3$	$^{63}CuSiO$	$^{63}CuNH_3$
B3LYP	6-311G	2518 (59.1, 56.2)[c]	3344 (19.3, 15.6)[c]	30 (57.7, 68.1)[c]	3617 (14.7)	1251 (65.6)
	6-311+G	5647 (8.2, 1.7)[c]	3891 (6.1, 1.8)[c]	5 (93.0, 94.7)[c]	4131 (2.5)	3165 (12.9)
	6-311+G(d)	5647 (8.2, 1.7)[c]	4106 (0.9, 3.7)[c]	6 (91.5, 93.6)[c]	4186 (1.2)	3325 (8.5)
	EPR-III[d]	5647 (8.2, 1.7)[c]	4068 (1.8, 2.7)[c]	8 (88.7, 91.5)[c]	e	3354 (7.7)
	6-31++G(d,p)[d]	5647 (8.2, 1.7)[c]	4071 (1.7, 2.8)[c]	8 (88.7, 91.5)[c]	4176 (1.5)	3336 (8.1)
M06	6-311G	2600 (57.7, 54.8)[c]	3492 (15.7, 11.8)[c]	15 (78.9, 84.0)[c]	3899 (8.0)	1529 (57.9)
	6-311+G	5661 (8.0, 1.5)[c]	3925 (5.2, 0.9)[c]	17 (76.1, 81.9)[c]	4154 (2.0)	3318 (8.6)
	6-311+G(d)	5661 (8.0, 1.5)[c]	4153 (0.3, 4.8)[c]	17(76.1, 81.9)[c]	4173 (1.5)	3493 (3.8)
	EPR-III[d]	5661 (8.0, 1.5)[c]	4127 (0.4, 4.2)[c]	7 (90.1, 92.6)[c]	e	3534 (2.7)
	6-31++G(d,p)[d]	5661 (8.0, 1.5)[c]	4125 (0.4, 4.1)[c]	20 (71.8, 78.7)[c]	4152 (2.0)	3542 (2.5)
BHandHLYP	6-311G	112 (98.2, 98.1)[c]	3513 (15.1, 11.3)[c]	77 (8.5, 18.1)[c]	3731 (12.0)	814 (77.6)
	6-311+G	5241 (14.8, 8.8)[c]	4059 (2.0, 2.5)[c]	43 (39.4, 54.3)[c]	4128 (2.6)	3198 (11.9)
	6-311+G(d)	5241 (14.8, 8.8)[c]	4377 (5.7, 10.5)[c]	48 (32.4, 48.9)[c]	4221 (0.4)	3344 (7.9)
	EPR-III[d]	5241 (14.8, 8.8)[c]	4317 (4.2, 9.0)[c]	52 (26.8, 44.7)[c]	e	3377 (7.0)
	6-31++G(d,p)[d]	5241 (14.8, 8.8)[c]	4324 (4.4, 9.2)[c]	48 (32.4, 48.9)[c]	4206 (0.8)	3374 (7.1)
Experimental	Argon	6151[f]	4142[h]	71[h]	4238[k]	3632[l]
	Adam	5746[g]	3961[i]	94[j]	-	-

[a]Hyperfine interaction in MHz. [b]% difference $[(a_{63Cu,\,exp} - a_{63Cu,\,calc})/a_{63Cu,\,exp}] \times 100$. [c]The two numbers within parentheses represent the % difference as defined in b, the first % difference was calculated using a_{63Cu}, Ar while the second calculated using a_{63Cu}, adamantane. [d]The 6-311+G(d) basis set was used for ^{63}Cu. [e]Si atoms are outside the basis set range. [f]Ref. 27. [g]Ref. 36. [h]Ref. 29. [i]Ref. 45. [j]Ref. 49. [k]Ref. 44. [l]Ref. 47.

Table 24. Predicted ^{63}Cu nuclear hyperfine interaction,[a] a_{63Cu}, of π-bonded mononuclear-Cu complexes. (The values in parentheses are the % difference between the calculated and experimental hyperfine interaction values.)[b]

Functional	Basis Set	π - Bonded Complex			
		$^{63}Cu[C_2H_4]$	$^{63}Cu[C_2H_4]_2$	$^{63}Cu[C_2H_2]_2$	^{63}Cu[HCN]
B3LYP	6-311G	2985 (25.3, 20.0)[c]	117 (5.6, 4.9)[c]	111 (12.6, 11.2)[c]	2580
	6-311+G	4375 (9.4, 17.3)[c]	99 (20.2, 19.5)[c]	76 (40.2, 39.2)[c]	4059
	6-311+G(d)	4243 (6.1, 13.8)[c]	91 (26.6, 26.0)[c]	74 (41.7, 40.8)[c]	4238
	EPR-III[d]	4252 (6.4, 14.0)[c]	90 (27.4, 26.8)[c]	76 (40.2, 39.2)[c]	4137
	6-31++G(d,p)[d]	4188 (4.8, 12.3)[c]	92 (25.8, 25.2)[c]	75 (40.9, 40.0)[c]	4147
M06	6-311G	3245 (18.8, 13.0)[c]	122 (1.6, 0.8)[c]	106 (16.5, 15.2)[c]	2671
	6-311+G	4131 (3.3, 10.8)[c]	136 (9.7, 10.6)[c]	104 (18.1, 16.8)[c]	4193
	6-311+G(d)	4059 (1.5, 8.8)[c]	129 (4.0, 4.9)[c]	105 (17.3, 16.0)[c]	4444
	EPR-III[d]	4075 (1.9, 9.2)[c]	127 (2.4, 3.3)[c]	102 (19.7,18.4)[c]	4137
	6-31++G(d,p)[d]	3982 (0.4, 6.8)[c]	130 (4.8, 5.7)[c]	106 (16.5, 15.2)[c]	4374
BHandHLYP	6-311G	3050 (23.7, 18.2)[c]	128 (3.2, 4.1)[c]	119 6.3, 4.8)[c]	2248
	6-311+G	5234 (30.9, 40.3)[c]	95 (23.4, 22.8)[c]	58 (54.3, 53.6)[c]	4070
	6-311+G(d)	5175 (29.4, 38.7)[c]	76 (38.7, 38.2)[c]	50 (60.6, 60.0)[c]	4368
	EPR-III[d]	5243 (31.1, 40.6)[c]	72 (41.9, 41.5)[c]	50 (60.6, 60.0)[c]	4200
	6-31++G(d,p)[d]	5058 (26.5, 35.6)[c]	79 (36.3, 35.8)[c]	53 (58.3, 57.6)[c]	4275
Experimental	Argon	3998[e]	124[e]	127[e]	-
	Adam	3730[f]	123[f]	125[g]	3884 – 4217[h]

[a]Hyperfine interaction in MHz. [b]% difference $[(a_{63Cu,\,exp} - a_{63Cu,\,calc})/a_{63Cu,\,exp}] \times 100$. [c]The two numbers within parentheses represent the % difference as defined in b, the first % difference was calculated using a_{63Cu}, Ar while the second calculated using a_{63Cu}, adamantane. [d]The 6-311+G(d) basis set was used for ^{63}Cu. [e]Ref. 37. [f]Ref. 38. [g]Ref. 41. [h]Ref. 42.

We studied the abilities of the five basis sets at predicting the ligand hyperfine interaction values, treating all non-metal atoms at the same level, Table 25. The results of the predicted a_{13C} values for the bent CuCO and planar $Cu(CO)_3$ structures along with thea_{14N} value for the bent $CuNH_3$ complex. Looking first at CuCO, any combination of the five basis sets with the B3LYP or M06 functionals results in an overestimation of a_{13C} while the BHandHLYP functional underestimates a_{13C}. Treatment of the ^{13}C atom with the B3LYP/6-311+G or B3LYP/6-311+G(d) level of theory resulted in deviations from the experimental values between 3.1-9.4 % and 0.5-5.6%, respectively. The a_{14N} value of $CuNH_3$ is always overestimated, but good agreement (<10 MHz) is achieved with the M06 or BHandHLYP functional and the 6-311+G(d) basis set. Finally, for $Cu(CO)_3$, the a_{13C} value is underestimated by about 10 MHz with the B3LYP and M06 functionals and only by 1-2 MHz using the BHandHLYP and the 6-311+G, 6-311+G(d), EPR-III or 6-31++G(d,p) basis sets.

4.5.2. Internal-Energy Calculations

DFT was used to investigate the relative stability of mononuclear metal complexes and metallacycles proposed as intermediates in this study, by comparing the internal energy values. We undertook two series of calculations with the B3LYP, M06 and BHandHLYP functionals. The first series used the 6-311+G(d) basis set for all atoms. This was expected to give good results, given that the a_{63Cu} values estimated using the 6-311+G(d) basis set for $^{63}CuCO$, $^{63}CuSiO$, and $^{63}CuNH_3$ were in good agreement with the experimental values. The second series of calculations treated all metal atoms (Cu, Ag or Au) with the LANL2DZ basis set and corresponding ECPs while the 6-311+G(d) basis

set was used for the nonmetal atoms. This method allows for the comparison of the Cu, Ag and Au-containing species with one another, as they are calculated at the same level of theory.

Table 25. Predicted nuclear hyperfine interaction,[a] a_{Nu}, of the ligand atoms in Cu-containing radicals. (The values in parentheses are the % difference between the calculated and experimental hyperfine interaction values.)[b]

Functional	Basis Set	a_{13C}	a_{13C}	a_{14N}
		$^{63}CuCO$	$^{63}Cu(CO)_3$	$^{63}CuNH_3$
B3LYP	6-311G	264 (46.7, 38.2)[c]	3 (84.2, 86.4) [c]	97 (64.4)
	6-311+G	197 (9.4, 3.14) [c]	11 (42.1, 50.0) [c]	86 (45.8)
	6-311+G(d)	190 (5.6, 0.5) [c]	14 (26.3, 36.4) [c]	87 (47.5)
	EPR-III[d]	195 (8.3, 2.1) [c]	11 (42.1, 50.0) [c]	87 (47.5)
	6-31++G(d,p)[d]	183 (1.7, 4.2) [c]	0 (100.0) [c]	74 (25.4)
M06	6-311G	265 (47.2, 38.7) [c]	12 (36.8, 45.5) [c]	83 (40.7)
	6-311+G	219 (21.7, 14.7) [c]	6 (68.4, 72.7) [c]	82 (39.0)
	6-311+G(d)	211 (17.2, 10.5) [c]	2 (89.5, 90.9) [c]	85 (44.1)
	EPR-III[d]	201 (11.7, 5.2) [c]	10 (47.4, 54.5) [c]	82 (39.0)
	6-31++G(d,p)[d]	197 (9.4, 3.1) [c]	11 (42.1, 50.0) [c]	69 (16.9)
BHandHLYP	6-311G	223 (23.9, 16.8) [c]	2 (89.5, 90.9) [c]	82 (39.0)
	6-311+G	167 (7.2, 12.6) [c]	18 (5.5, 18.1) [c]	72 (22.0)
	6-311+G(d)	158 (12.2, 17.3) [c]	22 (15.8, 0.0) [c]	72 (22.0)
	EPR-III[d]	163 (9.4, 14.7) [c]	20 (5.2, 9.1) [c]	73 (23.7)
	6-31++G(d,p)[d]	142 (21.1, 25.7) [c]	22 (15.8, 0.0) [c]	60 (1.7)
Experimental	Argon	180[e]	19[e]	59[h]
	Adam	191[f]	22[g]	-

[a]Hyperfine interaction in MHz. [b]% difference $[(a_{exp} - a_{calc})/a_{exp}] \times 100$. [c]The two numbers within parentheses represent the % difference as defined in b, the first % difference was calculated using a_{63Cu}, Ar while the second calculated using a_{63Cu}, adamantane. [d]The 6-311+G(d) basis set was used for ^{63}Cu. [e]Ref. 29. [f]Ref. 45. [g]Ref. 49. [h]Ref. 47.

The difference in energy between the mononuclear metal complexes or corresponding metallacycles, and the reactants, i.e., the free metal atoms and substrate molecule, was calculated using the DFT results, Table 26. The DFT calculations were carried out with double precision and the differences in energy reflect this precision. In the table, a negative value signifies that the molecule is lower in energy than the reactants, while a positive sign represents a higher energy value. The information in Table 26 can be more easily viewed in the energy diagrams shown in Figures 96 and 97.

The reactants (metal atom and substrate) are set to 0 kcal/mol as a reference. It is important to mention that the reactants were run in separate calculations with no correction for the basis set superposition error. Having said that, our main interest was to compare the energy between the mononuclear metal complexes and corresponding metallacyclic intermediates. Turning to the first series of calculations, Figure 96 (computed with the 6-311+G(d) basis set), all three mononuclear complexes are lower in energy when compared to the energy of free Cu atoms and ethylene oxide (EO), ethylene sulfide (ES) or aziridine (Az) for all three functionals, namely, B3LYP, M06 and BHandHLYP. The relative energy differences were found to be CuEO < CuES < CuAz. On the other hand, the metallacycles do not follow the same trend. Cupraoxetane and cuprathietane are lower in energy with respect to their mononuclear Cu complexes, while the cupraazetane is higher in energy than the complex. In fact, at the BHandHLYP level of theory the energy of the cupraazetane is higher than the reactants.

Table 26. Energy differences[a] of proposed mononuclear metal complexes and metallacycles, relative to the corresponding reactants.

Reaction	Mononuclear Complex			Metallacycle		
	B3LYP	M06	BHandHLYP	B3LYP	M06	BHandHLYP
Cu + EO[b]	-3.3310	-5.3560	-2.8940	-12.0839	-9.0901	-3.7718
Cu + ES[b]	-6.5171	-12.4610	-4.1143	-18.6924	-18.4537	-12.2173
Cu + Az[b]	-11.0906	-12.7106	-9.3660	-6.5363	-4.1344	2.9548
Cu + EO[c]	-6.3105	-7.9439	-4.7560	-12.8585	-9.3255	-3.0900
Cu + ES[c]	-8.1146	-11.3419	-5.1815	-18.7244	-17.6948	-11.5247
Cu + Az[c]	-13.8644	-14.8411	-11.1025	-7.8002	-5.0798	2.4237
Ag + EO[c]	-2.1709	-4.4086	-2.0014	10.7859	11.4762	15.4671
Ag + ES[c]	-3.5480	-7.2357	-2.4516	1.6831	0.5867	4.0704
Ag + Az[c]	-2.8281	-4.6415	-1.9657	2.6321	6.8783	3.8653
Au + EO[c]	-2.8281	-4.6415	-1.9657	2.6321	6.8783	3.8653
Au + ES[c]	-9.8980	-11.6338	-6.2075	-6.4699	-3.3376	0.2358
Au + Az[c]	-10.6153	-10.7257	-8.0668	-0.5449	4.9558	3.1411

[a]Energy in kcal/mol. [b]All atoms treated with the 6-311+G(d) basis set. [c]Metal atoms treated with LanL2DZ and nonmetal atoms with 6-311+G(d) basis set.

Figure 97 shows the plots corresponding to the second series of calculations where all metal atoms are treated with the LanL2DZ basis set and nonmetal atoms with the 6-311+G(d) basis set. In general, the results for Cu closely resemble those presented in Figure 96. However, the LanL2DZ series, predicts slightly larger energy differences between the reactants and the mononuclear-Cu complexes or cupracyclic intermediates. For example, the B3LYP/6-311+G(d) level of theory predicts that Cu-ethylene oxide is 3.3 kcal/mol more stable than the reactants compared to 6.3 kcal/mol found using B3LYP/LanL2DZ. Similarly, the energy differences for Cu-ethylene sulfide and Cu-aziridine complexes increases from 6.5 to 8.1 kcal/mol and from 11.1 to 13.9 kcal/mol, respectively. The same observation is made with the ethylene sulfide and aziridine complexes as being 6.5 versus 8.1 kcal/mol and 11.1 vs 13.9 Kcal/mol, respectively.

As was found for Cu, the energy difference for the Ag and Au complexes with respect to the reactants increased in the order M-EO < M-ES < M-Az for all three functionals used. However, the Ag and Au-metallacycles do not adhere to the same trend observed for Cu, in that they are all higher in energy than the corresponding mononuclear Ag- and Au-complexes.

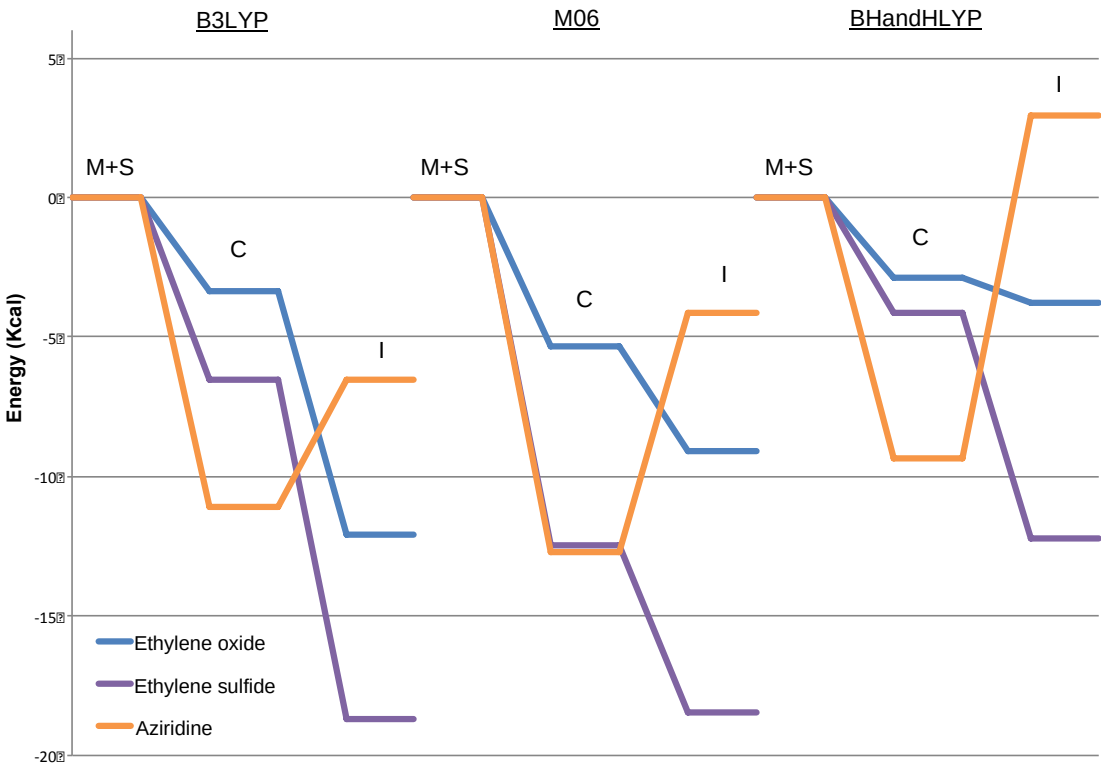

Figure 96. Energy diagram comparing the stability of mononuclear Cu-complexes (C) and metallacycles (I) resulting from the reaction of Cu atoms with ethylene oxide, ethylene sulfide and aziridine (M + S) computed at the B3LYP, M06, and BHandHLYP level of theory with the 6-311+G(d) basis set.

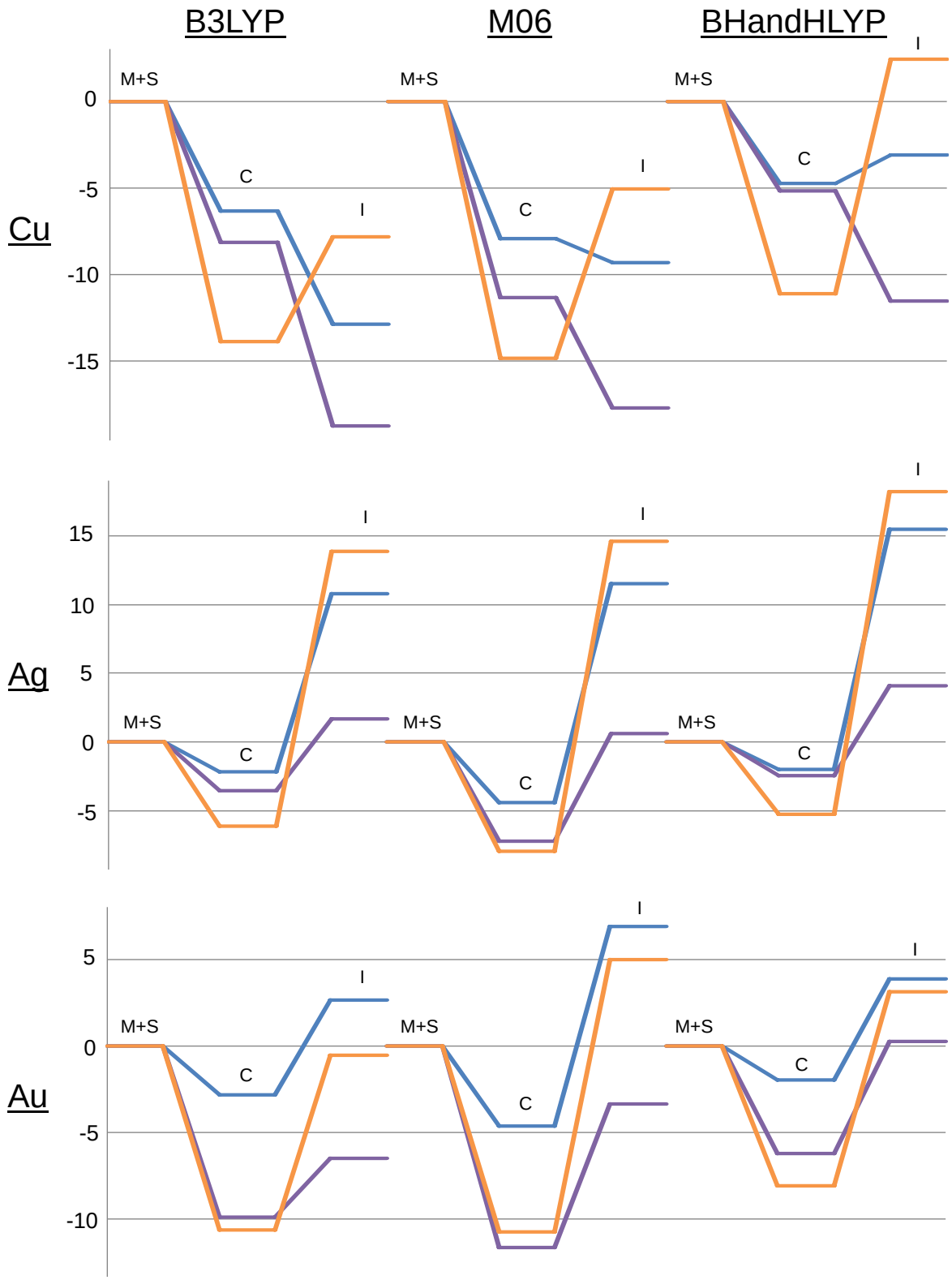

Figure 97. Energy diagram (kcal/mol) comparing the stability of mononuclear Group 11 metal complexes (C) and metallacycles (I) from reactions of Cu, Ag or Au atoms (M) with substrates (S), ethylene oxide (blue), ethylene sulfide (purple) and aziridine (orange).

5. Discussion

Reactions of Group 11 metal atoms with three-membered heterocyclic compounds have led to the formation of many paramagnetic products characterized by EPR spectroscopy at cryogenic temperatures. The trapped intermediates have been categorized based on the magnitude of the hyperfine interaction, i.e., metal-heterocyclic complexes and metallacycles. Furthermore, organic radicals that resonate at *g*-values ~2.00 and unassigned radicals with resolved hyperfine interaction are also included in the discussion.

5.1. Mononuclear-Metal-Ring Complexes

5.1.1. Three-Membered Heterocyclic Compounds

In the series of reactions between Group 11 metal atoms and the three-membered heterocyclic compounds, there was almost always a new paramagnetic species formed with a large value for the metal hyperfine interaction (3122 – 4349 MHz for ^{63}Cu, 1291 – 1619 MHz for ^{107}Ag, and 1374 – 2652 MHz for ^{197}Au) and *g*-value deviating from that of a free electron, Table 27. (The values for the ^{65}Cu and ^{109}Ag isotopomers have been excluded for the sake of clarity.) These species have been assigned to mononuclear metal complexes, M-$\overline{\text{XCH}_2\text{CH}_2}$ based on; 1) comparison to similar 1:1 metal-substrate complexes reported in the literature, 2) EPR experiments with aziridine and 3) DFT calculations of the Cu nuclear hyperfine interaction.

Table 27. Summary of the isotropic magnetic parameters[a] and calculated unpaired spin populations (ρ_{ns})[b] for mononuclear-metal-ring complexes formed in this study.

Species	Assignment	g_{iso}	$a_{iso\ (M)}$	$a_{iso\ (N)}$	ρ_{ns} (M)	ρ_{2s} (N)
^{63}Cu-EO-1	^{63}Cu-$\overline{OCH_2CH_2}$	2.0091	4349	-	0.73	-
^{63}Cu-EB-1	^{63}Cu-$\overline{OCH_2CH}CH_2CH_3$	2.0101	4293	-	0.72	-
^{63}Cu-EB-2		2.0043	4469	-	0.75	-
^{63}Cu-SO-1	^{63}Cu-$\overline{OCH_2CH}C_6H_5$	2.0099	3740	-	0.62	-
^{63}Cu-SO-2		2.0011	3920	-	0.65	-
^{63}Cu-ES-1	^{63}Cu-$\overline{SCH_2CH_2}$	2.0082	3625	-	0.60	-
^{63}Cu-Az-1	^{63}Cu-$\overline{NHCH_2CH_2}$	2.0094	3223	69	0.54	0.04
^{63}Cu-Az-2		2.0083	3122	65	0.52	0.04
^{107}Ag-EO	^{107}Ag-$\overline{OCH_2CH_2}$	2.0016	1619	-	0.88	-
^{107}Ag-SO-1	^{107}Ag-$\overline{OCH_2CH}C_6H_5$	2.0009	1524	-	0.83	-
^{107}Ag-SO-2		2.0001	1462	-	0.80	-
^{107}Ag-ES-1	^{107}Ag-$\overline{SCH_2CH_2}$	1.9988	1401	-	0.77	-
^{107}Ag-Az-1	^{107}Ag-$\overline{NHCH_2CH_2}$	2.0000	1362	55	0.74	0.03
^{107}Ag-Az-2		1.9995	1291	55	0.71	0.03
^{197}Au-EO-1	^{197}Au-$\overline{OCH_2CH_2}$	2.0232	2652	-	0.92	-
^{197}Au-ES	^{197}Au-$\overline{SCH_2CH_2}$	1.9862	1542	-	0.54	-
^{197}Au-Az-1	^{197}Au-$\overline{NHCH_2CH_2}$	2.0378	1374	100	0.48	0.06
^{197}Au-Az-2		2.0332	1474	101	0.51	0.06

[a]Hyperfine presented in MHz. [b]Value for an electron in the s-orbital of the atom (a_{iso}^{o} (atom) in MHz), ^{63}Cu, 5995, ^{107}Ag, 1831, ^{197}Au, 2876, and ^{14}N, 1811.[30]

5.1.1.1. Structural Assignment

Assignment of the paramagnetic products formed in the reactions of ethylene oxide, ethylene sulfide and aziridine with Group 11 metal atoms to mononuclear-metal-heterocyclic complexes, Table 27, is supported by a comparison of the experimental metal hyperfine interaction, a_M values, with those reported for similar metal-centered complexes prepared by matrix-isolation techniques, Tables 1-3 (section 1.3). Since the values of a_{63Cu} are large, one can immediately rule out the possibility of metal-carbon bond addition products, $a_M \approx 1372 - 375$ MHz or di- and tri-ligand complexes $a_M \approx 91 - 131$ MHz, as they have much smaller values. The magnitude of a_{63Cu} , 4349 MHz, 3625 MHz, and 3223 MHz obtained for ^{63}Cu-EO-1, ^{63}Cu-ES-1, and ^{63}Cu-Az-1, respectively,

are similar to those reported for the 1:1 ^{63}Cu:substrate complexes exhibiting π-interactions (4341 - 3601 MHz) and σ-interactions (4238 – 3632 MHz). The same trends can be observed when comparing the $a_{^{107}Ag}$ values 1619 MHz, 1401 MHz, and 1362 MHz, obtained for ^{107}Ag-EO, ^{107}Ag-ES-1, and ^{107}Ag-Az-1, respectively, which fall within the range of 1698 - 1116 MHz, found for mononuclear Ag-substrate complexes. Once again, the $a_{^{197}Au}$ values, 2652 MHz, 1542 MHz and 1374 MHz, obtained for ^{197}Au-EO-1, ^{197}Au-ES, and ^{197}Au-Az-1, respectively, are close to the values (2693 – 1611 MHz) reported in the literature for mononuclear Au-substrate complexes.

In the case of aziridine and its isotopomer, aziridine-^{15}N, the paramagnetic species with large metal hyperfine interaction could undoubtedly be assigned to the mononuclear metal complex **(1)** arising from the σ-donation of the lone pair electrons on the nitrogen to the metal.

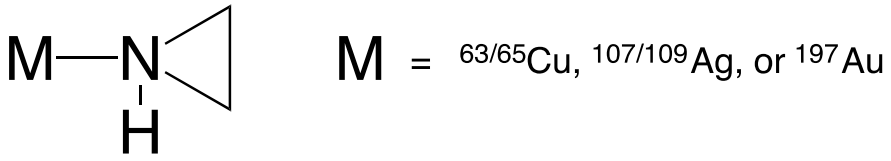

(1)

Comparing the m_I = +1/2 transition of species $^{63/65}$Cu-Az-1, $^{107/109}$Ag-Az-1, ^{197}Au-Az-1 with the spectra corresponding to $^{63/65}$Cu-Az^{15}N-1, $^{107/109}$Ag-Az^{15}N-1, and ^{197}Au-Az^{15}N-1, respectively, we see that the triplets arising from the interaction of the unpaired electron with the magnetic moment of the ^{14}N nucleus becomes a doublet upon substitution with ^{15}N, Figure 98. This proves that the unpaired electron situated on the metal atom is in close proximity to the nitrogen atom of the aziridine ligand.

The Group 11 metal atom -ethylene sulfide and -ethylene oxide reactions also yielded products with a large metal hyperfine interaction. However, no superhyperfine interaction was observed, contrary to that found in the case of aziridine. The natural abundance of the ligands' magnetic nuclei, ^{17}O and ^{33}S, were too low to observe in the EPR spectra. Nonetheless, these systems have lone pairs on the O and S atoms which, like aziridine, can enter into a σ-bonding interaction with the metal center. Repeating the $^{63/65}Cu$ atom experiments with ethylene oxide-d_4 and ethylene oxide-$^{13}C_2$, yielded $^{63/65}$Cu-EO-d_4-1 and $^{63/65}$Cu-EO-^{13}C-1, respectively. The EPR spectra of these systems are identical to that of $^{63/65}$Cu-EO-1. Isotopic substitution had no effect on the line width of the transition lines indicating that there was no significant interaction of the unpaired electron with either ^{13}C or ^{2}H. In a similar fashion, the line width of the $m_I = \pm 1/2$ transitions for the mononuclear ^{107}Ag-ethylene sulfide complex, ^{107}Ag-$\overline{SCH_2CH_2}$ were not affected when the reaction was repeated with ethylene sulfide-d_4.

A second species with a slightly smaller a_M was observed in the Group 11 metal-aziridine and –aziridine-^{15}N reactions, i.e., the a_M of M-Az-2 differs from that of M-Az-1 by 3 % (M = ^{63}Cu), 5 % (M = ^{107}Ag) and 7 % (M = ^{197}Au), respectively. On the other hand, the magnitude of the nitrogen hyperfine interaction for M-Az-1 and M-Az-2 is almost identical. In addition we can rule out the possibility of the second species being a di-ligand metal complex, as one would expect to see additional nitrogen hyperfine interaction. Thus $^{63/65}$Cu-Az-2, $^{107/109}$Ag-Az-2, and ^{197}Au-Az-2 must be the same species

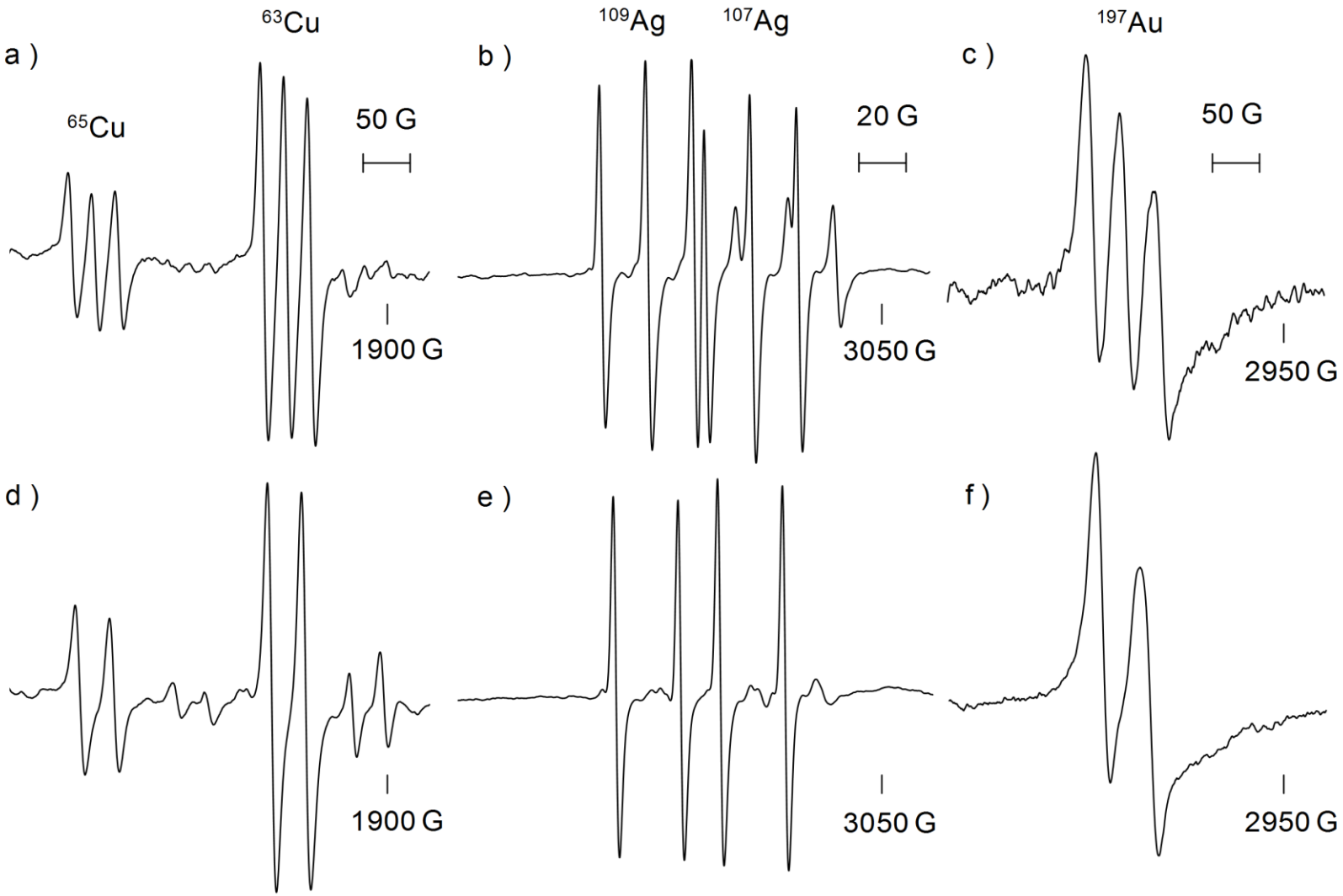

Figure 98. The m_I = +1/2 EPR transition for a paramagnetic product formed in the reaction of aziridine with a) $^{63/65}$Cu atoms at 120 K, b) $^{107/109}$Ag atoms at 220 K and c) ^{197}Au atoms at 180 K. Below each spectrum in d), e) and f) is the corresponding spectrum at the same temperature, from reactions with aziridine-^{15}N.

in a second trapping site in the adamantane matrix. This phenomenon has been observed in studies by Howard *et al.*,[36] where Ag and Au atoms were isolated in multiple trapping sites in adamantane. The magnitude of $a_{^{107}Ag}$ for the two trapping sites of $^{107}Ag^0$ differ by 90 MHz (5 %). From the intensity of the spectral lines, the trapping site with $a_{^{107}Ag}$ = 1682 MHz is preferred. Three magnetically different trapping sites, varying by 78 MHz (3 %) were observed for $^{197}Au^0$ atoms in adamantane. Similarly the co-deposition of Cu atoms and benzene,[36] 1-butene,[40] or cyclooctadiene,[40] resulted in mononuclear complexes in two trapping sites varying in $a_{^{63}Cu}$ by 186 MHz (4.5 %), 211 MHz (5.5 %), and 188 MHz (5.0 %), respectively. Interestingly only one species with a large a_M value was found in the experiments involving ethylene oxide and ethylene sulfide. It is not apparent why in certain cases the paramagnetic product is trapped in two sites while in others only one site is observed. This may be due to the size and shape of the paramagnetic product formed.

In summary, our substrates more closely resemble those considered to form σ bonds with the metal center. Thus the complex, M-$\overline{XCH_2CH_2}$, is formed in the reactions of ethylene oxide, ethylene sulfide and aziridine, from the interaction of the metal atoms with the lone pair of electrons of the heteroatom (O, S or N) of the ring. The a_M values of these complexes were of the same order of magnitude of known σ-bonded complexes reported in the literature. The a_M value increases in the order of, M-$\overline{OCH_2CH_2}$ > M-$\overline{SCH_2CH_2}$ > M-$\overline{NHCH_2CH_2}$. In addition support for the assignment comes from the experiments where aziridine-^{14}N was replaced by isotopically labelled aziridine-^{15}N.

DFT calculations have been valuable in predicting the nuclear hyperfine interaction, a_{Nu}, of paramagnetic species.[107] Comparison of predicted values with those obtained experimentally help to confirm structural assignments. In this study, we used the functionals, B3LYP, M06, or BHandHLYP and a number of basis sets (6-311G, 6-311+G, 6-311+G(d), EPR-III, or 6-31++G(d,p)) to predict the a_{63Cu} values of several known Cu-containing systems, Tables 23 and 24 (section 4.5.1). The % difference between the calculated and experimental values lie anywhere between 98 and 0.3 %. However, the relative order of a_M for the systems tested is, in general, correctly predicted by the DFT calculations. There appears to be no single combination of functional and basis set capable of modeling every Cu-containing system known. From the series of calculations, we observed that the best combinations of functionals and basis sets (lowest % difference between calculated and experimental a_{63Cu}) depended on the nature of the interactions between the metal and ligand, i.e., mono-ligand complexes, $^{63}CuCO$, $^{63}CuSiO$, and $^{63}CuNH_3$ were best modeled at the B3LYP/6-311+G, B3LYP/6-311+G(d), M06/6-311+G or B3LYP/6-311+G(d) levels of theory, while the di-and tri-ligand complexes, $^{63}Cu(C_2H_4)_2$, $^{63}Cu(C_2H_2)_2$, and $^{63}Cu(CO)_3$ were best modeled at the BHandHLYP/6-311G level of theory.

After testing the ability of the DFT methods to predict the a_{63Cu} values of known Cu-containing complexes, calculations were extended to include $^{63}Cu\text{-}\overline{OCH_2CH_2}$, $^{63}Cu\text{-}\overline{NHCH_2CH_2}$, and $^{63}Cu\text{-}\overline{SCH_2CH_2}$, Table 28. As observed experimentally, the calculated a_{63Cu} values increase in the order a_{63Cu} (^{63}Cu-EO) > a_{63Cu} (^{63}Cu-ES) > a_{63Cu} (^{63}Cu-Az) for all calculations with the exception of those carried out using the 6-311G basis set. This is not surprising as the a_{63Cu} calculated at the B3LYP/6-311G, M06/6-311G, and

BHandHLYP/6-311G level of theory for a series of known Cu-centered radicals was not in good agreement with the experimental values.

Table 28. Comparison of experimental and theoretical nuclear hyperfine interaction,[a] a_{63Cu}, of mononuclear Cu complexes formed with ethylene oxide, ethylene sulfide and aziridine. (The values in parentheses are the % difference between the calculated and experimental hyperfine interaction values.)[b]

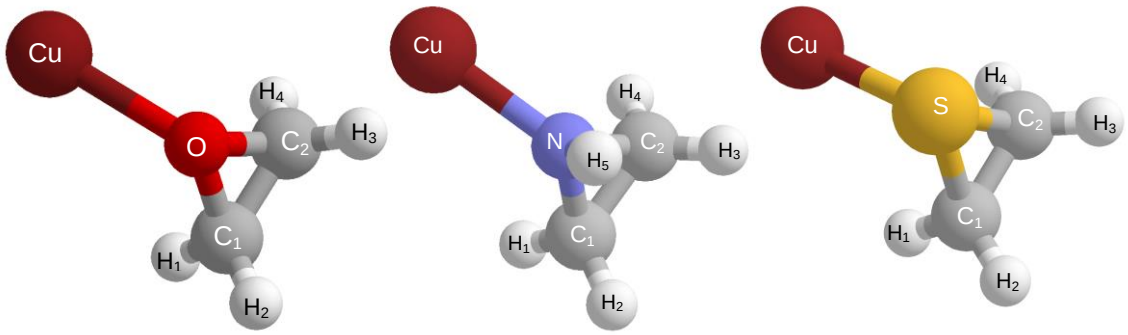

Functional	Basis Set	^{63}Cu-$\overline{OCH_2CH_2}$	^{63}Cu-$\overline{NHCH_2CH_2}$		^{63}Cu-$\overline{SCH_2CH_2}$
		a_{63Cu}	a_{63Cu}	a_{14N}	a_{63Cu}
B3LYP	6-311G	2022 (53.5)	1342 (58.2)	98 (40.0)	2731 (24.7)
	6-311+G	4310 (0.9)	3209 (0.2)	85 (21.4)	4093 (12.9)
	6-311+G(d)	4682 (7.7)	3469 (7.9)	77 (10.0)	3956 (9.1)
	EPR-III[c]	4690 (7.8)	3461 (7.6)	80 (14.3)	d
	6-31++G(d,p)[c]	4669 (7.4)	3447 (7.2)	68 (2.3)	3936 (8.6)
M06	6-311G	2248 (48.3)	1554 (51.7)	89 (27.1)	2791 (23.0)
	6-311+G	4571 (5.1)	3290 (2.3)	85 (21.4)	4153 (14.6)
	6-311+G(d)	4958(14.0)	3617 (12.5)	78 (11.4)	4039 (11.4)
	EPR-III[c]	5006 (15.1)	3605 (12.1)	78 (11.4)	d
	6-31++G(d,p)[c]	4920 (13.1)	3606 (12.1)	67 (4.3)	4013 (10.7)
BHandHLYP	6-311G	1244 (71.4)	843 (73.8)	82 (17.1)	3120 (13.9)
	6-311+G	4162 (4.3)	3199 (0.5)	68 (2.9)	4169 (15.0)
	6-311+G(d)	4505 (3.6)	3474 (8.0)	62 (11.4)	4039 (11.4)
	EPR-III[c]	4531 (4.2)	3468 (7.8)	64 (8.6)	d
	6-31++G(d,p)[c]	4497 (3.4)	3478 (8.1)	52 (25.7)	4039 (11.4)
Experimental	Adam	4349	3216	70	3625

[a]Hyperfine interaction in MHz. [b]% difference $[(a_{exp} - a_{calc})/a_{exp}] \times 100$. [c]The 6-311+G(d) basis set was used for ^{63}Cu. [d]S atoms outside the basis set range.

Agreement between experimental and calculated a_{63Cu} values improved considerably when the 6-311+G basis set was used, i.e., the % difference ranges from 0.9 – 4.3 % for ^{63}Cu-$\overline{OCH_2CH_2}$, 0.2 – 2.3 % for ^{63}Cu-$\overline{NHCH_2CH_2}$ and 12.9 – 14.6 % for ^{63}Cu-$\overline{SCH_2CH_2}$, respectively. Changing the basis set to 6-311+G(d) overestimated the a_{63Cu} values by 3.6 – 14.0 % for ^{63}Cu-$\overline{OCH_2CH_2}$, 7.9 – 12.5 % for ^{63}Cu-$\overline{NHCH_2CH_2}$ and 9.1 – 11.4 % for ^{63}Cu-$\overline{SCH_2CH_2}$. Treatment of the ligand atoms with the EPR-III or 6-31++G(d,p) basis set while maintaining the 6-311+G(d) basis set for the Cu atom, caused slight changes in a_{63Cu} of < 1 % for all three complexes, ^{63}Cu-$\overline{OCH_2CH_2}$, ^{63}Cu-$\overline{NHCH_2CH_2}$, and ^{63}Cu-$\overline{SCH_2CH_2}$, while the a_{14N} value of ^{63}Cu-$\overline{NHCH_2CH_2}$ was greatly affected, deviating from the experimental value by 2.3-25.7 %. It is interesting that for ^{63}Cu-$\overline{NHCH_2CH_2}$, the BHandHLYP/6-311+G level of theory gave the lowest % deviation from the experimental values, i.e., 0.5% and 2.9% for a_{63Cu} and a_{14N}, respectively. However, the a_{63Cu} values calculated at the B3LYP/6-311+G(d) level of theory were in the best agreement with the experimental values for all three Cu complexes, i.e., % deviation was ≤ 9. This is consistent with that found for the σ-bonded complexes, $^{63}CuNH_3$, ^{63}CuCO, and ^{63}CuSiO, which deviate from the experimental a_{63Cu} values by 8.5 %, 0.9 - 3.7 %, and 1.2 %, respectively. These DFT calculations support the proposed formation of the ^{63}Cu-$\overline{XCH_2CH_2}$ complexes where (X = O, S and NH).

5.1.2. Substituted Oxiranes

Successful reactions between Group 11 metal atoms with three-membered heterocyclic compounds led us to expand the study to more complex substrates. Species with large hyperfine interaction values were formed in the reactions of $^{63/65}$Cu atoms with 1,2-

epoxybutane or styrene oxide and $^{107/109}$Ag atoms with styrene oxide. To our surprise no new products formed in the reactions of ^{197}Au atoms and styrene oxide only isolated gold atoms, $^{197}Au^0$, were visible in the EPR spectrum. Not even a weak mononuclear complex such as the one observed in the reaction with ethylene oxide was found.

The species labelled ^{63}Cu-EB-1 and ^{63}Cu-EB-2 are assigned to the mononuclear ^{63}Cu atom-1,2-epoxybutane complex, ^{63}Cu-$\overline{OCH_2CH}CH_2CH_3$, in two different trapping sites since the a_{63Cu} values of 4293 MHz and 4469 MHz, respectively, only differ by 1.3% and 2.8% from the values found for ^{63}Cu-$\overline{OCH_2CH_2}$.

In the case of styrene oxide, two products, ^{63}Cu-SO-1 and ^{63}Cu-SO-2, formed when reacted with Cu atoms, having a_{63Cu} values of 3740 MHz and 3920 MHz, respectively, Table 27. There are two sites in the styrene oxide molecule where complexation can occur with Cu atoms, namely, the benzene ring and the oxygen atom. An a_{63Cu} of 4341 MHz was reported[36] for ^{63}Cu(C_6H_6), whereas for ^{63}Cu-$\overline{OCH_2CH_2}$ and ^{63}Cu-$\overline{OCH_2CH}CH_2CH_3$ the a_{63Cu} values were found to be 4368 MHz and 4293 MHz, respectively. It is not possible to definitively assign a structure to ^{63}Cu-SO-1 and ^{63}Cu-SO-2 based on the hyperfine interactions alone. However, we favour the formation ^{63}Cu-$\overline{OCH_2CH}C_6H_5$ because (1) a Cu($C_6H_5\overline{CHCH_2O}$) monoarene complex is not expected to be stable as it does not follow the 18 valence electron rule, (2) the Cu-ethylene oxide, -1,2-epoxybutane, and –styrene oxide deposits were of similar colour suggesting similarity in the type of bonding interaction, (3) the species formed in the Cu-styrene oxide reaction persists to *ca.* 190 K which is similar to that observed for ^{63}Cu-$\overline{OCH_2CH_2}$ (180 K) and ^{63}Cu-$\overline{OCH_2CH}CH_2CH_3$ (180 K), (4) Howard *et al.*[36] did not detect Cu-arene complexes

in the Cu atom reactions of substituted arenes, i.e., toluene, methoxybenzene, o-, m-, p-, xylenes, mesitylene, and perfluorobenzene. Although Cu-cyanobenzene complexes were detected they were very unstable.

In the reaction of $^{107/109}$Ag atoms with styrene oxide, three species with large $a_{^{107}Ag}$ values, ^{107}Ag-SO-1 (1524 MHz), ^{107}Ag-SO-2 (1462 MHz), and ^{107}Ag-SO-3 (1601 MHz), were observed. The intensity of the transition lines for ^{107}Ag-SO-1 > ^{107}Ag-SO-2 >> ^{107}Ag-SO-3. The $a_{^{107}Ag}$ values of ^{107}Ag-SO-1 and ^{107}Ag-SO-2 differ by 4 %. These are believed to be the same species in two different adamantane trapping sites. Support for this comes from the fact that $^{107/109}$Ag atoms deposited in adamantane are found in two different sites with the $a_{^{107}Ag}$ values differing by 5 %. Similarly to the reaction with Cu atoms, the styrene oxide presents two possible reactive sites, namely, the oxygen atom of the heterocycle and the benzene ring. Values of $a_{^{107}Ag}$ = 1698 and 1579 MHz were reported[36] for the Ag(C_6H_5) complex observed in two trapping sites from the reaction of Ag atoms and benzene. The values of $a_{^{107}Ag}$ for ^{107}Ag(C_6H_5) are larger than that observed for ^{107}Ag-SO-1 and ^{107}Ag-SO-2, while on the other hand ^{107}Ag-SO-3 is well within the range of the two trapping sites. Unlike reactions of Cu and substituted benzenes, Ag atoms formed detectable Ag-arene complexes, i.e., with toluene, mesitylene, cyanobenzene and methoxybenzene, having $a_{^{107}Ag}$ values ranging from 1555 – 1645 MHz.[36] It is reasonable to assign ^{107}Ag-SO-1 and ^{107}Ag-SO-2 to the mononuclear Ag-heterocyclic complex, ^{107}Ag-$\overline{OCH_2CH}C_6H_5$ and ^{107}Ag-SO-3 to the complex formed with the benzene group of the styrene oxide molecule, ^{107}Ag(C_6H_5-R). However, definitive assignments cannot be made without additional information.

In a final note, it is interesting to mention that for both the ^{63}Cu and ^{107}Ag-styrene oxide reactions we observed smaller hyperfine interaction values than those expected for coordination to the epoxide ring alone. Addition of the phenyl group as a substituent on the ethylene oxide ring may thus result in a stronger complex formed between the metal and the heteroatom, accounting for the lower a_{63Cu} or a_{107Ag} values observed. Previous reports have demonstrated that the a_{63Cu} and a_{107Ag} values of Cu atom-cyanide complexes (side-on bonding) decreased when C_6H_5CN was used in lieu of HCN (*vide supra* Table 1), supporting this conclusion.

5.1.3. Type of Bonding-Interactions

As mentioned above, the heteroatoms in the three-membered rings (O, S or NH) have at least one lone pair of electrons that is believed to form a σ bond with the metal atoms. The mononuclear metal-heterocyclic complexes should thus exhibit similar interactions to those found in the σ-bonded complexes formed with :PF_3 and :NH_3, i.e., $^{63}CuPF_3$, $^{107}AgPF_3$, and $^{63}CuNH_3$, respectively. To confirm this one can compare the calculated unpaired spin population contributions of each atom (ρ_n) in the molecule estimated from the EPR parameters, i.e., a_{iso} and a_{dip} (when available).

The unpaired spin population of the metal "s" orbitals, ρ_{ns}, in the M-$\overline{XCH_2CH_2}$ complexes are recorded in Table 27. The values of ρ_{4s} for the ^{63}Cu-$\overline{XCH_2CH_2}$ complexes range from 0.52 – 0.73 and are comparable to 0.70 and 0.61 reported for $^{63}CuPF_3$ and $^{63}CuNH_3$, respectively (see Table 1, section 1.3.). For ^{107}Ag-$\overline{XCH_2CH_2}$, the values of ρ_{5s} range from 0.71 – 0.88, which are comparable to the values of 0.92 and 0.61 determined for $^{107}AgPF_3$ and ^{107}AgPN, respectively. Although EPR evidence for $^{197}AuNH_3$ or

$^{197}AuPF_3$ has yet to be reported, the values of ρ_{6s} for the $^{197}Au\text{-}\overline{XCH_2CH_2}$ complexes, which fall in the range of 0.48 – 0.92, are comparable to those of 0.59 and 0.54 for the σ-bonded complexes, $^{197}AuCO$ and $^{197}AuSiO$, respectively.

In general, the EPR spectra of $M\text{-}\overline{XCH_2CH_2}$ are isotropic, with the exception of $^{197}Au\text{-}\overline{NHCH_2CH_2}$. The anisotropic EPR parameters obtained for $^{197}Au\text{-}\overline{NHCH_2CH_2}$ can be used to gain additional information about the ^{197}Au-ligand bond.

Using the magnetic parameters for species ^{197}Au-Az-1, i.e., $a_{Au_\perp}$ = 1352 MHz, $a_{Au_\parallel}$ = 1417 MHz, $a_{N_\perp}$ = 92 MHz, and $a_{N_\parallel}$ = 114 MHz, the values of a_{dip} for Au and N are 21.7 MHz and 7.24 MHz, respectively, assuming the same sign for $a_\parallel$ and $a_{Au_\perp}$. This translates into a Au "6p" unpaired spin contribution, ρ_{6p}, of 0.04 and N "2p" unpaired spin contribution, ρ_{2p}, of 0.13 (equation (18), section 1.2.5.).[30,49] The sum of the unpaired metal (M) and ligand (L) spin contributions to the SOMO ($\Sigma\rho = M\rho_{ns} + M\rho_{np} + L\rho_{ns} + L\rho_{np}$), is = 0.48 + 0.40 + 0.06 + 0.13 or, 1.07. Similarly, the Au and N a_{dip} values of ^{197}Au-Az-2, determined from the magnetic parameters, $a_{Au_\perp}$ = 1452 MHz, $a_{Au_\parallel}$ = 1527 MHz, $a_{N_\perp}$ = 104 MHz, and $a_{N_\parallel}$ = 97 MHz, are 25.2 MHz and -2.37 MHz, respectively. Consequently these values give the unpaired spin contributions of the Au and N p-orbitals, i.e., ρ_{6p} and ρ_{2p} of 0.46 and -0.04, respectively. The total unpaired spin density contribution in this molecule is then, $\Sigma\rho$ = 0.51 + 0.46 + 0.06 + -0.04 = 0.99.

The values of the spin contribution demonstrate that bonding in $^{197}Au\text{-}\overline{NHCH_2CH_2}$ involves almost exclusively metal and ligand, s and p orbitals. Examination of the magnetic parameters of the ^{197}AuCO complex, formed by co-deposition of metal

atoms and CO in an argon matrix,[72] shows similar unpaired spin density distributions to that of ^{197}Au-$\overline{\text{NHCH}_2\text{CH}_2}$, Table 29. Using the estimated a^o_{dip} value of 54.6 MHz, determined by Howard *et al.*,[49] one can calculate the Au 6p unpaired spin contribution, ρ_{6p}, of 0.35 using equation (18). The total unpaired spin density contribution of Au and C in AuCO, $\Sigma\rho$, is equal to 0.59 + 0.35 + 0.09 + -0.05 or 0.98. There is an increase in the Au 6p spin density of ~5% when comparing ^{197}AuCO to ^{197}Au-$\overline{\text{NHCH}_2\text{CH}_2}$.

An interesting trend is observed when the unpaired metal and ligand contributions in M-$\overline{\text{NHCH}_2\text{CH}_2}$ are compared to those of other Cu and Ag complexes. Looking first at the σ-complexes formed with Cu atoms, the unpaired "s" metal spin population for the most intense trapping site of ^{63}Cu-$\overline{\text{NHCH}_2\text{CH}_2}$, 0.54, is less than that of ^{63}CuNH$_3$ (0.61) and ^{63}CuPF$_3$ (0.70). The ρ_{2s} values of the nitrogen atoms in ^{63}CuNH$_3$ (0.03) and ^{63}Cu-$\overline{\text{NHCH}_2\text{CH}_2}$ (0.04), are virtually identical. Unfortunately, the values of metal and ligand p-orbital contributions could not be determined experimentally, as the spectra were isotropic. The smaller ρ_{4s} value for ^{63}Cu-$\overline{\text{NHCH}_2\text{CH}_2}$, with respect to those for the complexes in Table 29, would suggest a larger unpaired 4p spin contribution.

Ag complexes, prepared using cryogenic techniques, gave results similar to those found with the Cu analogues. When comparing the ρ_{5s} for previously reported Ag-containing complexes, Table 29, Ag-$\overline{\text{NHCH}_2\text{CH}_2}$ (0.74) most resembles that of ^{107}AgSiO (0.74) and ^{107}AgNH$_3$ (0.67). The smaller ρ_{5s} value for ^{107}AgNH$_3$ in contrast to that for the ^{107}AgPF$_3$ complex may be due to the fact that it is trapped in a γ-irradiated AgNa-A zeolite instead of adamantane.[108] The environment (matrix) in which the atoms are trapped plays a role in the magnitude of the hyperfine interaction, i.e., two trapping sites

for Ag^0 atoms are observed in the AgNa-A zeolite,[109] but the values are much smaller than those obtained in either argon or adamantane, i.e., 1328 MHz for the minor and 1398 MHz the major trapping site. Similarly in comparing the ρ_{ns} for the :NH_3, :PF_3, and :$\overline{NHCH_2CH_2}$ ligands, ρ_{3s} (PF_3) = ρ_{2s} (NH_3) < ρ_{2s} ($\overline{NHCH_2CH_2}$).

Table 29. Analysis of hyperfine coupling tensors,[a] a_{iso} and a_{dip} with calculated unpaired spin population (ρ_n)[b] for metal and ligand atoms in σ-complexes.

	Metal				Ligand				Ref
	a_{iso}	a_{dip}	ρ_{ns}	ρ_{np}	a_{iso}	a_{dip}	ρ_{ns}	ρ_{np}	
$^{63}CuNH_3$	3632	-	0.61	-	59	-	0.03[a]	-	47
$^{63}CuCO$	4142	16	0.69	0.09	180	-4.0	0.05[d]	-0.04[d]	72
	3961	-	0.66	-	191	-	0.05[d]	-	45
$^{63}CuSiO$	4238	-	0.71	-	-	-	-	-	44
$^{63}CuPF_3$	4205	-	0.70	-	1100	-	0.08[e]	-	46
					90	-	0.02[f]	-	
^{63}Cu-Az-1[g]	3223	-	0.54	-	69	-	0.04[c]	-	[h]
^{63}Cu-Az-2	3122	-	0.52	-	65	-	0.04[c]	-	[h]
$^{107}AgNH_3$	1233	-	0.67	-	42	2.8	0.023[c]	0.05[c]	108
$^{107}AgCO$	1787	-	0.98	-	38	2	0.01[d]	0.02[d]	72
	1682	-	0.92	-	31	-	0.01[d]	-	65
$^{107}AgSiO$	1364	-	0.74	-	-	-	-	-	44
	1226	-	0.67	-	-	-	-	-	63
$^{107}AgPF_3$	1685	-	0.92	-	311	-	0.023[e]	-	67
					37	-	0.002[f]	-	
$^{107}AgPN$	1116	-	0.61	-	183	-	0.014[e]	-	68
					14.7	-	0.008[c]	-	
^{107}Ag-Az-1[g]	1362	-	0.74	-	55	-	0.03[c]	-	[h]
^{107}Ag-Az-2	1291	-	0.71	-	55	-	0.03[c]	-	[h]
$^{197}AuCO$	1705	19	0.59	0.35	327	-5.0	0.09[d]	-0.05[d]	72
$^{197}AuSiO$	1559	-	0.54	-	-	-	-	-	44
^{197}Au-Az-1	1374	21.7	0.48	0.40	100	7.2	0.06[c]	0.13[c]	[h]
^{197}Au-Az-2[g]	1474	25.2	0.51	0.46	101	-2.4	0.06[c]	-0.04[c]	[h]

[a]Hyperfine interaction in MHz. [b]Values for an electron in the s-orbital (a^o_{iso}) or p-orbital (a^o_{dip}) of the atom, taken from Ref. 30. a^o_{dip} values estimated for an electron in the p-orbital of Cu, Ag or Au metal atoms, taken from Ref. 49. [c]ρ_{2s} and ρ_{2p} for ^{14}N. [d]ρ_{2s} and ρ_{2p} for ^{13}C. [e]ρ_{3s} for ^{31}P. [f]ρ_{2s} for ^{19}F. [g]Most intense trapping site. [h]This work.

A comparison of the unpaired "ns" spin contributions of the Ag and N nuclei for the M-$\overline{NHCH_2CH_2}$ complexes, with those of similar structures reported in the literature,

suggests that they are σ-bonded complexes involving dative-type interactions between a lone pair of electrons on the ligand and the metal. More specifically, the electrons of the highest occupied molecular orbital of the heterocycle are donated to an empty sp-hybridized orbital on the metal center, with the unpaired electron localized in another sp-orbital projected away from the ligand.

Based on the magnitude of metal ρ_{ns} in the complexes presented in Table 27, one can determine that the relative M-L bond strength depends on the heterocycle involved in complexation. For example, looking at the complexes formed with Cu, ρ_{4s} contribution to the SOMO decreases in the order Cu-$\overline{OCH_2CH_2}$ > Cu-$\overline{SCH_2CH_2}$ > Cu-$\overline{NHCH_2CH_2}$, suggesting a greater "4p" spin contribution and an increase in the degree of hybridization on the metal to accommodate the ligand interaction. Pseudo-complexes, held together by van der Waals interactions would have large metal "s" spin contributions and small ligand unpaired spin contributions resulting in weaker interactions, as observed in the case of Ag---C_2H_4 and Ag---CO.[37,64] It is safe to say that the strength of the complexes for each metal series in the present study follows the order:

M-$\overline{NHCH_2CH_2}$ > M-$\overline{SCH_2CH_2}$ > M-$\overline{OCH_2CHC_6H_5}$ > M-$\overline{OCH_2CH_2}$.

Comparing the unpaired spin population contributions by the Group 11 metal and nitrogen atoms in the mononuclear metal-aziridine complexes, one finds that the strongest bond is formed with the Au atom, and decreases in the order:

Au-$\overline{NHCH_2CH_2}$ > Cu-$\overline{NHCH_2CH_2}$ > Ag-$\overline{NHCH_2CH_2}$.

The complexes also vary in relative stability when annealed in the cavity of the spectrometer. In general, the persistence of the EPR signals for the complexes follows the

order M-$\overline{NHCH_2CH_2}$ > M-$\overline{OCH_2CH_2}$ > M-$\overline{SCH_2CH_2}$. The EPR signals due to M-$\overline{NHCH_2CH_2}$ persisted to T ≈ 240 K for M = Cu, Ag and Au.

The increase in the a_{63Cu} values of ^{63}Cu-$\overline{OCH_2CH_2}$ or ^{63}Cu-$\overline{NHCH_2CH_2}$ as a function of increasing temperature is thought to be related to the strength of the M-L bond. When the sample was recooled to 77 K the initial a_{63Cu} value was obtained.

Howard *et al.*,[49,55] observed similar behaviour for the a_M values of the products of ^{63}Cu-CO or ^{107}Ag-CH_2CO reactions in adamantane as a function of temperature. They concluded that this phenomenon arises from the metal-ligand bending vibration. In the case of $^{63}Cu(CO)_3$ the authors were able to estimate the value of the out-of-plane bending mode from a least-squares fitting of the hyperfine data to a hyperbolic cotangent function. The hyperfine data collected at various temperatures, Tables 19 and 20 (Section 4.4.), in the present study show one of two types of trendlines, i.e., concave upward or concave downward. Larger deviations in the a_{63Cu} values of ^{63}Cu-$\overline{OCD_2CD_2}$ are due to the fact that accurate magnetic field positions for the m_I = +3/2 and +1/2 transition lines were difficult to obtain because they were found at very low field. It is interesting to note also that the 3.3% increase in the hyperfine interaction for ^{63}Cu-$\overline{OCD_2CD_2}$, Table 21, is very small compared to that of the 30% increase in a_{63Cu} for $Cu(CO)_3$ when the sample was annealed from 77 to 250 K.

The nitrogen hyperfine, a_N of M-$\overline{NHCH_2CH_2}$ did not change as a function of temperature, supporting the theory that the bending vibration is affected rather than stretching. If the magnetic nitrogen nuclei were shifting farther away from the unpaired electron a smaller value of a_N would be anticipated. It is intriguing to find that

complexes, ^{197}Au-$\overline{NHCH_2CH_2}$ and ^{197}Au-$\overline{SCH_2CH_2}$, did not exhibited any increases in hyperfine values when annealed in the spectrometer, leading one to conclude a tighter complex is formed (stronger interactions requires more energy to cause vibrations).

A final interesting note is how well the internal energies of the metal complexes, predicted by DFT, compliment the stability trends observed based on EPR evidence. Firstly, calculations with any of the three functionals, B3LYP, M06, or BHandHLYP, show that the internal energy, for all mononuclear metal-heterocyclic complexes formed with Cu, Ag or Au atoms, are lower relative to the respective energies for the metal and substrate alone, Table 26. Secondly, the most stable complexes (lowest in energy relative to the reactants) are formed with aziridine, ethylene oxide forms the least stable complexes of the three heterocycles, therefore the order of stability is:

$$M\text{-}\overline{NHCH_2CH_2} > M\text{-}\overline{SCH_2CH_2} > M\text{-}\overline{OCH_2CH_2}.$$

A portion of the alpha density matrix presented in Table 30, from calculations of mononuclear Cu-heterocyclic complexes at the B3LYP/6-311+G(d) level, show the contribution of the atomic orbitals (AOs) of O, N, or S and Cu atoms to the total density (over all the molecular orbitals). In comparing the values of ethylene oxide and aziridine, one notices that the nitrogen contribution to the total density is greater than that of the oxygen atom, leading us again to conclude that the Cu-$\overline{NHCH_2CH_2}$ interaction is stronger, coinciding with the EPR experiments.

Table 30. Density matrix calculated at the B3LYP/6-311+G(d) level of theory for mononuclear Cu complexes formed with oxirane, thiirane and aziridine.

		O		N		S	
		4s	5s	4s	5s	6s	7s
Cu	8s	0.08766	0.12891	**0.13346**	**0.20297**	0.11904	0.20769
	9s	0.07254	0.08798	**0.14984**	**0.15995**	0.10581	0.18594

5.2. Tri-ligand Cu-containing complexes

Ethylene oxide, ethylene oxide-d_4, ethylene oxide-$^{13}C_2$ and 1,2-epoxybutane all gave similar central features, A, A-d_4, A-^{13}C and B, respectively, when co-condensed with $^{63/65}$Cu atoms in adamantane, Figure 99. Isotropic substitution of ethylene oxide had no effect on the EPR spectrum indicating that the carbon and hydrogen atoms are not close enough to interact with the unpaired electron on the Cu atom. The EPR spectra of the central features are axial with $g_{\|} > g_{\perp}$ and $a_{\|}$ (^{63}Cu) > $a_{\perp}$ (^{63}Cu), Table 31. When looking at the literature, Table 1 (section 1.3.) and comparing the magnitude of a_{iso} for A-d_4, A-^{13}C and B, 117 MHz, 117 MHz and 119 MHz, respectively, one notices that they fall in the range found for multi-ligand Cu-complexes, i.e., 123 MHz for $^{63}Cu(C_2H_4)_2$,[38] 126 MHz for $^{63}Cu(C_2H_2)_2$,[41] and 120 MHz for $^{63}Cu[PMe]_3$ or $^{63}Cu[P(OMe)_3]_3$.[48] The EPR spectra reported for $^{63}Cu[PMe]_3$ and $^{63}Cu[P(OMe)_3]_3$ are both axial, falling in line with the observations made for the central features A and B. These tri-ligand Cu complexes are thought to arise from the donation of lone-pair electrons from three phosphorous ligands into the hybridized metal atom orbitals. A similar planar structure would be expected with ethylene oxide or 1,2-epoxybutane if the lone-pair electrons of the oxygen atom of three epoxide rings is donated a to the Cu atom.

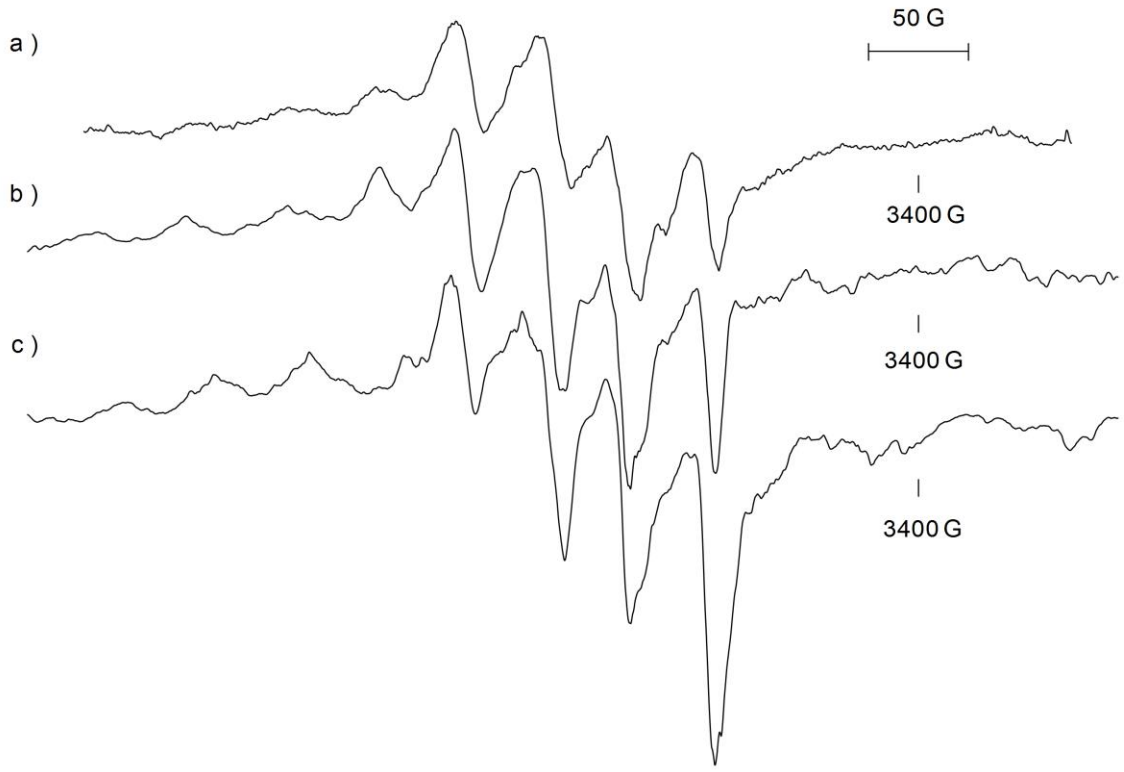

Figure 99. Central region of the EPR spectra recorded at 77 K for the reactions of $^{63/65}$Cu atoms with a) ethylene oxide-$^{13}C_2$, b) ethylene oxide-d_4 and c) 1,2-epoxybutane.

Table 31. Magnetic parameters[a] of A and B formed in the reaction $^{63/65}$Cu atoms with ethylene oxide and 1,2-epoxybutane.

	A-d_4	A-$^{13}C_2$	B	^{63}Cu(PMe)$_3$	$^{63}CuO_2$[b]
$a_{\parallel}$ (^{63}Cu)	138	138	130	293	a_{xx} = 106
$a_{\perp}$ (^{63}Cu)	110	110	110	34	a_{yy} = 123
					a_{zz} = 133
$g_{\parallel}$	2.1217	2.1217	2.1143	2.0023	g_{xx} = 2.0000
$g_{\perp}$	2.0075	2.0065	2.0073	2.0016	g_{yy} = 2.0070
					g_{zz} = 2.0810
g_{iso}	2.0456	2.0449	2.0430	2.0018	2.0290
a_{iso}	119[d]	119[d]	117[d]	120	120
ρ_{4s}[c]	0.02	0.02	0.02	0.02	0.02

[a]Hyperfine interaction in MHz. [b]Ref. 52. [c]Calculated using a_{iso} = 5995 MHz, for an electron in a Cu 4s orbital.[30] [d]Assuming that both $a_{\parallel}$ (^{63}Cu) and $a_{\perp}$ (^{63}Cu) are positive.

The calculations for the unpaired spin density contributions from the metal s-orbital, ρ_{4s}, is quite small, 0.02, Table 31. The a_{dip} of 9 MHz, calculated using equation

(17), is used to estimate the Cu "4p" unpaired spin density, ρ_{4p}, $a_{dip} = 1/3(a_{\parallel} - a_{\perp})$ = (138 -110)/3 = 9 MHz. More specifically, $\rho_{4p} = a_{dip}$ (Cu) /αP, where α is 0.4 for a p orbital and P is the atomic parameter for the unit spin population in the Cu "4p" orbital. P had been estimated to be 171 MHz[48] or 217 MHz[110] by two different research groups. This means for A and B $\rho_{4p} \approx 0.1$-0.13 assuming that there is limited rotational averaging of the hyperfine tensor occurring at 77 K. Without additional information from hyperfine splitting originating from the ligands one can only assume that the remaining (0.85-0.88) unpaired electron density is delocalized onto the ligands. In a previous study Howard *et al*.[52] reported a $\rho_{4s} = 0.02$ for $^{63}CuO_2$ formed in the reaction of Cu atoms with O_2 in adamantane. Isotropic substitution of ^{16}O for ^{17}O showed that the oxygen atom contributed significantly to the unpaired spin density. It was suggested that $^{63}CuO_2$ has similarities to a peroxyl with the unpaired electron largely confined to the π^* orbital of the adjacent oxygen nuclei. It is difficult to imagine how this bonding scheme could be applied to A and B. Also noteworthy are the large g_{iso} values for A and B, 2.046 and 2.043, respectively. This can be compared to the value of 2.0018 found for $^{63}Cu(PMe_3)_3$ and 2.029 for $^{63}CuO_2$. The positive shift in *g*-value (+0.04) from the value of a free electron (2.0023) indicates the admixture of the partially filled Cu 4s orbital with a filled Cu 3d orbital of similar energy.[52]

A and B are tentatively assigned to the tri-ligand Cu-heterocyclic complexes based on the similarity of their a_{63Cu} to those of the $^{63}Cu(PX_3)_3$ complexes, the axial pattern of the spectra, and the large *g*-values associated with Cu-O linked structures. In order to confirm this, the experiments would have to be repeated with ^{17}O labelled ethylene oxide.

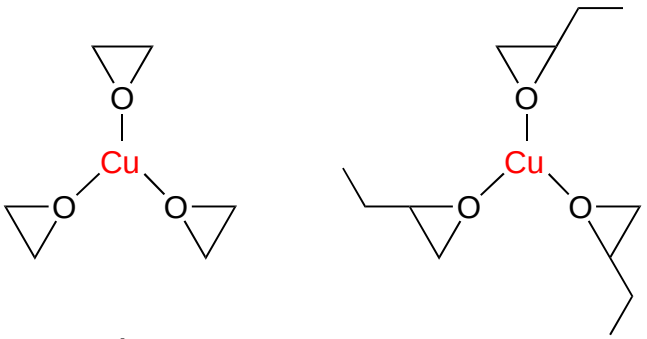

5.3. Metallacycles

The Cu-ethylene oxide, Cu-ethylene oxide-d_4, and Cu-1,2-epoxybutane reaction mixtures that generated the anisotropic central features discussed in Section 5.2., were irradiated with a Hg-Xe lamp for 6 h. This led to the appearance of features labelled A-UV, A-d_4-UV, and B-UV, respectively. Upon closer examination of Figure 30 (section 4.1.1.3), it is believed that, A-d_4-UV, was present prior to irradiating the sample and that either light caused the original anisotropic 77 K spectrum to diminish in intensity, revealing the underlying signals, or the UV light promoted the formation of A-d_4-UV, thus increasing its concentration in the reaction mixture. The isotropic quartet observed for A-d_4-UV has an $a_{^{63}Cu}$ of 196 MHz and *g*-value of 2.0000. The isotropic $a_{^{63}Cu}$ translates to an unpaired Cu 4s orbital spin contribution, ρ_{4s}, of 0.03. Small ρ_{4s} values have been reported in the literature for Cu β-substituted vinyls, e.g., $^{63}CuCH{=}\dot{C}H$ (ρ_{4s} = 0.09) and $CH_2C(^{63}Cu)O$ (ρ_{4s} = <0.01), or Cu insertion products, e.g., $H^{63}CuNH_2$ (ρ_{4s} = 0.04) and $H^{63}CuCH_3$ (ρ_{4s} = 0.05).

A possible structure for the radical giving rise to this EPR spectrum is a four-membered metallacycle, $\overline{CuOCH_2CH_2}$, formed by insertion of Cu-atoms into the C-O

bond of ethylene oxide. Reactions of ethylene oxide with other first-row transition metals, namely, Ni^0 or Fe^0 atoms, in argon matrices at 10 K, resulted in C-O bond activation forming analagous metallacyclic intermediates, i.e., nickelaoxetane and ferraoxetane, characterized by IR spectroscopy.[111,112] Formation of the Cu atom N-H and C-H insertion products, $H^{63}CuNH_2$ and $H^{63}CuCH_3$, studied by EPR spectroscopy, required UV light to promote the reaction via excitation of the unpaired electron in the Cu 4s orbital into a vacant 4p orbital, $^2P \leftarrow {}^2S$.

The UV irradiated Cu-ethylene oxide and Cu-ethylene oxide-d_4 reaction mixtures gave rise to the same spectral feature at $g \approx 2.0000$ whereas the Cu atom-1,2-epoxybutane reaction mixture yielded a more complex quartet of triplets, B-UV, Figure 38 (Section 4.1.1.3). The quartet and triplet spacings of 192 and 54 MHz, respectively, suggest that the unpaired electron interacts with a Cu nucleus and two equivalent H nuclei. The magnitude of the a_{63Cu} values for features A and B are very similar, 192 and 196 MHz, respectively. Since the 1,2-epoxybutane molecule is asymmetrical, insertion into the C_1-O or C_2-O bonds of the ring should yield two different products, $\overline{OCuCH_2CH}CH_2CH_3$ and $\overline{CuOCH_2CH}CH_2CH_3$, respectively. Reactions of 1,2-epoxybutane with Al or Ga atoms under similar conditions (adamantane matrix at 77 K) yielded both C_1-O and C_2-O insertion products.[113,114]

In the reaction of $^{63/65}$Cu atoms with ethylene sulfide, Figure 44 (Section 4.1.2.), there was a well-defined quartet, ^{63}Cu-ES-2, with a spacing of a_{63Cu} = 439 MHz centered at g = 1.9993 was observed. This species formed spontaneously, i.e., without subjecting the sample to UV irradiation. The Cu "4s" spin contribution, ρ_{4s}, is 0.07. This is

comparable to that for $H^{63}CuCH_3$, $H^{63}CuNH_2$, $^{63}\overline{CuOCH_2CH_2}$ insertion products. This species is therefore assigned to the C-S insertion product, cuprathietane, $\overline{CuSCH_2CH_2}$.

The a_{63Cu} values of $\overline{CuOCH_2CH_2}$ (**A**), $\overline{CuSCH_2CH_2}$ (**B**), $\overline{OCuCH_2CH}CH_2CH_3$ (**C**), $\overline{CuOCH_2CH}CH_2CH_3$ (**D**), $HCuNH_2$ (**E**) and $HCuCH_3$ (**F**) were estimated using the three DFT functionals, B3LYP, M06, and BHandHLYP with a number of different basis sets, Table 32, in an attempt to obtain support for the structural assignments. With the odd exception, agreement between the estimated and experimental a_{63Cu} values is poor, as is evidenced by the large % deviation values, Table 32. As a result, the reliability of DFT calculations to predict the a_{63Cu} values is limited.

Despite the poor performance in predicting a_{63Cu}, interesting information about the expected H hyperfine interaction values of **A**, **B**, **C**, and **D** was obtained, Table 33. In all cases, a_H for the ring hydrogens, H_1, H_2, and H_3 are small. This is consistent with the absence of superhyperfine structure in the products formed in the Cu-ethylene oxide and Cu-ethylene sulfide reactions. For structure **D**, Cu atom C_2-O insertion product, H_4 and H_5 are estimated to have relatively large hyperfine interaction values. This is surprising since these are farther away from the Cu atom assumed to bear most of the unpaired electron density. The large values for a_{H4} and a_{H5} would account for the two hydrogen nuclei observed in the experimental spectrum obtained in the Cu-1,2-epoxybutane reaction and inequivalence in H_4 and H_5 predicted by DFT calculations is due to the relative orientation of the two atoms. This is only one possible orientation of the molecule and others might exist where the ethyl side chain is slightly rotated with respect to the ring. Rapid rotation of the ethyl side chain would render the hydrogen

Table 32. DFT predictions for a_{Cu}[a] of Cu-containing metallacycles (A, B, C and D) as well as $HCuNH_2$ and $HCuCH_3$.

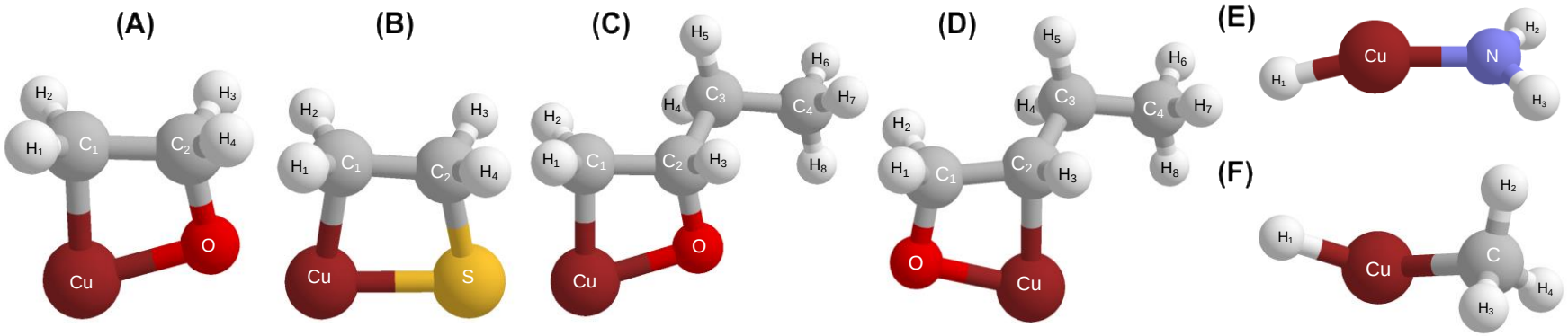

Functional	Basis Set	(A)	(B)	(C)	(D)	(E)	(F)
B3LYP	6-311G	495 (>100)	229 (47.8)	446 (>100)	415 (>100)	178 (27.9)	434 (32.3)
	6-311+G	336 (71.4)	226 (48.5)	310 (61.5)	276 (43.8)	115 (53.4)	521 (58.8)
	6-311+G(d)	305 (55.6)	273 (37.8)	272 (41.7)	236 (22.9)	7 (97.2)	517 (57.6)
	EPR-III[b]	316 (61.2)	*c*	285 (48.4)	244 (27.1)	0 (100.0)	518 (57.9)
	6-31++G(d,p)[b]	314 (60.2)	273 (37.8)	282 (46.9)	242 (26.0)	13 (94.7)	514 (56.7)
M06	6-311G	195 (0.5)	11 (97.5)	163 (15.1)	125 (34.9)	69 (72.1)	156 (52.4)
	6-311+G	162 (17.3)	108 (75.4)	146 (24.0)	96 (50.0)	232 (6.1)	*d*
	6-311+G(d)	124 (36.7)	141 (67.9)	105 (45.3)	55 (71.4)	110 (55.5)	*d*
	EPR-III[b]	131 (33.2)	*c*	112 (42.7)	62 (67.7)	103 (58.3)	*d*
	6-31++G(d,p)[b]	122 (37.8)	122 (72.2)	104 (45.8)	47 (75.5)	109 (55.9)	*d*
BHandHLYP	6-311G	819 (>100)	507 (15.5)	778 (>100)	820 (>100)	250 (1.2)	425 (29.6)
	6-311+G	731 (>100)	495 (12.8)	708 (>100)	756 (>100)	234 (5.3)	671 (>100)
	6-311+G(d)	702 (>100)	560 (27.6)	676 (>100)	716 (>100)	105 (57.5)	664 (>100)
	EPR-III[b]	702 (>100)	*c*	679 (>100)	714 (>100)	252 (2.0)	659 (>100)
	6-31++G(d,p)[b]	697 (>100)	564 (28.5)	673 (>100)	720 (>100)	162 (34.4)	656 (>100)
Experimental		196	439	192	192	247[e]	328[f]

[a]Hyperfine interaction in MHz. [b]Cu treated with 6-311+G(d) basis set. [c]S atoms outside basis set range. [d]No stationary point found. [e]Ref. 47. [f]Ref. 56.

Table 33. DFT predictions for a_H[a] of cupraoxetanes and cuprathietane.

(A) (B) (C) (D)

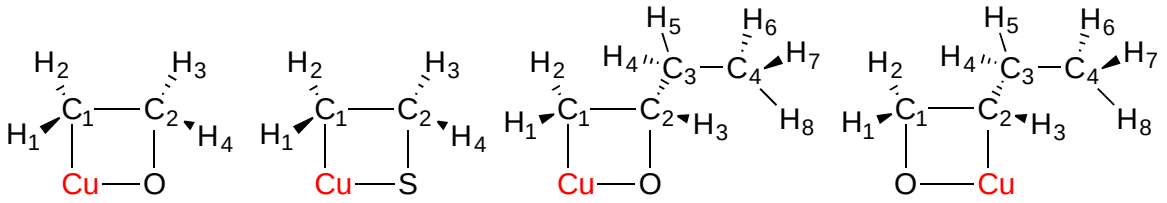

Molecule	Basis Set[b]	H_1	H_2	H_3	H_4	H_5
(A)	6-311G	1.4	2.4	2.0	3.0	-
	6-311+G	1.4	1.4	1.3	1.3	-
	6-311+G(d)	1.2	1.2	1.0	1.0	-
	EPR-III	2.1	2.1	1.0	1.0	-
	6-31++G(d,p)	0.8	0.8	0.9	0.9	-
(B)	6-311G	6.9	7.4	1.1	8.4	-
	6-311+G	4.0	4.0	6.0	6.0	-
	6-311+G(d)	0.5	0.5	4.0	4.0	-
	EPR-III	-	-	-	-	-
	6-31++G(d,p)	0.9	0.9	3.9	3.9	-
(C)	6-311G	1.3	0.9	2.9	0.5	0.8
	6-311+G	1.1	0.2	1.6	0.6	0.5
	6-311+G(d)	1.3	2.7	1.4	0.4	2.1
	EPR-III	2.1	3.6	1.4	0.5	2.3
	6-31++G(d,p)	1.0	1.4	2.3	0.4	2.1
(D)	6-311G	0.7	3.5	5.4	6.2	27.2
	6-311+G	1.5	2.2	4.6	12.9	47.3
	6-311+G(d)	0.7	2.8	6.6	13.3	49.1
	EPR-III	0.7	2.9	8.0	14.9	53.6
	6-31++G(d,p)	0.6	2.6	6.4	13.2	49.0

[a]Hyperfine interaction in MHz. [b]B3LYP functional used for all calculations.

nuclei equivalent. Most likely the magnitude of a_{H5} originates from the orientation with respect to the plane of the metallacycle. The (Cu-C_2-C_3-H_5) dihedral angle in **D**, is 170^O, allowing the alignment of the hydrogen s orbital with a Cu d orbital, giving rise to a_H = 54 MHz. The experimental data and DFT calculations of the hyperfine interaction led us to suggest that the Cu atom C_2-O insertion product, **D**, is formed in the Cu atom-1,2-epoxybutane reaction.

It is interesting to note that reactions of $^{63/65}$Cu atoms did not form the C-N insertion product, $\overline{CuNHCH_2CH_2}$, when reacted with aziridine. In reanalyzing the DFT calculations, Table 42 Section (4.5.2.), it is evident that Cu atom C-O and C-S insertion products of ethylene oxide and ethylene sulfide, are lower in energy than the complex, while the Cu atom C-N insertion product of aziridine is in higher energy (making it a less favorable reaction). Another question one might ask is why the C-S insertion product formed without the aid of UV irradiation. This can also be explained with the DFT calculations. From Figure 95 (*vide supra*), it is obvious that cuprathietane is of much lower energy than the cupraoxetane meaning that: a) it is predicted to be more stable, and b) it could potentially have a lower energy barrier (not requiring energy provided by the UV irradiation). However, modeling of the transition states would have to be done in order to test this hypothesis.

Metallacyclic intermediates were not detected in the Ag and Au atom reactions. This is not surprising when looking at the DFT results. As mentioned above both Ag and Au are predicted to form stable mononuclear complexes, but less stable metallacyclic intermediates with geometries adopting a structure with longer bonds between the metal and heteroatom from the ring (See Appendix 8.1.1.). Generally speaking, in the reactions of Ag and Au atoms with ethylene oxide and aziridine, the calculations predict an increase of more than 10 kcal/mol in going from the metal-heterocyclic complex to the metallacyclic intermediate and an increase of less than 7 kcal/mol for ethylene sulfide.

5.4. Ring-opened Styrene oxide Radical

The central features generated by $^{63/65}$Cu- and $^{107/109}$Ag-styrene oxide reaction mixtures, Figure 100, dominated the EPR spectra. At 160 K these centers are best described as doublets of triplets with the intensity of the transition lines being 1:3:3:1. This signal is typical of that expected for an alkyl radical containing α and β hydrogens. The α-hydrogens interchange positions rapidly, through rotation, causing them to be equivalent in the magnetic field. The magnitude of the isotropic β-hydrogen varies as a function of the dihedral angle, θ, more specifically, the angle formed between the C_β-H_β bond and the p_π orbital, equation (19),

$$a_{H_\beta} = B_0 + B \cos^2 \theta \qquad (19)$$

where constants B_0 and B have been empirically determined to be 4 G and 50 G, respectively.[115] The spectral pattern is thus interpreted as the ring-opened styrene oxide radical, $C_6H_5CH(O^-)\dot{C}H_2$ with two equivalent hydrogens, a_{H_α} = 56.0 MHz and a single β-hydrogen, a_{H_β} = 68.9 MHz (θ = 65.7°). The magnitude of a_{H_β} and calculated dihedral angle for the C_β-H_β bond relative to the p_π orbital are both larger than that found for the ring opened 1,2-epoxybutane, $CH_2CH_3CH(O^-)\dot{C}H_2$, θ = 56°.[113] The bulky phenyl group on C_β is likely responsible for this difference, creating a more stable radical that exists above 250 K.

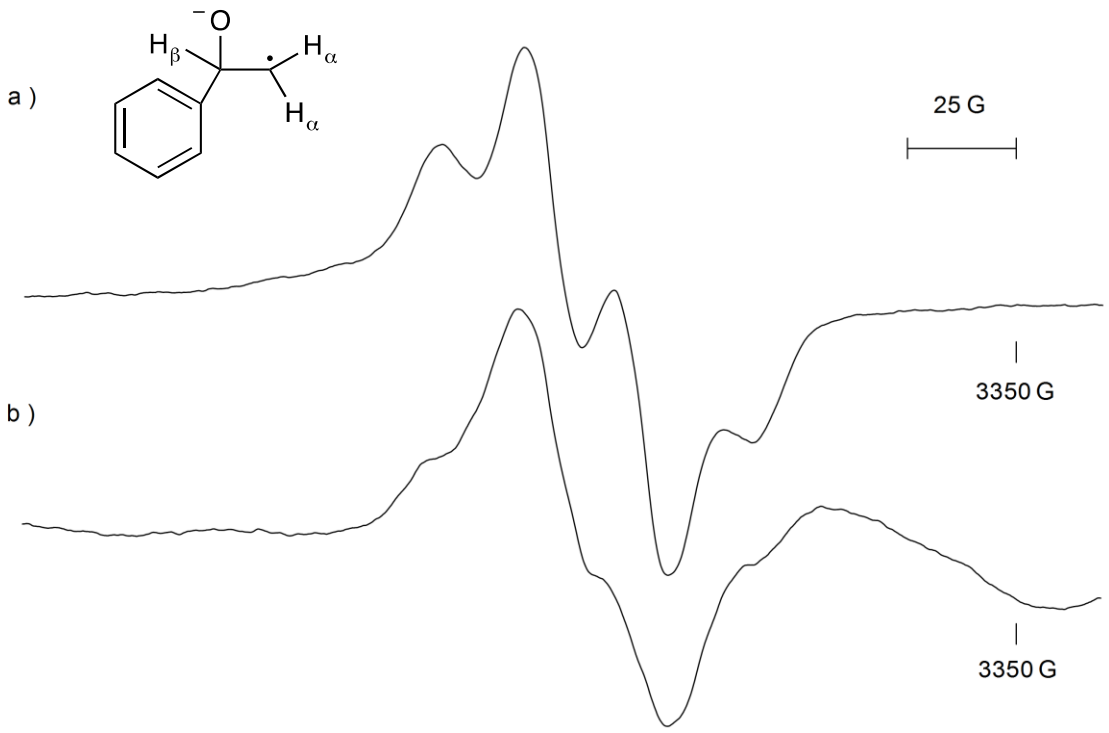

Figure 100. Comparing the central EPR features C and G at 160 K from reactions of styrene oxide with a) $^{63/65}$Cu atoms (*v* = 9118 MHz, m.p. = 2 mW) and b) $^{107/109}$Ag atoms (*v* = 9119 MHz, m.p. = 2 mW).

There has been experimental evidence by other groups for argentaoxetanes formed from ethylene oxide or styrene oxide on Ag (111) and Ag (110) surfaces.[116,117] Researchers are still unsure whether if the ring-opened radical (not observed) is formed first, followed by rapid closure into the metallacycle or the reverse, where the metallacycle is first formed and opens due to ring-strain. The former mechanism whereby the metal coordinates to the oxygen atom first (EPR evidence for a mononuclear complex) leading to homolytic cleavage of the less hindered C-O bond and oxidative addition to the metal center, is the mechanism preferred by Enever *et al.*[117] In the case of $C_6H_5CH(O^-)\dot{C}H_2$, perhaps too much energy is required to close the ring, and thus remains in the form $C_6H_5CH(O^-M^+)\dot{C}H_2$.

5.5. Other Small Central Radicals

The discussion thus far has been primarily focused on complexation and activation of bonds in three-membered heterocycles with Group 11 metal atoms. We would like to mention, in this section, some other interesting radicals discovered during the course of this study.

In the reactions of $^{107/109}$Ag and ^{197}Au with aziridine and aziridine-^{15}N we observed the characteristic EPR spectrum for the aziridino radical, $\overline{\dot{N}CH_2CH_2}$. The transition lines for $\overline{\dot{N}CH_2CH_2}$ were more intense in the case of ^{197}Au atom reactions suggesting that the Au atoms are more effective in facilitating N-H abstraction. Selective N-H bond cleavage by transition metals is of great interest to chemists as it opens new catalytic reaction routes for the cross-couplings of two substrates and functionalization of amines.[118–120] Several studies have shown that Cu^I metal complexes, i.e., $CuBr(SMe)_2$, are important in the formation of mononuclear metal-amido species via N-H bond activation[118] and also the oxidative C-H/N-H cross-coupling between formamides and amides. It was therefore surprising Cu atoms did not activate the formation of $\overline{\dot{N}CH_2CH_2}$. Nonetheless, the possibility that the reaction occurs and more stable diamagnetic products are rapidly formed cannot be ruled out.

In the reaction of $^{107/109}$Ag atoms with ethylene sulfide the EPR signal, H, centered at g ~ 2.0023 was much more intense than the transitions corresponding to the mononuclear metal-ring complex, Figure 64. The best simulation assumed the interaction of the unpaired electron with a Ag nucleus (a_{107Ag} = 53.6 MHz or a_{109Ag} = 61.7 MHz) and eight equivalent hydrogen nuclei ($a_H(8)$ = 21.7 MHz), taking into consideration two

overlapping species resulting from the two Ag isotopes, ^{107}Ag and ^{109}Ag. This was confirmed by repeating the reaction with isotopically enriched ethylene sulfide-d_4, i.e., collapse of the multi-lined pattern obtained for the Ag-ethylene sulfide to a doublet due to a_{Ag}. This is consistent with what one would expect for a tight ion pair, $Ag^+[C_2H_4SSC_2H_4]^-$. Similarly, in the reaction of ^{197}Au atoms with ethylene sulfide, an intense feature, L, centered at g = 2.0080 was observed, Figure 82. A good simulation of L was achieved assuming the presence of one Au nuclei, with a_{Au} = 48 MHz and eight equivalent hydrogen nuclei, with a_H (8) = 22 MHz. This species is therefore assigned to the tight ion pair $Au^+[C_2H_4SSC_2H_4]^-$. Reactions of Al and Ga atoms with H_2S in adamantane matrices afforded a similar tight ion pair, M^+HSSH^-.[121] It is believed that significant electron transfer from the metal atom to the H_2S molecule results in the formation of $M^+H_2S^-$, which subsequently reacts with another molecule of H_2S in the matrix to generate the disulfide anion/metal tight ion pair, M^+HSSH^- and H_2. The magnitude of the hydrogen nuclei, a_H of 21 MHz for Al^+HSSH^- is practically identical to the value of a_H = 22 MHz observed for $Ag^+[C_2H_4SSC_2H_4]^-$.

Annealing the Ag-ethylene sulfide reaction mixture to temperatures above 140 K resulted in the formation a new radical centered at g = 2.0187, partially masking the radical anion signal of $Ag^+[C_2H_4SSC_2H_4]^-$. An identical quartet pattern was observed at 220 K whether the reaction was carried out with ethylene sulfide of ethylene sulfide-d_4. This is due to interaction of the unpaired electron with three equivalent neighboring Ag nuclei, where, a_{Ag} = 32.4 MHz. Cooling the sample back to 77 K did not regenerate the spectrum for the tight ion pair, but rather an anisotropic feature with no hyperfine

interaction, $g_{\|}$ =2.0019 and $g_{\perp}$ =2.0297 (g_{iso} = 2.0205), was observed. When slowly warming the sample back to 220 K, the quartet with a_{Ag} = 32.4 MHz Ag hyperfine was reestablished.

Small silver clusters, Ag_3, have been trapped in both hexadeuterobenzene (C_6D_6)[122] and N_2[123] under matrix isolation conditions. The EPR parameters of a_{Ag} (2) = 827 MHz, a_{Ag} (1) = 108 MHz and g = 1.9622, led Howard *et al*.[122] to propose a bent structure with the unpaired electron localized in the s atomic orbitals of the terminal atoms. They were surprised to find a large shift from the g-value of a free electron (2.0023), suggesting this effect is caused by intramolecular spin-orbit interactions. For Ag_3 clusters isolated in N_2, the anisotropic magnetic parameters, $g_{\|}$ =1.9933, $g_{\perp}$ =1.9558, $a_{Ag_{\|}}$ (1) = 871 MHz, $a_{Ag_{\perp}}$ (1) = 869 MHz, $a_{Ag_{\|}}$ (2) = 213 MHz and $a_{Ag_{\perp}}$ (2) = 204 MHz were reported.[123] These parameters suggest that the unpaired spin population is primarily located on one nucleus with smaller contributions from two equivalent nuclei. The acute triangular structure proposed to account for the spin distribution is in sharp contrast to the isomer found in C_6D_6 possessing obtuse angles.

EPR analysis of neutral Ag clusters trapped in zeolite materials gave an isotropic quartet with an intensity ratio of 1:3:3:1, with parameters, a_{Ag} (3) = 283 MHz and g = 2.0430.[124] There is a dramatic positive shift in g and large reduction in hyperfine splitting in comparison to that found for the naked Ag_3 clusters isolated in C_6D_6 or N_2 mentioned above. It is obvious that the environment greatly influences the EPR parameters of Ag_3 clusters. A more recent study has found an even more reduced

hyperfine interaction, i.e., a_{Ag} ~151 MHz when linear Ag_3 is formed in metal-organic frameworks (MOFs).[125]

The hyperfine interactions of naked metal clusters are also affected when they interact with ligands. For example, EPR studies of Ag atoms and C_2H_4 in adamantane, yielded $Ag_3[C_2H_4]$ with hyperfine interaction values smaller than those of the naked clusters, i.e., a_{Ag_x} (1) = 605 MHz, a_{Ag_y} (1) = 475 MHz, a_{Ag_z} (1) = 300 MHz, $a_{Ag_\perp}$ (2) = 200 MHz, $a_{Ag_\parallel}$ (2) = 215 MHz. Comparing the a_{iso} values for the central Ag atoms of Ag_3 in N_2, 870 MHz, with that of $Ag_3[C_2H_4]$, 460 MHz, one notices a large (47%) decrease in hyperfine interaction value.

It is quite possible that Ag_3 clusters may be formed in our reaction and interact with some sulfur-ligand in the matrix. Sulfur-containing rings notoriously undergo desulfurization and ring opening reactions leading to a number of products such as, sulfur allotropes (cyclo-S_n) or ethenethiol.[126,127] Of course none of our tentative conclusions can be asserted without further experiments. Mass spectrometry could be a good way to prove the presence of Ag_3 clusters, as they seem to be stable at room temperature in the EPR samples.

5.6. Unassigned EPR signals

There are a few EPR spectra that could not be assigned to any particular radical. They are D and D-^{15}N, ^{63}Cu-EO-d$_4$-2, ^{63}Cu-EO-^{13}C-2, $^{107/109}$Ag-ES-2, $^{107/109}$Ag-ES-3 and $^{107/109}$Ag-ES-d$_4$-2. In general, these represent a minor product based on the relative intensities of the transition lines of all radicals present in the various reaction mixtures.

Further experiments would have to be carried out to try and elucidate the structures of these unknown radicals. Since they were not the major products formed in the reaction, their identification was not pursued at this time.

6. Conclusion

The current study involving reactions between Group 11 metal atoms and three-membered heterocyclic compounds under cryogenic matrix-isolation conditions resulted in the formation and characterization of several novel paramagnetic species. The major findings of the thesis are listed below:

1) The major products formed in the reactions are mononuclear metal-heterocyclic complexes with relative stabilities following the order:

   $M\text{-}\overline{NHCH_2CH_2} > M\text{-}\overline{SCH_2CH_2} > M\text{-}\overline{OCH_2CH}C_6H_5 > M\text{-}\overline{OCH_2CH_2}$.

   Internal energy values, calculated using the B3LYP, M06 or BHandHLYP functionals in combination with the 6-311+G(d) basis set, are in agreement with this finding.

2) Tri-ligand complexes closely resembling $^{63}Cu(PX)_3$ (X = CH_3 or OCH_3), reported by M. Histed *et al.*,[48] are formed in the reaction of $^{63/65}$Cu atoms and oxiranes, ethylene oxide or 1,2-epoxybutane at 77 K.

3) We report for the first time evidence for the isolation of cupraoxetane, $\overline{CuOCH_2CH_2}$ and cuprathietane, $\overline{CuSCH_2CH_2}$ intermediates at 77 K. The insertion of $^{63/65}$Cu atoms into the C-S bond of ethylene sulfide occurred spontaneously, while C-O bond activation of oxiranes required UV irradiation of the samples.

4) In general, the relative a_{63Cu} values predicted by the functionals tested were in good agreement with the experimental values. The 6-311+G and 6-311+G(d) basis sets functioned best, while the EPR-III basis set failed to improve the hyperfine of magnetic ligand atoms and resulted in long computation times.

5) Other interesting radicals detected in the reactions were the ring-opened styrene oxide ($C_6H_5CH(O^-)\dot{C}H_2$), aziridino, ($\overline{\dot{N}CH_2CH_2}$), disulfide anions ($M^+[C_2H_4SSC_2H_4]^-$) and Ag_3-R sulfur complexes where R has not been well characterized.

The magnetic parameters and calculated spin populations for the paramagnetic species observed in the reactions of Cu, Ag or Au reactions with three-membered heterocyclic compounds have been summarized, Table 34. The findings in this thesis support mechanisms proposed for the catalytic transformations of three-membered rings mediated by Group 11 metals. More specifically, we have shown that mononuclear metal-ligand complexes and metallacyclic intermediates do exist along the reaction pathway.

This project still has some unanswered questions that can lead to future investigations. The experiments could be extended to include the reaction of Group 11 metals with phosphirane, $\overline{PHCH_2CH_2}$ (isoelectronic with thiirane). Based on our predictions it will form a slightly more stable complex with the metals than that observed for the strongest M-$\overline{NHCH_2CH_2}$ complexes. Subsequently, a better comparison of bonding can be made between the M-$\overline{PHCH_2CH_2}$ and known M-PF_3 complexes. Secondly, we could examine the reactions of the Group 11 metals with acyclic compounds, namely, dimethyl ether, dimethyl sulfide and dimethyl amine, to see if the intrinsic ring strain of the molecules affects the strength of the observed complexes and if C-X bond activation occurs. More elaborate molecules such as vinyl oxiranes, thiirane and aziridines could be used to get a better comparison with the catalytic ring expansion studies found in the literature. Further effort must be spent in improving the DFT

calculations so that the nuclear hyperfine interaction values of Ag-and Au-containing species can also be mimicked.

Table 34. Summary of magnetic parameters[a] and calculated spin populations[b] for paramagnetic species observed in reactions of Group 11 metal atoms with three-membered heterocyclic compounds.

Species	Assignment	g_{iso}	$a_{iso\ (M)}$	$a_{iso\ (N)}$	ρ_{ns} (M)	ρ_{2s} (N)
Mononuclear-metal complexes						
^{63}Cu-EO-1	Cu-$\overline{OCH_2CH_2}$	2.0091	4349	-	0.73	-
^{63}Cu-EO-d_4-1	Cu-$\overline{OCD_2CD_2}$	2.0098	4336	-	0.72	-
^{63}Cu-EO-^{13}C-1	Cu-$\overline{O^{13}CH_2{}^{13}CH_2}$	2.0095	4347	-	0.73	-
^{63}Cu-EB-1	Cu-$\overline{OCH_2CH}CH_2CH_3$	2.0101	4293	-	0.72	-
^{63}Cu-EB-2		2.0043	4469	-	0.75	-
^{63}Cu-SO-1	Cu-$\overline{OCH_2CHC_6H_5}$	2.0099	3740	-	0.62	-
^{63}Cu-SO-2		2.0011	3920	-	0.65	-
^{63}Cu-ES-1	Cu-$\overline{SCH_2CH_2}$	2.0082	3625	-	0.60	-
^{63}Cu-Az-1	Cu-$\overline{NHCH_2CH_2}$	2.0094	3223	69	0.54	0.04
^{63}Cu-Az-2		2.0083	3122	65	0.52	0.04
^{63}Cu-Az^{15}N-1	Cu-$\overline{^{15}NHCH_2CH_2}$	2.0096	3221	103	0.54	-
^{63}Cu-Az^{15}N-2		2.0074	3122	93	0.52	-
^{107}Ag-EO	Ag-$\overline{OCH_2CH_2}$	2.0016	1619	-	0.88	-
^{107}Ag-SO-1	Ag-$\overline{OCH_2CHC_6H_5}$	2.0009	1524	-	0.83	-
^{107}Ag-SO-2		2.0001	1462	-	0.80	-
^{107}Ag-SO-3	Ag[C_6H_5]-R	2.0018	1601	-	0.88	-
^{107}Ag-ES-1	Ag-$\overline{SCH_2CH_2}$	1.9988	1401	-	0.77	-
^{107}Ag-ES-d_4-1	Ag-$\overline{SCD_2CD_2}$	1.9991	1400	-	0.76	-
^{107}Ag-Az-1	Ag-$\overline{NHCH_2CH_2}$	2.0000	1362	55	0.74	0.03
^{107}Ag-Az-2		1.9995	1291	55	0.71	0.03
^{107}Ag-Az^{15}N-1	Ag-$\overline{^{15}NHCH_2CH_2}$	1.9999	1360	78	0.74	-
^{107}Ag-Az^{15}N-2		1.9992	1290	78	0.71	-
^{197}Au-EO-1	Au-$\overline{OCH_2CH_2}$	2.0232	2652	-	0.92	-
^{197}Au-ES	Au-$\overline{SCH_2CH_2}$	1.9862	1542	-	0.54	-
^{197}Au-Az-1	Au-$\overline{NHCH_2CH_2}$	2.0378	1374	100	0.48	0.06
^{197}Au-Az-2		2.0332	1474	101	0.51	0.06
^{197}Au-Az^{15}N-1	Au-$\overline{^{15}NHCH_2CH_2}$	2.0378	1374	139	0.48	-
^{197}Au-Az^{15}N-2		2.0328	1475	142	0.51	-
Tri-ligand complexes						
A-d_4	Cu($\overline{OCD_2CD_2}$)$_3$	2.0456	119	-	0.2	-
A-^{13}C	Cu($\overline{O^{13}CH_2{}^{13}CH_2}$)$_3$	2.0449	119	-	0.2	-
B	Cu($\overline{OCH_2CHCH_2CH_3}$)$_3$	2.0430	117	-	0.2	-

Table 34. continued.

Species	Assignment	g_{iso}	a_{iso} (M)	a_{iso} (N)	ρ_{ns} (M)	ρ_{2s} (N)
Metallacycles						
A-UV	$\overline{CuOCH_2CH_2}$	2.0005	189	-	0.03	-
A-d_4-UV	$\overline{CuOCD_2CD_2}$	2.0000	196	-	0.03	-
B-UV	$\overline{CuOCH_2CH}CH_2CH_3$	2.0009	192	54[c]	0.03	0.4[d]
^{63}Cu-ES-2	$\overline{CuSCH_2CH_2}$	1.9993	439	-	0.07	-
Central Radicals						
H	$Ag^+[C_2H_4SSC_2H_4]^-$	2.0054	54	22[c]	0.03	0.02[d]
H-d_4	$Ag^+[C_2D_4SSC_2D_4]^-$	2.0054	54	3[e]	0.03	-
L	$Au^+[C_2H_4SSC_2H_4]^-$	2.0080	48	22[c]	0.02	0.02[d]
	$\overline{\dot{N}CH_2CH_2}$	2.0041	86[c]	35	0.06[d]	0.02
	$\overline{^{15}\dot{N}CH_2CH_2}$	2.0046	85[c]	49	0.06[d]	-
C and G	$C_6H_5CH(O^-)\dot{C}H_2$	2.0018	56(α)[c]	69(β)[c]	0.04(α)[d]	0.05(β)[d]
Unknown species						
^{63}Cu-EO-d_4-2		2.0113	4005	-	0.67	-
^{63}Cu-EO-^{13}C-2		2.0101	4030	-	0.67	-
^{107}Ag-ES-3		1.9974	1376	-	0.75	-
^{107}Ag-ES-d_4-2		1.9974	1374	-	0.75	-

[a]Hyperfine interaction in MHz. [b]Value for an electron in the s-orbital of the atom (a^o_{iso} (atom) in MHz), ^{63}Cu, 5995; ^{107}Ag, 1831; ^{197}Au, 2876, ^{14}N, 1811 and ^{1}H, 1427. [c]a_H. [d]ρ_{1s} (H). [e]a_D.

7. References

(1) Bergmeier, S.; Lapinsky, D. In *Progress in Heterocyclic Chemistry*; Elsevier, London, 2009; pp 69–93.

(2) Álvarez-Builla, J.; Vaquero, J. J.; Barluenga, J. *Modern Heterocyclic Chemistry*; Wiley-VCH: Weinheim, 2011.

(3) Raynaud, J.; Absalon, C.; Gnanou, Y.; Taton, D. *J. Am. Chem. Soc.* **2009**, *131*, 3201.

(4) Fan, Y.; Yao, J.; Du, R.; Hou, L.; Zhou, J.; Lu, Y.; Meng, Q.; Zhang, Q. *Pharm. Res.* **2013**, *30*, 1215.

(5) Brichacek, M.; Batory, L. A.; McGrath, N. A.; Njardarson, J. T. *Tetrahedron* **2010**, *66*, 4832.

(6) Weissermel, K.; Arpe, H.-J. *Industrial Organic Chemistry*, 5th ed.; Wiley, New York, 2010.

(7) Chawla, R.; Singh, A. K.; Yadav, L. D. S. *RSC Adv.* **2013**, *3*, 11385.

(8) Huang, C. Y.; Doyle, A. G. *Chem. Rev.* **2014**, *114*, 8153.

(9) Tsuda, T.; Chujo, Y.; Saegusa, T. *J. Chem. Soc., Chem. Commun.* **1976**, 415.

(10) Bäckvall, J.-E.; Karlsson, O.; Ljunggren, S. O. *Tetrahedron Lett.* **1980**, *21*, 4985.

(11) Guo, C.-H.; Wu, H.-S.; Zhang, X.-M.; Song, J.-Y.; Zhang, X. *J. Phys. Chem. A.* **2009**, *113*, 6710.

(12) Batory, L. A.; McInnis, C. E.; Njardarson, J. T. *J. Am. Chem. Soc.* **2006**, *128*, 16054.

(13) Rogers, E.; Araki, H.; Batory, L. A.; McInnis, C. E.; Njardarson, J. T. *J. Am. Chem. Soc.* **2007**, *129*, 2768.

(14) Brichacek, M.; Lee, D.; Njardarson, J. T. *Org. Lett.* **2008**, *10*, 5023.

(15) Njardarson, J. T. *Synlett* **2013**, *24*, 787.

(16) Merino, E.; Fernández, L.; Nevado, C. In *The Chemistry of Organogold Compounds*; Rappoport, Z.; Marek, I.; Liebman, J. F., Eds.; Wiley, Sussex, 2015; pp 235–305.

(17) Mack, D. J.; Njardson, J. T. *ACS Catal.* **2013**, *3*, 272.

(18) Luhowy, R.; Meneghini, F. *J. Org. Chem.* **1973**, *38*, 2405.

(19) Usui, Y.; Noma, J.; Hirano, M.; Komiya, S. *J. Chem. Soc., Dalt. Trans.* **1999**, 4397.

(20) Desnoyer, A. N.; Bowes, E. G.; Patrick, B. O.; Love, J. A. *J. Am. Chem. Soc.* **2015**, *137*, 12748.

(21) Desmarais, F. K.; Joly, H. A. *Organometallics* **2015**, *34*, 1264.

(22) Weil, J. A.; Bolton, J. R.; Werts, J. E. *Electron Paramagnetic Resonance: Elementary Theory and Practical Applications*; Wiley-Interscience, 1994.

(23) Sajfutdinov, R. G.; Larina, L. I.; Vakul'skaya, T. I.; Voronkov, M. G. *Electron Paramagnetic Resonance in Biochemistry and Medicine*; Kluwer: New York, 2012; Vol. 33.

(24) Weltner, W., Jr. J. *Magnetic Atoms and Molecules*; Dover Publications: New, York, 1983.

(25) Morton, J. R.; Preston, K. F.; Boate, A. R. *J. Magn. Res.* **1976**, *24*, 259.

(26) Breit, G.; Rabi, I. I. *Phys. Rev.* **1931**, *38*, 2082.

(27) Kasai, P. H.; Mcleod, D, J. *J. Chem. Phys.* **1971**, *55*, 1566.

(28) Abragam, A.; Bleaney, B. *Electron Paramagnetic Resonance of Transition Ions*, 1st ed.; Oxford: London, 1970.

(29) Kasai, P. H.; Jones, P. M. *J. Am. Chem. Soc.* **1985**, *107*, 813.

(30) Morton, J. R.; Preston, K. F. *J. Magn. Res.* **1978**, *30*, 577.

(31) Blackborow, J. R.; Young, D. *Metal-Vapour Synthesis in Organometallic Chemistry*; Springer-Verlag: New York, 1979.

(32) Kasai, P. H. *Acc. Chem. Res.* **1971**, No. 4, 329.

(33) Hauge, R. H.; Fredin, L.; Kafafi, Z. H.; Margrave, J. L. *Appl. Spectrosc.* **1986**, *40*, 588.

(34) Bennett, J. E.; Mile, B.; Thomas, A.; Ward, B. *Adv. Phys. Org. Chem.* **1970**, *8*, 1.

(35) Kharisov, B. I.; Garnovskii, A. D.; Blanco, L. M.; Burlov, A. S.; García-Luna, A. *J. Coord. Chem.* **1999**, *49*, 113.

(36) Buck, A. J.; Mile, B.; Howard, J. A. *J. Am. Chem. Soc.* **1983**, *105*, 3381.

(37) Kasai, P. H.; Watanabe, T.; Mcleod, D, J. *J. Am. Chem. Soc.* **1980**, *102*, 179.

(38) Howard, J. A.; Joly, H. A.; Mile, B. *J. Phys. Chem.* **1990**, *94*, 1275.

(39) Kasai, P. H. *J. Am. Chem. Soc.* **1984**, *106*, 3069.

(40) Chenier, J. H. B.; Joly, H. A.; Howard, J. A.; Mile, B. *J. Chem. Soc., Faraday Trans.* **1990**, *86*, 3329.

(41) Howard, J. A.; Sutcliffe, R.; Tse, J. S.; Mile, B. *Organometallics* **1984**, *3*, 859.

(42) Howard, J. A.; Sutcliffe, R.; Mile, B. *J. Phys. Chem.* **1984**, *88*, 5155.

(43) Howard, J. A.; Sutcliffe, R.; Dahmane, H.; Mile, B. *Organometallics* **1985**, *4*, 697.

(44) Williams, A. P.; Van Zee, R. J.; Weltner, W., Jr. *J. Am. Chem. Soc.* **1996**, *188*, 4498.

(45) Chenier, J. H. B.; Howard, J. A.; Mile, B. *J. Phys. Chem.* **1989**, *93*, 114.

(46) Histed, M.; Howard, J. A.; Jones, R.; Tomietto, M. *J. Phys. Chem.* **1992**, *96*, 1141.

(47) Doan, V.; Kasai, P. H. *J. Phys. Chem. A.* **1997**, *101*, 8115.

(48) Histed, M.; Howard, J. A.; Joly, H. A.; Mile, B. *Chem. Phys. Lett.* **1990**, *174*, 411.

(49) Howard, J. A.; Mile, B.; Morton, J. R.; Preston, K. F.; Sutcliffe, R. *J. Phys. Chem.* **1986**, *90*, 1033.

(50) Howard, J. A.; Mile, B.; Morton, J. R.; Preston, K. F. *J. Phys. Chem.* **1986**, *90*, 2027.

(51) Kasai, P. H.; Jones, P. M. *J. Phys. Chem.* **1986**, *90*, 4239.

(52) Howard, J. A.; Sutcliffe, R.; Mile, B. *J. Phys. Chem.* **1984**, *88*, 4351.

(53) Chenier, J. H. B.; Howard, J. A; Mile, B.; Sutcliffe, R. *J. Am. Chem. Soc.* **1983**, *105*, 788.

(54) Chenier, J. H. B.; Howard, J. A.; Mile, B. *J. Am. Chem. Soc.* **1985**, *107*, 4190.

(55) Genin, F.; Howard, J. A.; Mile, B.; Hampson, C. A. *J. Chem. Soc., Faraday Trans. I* **1989**, *85*, 3963.

(56) Parnis, J. M.; Mitchell, S. A.; Garcia-Prieto, J.; Ozin, G. A. *J. Am. Chem. Soc.* **1985**, *107*, 8169.

(57) Knight, L. B., Jr.; Cobranchi, S. T.; Gregory, B. W.; Jones, G. C., J. *J. Chem. Phys.* **1988**, *88*, 524.

(58) Kasai, P. H.; Whipple, E. B.; Weltner, W., Jr. *J. Chem. Phys.* **1966**, *44*, 2581.

(59) Knight, L. B., Jr.; Cobranchi, S. T.; Petty, J.; Cobranchi, D. P. *J. Chem. Phys.* **1989**, *91*, 4587.

(60) Howard, J. A.; Joly, H. A.; Mile, B. *J. Phys. Chem.* **1990**, 94, 6627.

(61) Kasai, P. H. *J. Phys. Chem.* **1982**, *86*, 3684.

(62) Howard, J. A.; Sutcllffe, R.; Mile, B. *J. Phys. Chem.* **1984**, *88*, 5155.

(63) Chenier, J. H. B.; Howard, J. A.; Joly, H. A.; Mile, B.; Timms, P. L. *J. Chem. Soc., Chem. Commun.* **1990**, 581.

(64) Kasai, P. H.; Jones, P. M. *J. Phys. Chem.* **1985**, *89*, 1147.

(65) Chenier, J. H. B.; Hampson, C. A.; Howard, J. A.; Mile, B. *J. Phys. Chem.* **1988**, 92, 2745.

(66) Hampson, C. A.; Howard, J. A.; Mile, B. *J. Chem. Soc., Chem. Commun.* **1985**, 966.

(67) Histed, M.; Howard, J. A.; Jones, R.; Tomietto, M.; Joly, H. A. *J. Phys. Chem.* **1992**, *96*, 1144.

(68) Howard, J. A.; Jones, R.; Tse, J. S.; Tomietto, M.; Timms, P. L.; Seeley, A. J. *J. Phys. Chem.* **1992**, *96*, 9144.

(69) Hayton, L. J.; Mile, B.; Timms, P. L.; Harvey, J. N. *J. Chem. Soc., Dalt. Trans.* **2002**, 1327.

(70) Kasai, P. H. *J. Phys. Chem.* **1990**, *94*, 3539.

(71) Kasai, P. H. *J. Am. Chem. Soc.* **1983**, *105*, 6704.

(72) Kasai, P. H.; Jones, P. M. *J. Am. Chem. Soc.* **1985**, *107*, 6385.

(73) Dewar, M. J. S. *Bull Soc. Chim. Fr.* **1951**, *18*, C71.

(74) Chatt, J.; Duncanson, L. A. *J. Chem. Soc.* **1953**, 2939.

(75) Mile, B.; Howard, J. A.; Tse, J. S. *Organometallics* **1988**, *7*, 1278.

(76) Ball, D. W.; Hauge, R. H.; Margrave, J. L. *Inorg. Chem.* **1989**, *28*, 1599.

(77) Gong, Y.; Andrews, L. *Inorg. Chem.* **2012**, *51*, 667.

(78) Kauffman, J. W.; Hauge, R. H.; Margrave, J. L. *J. Phys. Chem.* **1985**, *89*, 3541.

(79) Chang, S.; Kafafi, Z. H.; Hauge, R. H.; Billups, W. E.; Margrave, J. L. *J. Am. Chem. Soc.* **1987**, *109*, 4508.

(80) Cho, H.-G.; Andrews, L. *Dalton Trans.* **2011**, *40*, 11115.

(81) Cho, H.-G.; Andrews, L. *Inorg. Chem.* **2011**, *50*, 10319.

(82) Cho, H.-G.; Andrews, L. *Organometallics* **2013**, *32*, 2753.

(83) Parr, R. G.; Yang, W. *Density-Functional Theory of Atoms and Molecules*; Oxford Science Publications: New York, 1989.

(84) Kohn, W.; Sham, L. J. *Phys. Rev.* **1965**, *140*, A1133.

(85) Becke, A. D. *J. Chem. Phys.* **1993**, *98*, 5648.

(86) Becke, A. D. *Phys. Rev. A.* **1988**, *38*, 3098.

(87) Lee, C.; Yang, W.; Parr, R. G. *Phys. Rev. B* **1988**, *37*, 785.

(88) Frisch, M. J.; Trucks, G. W.; Schlegel, H. B.; Scuseria, G. E.; Robb, M. A.; Cheeseman, J. R.; Scalmani, G.; Barone, V.; Mennucci, B.; Petersson, G. A.; Nakatsuji, H.; Caricato, M.; Li, X.; Hratchian, H. P.; Izmaylov, A. F.; Bloino, J.; Zheng, G.; Sonnenberg, J. L.; Hada, M.; Ehara, M.; Toyota, K.; Fukuda, R.; Hasegawa, J.; Ishida, M.; Nakajima, T.; Honda, Y.; Kitao, O.; Nakai, H.; Vreven, T.; Montgomery, J. A., Jr.; Peralta, J. E.; Ogliaro, F.; Bearpark, M.; Heyd, J. J.; Brothers, E.; Kudin, K. N.; Staroverov, V. N.; Kobayashi, R.; Normand, J.; Raghavachari, K.; Rendell, A.; Burant, J. C.; Iyengar, S. S.; Tomasi, J.; Cossi, M.; Rega, N.; Millam, J. M.; Klene, M.; Knox, J. E.; Cross, J. B.; Bakken, V.; Adamo, C.; Jaramillo, J.; Gomperts, R.; Stratmann, R. E.; Yazyev, O.; Austin, A. J.; Cammi, R.; Pomelli, C.; Ochterski, J. W.; Martin, R. L.; Morokuma, K.; Zakrzewski, V. G.; Voth, G. A.; Salvador, P.; Dannenberg, J. J.; Dapprich, S.; Daniels, A. D.; Farkas, Ö .; Foresman, J. B.; Ortiz, J. V.; Cioslowski, J.; Fox, D. J. *Gaussian 09*, revision A.1; Gaussian, Inc.: Wallingford, CT, 2009.

(89) Zhao, Y.; Truhlar, D. G. *Theor. Chem. Acc.* **2008**, *120*, 215.

(90) Foresman, J. B.; Frish, A. *Exploring Chemistry with Electronic Structure Methods*, 2nd ed.; Gaussian Inc., 1996.

(91) Wachters, A. J. H. *J. Chem. Phys.* **1970**, *52*, 1033.

(92) Hay, P. J. *J. Chem. Phys.* **1977**, *66*, 4377.

(93) Wadt, W. R.; Hay, P. J. *J. Chem. Phys.* **1985**, *82*, 272.

(94) Wadt, W. R.; Hay, P. J. *J. Chem. Phys.* **1985**, *82*, 284.

(95) Wadt, W. R.; Hay, P. J. *J. Chem. Phys.* **1985**, *82*, 299.

(96) Chaikittisilp, W.; Didas, S. A.; Kim, H.-J.; Jones, C. W. *Chem. Mater.* **2013**, *25*, 613.

(97) Gibson, M. S.; Bradshaw, R. W. *Angew. Chem. Int. Ed.* **1968**, *7*, 919.

(98) Betley, T. A.; Peters, J. C. *J. Am. Chem. Soc.* **2004**, *126*, 6252.

(99) Lui, N.; Heinrich, J.-D. Process for the Preparation of 2,2-Difluoroethylamine, 2013. Patent US8450528 B2.

(100) Gross, H.; Grassi, G.; Quack, M. *Chem. Eur. J.* **1998**, *4*, 441.

(101) FORTRAN programs provided by Drs. J. R. Morton and K. F. Preston (NRC, Ottawa).

(102) EPR-NMR, *Version 6.4*, M. J. Mombourquette and J. A. Weil, University of Saskatchewan.

(103) Howard, J. A.; Sutcllffe, R. *J. Phys. Chem.* **1983**, *87*, 2268.

(104) Danen, W. C.; Kensler, T. T. *Tetrahedron Lett.* **1971**, *25*, 2247.

(105) Jiang, L.; Xu, Q. *J. Phys. Chem. A.* **2007**, *111*, 2690.

(106) Giard, A.; Xerri, B.; Ciofini, I.; Berthomieu, D. *Chem. Phys. Lett.* **2014**, *614*, 226.

(107) Brunet, F. D.; Feola, J. C.; Joly, H. A. *J. Phys. Chem. A.* **2012**, *116*, 2439.

(108) Yahiro, H.; Manabe, K.; Itagaki, Y.; Shiotani, M. *J. Chem. Soc., Faraday Trans.* **1998**, *94*, 805.

(109) Wasowicz, T.; Mikosz, J.; Michalik, J. *J. Chem. Soc., Perkin Trans. 2* **1992**, 1487.

(110) Lindsay, D. M.; Kasai, P. H. *J. Magn. Reson.* **1985**, *64*, 278.

(111) Kline, E. S.; Hauge, R. H.; Margrave, J. L.; Kafafi, Z. H. *High Temp. Sci.* **1990**, *30*, 69.

(112) Kafafi, Z. H.; Hauge, R. H.; Billups, W. E.; Margrave, J. L. *J. Am. Chem. Soc.* **1987**, *109*, 4775.

(113) Joly, H. A.; Beaudet, L.; Dai, X. *J. Phys. Chem. A.* **2006**, *110*, 5656.

(114) Joly, H. A.; Beaudet, L.; Levesque, M.; Myre, M. *J. Phys. Chem. A.* **2011**, *115*, 11841.

(115) Kasai, P. H. *J. Am. Chem. Soc.* **1991**, *113*, 1539.

(116) Linic, S.; Barteau, M. A. *J. Am. Chem. Soc.* **2002**, *124*, 310.

(117) Enever, M.; Linic, S.; Uffalussy, K.; Vohs, J. M.; Barteau, M. A. *J. Phys. Chem. B* **2005**, *109*, 2227.

(118) de Boer, S. Y.; Gloaguen, Y.; Reek, J. N. H.; Lutz, M.; van der Vlugt, J. I. *Dalt. Trans.* **2012**, *41*, 11276.

(119) Li, X.; Li, B.; You, J.; Lan, J. *Org. Biomol. Chem.* **2013**, *11*, 1925.

(120) Dhara, S.; Singha, R.; Ahmed, A.; Mandal, H.; Ghosh, M.; Nuree, Y.; Ray, J. K. *RSC Adv.* **2014**, *4*, 45163.

(121) Joly, H. A.; Howard, J. A.; Tomietto, M.; Tse, J. S. *J. Chem. Soc., Faraday Trans.* **1994**, *90*, 3145.

(122) Howard, J. A.; Preston, K. F.; Mile, B. *J. Am. Chem. Soc.* **1981**, *103*, 6226.

(123) Kernisant, K.; Thompson, G. A.; Lindsay, D. M. *J. Chem. Phys.* **1985**, *82*, 4739.

(124) Michalik, J.; Kevan, L. *J. Am. Chem. Soc.* **1986**, *108*, 4247.

(125) Houk, R. J. T.; Jacobs, B. W.; El Gabaly, F.; Chang, N. N.; Talin, A. A.; Graham, D. D.; House, S. D.; Robertson, I. M.; Allendorf, M. D.; Gabaly, F. E. *Nano Lett.* **2009**, *9*, 3413.

(126) Blazevska-Gilev, J.; Urbanova, M.; Pokorna, D.; Subrt, J.; Pola, J. *J. Anal. Appl. Pyrolysis* **2012**, *93*, 165.

(127) Chin, W. S.; Ek, B. W.; Mok, C. Y.; Huang, H. H. *J. Chem. Soc., Perkin Trans. 2* **1994**, 883.

8. Appendix

8.1. Computational Details

The geometry of all optimized structures, bond lengths, bond angles and dihedral angles are included in this section along with the internal energy (presented in hartrees) and isotropic hyperfine (presented in MHz) when available. All structures shown below are representations, taken from the B3LYP/6-311+G(d) calculations.

8.1.1. DFT Calculations for Energy Diagrams

Below are the optimized geometrical information and internal energy (hartrees) values for the structures used in generating the energy diagrams, Figures 96 and 97, for the reaction path of Group 11 metal atoms with ethylene oxide, ethylene sulfide and aziridine. Recorded in Table S1 are the internal energy values for Group 11 metal atoms computed with the Gaussian 09W program.

Table S1. Calculated internal energy[a] of Group 11 atoms (i.e., total electronic energy for atoms) with the B3LYP, M06, and BHandHLYP functionals.

Reactants	Basis Set	Functional		
		B3LYP	M06	BHandHLYP
$^{63}Cu^{0}$	6-311+G(d)	-1640.4722572	-1640.3658386	-1640.3569407
	LanL2DZ	-196.1168077	-196.1467860	-195.9154678
$^{107}Ag^{0}$	LanL2DZ	-145.7586864	-145.7602650	-145.6265091
$^{197}Au^{0}$	LanL2DZ	-135.4397853	-135.4101662	-135.2837619

[a]Energy presented in Hartrees.

Ethylene oxide

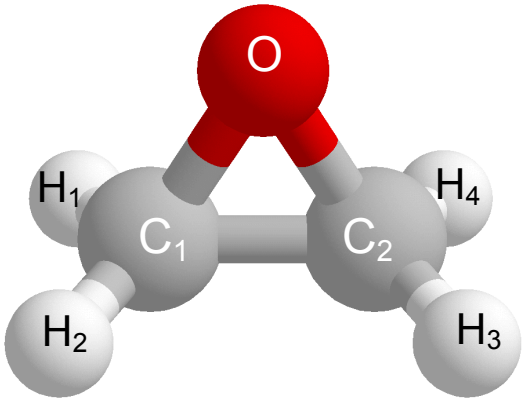

	B3LYP	M06	BHandHLYP
$O\text{-}C_1$	1.431 Å	1.408 Å	1.410 Å
$O\text{-}C_2$	1.431 Å	1.408 Å	1.410 Å
$C_1\text{-}C_2$	1.466 Å	1.456 Å	1.455 Å
$C_1\text{-}H_1$	1.087 Å	1.091 Å	1.079 Å
$C_1\text{-}H_2$	1.087 Å	1.091 Å	1.079 Å
$C_2\text{-}H_3$	1.087 Å	1.091 Å	1.079 Å
$C_2\text{-}H_4$	1.087 Å	1.091 Å	1.079 Å
$\angle C_1\text{-}O\text{-}C_2$	61.7º	62.3º	62.1º
$\angle O\text{-}C_1\text{-}C_2$	59.2º	58.9º	58.9º
$\angle C_1\text{-}C_2\text{-}O$	59.2º	58.9º	58.9º
$\angle O\text{-}C_1\text{-}H_1$	115.0º	115.3º	115.0º
$\angle O\text{-}C_1\text{-}H_2$	115.0º	115.3º	115.0º
$\angle O\text{-}C_2\text{-}H_3$	115.0º	115.3º	115.0º
$\angle O\text{-}C_2\text{-}H_4$	115.0º	115.3º	115.0º
$\angle H_1\text{-}C_1\text{-}H_2$	115.6º	115.4º	115.6º
$D(O\text{-}C_2\text{-}C_1\text{-}H_1)$	-103.0º	-103.3º	-103.0º
$D(O\text{-}C_2\text{-}C_1\text{-}H_2)$	103.0º	103.3º	103.0º
$D(O\text{-}C_1\text{-}C_2\text{-}H_3)$	-103.0º	-103.3º	-103.0º
$D(O\text{-}C_1\text{-}C_2\text{-}H_4)$	103.0º	103.3º	103.0º
$D(H_1\text{-}C_1\text{-}C_2\text{-}H_3)$	154.0º	153.3º	154.0º
$D(H_2\text{-}C_1\text{-}C_2\text{-}H_3)$	0.0º	0.0º	0.0º
Energy[a]	-153.829969	-153.72902	-153.734127

[a]Potential energy at the equilibrium geometry.

Ethylene sulfide

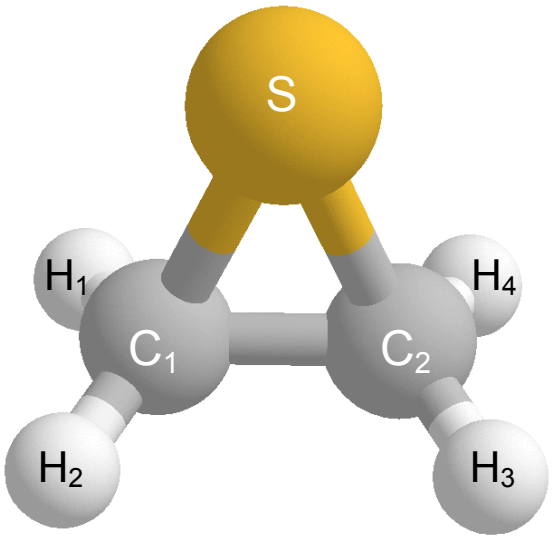

	B3LYP	M06	BHandHLYP
S-C_1	1.838 Å	1.813 Å	1.817 Å
S-C_2	1.838 Å	1.813 Å	1.817 Å
C_1-C_2	1.479 Å	1.471 Å	1.470 Å
C_1-H_1	1.084 Å	1.088 Å	1.076 Å
C_1-H_2	1.084 Å	1.088 Å	1.076 Å
C_2-H_3	1.084 Å	1.088 Å	1.076 Å
C_2-H_4	1.084 Å	1.088 Å	1.076 Å
∠C_1-S-C_2	47.4º	47.9º	47.7º
∠S-C_1-C_2	66.3º	66.1º	66.1º
∠C_1-C_2-S	66.3º	66.1º	66.1º
∠S-C_1-H_1	115.0º	115.4º	115.1º
∠S-C_1-H_2	115.0º	115.4º	115.1º
∠S-C_2-H_3	115.0º	115.4º	115.1º
∠S-C_2-H_4	115.0º	115.4º	115.1º
∠H_1-C_1-H_2	114.7º	114.6º	114.8º
D(S-C_2-C_1-H_1)	106.7º	107.1º	106.8º
D(S-C_2-C_1-H_2)	-106.7º	-107.1º	-106.8º
D(S-C_1-C_2-H_3)	-106.7º	-107.1º	-106.8º
D(S-C_1-C_2-H_4)	106.7º	107.1º	106.8º
D(H_1-C_1-C_2-H_3)	146.6º	145.9º	146.4º
D(H_2-C_1-C_2-H_3)	0.0º	0.0º	0.0º
Energy[a]	-476.8274136	-476.7272955	-476.7494948

[a]Potential energy at the equilibrium geometry.

Aziridine

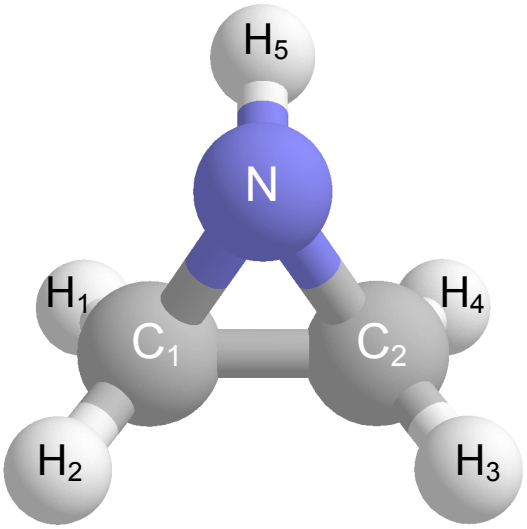

	B3LYP	M06	BHandHLYP
$N\text{-}C_1$	1.472 Å	1.456 Å	1.454 Å
$N\text{-}C_2$	1.472 Å	1.456 Å	1.454 Å
$C_1\text{-}C_2$	1.485 Å	1.447 Å	1.474 Å
$C_1\text{-}H_1$	1.086 Å	1.089 Å	1.079 Å
$C_1\text{-}H_2$	1.085 Å	1.087 Å	1.077 Å
$C_2\text{-}H_3$	1.085 Å	1.087 Å	1.077 Å
$C_2\text{-}H_4$	1.086 Å	1.089 Å	1.079 Å
$N\text{-}H_5$	1.016 Å	1.018 Å	1.005 Å
$\angle C_1\text{-}N\text{-}C_2$	60.6º	60.8º	60.9º
$\angle N\text{-}C_1\text{-}C_2$	59.7º	59.6º	59.5º
$\angle C_1\text{-}C_2\text{-}N$	59.7º	59.6º	59.5º
$\angle N\text{-}C_1\text{-}H_1$	118.7º	118.7º	118.5º
$\angle N\text{-}C_1\text{-}H_2$	114.7º	114.9º	114.9º
$\angle N\text{-}C_2\text{-}H_3$	114.7º	114.9º	114.9º
$\angle N\text{-}C_2\text{-}H_4$	118.7º	118.7º	118.5º
$\angle C_1\text{-}N\text{-}H_5$	110.8º	110.9º	111.6º
$\angle C_2\text{-}N\text{-}H_5$	110.8º	110.9º	111.6º
$\angle H_1\text{-}C_1\text{-}H_2$	114.7º	114.6º	114.7º
$D(N\text{-}C_2\text{-}C_1\text{-}H_1)$	-108.6º	-108.8º	-108.4º
$D(N\text{-}C_2\text{-}C_1\text{-}H_2)$	102.8º	102.9º	102.9º
$D(N\text{-}C_1\text{-}C_2\text{-}H_3)$	-102.8º	-102.9º	-102.9º
$D(N\text{-}C_1\text{-}C_2\text{-}H_4)$	-108.6º	-108.8º	-108.4º
$D(C_1\text{-}C_2\text{-}N\text{-}H_5)$	102.8º	103.0º	103.4º
$D(C_2\text{-}C_1\text{-}N\text{-}H_5)$	-102.8º	-103.0º	-103.4º
$D(H_1\text{-}C_1\text{-}C_2\text{-}H_3)$	148.7º	148.3º	148.7º
$D(H_2\text{-}C_1\text{-}C_2\text{-}H_3)$	0.0º	0.0º	0.0º
Energy[a]	-133.9537586	-133.8526374	-133.8621957

[a]Potential energy at the equilibrium geometry.

Cu-$\overline{OCH_2CH_2}$

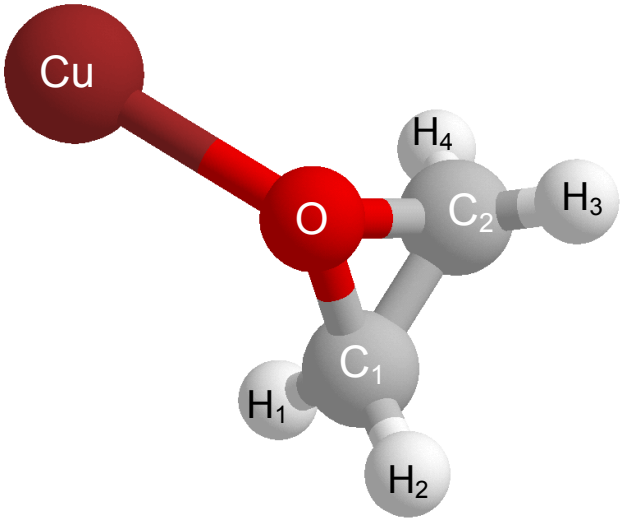

	B3LYP	M06	BHandHLYP
Cu-O	2.222 Å	2.275 Å	2.285 Å
O-C_1	1.446 Å	1.422 Å	1.421 Å
O-C_2	1.446 Å	1.422 Å	1.421 Å
C_1-C_2	1.464 Å	1.454 Å	1.454 Å
C_1-H_1	1.086 Å	1.091 Å	1.078 Å
C_1-H_2	1.085 Å	1.089 Å	1.077 Å
C_2-H_3	1.085 Å	1.089 Å	1.077 Å
C_2-H_4	1.086 Å	1.091 Å	1.078 Å
∠Cu-O-C_1	127.1º	112.2º	129.3º
∠C_1-O-C_2	60.8º	61.5º	61.5º
∠O-C_1-H_1	114.5º	114.4º	114.7º
∠O-C_1-H_2	113.9º	114.6º	114.2º
∠O-C_2-H_3	113.9º	114.6º	114.2º
∠O-C_2-H_4	114.5º	114.4º	114.7º
∠H_1-C_1-H_2	116.1º	116.1º	116.0º
D(Cu-O-C_1-C_2)	-116.4º	-104.1º	-119.2º
D(Cu-O-C_1-H_1)	-5.2º	-6.7º	-8.2º
D(Cu-O-C_1-H_2)	131.7º	144.1º	129.2º
D(Cu-O-C_2-H_3)	-131.7º	-144.1º	-129.2º
D(Cu-O-C_2-H_4)	5.2º	6.7º	8.2º
Energy[a]	-349.9568332	-349.8884654	-349.6571740

[a]Potential energy at the equilibrium geometry.

Ag-$\overline{OCH_2CH_2}$

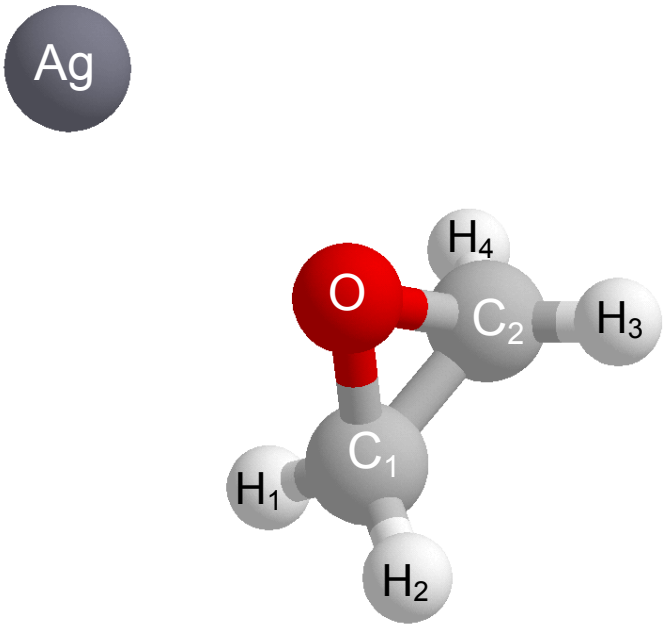

	B3LYP	M06	BHandHLYP
Ag-O	2.746 Å	2.715 Å	2.764 Å
O-C_1	1.438 Å	1.416 Å	1.416 Å
O-C_2	1.438 Å	1.416 Å	1.416 Å
C_1-C_2	1.465 Å	1.454 Å	1.455 Å
C_1-H_1	1.087 Å	1.092 Å	1.078 Å
C_1-H_2	1.086 Å	1.089 Å	1.078 Å
C_2-H_3	1.086 Å	1.089 Å	1.078 Å
C_2-H_4	1.087 Å	1.092 Å	1.078 Å
∠Ag-O-C_1	126.3º	106.2º	131.8º
∠C_1-O-C_2	61.3º	61.8º	61.8º
∠O-C_1-H_1	114.7º	114.7º	114.9º
∠O-C_1-H_2	114.5º	115.0º	114.7º
∠O-C_2-H_3	114.5º	115.0º	114.7º
∠O-C_2-H_4	114.7º	114.7º	114.9º
∠H_1-C_1-H_2	115.8º	100.0º	115.8º
D(Ag-O-C_1-C_2)	-115.8º	-115.8º	-122.4º
D(Ag-O-C_1-H_1)	-4.7º	-10.7º	-11.4º
D(Ag-O-C_1-H_2)	132.7º	148.5º	126.3º
D(Ag-O-C_2-H_3)	-132.7º	-148.5º	-126.3º
D(Ag-O-C_2-H_4)	4.7º	10.7º	11.4º
Energy[a]	-299.5921149	-299.4963105	-299.3638256

[a]Potential energy at the equilibrium geometry.

Au-$\overline{OCH_2CH_2}$

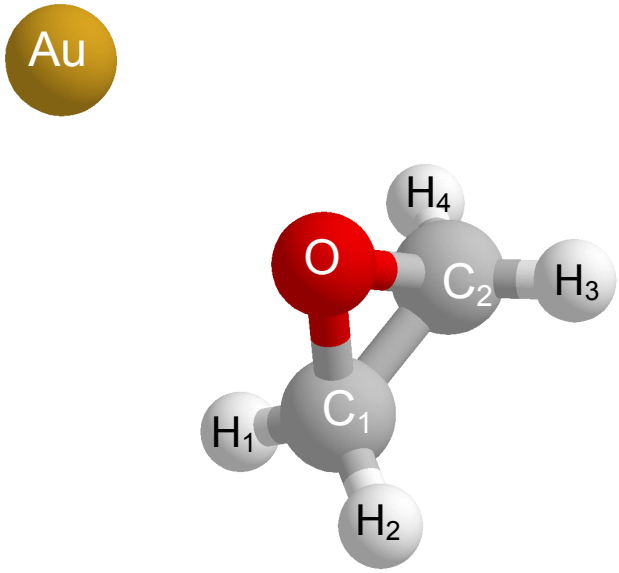

	B3LYP	M06	BHandHLYP
Au-O	2.689 Å	2.719 Å	2.799 Å
O-C_1	1.440 Å	1.417 Å	1.416 Å
O-C_2	1.440 Å	1.417 Å	1.416 Å
C_1-C_2	1.465 Å	1.455 Å	1.454 Å
C_1-H_1	1.086 Å	1.091 Å	1.078 Å
C_1-H_2	1.086 Å	1.089 Å	1.078 Å
C_2-H_3	1.086 Å	1.089 Å	1.078 Å
C_2-H_4	1.086 Å	1.091 Å	1.078 Å
∠Au-O-C_1	120.3º	109.4º	121.9º
∠C_1-O-C_2	61.1º	61.8º	61.8º
∠O-C_1-H_1	114.6º	114.8º	114.8º
∠O-C_1-H_2	114.2º	114.7º	114.6º
∠O-C_2-H_3	114.2º	114.7º	114.6º
∠O-C_2-H_4	114.6º	114.8º	114.8º
∠H_1-C_1-H_2	116.0º	115.8º	115.8º
D(Au-O-C_1-C_2)	-110.2º	-102.1º	-111.9º
D(Au-O-C_1-H_1)	1.0º	8.7º	0.9º
D(Au-O-C_1-H_2)	138.2º	146.5º	136.8º
D(Au-O-C_2-H_3)	-138.2º	-146.5º	-136.8º
D(Au-O-C_2-H_4)	-1.0º	-8.7º	-0.9º
Energy[a]	-289.2742612	-289.1465829	-289.0210214

[a]Potential energy at the equilibrium geometry.

Cu-$\overline{SCH_2CH_2}$

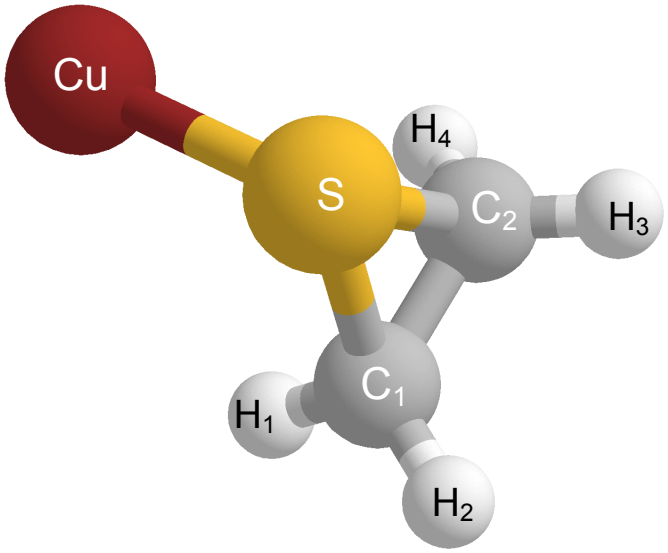

	B3LYP	M06	BHandHLYP
Cu-S	2.506 Å	2.499 Å	2.606 Å
S-C_1	1.847 Å	1.823 Å	1.824 Å
S-C_2	1.847 Å	1.823 Å	1.824 Å
C_1-C_2	1.474 Å	1.465 Å	1.466 Å
C_1-H_1	1.085 Å	1.089 Å	1.076 Å
C_1-H_2	1.084 Å	1.087 Å	1.076 Å
C_2-H_3	1.084 Å	1.087 Å	1.076 Å
C_2-H_4	1.085 Å	1.089 Å	1.076 Å
∠Cu-S-C_1	102.2º	94.7º	100.8º
∠C_1-S-C_2	47.0º	47.4º	47.4º
∠S-C_1-H_1	114.2º	114.1º	114.6º
∠S-C_1-H_2	113.9º	114.2º	114.2º
∠S-C_2-H_3	113.9º	114.2º	114.2º
∠S-C_2-H_4	114.2º	114.1º	114.6º
∠H_1-C_1-H_2	115.4º	115.5º	115.3º
D(Cu-S-C_1-C_2)	-95.4º	-92.1º	-94.8º
D(Cu-S-C_1-H_1)	16.6º	19.4º	16.9º
D(Cu-S-C_1-H_2)	152.0º	155.3º	152.9º
D(Cu-S-C_2-H_3)	-152.0º	-155.3º	-152.9º
D(Cu-S-C_2-H_4)	-16.6º	-19.4º	-16.9º
Energy[a]	-672.9571527	-672.8921559	-672.6732199

[a]Potential energy at the equilibrium geometry.

Ag-$\overline{SCH_2CH_2}$

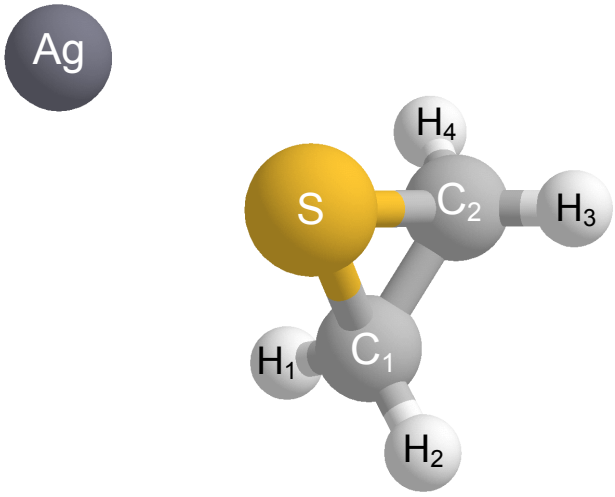

	B3LYP	M06	BHandHLYP
Ag-S	2.986 Å	2.924 Å	3.068 Å
S-C_1	1.842 Å	1.820 Å	1.821 Å
S-C_2	1.842 Å	1.820 Å	1.821 Å
C_1-C_2	1.476 Å	1.467 Å	1.468 Å
C_1-H_1	1.084 Å	1.089 Å	1.076 Å
C_1-H_2	1.084 Å	1.087 Å	1.076 Å
C_2-H_3	1.084 Å	1.087 Å	1.076 Å
C_2-H_4	1.084 Å	1.089 Å	1.076 Å
∠Ag-S-C_1	100.8º	92.1º	100.0º
∠C_1-S-C_2	47.2º	47.5º	47.5º
∠S-C_1-H_1	114.5º	114.6º	114.8º
∠S-C_1-H_2	114.2º	114.6º	114.5º
∠S-C_2-H_3	114.2º	114.6º	114.5º
∠S-C_2-H_4	114.5º	114.6º	114.8º
∠H_1-C_1-H_2	115.2º	115.2º	115.1º
D(Ag-S-C_1-C_2)	-94.8º	-90.9º	-94.4º
D(Ag-S-C_1-H_1)	17.1º	20.5º	17.2º
D(Ag-S-C_1-H_2)	153.0º	156.8º	153.6º
D(Ag-S-C_2-H_3)	-153.0º	-156.8º	-153.6º
D(Ag-S-C_2-H_4)	-17.1º	-20.5º	-17.2º
Energy[a]	-622.5917541	-622.4990914	-622.3799107

[a]Potential energy at the equilibrium geometry.

Au-$\overline{SCH_2CH_2}$

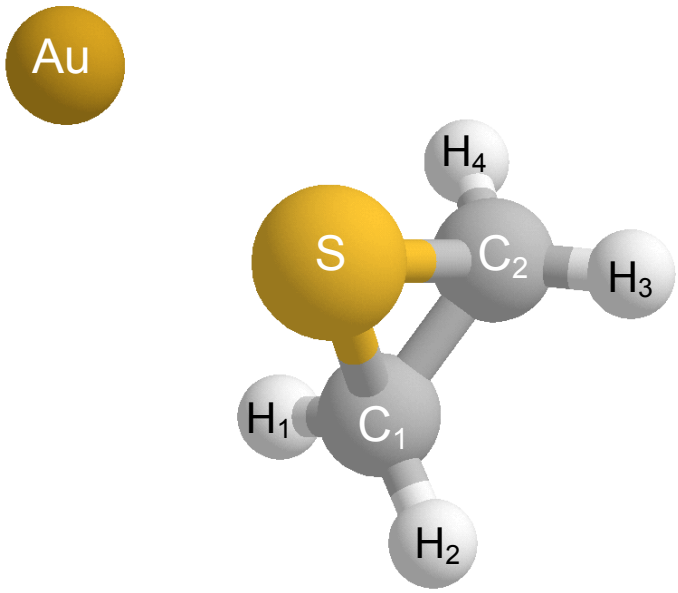

	B3LYP	M06	BHandHLYP
Ag-S	2.676 Å	2.713 Å	2.721 Å
S-C_1	1.847 Å	1.824 Å	1.824 Å
S-C_2	1.847 Å	1.824 Å	1.824 Å
C_1-C_2	1.474 Å	1.465 Å	1.466 Å
C_1-H_1	1.083 Å	1.088 Å	1.075 Å
C_1-H_2	1.084 Å	1.087 Å	1.076 Å
C_2-H_3	1.084 Å	1.087 Å	1.076 Å
C_2-H_4	1.083 Å	1.088 Å	1.075 Å
∠Ag-S-C_1	102.5º	97.5º	102.1º
∠C_1-S-C_2	47.0º	47.4º	47.4º
∠S-C_1-H_1	113.8º	114.0º	114.3º
∠S-C_1-H_2	113.7º	114.0º	113.9º
∠S-C_2-H_3	113.7º	114.0º	113.9º
∠S-C_2-H_4	113.8º	114.0º	114.3º
∠H_1-C_1-H_2	115.6º	115.5º	115.5º
D(Ag-S-C_1-C_2)	-95.5º	-93.3º	-95.4º
D(Ag-S-C_1-H_1)	16.8º	18.7º	16.6º
D(Ag-S-C_1-H_2)	151.8º	154.3º	152.3º
D(Ag-S-C_2-H_3)	-151.8º	-154.3º	-152.3º
D(Ag-S-C_2-H_4)	-16.8º	-18.7º	-16.6º
Energy[a]	-612.2829724	-612.1560014	-612.0431490

[a]Potential energy at the equilibrium geometry.

Cu-$\overline{NHCH_2CH_2}$

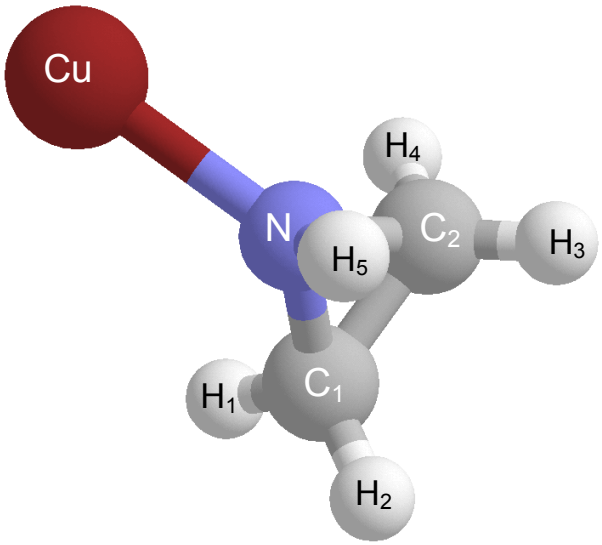

	B3LYP	M06	BHandHLYP
Cu-N	2.107 Å	2.099 Å	2.149 Å
N-C_1	1.481 Å	1.465 Å	1.463 Å
N-C_2	1.481 Å	1.465 Å	1.463 Å
N-H_5	1.016 Å	1.017 Å	1.005 Å
C_1-C_2	1.481 Å	1.469 Å	1.470 Å
C_1-H_1	1.084 Å	1.088 Å	1.076 Å
C_1-H_2	1.085 Å	1.087 Å	1.077 Å
C_2-H_3	1.085 Å	1.087 Å	1.077 Å
C_2-H_4	1.084 Å	1.088 Å	1.076 Å
∠Cu-N-C_1	125.2º	118.4º	124.5º
∠Cu-N-H_5	112.9º	120.5º	113.3º
∠C_1-N-C_2	60.0º	60.2º	60.3º
∠N-C_1-H_1	114.3º	113.9º	114.6º
∠N-C_1-H_2	117.2º	117.5º	117.3º
∠N-C_2-H_3	117.2º	117.5º	117.3º
∠N-C_2-H_4	114.3º	113.9º	114.6º
D(Cu-N-C_1-C_2)	-114.1º	-108.3º	-113.5º
D(Cu-N-C_1-H_1)	2.5º	3.3º	2.0º
D(Cu-N-C_1-H_2)	136.9º	142.9º	137.6º
D(Cu-N-C_2-H_3)	-136.9º	-142.9º	-137.6º
D(Cu-N-C_2-H_4)	-2.5º	-3.3º	-2.0º
D(H_5-N-C_1-C_2)	103.3º	103.8º	103.7º
Energy[a]	-330.0926607	-330.0230742	-329.7953565

[a]Potential energy at the equilibrium geometry.

Ag-$\overline{NHCH_2CH_2}$

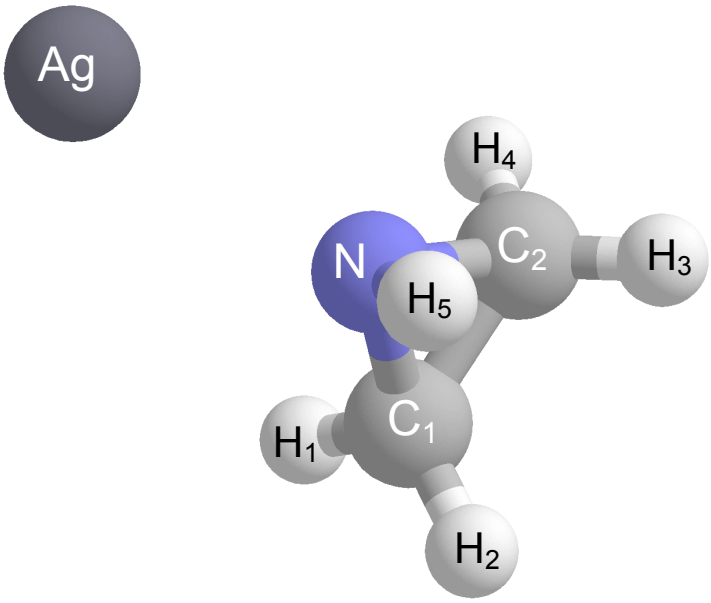

	B3LYP	M06	BHandHLYP
Ag-N	2.520 Å	2.504 Å	2.544 Å
N-C_1	1.476 Å	1.461 Å	1.459 Å
N-C_2	1.476 Å	1.461 Å	1.459 Å
N-H_5	1.016 Å	1.017 Å	1.005 Å
C_1-C_2	1.483 Å	1.470 Å	1.471 Å
C_1-H_1	1.084 Å	1.089 Å	1.076 Å
C_1-H_2	1.085 Å	1.088 Å	1.077 Å
C_2-H_3	1.085 Å	1.088 Å	1.077 Å
C_2-H_4	1.084 Å	1.089 Å	1.076 Å
∠Ag-N-C_1	123.9º	114.2º	123.8º
∠Ag-N-H_5	114.3º	125.6º	114.1º
∠C_1-N-C_2	60.3º	60.4º	60.6º
∠N-C_1-H_1	114.4º	114.2º	114.7º
∠N-C_1-H_2	117.9º	118.1º	117.8º
∠N-C_2-H_3	117.9º	118.1º	117.8º
∠N-C_2-H_4	114.4º	114.2º	114.7º
D(Ag-N-C_1-C_2)	-113.0º	-105.2º	-113.0º
D(Ag-N-C_1-H_1)	-1.4º	-6.4º	-1.4º
D(Ag-N-C_1-H_2)	138.5º	146.5º	138.8º
D(Ag-N-C_2-H_3)	-138.5º	-146.5º	-138.7º
D(Ag-N-C_2-H_4)	1.4º	6.4º	1.4º
D(H_5-N-C_1-C_2)	103.5º	103.8º	103.7º
Energy[a]	-279.7221904	-279.6255630	-279.4970750

[a]Potential energy at the equilibrium geometry.

Au-$\overline{NHCH_2CH_2}$

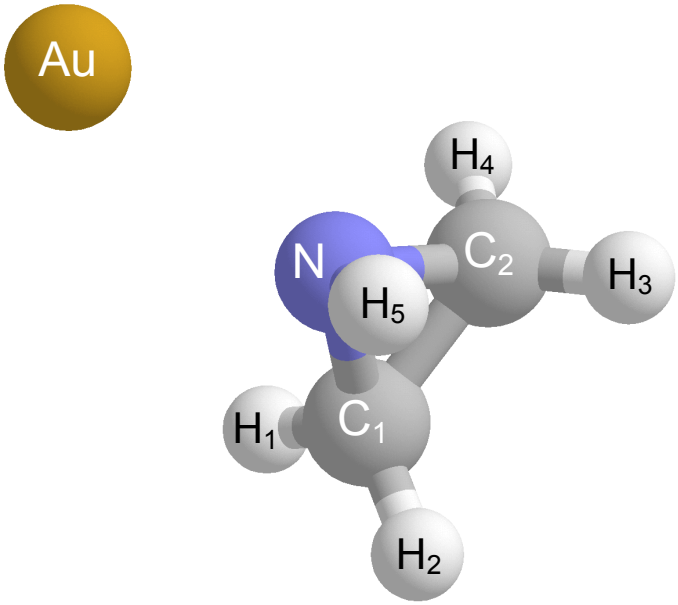

	B3LYP	M06	BHandHLYP
Au-N	2.374 Å	2.418 Å	2.392 Å
N-C_1	1.474 Å	1.460 Å	1.459 Å
N-C_2	1.474 Å	1.460 Å	1.459 Å
N-H_5	1.014 Å	1.016 Å	1.004 Å
C_1-C_2	1.484 Å	1.472 Å	1.472 Å
C_1-H_1	1.083 Å	1.087 Å	1.075 Å
C_1-H_2	1.085 Å	1.088 Å	1.077 Å
C_2-H_3	1.085 Å	1.088 Å	1.077 Å
C_2-H_4	1.083 Å	1.087 Å	1.075 Å
∠Au-N-C_1	124.5º	119.1º	124.1º
∠Au-N-H_5	112.0º	118.4º	112.5º
∠C_1-N-C_2	60.5º	60.6º	60.6º
∠N-C_1-H_1	114.3º	114.1º	114.5º
∠N-C_1-H_2	117.2º	117.7º	117.3º
∠N-C_2-H_3	117.2º	117.7º	117.3º
∠N-C_2-H_4	114.3º	114.1º	114.5º
D(Au-N-C_1-C_2)	-113.6º	-108.9º	-113.4º
D(Au-N-C_1-H_1)	2.1º	2.7º	1.8º
D(Au-N-C_1-H_2)	137.4º	142.5º	137.9º
D(Au-N-C_2-H_3)	-137.4º	-142.5º	-137.9º
D(Cu-N-C_2-H_4)	-2.1º	-2.7º	-1.8º
D(H_5-N-C_1-C_2)	104.5º	104.6º	104.4º
Energy[a]	-269.4104604	-269.2798961	-269.1588129

[a]Potential energy at the equilibrium geometry.

$CuOCH_2CH_2$

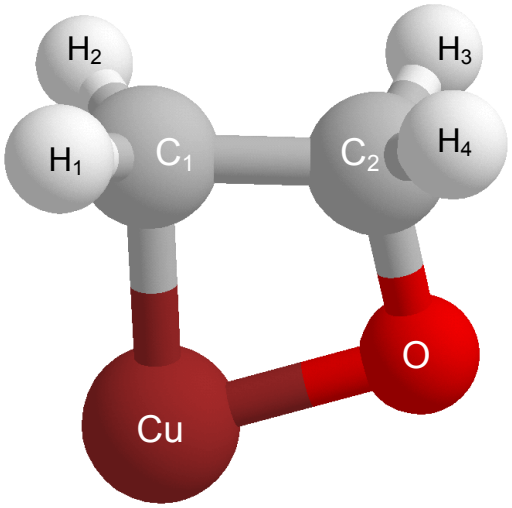

	B3LYP	M06	BHandHLYP
$Cu-C_1$	2.011 Å	1.993 Å	2.050 Å
Cu-O	1.910 Å	1.910 Å	1.904 Å
$O-C_2$	1.437 Å	1.415 Å	1.415 Å
C_1-C_2	1.517 Å	1.507 Å	1.504 Å
C_1-H_1	1.088 Å	1.091 Å	1.080 Å
C_1-H_2	1.088 Å	1.091 Å	1.080 Å
C_2-H_3	1.097 Å	1.101 Å	1.089 Å
C_2-H_4	1.097 Å	1.101 Å	1.089 Å
$\angle C_1-Cu-O$	72.8º	71.9º	70.8º
$\angle Cu-O-C_2$	94.8º	95.5º	97.2º
$\angle O-C_2-C_1$	104.0º	103.4º	103.6º
$\angle C_2-C_1-Cu$	88.3º	89.2º	88.5º
$\angle Cu-C_1-H_1$	107.6º	106.3º	106.3º
$\angle Cu-C_1-H_2$	107.6º	106.3º	106.3º
$\angle O-C_2-H_3$	109.9º	110.5º	110.1º
$\angle O-C_2-H_4$	109.8º	110.5º	110.1º
$D(C_1-Cu-O-C_2)$	0.0º	0.0º	0.0º
$D(O-Cu-C_1-H_1)$	118.2º	118.7º	118.6º
$D(O-Cu-C_1-H_2)$	-118.2º	-118.7º	-118.6º
$D(Cu-O-C_2-H_3)$	120.1º	120.0º	120.1º
$D(Cu-O-C_2-H_4)$	-120.1º	-120.0º	-120.1º
Energy[a]	-349.9672681	-349.8906671	-349.6545190

[a]Potential energy at the equilibrium geometry.

$AgOCH_2CH_2$

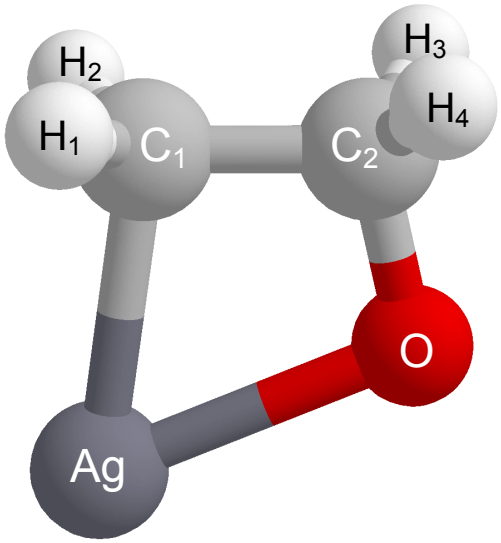

	B3LYP	M06	BHandHLYP
Ag-C_1	2.258 Å	2.258 Å	2.273 Å
Ag-O	2.264 Å	2.255 Å	2.309 Å
O-C_2	1.421 Å	1.402 Å	1.404 Å
C_1-C_2	1.506 Å	1.498 Å	1.497 Å
C_1-H_1	1.086 Å	1.089 Å	1.078 Å
C_1-H_2	1.086 Å	1.089 Å	1.078 Å
C_2-H_3	1.098 Å	1.103 Å	1.089 Å
C_2-H_4	1.098 Å	1.103 Å	1.089 Å
∠C_1-Ag-O	61.2º	60.8º	59.4º
∠Ag-O-C_2	98.6º	99.3º	99.6º
∠O-C_2-C_1	103.8º	103.8º	102.9º
∠C_2-C_1-Ag	96.3º	96.2º	98.2º
∠Ag-C_1-H_1	101.6º	101.1º	102.3º
∠Ag-C_1-H_2	101.6º	101.1º	102.3º
∠O-C_2-H_3	110.3º	110.9º	110.2º
∠O-C_2-H_4	110.3º	110.9º	110.2º
D(C_1-Ag-O-C_2)	0.0º	0.0º	0.0º
D(O-Ag-C_1-H_1)	120.3º	120.4º	120.2º
D(O-Ag-C_1-H_2)	-120.3º	-120.4º	-120.2º
D(Ag-O-C_2-H_3)	119.8º	120.0º	119.8º
D(Ag-O-C_2-H_4)	-119.8º	-120.0º	-119.8º
Energy[a]	-299.5714669	-299.4709965	-299.3359877

[a]Potential energy at the equilibrium geometry.

$AuOCH_2CH_2$

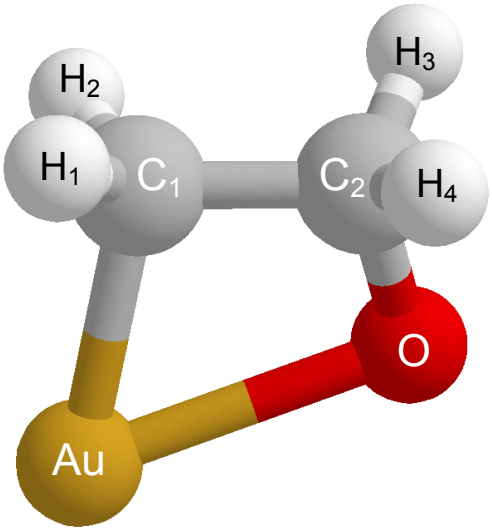

	B3LYP	M06	BHandHLYP
Au-C_1	2.079 Å	2.089 Å	2.049 Å
Au-O	2.463 Å	2.455 Å	3.395 Å
O-C_2	1.405 Å	1.391 Å	1.365 Å
C_1-C_2	1.528 Å	1.521 Å	1.512 Å
C_1-H_1	1.089 Å	1.091 Å	1.085 Å
C_1-H_2	1.089 Å	1.091 Å	1.085 Å
C_2-H_3	1.099 Å	1.102 Å	1.101 Å
C_2-H_4	1.099 Å	1.102 Å	1.101 Å
$\angle C_1$-Au-O	60.8º	60.4º	45.5º
$\angle$Au-O-C_2	89.8º	91.5º	61.5º
$\angle$O-C_2-C_1	104.6º	104.7º	116.2º
$\angle C_2$-C_1-Au	102.4º	103.3º	113.6º
$\angle$Au-C_1-H_1	105.9º	104.9º	105.9º
$\angle$Au-C_1-H_2	104.3º	104.9º	105.5º
$\angle$O-C_2-H_3	110.2º	110.9º	104.7º
$\angle$O-C_2-H_4	111.2º	110.9º	108.6º
D(C_1-Au-O-C_2)	-10.4º	0.0º	-31.3º
D(O-Au-C_1-H_1)	131.0º	120.8º	148.7º
D(O-Au-C_1-H_2)	-109.9º	-120.8º	-95.5º
D(Au-O-C_2-H_3)	131.8º	119.3º	155.0º
D(Au-O-C_2-H_4)	-106.9º	-119.3º	-94.0º
Energy[a]	-289.2655598	-289.1282250	-289.0117292

[a]Potential energy at the equilibrium geometry.

$CuSCH_2CH_2$

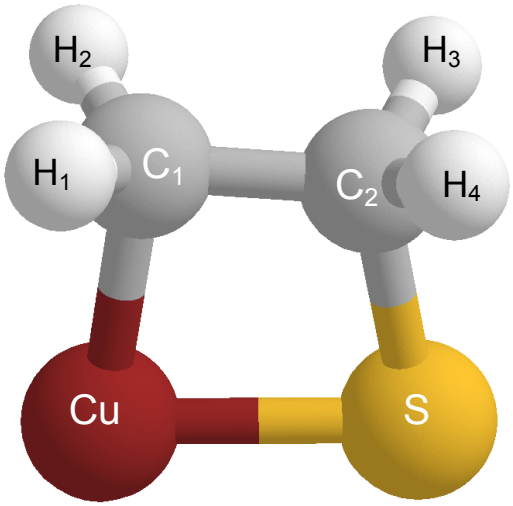

	B3LYP	M06	BHandHLYP
$Cu-C_1$	2.036 Å	2.028 Å	2.123 Å
Cu-S	2.244 Å	2.213 Å	2.236 Å
$S-C_2$	1.891 Å	1.877 Å	1.867 Å
C_1-C_2	1.507 Å	1.493 Å	1.490 Å
C_1-H_1	1.089 Å	1.091 Å	1.080 Å
C_1-H_2	1.089 Å	1.091 Å	1.080 Å
C_2-H_3	1.090 Å	1.093 Å	1.082 Å
C_2-H_4	1.090 Å	1.093 Å	1.082 Å
$\angle C_1-Cu-S$	78.6º	78.5º	75.9º
$\angle Cu-S-C_2$	79.6º	80.1º	82.5º
$\angle S-C_2-C_1$	105.6º	105.2º	105.5º
$\angle C_2-C_1-Cu$	96.2º	96.2º	96.21
$\angle Cu-C_1-H_1$	105.6º	104.3º	102.6º
$\angle Cu-C_1-H_2$	105.6º	104.3º	102.6º
$\angle S-C_2-H_3$	107.9º	108.2º	108.3º
$\angle S-C_2-H_4$	107.9º	108.2º	108.3º
$D(C_1-Cu-S-C_2)$	0.0º	0.0º	0.0º
$D(S-Cu-C_1-H_1)$	119.6º	119.9º	120.2º
$D(S-Cu-C_1-H_2)$	-119.6º	-119.9º	-120.2º
$D(Cu-S-C_2-H_3)$	120.8º	120.8º	120.8º
$D(Cu-S-C_2-H_4)$	-120.8º	-120.8º	-120.8º
Energy[a]	-672.9740606	-672.9022799	-672.6833283

[a]Potential energy at the equilibrium geometry.

$AgSCH_2CH_2$

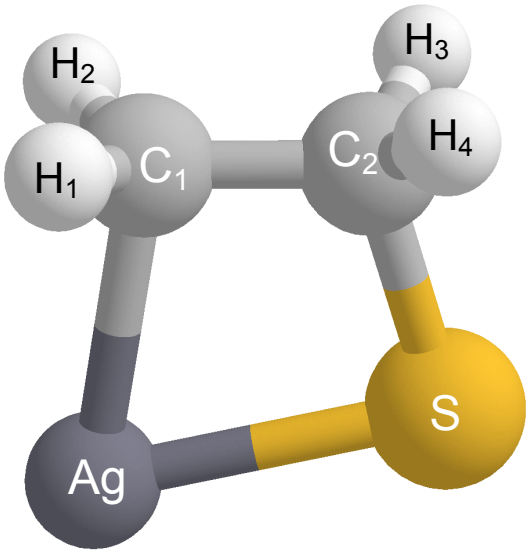

	B3LYP	M06	BHandHLYP
Ag-C_1	2.360 Å	2.403 Å	2.612 Å
Ag-O	2.492 Å	2.450 Å	2.444 Å
O-C_2	1.885 Å	1.871 Å	1.864 Å
C_1-C_2	1.492 Å	1.480 Å	1.477 Å
C_1-H_1	1.086 Å	1.089 Å	1.077 Å
C_1-H_2	1.086 Å	1.089 Å	1.077 Å
C_2-H_3	1.090 Å	1.093 Å	1.082 Å
C_2-H_4	1.090 Å	1.093 Å	1.082 Å
∠C_1-Ag-O	68.4º	68.0º	65.3º
∠Ag-O-C_2	85.1º	86.2º	91.0º
∠O-C_2-C_1	107.2º	107.7º	109.2º
∠C_2-C_1-Ag	99.4º	97.6	94.5º
∠Ag-C_1-H_1	99.7º	99.1º	95.8º
∠Ag-C_1-H_2	99.7º	99.1º	95.8º
∠O-C_2-H_3	107.7º	108.1º	107.4º
∠O-C_2-H_4	107.7º	108.1º	107.4º
D(C_1-Ag-O-C_2)	0.0º	0.0º	0.0º
D(O-Ag-C_1-H_1)	120.8º	126.1º	120.8º
D(O-Ag-C_1-H_2)	-120.8º	-126.1º	-120.8º
D(Ag-O-C_2-H_3)	121.0º	115.2º	121.4º
D(Ag-O-C_2-H_4)	-121.0º	-115.2º	-121.4º
Energy[a]	-622.5834178	-622.4866256	-622.3695173

[a]Potential energy at the equilibrium geometry.

$AuSCH_2CH_2$

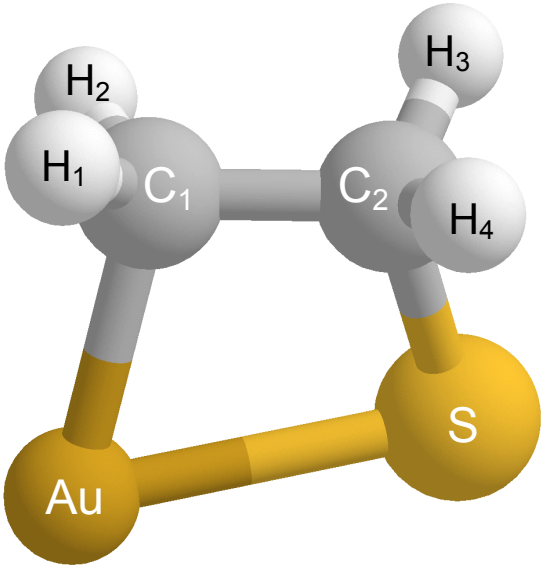

	B3LYP	M06	BHandHLYP
Au-C_1	2.111 Å	2.136 Å	2.099 Å
Au-S	2.619 Å	2.557 Å	2.630 Å
S-C_2	1.858 Å	1.849 Å	1.836 Å
C_1-C_2	1.515 Å	1.503 Å	1.510 Å
C_1-H_1	1.089 Å	1.092 Å	1.081 Å
C_1-H_2	1.089 Å	1.092 Å	1.081 Å
C_2-H_3	1.093 Å	1.096 Å	1.084 Å
C_2-H_4	1.093 Å	1.096 Å	1.084 Å
∠C_1-Au-S	68.9º	69.1º	68.0º
∠Au-S-C_2	77.8º	79.2º	78.1º
∠S-C_2-C_1	106.3º	106.0º	106.1º
∠C_2-C_1-Au	103.6º	102.3º	104.8º
∠Au-C_1-H_1	105.5º	105.7º	105.8º
∠Au-C_1-H_2	103.5º	103.4º	103.8º
∠S-C_2-H_3	108.8º	108.7º	109.2º
∠S-C_2-H_4	109.4º	109.4º	109.4º
D(C_1-Au-S-C_2)	13.3º	14.5º	12.3º
D(S-Au-C_1-H_1)	135.2º	134.8º	13542º
D(S-Au-C_1-H_2)	-106.7º	-106.8º	-107.8º
D(Au-S-C_2-H_3)	134.6º	134.8º	133.8º
D(Au-S-C_2-H_4)	-106.0º	-106.2º	-106.9º
Energy[a]	-612.2775094	-612.1427805	-612.0328809

[a]Potential energy at the equilibrium geometry.

$CuNHCH_2CH_2$

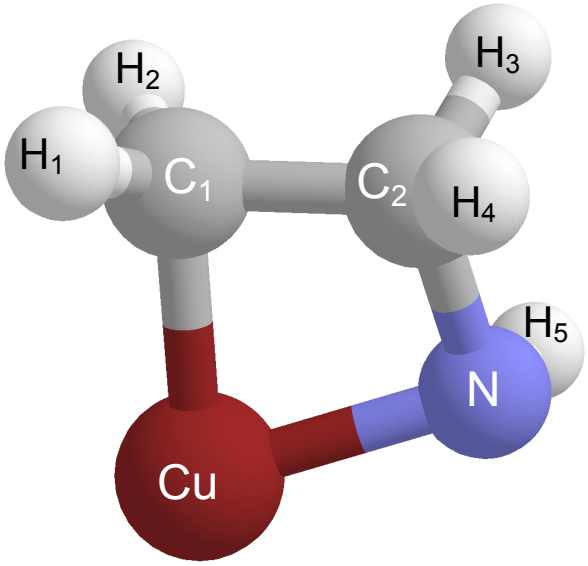

	B3LYP	M06	BHandHLYP
$Cu-C_1$	2.018 Å	1.994 Å	2.038 Å
Cu-N	1.977 Å	1.975 Å	2.027 Å
$N-C_2$	1.499 Å	1.486 Å	1.477 Å
C_1-C_2	1.523 Å	1.511 Å	1.511 Å
C_1-H_1	1.089 Å	1.092 Å	1.081 Å
C_1-H_2	1.089 Å	1.092 Å	1.081 Å
C_2-H_3	1.097 Å	1.099 Å	1.089 Å
C_2-H_4	1.097 Å	1.099 Å	1.089 Å
$N-H_5$	1.025 Å	1.026 Å	1.014 Å
$\angle C_1-Cu-N$	73.9º	73.3º	70.9º
$\angle Cu-N-C_2$	90.7º	90.7º	91.9º
$\angle N-C_2-C_1$	105.3º	104.4º	104.1º
$\angle C_2-C_1-Cu$	88.4º	89.3º	90.5º
$\angle Cu-C_1-H_1$	110.6º	109.8º	109.1º
$\angle Cu-C_1-H_2$	108.4º	107.9º	109.3º
$\angle N-C_2-H_3$	111.6º	111.9º	111.8º
$\angle N-C_2-H_4$	108.0º	108.2º	108.4º
$\angle Cu-N-H_5$	109.4º	98.6º	107.5º
$D(C_1-Cu-N-C_2)$	-8.6º	-10.0º	-14.1º
$D(N-Cu-C_1-H_1)$	127.1º	128.8º	129.0º
$D(N-Cu-C_1-H_2)$	-108.3º	-107.1º	-107.0º
$D(Cu-N-C_2-H_3)$	133.7º	135.7º	136.7º
$D(Cu-N-C_2-H_4)$	-107.5º	-105.5º	-104.4º
$D(C_1-Cu-N-H_5)$	100.8º	98.6º	107.5º
Energy[a]	-330.0829967	-330.0075186	-329.7738011

[a]Potential energy at the equilibrium geometry.

$AgNHCH_2CH_2$

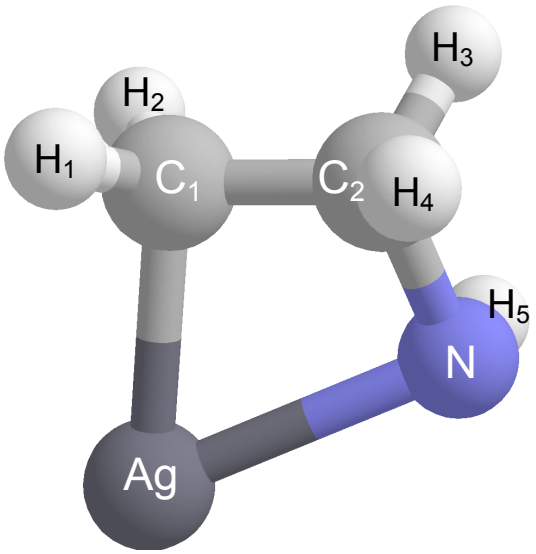

	B3LYP	M06	BHandHLYP
Ag-C_1	2.232 Å	2.206 Å	2.194 Å
Ag-N	2.415 Å	2.447 Å	2.689 Å
N-C_2	1.482 Å	1.468 Å	1.455 Å
C_1-C_2	1.515 Å	1.507 Å	1.516 Å
C_1-H_1	1.087 Å	1.091 Å	1.081 Å
C_1-H_2	1.087 Å	1.091 Å	1.081 Å
C_2-H_3	1.098 Å	1.102 Å	1.092 Å
C_2-H_4	1.098 Å	1.102 Å	1.092 Å
N-H_5	1.027 Å	1.029 Å	1.016 Å
∠C_1-Ag-N	61.9º	61.1º	57.6º
∠Ag-N-C_2	91.0º	89.9º	85.1º
∠N-C_2-C_1	106.0º	105.8º	107.2º
∠C_2-C_1-Ag	97.5º	98.6º	103.7º
∠Ag-C_1-H_1	104.6º	105.0º	106.2º
∠Ag-C_1-H_2	105.4º	106.0º	107.1º
∠N-C_2-H_3	111.8º	112.0º	111.4º
∠N-C_2-H_4	107.8º	108.0º	108.0º
∠Ag-N-H_5	102.1º	100.7º	100.5º
D(C_1-Ag-N-C_2)	-12.1º	-18.2º	-20.5º
D(N-Ag-C_1-H_1)	132.3º	133.8º	136.2º
D(N-Ag-C_1-H_2)	-107.7º	-106.4º	-105.0º
D(Ag-N-C_2-H_3)	139.0º	141.0º	143.3º
D(Ag-N-C_2-H_4)	-102.2º	-100.3º	-98.2º
D(C_1-Ag-N-H_5)	95.5º	93.3º	90.7º
Energy[a]	-279.6903982	-279.5896597	-279.4597344

[a]Potential energy at the equilibrium geometry.

AuNHCH$_2$CH$_2$

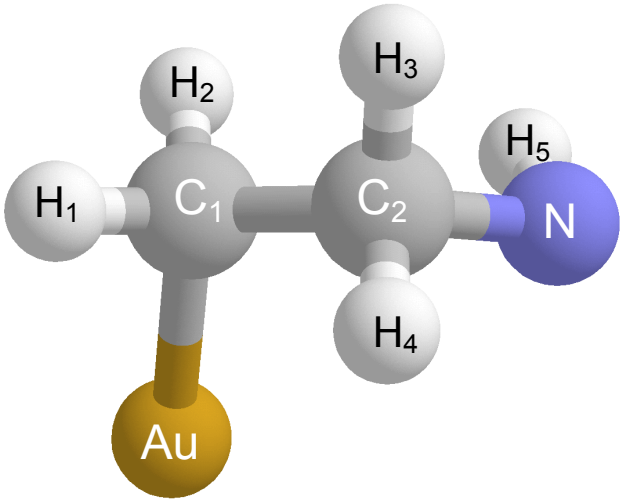

	B3LYP	M06	BHandHLYP
Au-C_1	2.060 Å	2.069 Å	2.052 Å
Au-N	3.389 Å	3.114 Å	3.341 Å
N-C_2	1.443 Å	1.439 Å	1.437 Å
C_1-C_2	1.525 Å	1.516 Å	1.517 Å
C_1-H_1	1.092 Å	1.094 Å	1.084 Å
C_1-H_2	1.092 Å	1.094 Å	1.084 Å
C_2-H_3	1.110 Å	1.109 Å	1.099 Å
C_2-H_4	1.110 Å	1.109 Å	1.099 Å
N-H_5	1.028 Å	1.030 Å	1.017 Å
∠C_1-Au-N	48.1º	51.9º	48.2º
∠Au-N-C_2	62.3º	70.1º	63.6º
∠N-C_2-C_1	116.9º	112.4º	115.5º
∠C_2-C_1-Au	112.9º	109.9º	113.1º
∠Au-C_1-H_1	104.8º	106.1º	105.3º
∠Au-C_1-H_2	104.9º	105.5º	105.6º
∠N-C_2-H_3	106.6º	109.3º	107.1º
∠N-C_2-H_4	108.7º	108.9º	108.7º
∠Au-N-H_5	78.7º	88.1º	83.0º
D(C_1-Au-N-C_2)	-32.1º	-24.7º	-27.9º
D(N-Au-C_1-H_1)	147.5º	145.6º	147.6º
D(N-Au-C_1-H_2)	-97.3º	-98.1º	-97.2º
D(Au-N-C_2-H_3)	151.7º	149.6º	151.5º
D(Au-N-C_2-H_4)	-95.1º	-94.2º	-94.1º
D(C_1-Au-N-H_5)	88.5º	83.6º	85.5º
Energy[a]	-269.3944122	-269.2549060	-269.1409519

[a]Potential energy at the equilibrium geometry.

8.1.2. Predicted hyperfine interaction, a_{Nu} and geometry of small molecules (Energy corresponds to potential energy values at these optimized equilibrium geometries).

CuCO

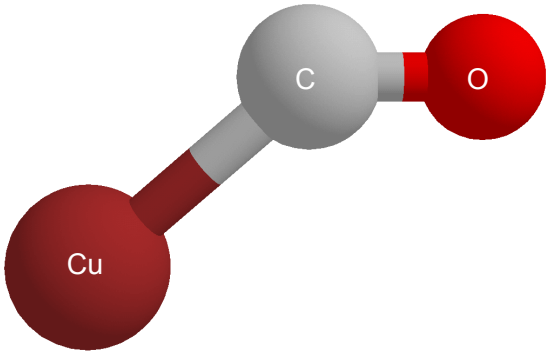

B3LYP	6-311G	6-311+G	6-311+G(d)	EPR-III	6-31++G(d,p)
Cu-C	1.842 Å	1.940 Å	1.966 Å	1.960 Å	1.960 Å
C-O	1.175 Å	1.169 Å	1.144 Å	1.140 Å	1.153 Å
∠Cu-C-O	140.1º	140.1º	138.6º	140.2º	138.73º
a_{63Cu}	3344	3891	4106	4068	4071
a_{13C}	264	197	190	195	183
a_{17O}	-11	-11	-10	-12	-15
Energy	-1753. 7132797	-1753. 7892716	-1753. 8340045	-1753. 8525977	-1753. 8014543
M06					
Cu-C	1.837 Å	1.950 Å	1.983 Å	1.978 Å	1.974 Å
C-O	1.170 Å	1.164 Å	1.140 Å	1.136 Å	1.151 Å
∠Cu-C-O	139.9º	138.5º	136.7º	138.6º	136.5º
a_{63Cu}	3492	3925	4153	4127	4125
a_{13C}	265	220	211	201	197
a_{17O}	-10	-10	-10	-15	-14
Energy	-1753. 5403836	-1753. 6195508	-1753. 6660387	-1753. 6876024	-1753. 6364001
BHandHLYP					
Cu-C	1.909 Å	2.042 Å	2.120 Å	2.102 Å	2.103 Å
C-O	1.158 Å	1.149 Å	1.123 Å	1.120 Å	1.133 Å
∠Cu-C-O	136.4º	137.8º	136.1º	137.9º	136.4º
a_{63Cu}	3513	4059	4378	4317	4324
a_{13C}	223	167	158	163	141
a_{17O}	-17	-15	-11	-12	-14
Energy	-1753. 523306	-1753. 5947326	-1753. 6484064	-1753. 6666137	-1753. 617366

CuSiO

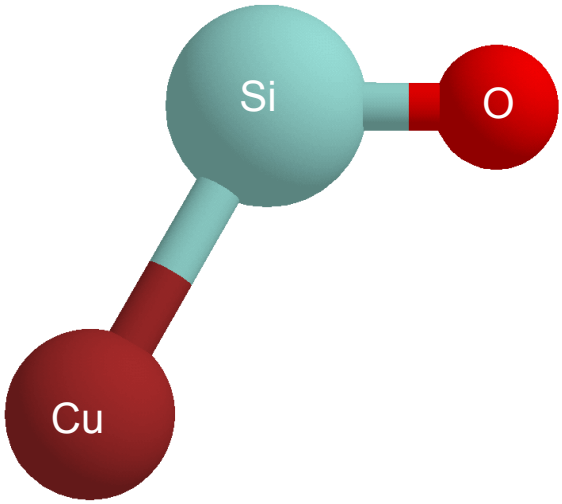

B3LYP	6-311G	6-311+G	6-311+G(d)	6-31++G(d,p)[a]
Cu-Si	2.255 Å	2.384 Å	2.359 Å	2.359 Å
Si-O	1.595 Å	1.598 Å	1.536 Å	1.543 Å
∠Cu-Si-O	121.1º	116.3º	118.0º	118.2º
a_{63Cu}	3617	4131	4186	4176
a_{29Si}	-340	-288	-299	-254
a_{17O}	-8	-8	-8	-18
Energy	-2005.1263132	-2005.2170935	-2005.2630145	-2005.2169891
M06				
Cu-Si	2.241 Å	2.369 Å	2.346 Å	2.343 Å
Si-O	1.581 Å	1.582 Å	1.525 Å	1.531 Å
∠Cu-Si-O	121.4º	117.7º	119.9º	120.7º
a_{63Cu}	3899	4154	4173	4152
a_{29Si}	-341	-328	-344	-303
a_{17O}	0.0	-10	-9	-17
Energy	-2004.9495677	-2005.0445472	-2005.0927339	-2005.0511168
BHandHLYP				
Cu-Si	2.337 Å	2.453 Å	2.438 Å	2.434 Å
Si-O	1.572 Å	1.576 Å	1.515 Å	1.521 Å
∠Cu-Si-O	115.9º	110.3º	113.6º	114.0º
a_{63Cu}	3731	4128	4221	4206
a_{29Si}	-248	-211	-234	-195
a_{17O}	-23	-23	-17	-26
Energy	-2004.9410272	-2005.0240471	-2005.0775666	-2005.035601

$CuNH_3$

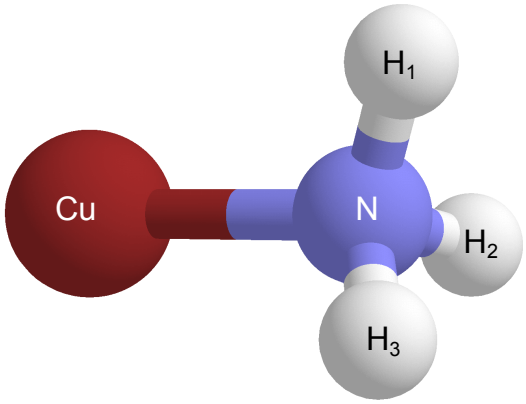

B3LYP	6-311G	6-311+G	6-311+G(d)	EPR-III	6-31++G(d,p)
Cu-N	1.998 Å	2.073 Å	2.085 Å	2.094 Å	2.093 Å
N-H_1	1.019 Å	1.018 Å	1.018 Å	1.016 Å	1.020 Å
N-H_2	1.019 Å	1.018 Å	1.018 Å	1.016 Å	1.020 Å
N-H_3	1.019 Å	1.018 Å	1.018 Å	1.016 Å	1.020 Å
∠Cu-N-H_1	109.4º	108.7º	111.3º	111.0º	111.1º
∠Cu-N-H_2	109.4º	108.7º	111.3º	110.9º	111.1º
∠Cu-N-H_3	109.4º	108.7º	111.3º	111.0º	111.0º
∠H_1-N-H_2	109.6º	110.3º	107.6º	107.9º	107.8º
∠H_1-N-H_3	109.5º	110.3º	107.6º	107.9º	107.8º
∠H_2-N-H_3	109.5º	110.3º	107.6º	107.9º	107.8º
a_{63Cu}	1251	3165	3325	3354	3336
a_{14N}	97	86	87	87	74
a_{H1}	-5	-3	-2	-2	-1
a_{H2}	-5	-3	-2	-2	-1
a_{H3}	-5	-3	-2	-2	-1
Energy	-1696.9689997	-1697.0528094	-1697.0648529	-1697.0792802	-1697.0563842
M06					
Cu-N	1.983 Å	2.066 Å	2.082 Å	2.097 Å	2.097 Å
N-H_1	1.018 Å	1.017 Å	1.018 Å	1.013 Å	1.018 Å
N-H_2	1.018 Å	1.017 Å	1.018 Å	1.013 Å	1.018 Å
N-H_3	1.018 Å	1.017 Å	1.018 Å	1.013 Å	1.018 Å
∠Cu-N-H_1	109.0º	108.1º	111.2º	110.7º	110.8º
∠Cu-N-H_2	109.0º	108.1º	111.2º	110.7º	110.8º
∠Cu-N-H_3	109.0º	108.1º	111.2º	110.7º	110.8º
∠H_1-N-H_2	109.9º	110.9º	107.7º	108.2º	108.2º
∠H_1-N-H_3	109.9º	110.9º	107.7º	108.2º	108.2º
∠H_2-N-H_3	109.9º	110.9º	107.7º	108.2º	108.2º
a_{63Cu}	1529	3318	3493	3534	3542
a_{14N}	83	82	85	82	69

a_{H1}	-9	-6	-4	-7	-4

	6-311G	6-311+G	6-311+G(d)	EPR-III	6-31++G(d,p)
a_{H2}	-9	-6	-4	-7	-4
a_{H3}	-9	-6	-4	-7	-4
Energy	-1696. 8184958	-1696. 9058764	-1696. 9157051	-1696. 9319080	-1696. 9097494
BHandHLYP					
Cu-N	2.012 Å	2.110 Å	2.127 Å	2.137 Å	2.127 Å
N-H_1	1.008 Å	1.006 Å	1.007 Å	1.006 Å	1.007 Å
N-H_2	1.008 Å	1.006 Å	1.007 Å	1.006 Å	1.007 Å
N-H_3	1.008 Å	1.006 Å	1.007 Å	1.006 Å	1.007 Å
∠Cu-N-H_1	108.8º	108.2º	111.3º	110.8º	111.3º
∠Cu-N-H_2	108.8º	108.2º	111.2º	110.8º	111.3º
∠Cu-N-H_3	108.8º	108.2º	111.3º	110.8º	111.3º
∠H_1-N-H_2	110.1º	110.7º	107.6º	108.1º	107.6º
∠H_1-N-H_3	110.1º	110.7º	107.6º	108.1º	107.6º
∠H_2-N-H_3	110.1º	110.7º	107.3º	108.1º	107.3º
a_{63Cu}	814	3198	3344	3377	3374
a_{14N}	82	72	72	73	60
a_{H1}	-6	-3	-3	-2	-2
a_{H2}	-6	-3	-3	-2	-2
a_{H3}	-6	-3	-3	-2	-2
Energy	-1696. 8163085	-1696. 8906283	-1696. 9047994	-1696. 9190326	-1696. 8979544

Cu[HCN]

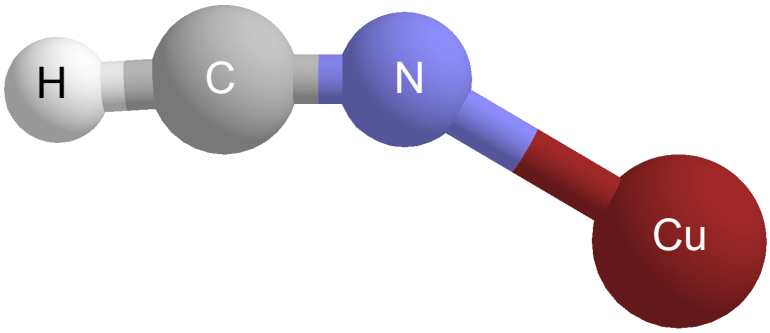

B3LYP	6-311G	6-311+G	6-311+G(d)	EPR-III	6-31++G(d,p)
Cu-N	1.865 Å	1.995 Å	2.034 Å	2.009 Å	2.012 Å
C-N	1.166 Å	1.165 Å	1.155 Å	1.150 Å	1.161 Å
H-C	1.065 Å	1.066 Å	1.070 Å	1.067 Å	1.072 Å
∠H-C-N	175.3º	176.1º	176.51º	176.9º	176.3º
∠C-N-Cu	163.0º	153.0º	149.53º	150.5º	152.0º
D(H-C-N-Cu)	0.0º	0.0º	0.0º	0.0º	0.0º
	6-311G	6-311+G	6-311+G(d)	EPR-III	6-31++G(d,p)
a_{63Cu}	2580	4059	4238	4137	4147
a_{14N}	103	67	63	65	55
a_{13C}	48	30	26	27	28
a_{H}	15	6	5	5	6
Energy	-1733. 8203890	-1733. 9026861	-1733. 9296139	-1733. 9473460	-1733. 9067715
M06					
Cu-N	1.861 Å	2.014 Å	2.074 Å	2.042 Å	2.052 Å
C-N	1.165 Å	1.163 Å	1.152 Å	1.148 Å	1.162 Å
H-C	1.067 Å	1.067 Å	1.072 Å	1.068 Å	1.073 Å
∠H-C-N	174.5º	176.0º	176.4º	177.1º	176.0º
∠C-N-Cu	157.8º	148.3º	143.6º	146.2º	144.6º
D(H-C-N-Cu)	0.0º	0.0º	0.0º	0.0º	0.0º
a_{63Cu}	2671	4193	4444	4137	4374
a_{14N}	104	71	65	65	56
a_{13C}	64	42	33	27	37
a_{H}	14	5	8	5	6
Energy	-1733. 6428564	-1733. 7291757	-1733. 7569218	-1733. 7774891	-1733. 7355104
BHandHLYP					
Cu-N	1.961 Å	2.136 Å	2.248 Å	2.181 Å	2.215 Å
C-N	1.145 Å	1.146 Å	1.136 Å	1.132 Å	1.142 Å
H-C	1.057 Å	1.057 Å	1.062 Å	1.060 Å	1.064 Å
∠H-C-N	180.0º	178.9º	179.4º	179.4º	179.4º
∠C-N-Cu	179.9º	159.3º	158.2º	159.0º	161.6º

D(H-C-N-Cu)	0.0º	0.0º	0.0º	0.0º	0.0º
	6-311G	6-311+G	6-311+G(d)	EPR-III	6-31++G(d,p)
a_{63Cu}	2248	4070	4368	4200	4275
a_{14N}	91	54	48	52	41
a_{13C}	26	16	13	14	12
a_{H}	13	5	4	4	4
Energy	-1733. 6390101	-1733. 716727	-1733. 7506335	-1733. 7674276	-1733. 7295594

Cu[C_2H_4]

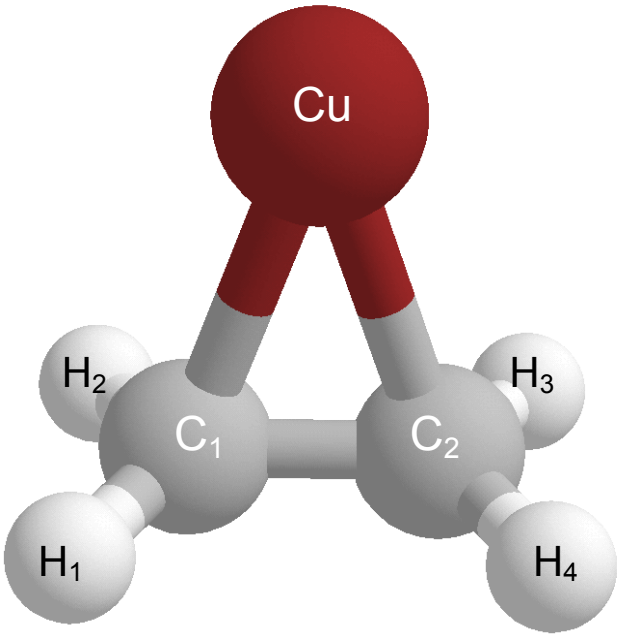

B3LYP	6-311G	6-311+G	6-311+G(d)	EPR-III	6-31++G(d,p)
$Cu\text{-}C_1$	2.088 Å	2.202 Å	2.162 Å	2.166 Å	2.153 Å
$Cu\text{-}C_2$	2.087 Å	2.798 Å	2.721 Å	2.701 Å	2.725 Å
$C_1\text{-}C_2$	1.372 Å	1.365 Å	1.362 Å	1.357 Å	1.369 Å
$C_1\text{-}H_1$	1.082 Å	1.085 Å	1.087 Å	1.085 Å	1.089 Å
$C_1\text{-}H_2$	1.082 Å	1.085 Å	1.087 Å	1.085 Å	1.089 Å
$C_2\text{-}H_3$	1.082 Å	1.082 Å	1.084 Å	1.082 Å	1.086 Å
$C_2\text{-}H_4$	1.082 Å	1.082 Å	1.084 Å	1.082 Å	1.086 Å
$\angle C_1\text{-}Cu\text{-}C_2$	38.4º	29.0º	29.7º	29.9º	29.7º
$\angle Cu\text{-}C_1\text{-}C_2$	70.8º	100.7º	98.5º	97.5º	99.0º
$\angle Cu\text{-}C_2\text{-}C_1$	70.8º	50.7º	51.8º	52.7º	51.3º
$\angle Cu\text{-}C_1\text{-}H_1$	106.4º	93.4º	94.7º	94.4º	94.7º
$\angle Cu\text{-}C_1\text{-}H_2$	106.4º	93.4º	94.7º	94.4º	94.7º
$\angle Cu\text{-}C_2\text{-}H_3$	106.4º	108.6º	107.7º	107.5º	107.9º
$\angle Cu\text{-}C_2\text{-}H_4$	106.4º	108.6º	107.7º	107.5º	107.9º
$\angle H_1\text{-}C_1\text{-}H_2$	116.1º	115.5º	115.5º	115.9º	115.8º
$D(Cu\text{-}C_2\text{-}C_1\text{-}H_1)$	98.0º	100.5º	100.7º	99.7º	100.9º
$D(Cu\text{-}C_2\text{-}C_1\text{-}H_2)$	-98.0º	-100.6º	-100.7º	-99.7º	-100.9º
$D(Cu\text{-}C_1\text{-}C_2\text{-}H_3)$	98.0º	88.7º	88.3º	88.6º	88.3º
$D(Cu\text{-}C_1\text{-}C_2\text{-}H_4)$	-98.0º	-88.6º	-88.3º	-88.6º	-88.3º
$D(H_1\text{-}C_1\text{-}C_2\text{-}H_3)$	-164.0º	-170.8º	-171.0º	-171.7º	-170.9º
$D(H_2\text{-}C_1\text{-}C_2\text{-}H_3)$	0.0º	12.0º	12.3º	11.1º	12.6º
a_{63Cu} (MHz)	2985	4375	4243	4252	4188
a_{13C1} (MHz)	37	28	26	10	51

a_{13C2} (MHz)	37	13	15	6	4
a_{H1} (MHz)	2	-20	-20	-7	-22
	6-311G	6-311+G	6-311+G(d)	EPR-III	6-31++G(d,p)
a_{H2} (MHz)	2	-20	-20	-7	-22
a_{H3} (MHz)	2	16	15	5	15
a_{H4} (MHz)	2	16	15	5	15
ENERGY (HF)	-1718. 9968802	-1719. 0683002	-1719. 0847003	-1719. 1043684	-1719. 0748007
M06					
Cu-C_1	2.063 Å	2.122 Å	2.102 Å	2.112 Å	2.093 Å
Cu-C_2	2.064 Å	2.738 Å	2.684 Å	2.655 Å	2.689 Å
C_1-C_2	1.367 Å	1.367 Å	1.362 Å	1.356 Å	1.370 Å
C_1-H_1	1.084 Å	1.088 Å	1.091 Å	1.085 Å	1.092 Å
C_1-H_2	1.084 Å	1.088 Å	1.091 Å	1.085 Å	1.092 Å
C_2-H_3	1.084 Å	1.084 Å	1.087 Å	1.081 Å	1.087 Å
C_2-H_4	1.084 Å	1.084 Å	1.087 Å	1.081 Å	1.087 Å
$\angle C_1$-Cu-C_2	38.7º	29.3º	30.0º	30.4º	30.1º
$\angle$Cu-C_1-C_2	70.7º	101.2º	99.4º	97.5º	99.8º
$\angle$Cu-C_2-C_1	70.7º	49.5º	50.6º	52.0º	50.1º
$\angle$Cu-C_1-H_1	106.5º	94.3º	95.1º	94.9º	95.2º
$\angle$Cu-C_1-H_2	106.5º	94.3º	95.1º	94.9º	95.2º
$\angle$Cu-C_2-H_3	106.5º	108.8º	108.0º	107.6º	108.1º
$\angle$Cu-C_2-H_4	106.5º	108.8º	108.0º	107.6º	108.1º
$\angle H_1$-C_1-H_2	116.2º	115.2º	115.2º	115.7º	115.5º
D(Cu-C_2-C_1-H_1)	98.0º	101.8º	100.6º	100.3º	102.0º
D(Cu-C_2-C_1-H_2)	-98.0º	-101.8º	-100.6º	-100.3º	-102.0º
D(Cu-C_1-C_2-H_3)	98.0º	88.4º	88.0º	88.4º	87.8º
D(Cu-C_1-C_2-H_4)	-98.0º	-88.4º	-88.30	-88.4º	-87.8º
D(H_1-C_1-C_2-H_3)	-164.0º	-169.8º	-171.0º	-171.3º	-170.2º
D(H_2-C_1-C_2-H_3)	0.0º	13.4º	13.7º	11.9º	14.1º
a_{63Cu}	3245	4131	4059	4075	3982
a_{13C1}	42	58	51	19	63
a_{13C2}	42	1	7	18	1
a_{H1}	-3	-34	-31	-34	-30
a_{H2}	-3	-34	-31	-34	-30
a_{H3}	-3	22	18	20	18
a_{H4}	-3	22	18	20	18
Energy	-1718. 8182899	-1718. 8941383	-1718. 9068226	-1718. 9293048	-1718. 8971615
BHandHLYP					
Cu-C_1	2.165 Å	3.640 Å	3.202 Å	3.763 Å	2.905 Å
Cu-C_2	2.165 Å	4.070 Å	3.576 Å	4.241 Å	3.306 Å
C_1-C_2	1.347 Å	1.324 Å	1.322 Å	1.316 Å	1.328 Å
C_1-H_1	1.073 Å	1.075 Å	1.078 Å	1.075 Å	1.079 Å
C_1-H_2	1.073 Å	1.075 Å	1.078 Å	1.075 Å	1.079 Å
C_2-H_3	1.073 Å	1.075 Å	1.078 Å	1.075 Å	1.079 Å

C_2-H_4	1.073 Å	1.075 Å	1.078 Å	1.075 Å	1.079 Å
$\angle C_1$-Cu-C_2	36.2º	18.7º	21.6º	17.7º	23.6º
	6-311G	6-311+G	6-311+G(d)	EPR-III	6-31++G(d,p)
$\angle$Cu-C_1-C_2	71.9º	99.3º	95.4º	102.2º	95.4º
$\angle$Cu-C_2-C_1	71.9º	61.9º	63.0º	60.2º	61.0º
$\angle$Cu-C_1-H_1	103.8º	85.4º	87.8º	83.8º	88.4º
$\angle$Cu-C_1-H_2	103.8º	85.4º	87.8º	83.8º	88.4º
$\angle$Cu-C_2-H_3	103.8º	104.4º	103.7º	105.1º	104.6º
$\angle$Cu-C_2-H_4	103.8º	104.4º	103.7º	105.1º	104.6º
$\angle H_1$-C_1-H_2	116.3º	116.2º	116.4º	116.6º	116.6º
D(Cu-C_2-C_1-H_1)	95.4º	90.3º	90.8º	90.2º	91.5º
D(Cu-C_2-C_1-H_2)	-95.4º	-90.3º	-90.8º	-90.2º	-91.5º
D(Cu-C_1-C_2-H_3)	95.4º	90.0º	89.9º	90.0º	89.8º
D(Cu-C_1-C_2-H_4)	-95.4º	-90.0º	-89.9	-90.0º	-89.8º
D(H_1-C_1-C_2-H_3)	-169.1º	-179.7º	-179.3º	-179.8º	-178.8º
D(H_2-C_1-C_2-H_3)	0.0º	0.4º	0.9º	0.2º	1.7º
a_{63Cu}	3050	5232	5175	5243	5058
a_{13C1}	35	4	8	4	18
a_{13C2}	35	4	8	3	6
a_{H1}	1	2	4	2	7
a_{H2}	1	2	4	2	7
a_{H3}	1	2	4	2	6
a_{H4}	1	2	4	2	6
Energy	-1718.8157093	-1718.8861982	-1718.9059782	-1718.9249672	-1718.8978334

$Cu(CO)_3$

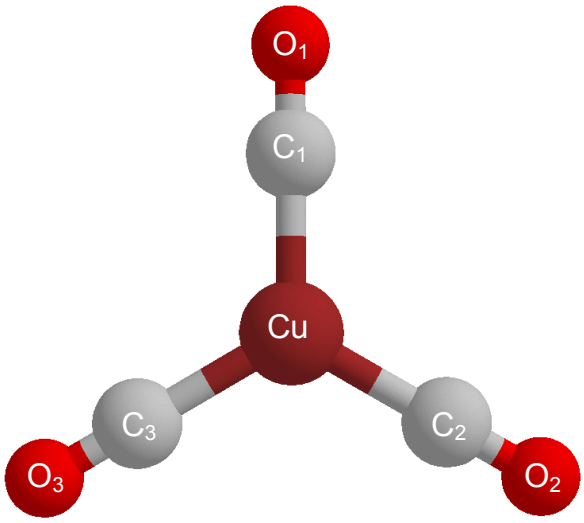

B3LYP	6-311G	6-311+G	6-311+G(d)	EPR-III	6-31++G(d,p)
$Cu\text{-}C_1$	1.833 Å	1.874 Å	1.884 Å	1.881 Å	1.883 Å
$Cu\text{-}C_2$	1.833 Å	1.874 Å	1.884 Å	1.881 Å	1.883 Å
$Cu\text{-}C_3$	1.833 Å	1.874 Å	1.884 Å	1.881 Å	1.883 Å
$C_1\text{-}O_1$	1.167 Å	1.163 Å	1.141 Å	1.138 Å	1.150 Å
$C_2\text{-}O_2$	1.167 Å	1.163 Å	1.141 Å	1.138 Å	1.150 Å
$C_3\text{-}O_3$	1.167 Å	1.163 Å	1.141 Å	1.138 Å	1.150 Å
$\angle C_1\text{-}Cu\text{-}C_2$	120.0º	120.0º	120.0º	120.0º	120.0º
$\angle C_1\text{-}Cu\text{-}C_3$	120.0º	119.9º	119.9º	120.1º	120.1º
$\angle C_2\text{-}Cu\text{-}C_3$	120.1º	120.1º	120.1º	119.9º	119.9º
$\angle Cu\text{-}C_1\text{-}O_1$	176.7º	180.0º	180.0º	180.0º	180.0º
$\angle Cu\text{-}C_2\text{-}O_2$	176.7º	180.0º	180.0º	180.0º	180.0º
$\angle Cu\text{-}C_3\text{-}O_3$	176.7º	180.0º	180.0º	180.0º	180.0º
$D(O_1\text{-}C_1\text{-}Cu\text{-}C_2)$	88.9º	180.0º	0.4º	0.2º	0.1º
$D(O_2\text{-}C_2\text{-}Cu\text{-}C_3)$	89.1º	180.0º	-0.4º	-0.3º	-0.4º
$D(O_3\text{-}C_3\text{-}Cu\text{-}C_1)$	88.5º	-0.3º	179.1º	179.7º	179.7º
a_{63Cu}	-30	6	6	8	8
a_{13C1} ($C_1\text{-}C_3$)	-3	-11	-14	-11	0
a_{17O1} ($O_1\text{-}O_3$)	-6	-5	-4	-6	-11
Energy	-1980.398291	-1980.4662471	-1980.5976575	-1980.6545059	-1980.5007996
M06					
$Cu\text{-}C_1$	1.823 Å	1.871 Å	1.883 Å	1.8811 Å	1.8795 Å
$Cu\text{-}C_2$	1.824 Å	1.871 Å	1.883 Å	1.8801 Å	1.8807 Å
$Cu\text{-}C_3$	1.824 Å	1.871 Å	1.884 Å	1.8806 Å	1.8805 Å

C_1-O_1	1.163 Å	1.159 Å	1.138 Å	1.1342 Å	1.1480 Å
C_2-O_2	1.163 Å	1.159 Å	1.138 Å	1.1342 Å	1.1480 Å
C_3-O_3	1.163 Å	1.159 Å	1.138 Å	1.1342 Å	1.1480 Å
	6-311G	6-311+G	6-311+G(d)	EPR-III	6-31++G(d,p)
∠C_1-Cu-C_2	120.0º	120.1º	120.1º	120.00º	120.13º
∠C_1-Cu-C_3	120.0º	119.8º	120.1º	119.96º	120.36º
∠C_2-Cu-C_3	119.9º	120.1º	119.8º	120.04º	119.51º
∠Cu-C_1-O_1	175.7º	180.0º	180.0º	179.99º	179.93º
∠Cu-C_2-O_2	175.8º	180.0º	180.0º	179.99º	179.85º
∠Cu-C_3-O_3	175.7º	180.0º	180.0º	179.98º	179.76º
D(O_1-C_1-Cu-C_2)	87.8º	-180.0º	0.0º	0.00º	0.12º
D(O_2-C_2-Cu-C_3)	87.8º	-180.0º	0.0º	0.00º	0.03º
D(O_3-C_3-Cu-C_1)	88.2º	0.0º	-180.0º	-180.00º	179.96º
a_{63Cu}	-15	-17	-17	-7	-20
a_{13C} (C_1-C_3)	12	6	2	-10	11
a_{17O} (O_1-O_3)	-5	-4	-4	-9	-9
Energy	-1980. 1044311	-1980. 1762673	-1980. 3121185	-1980. 3772845	-1980. 2241895
BHandHLYP					
Cu-C_1	1.854 Å	1.895 Å	1.909 Å	1.906 Å	1.909 Å
Cu-C_2	1.854 Å	1.895 Å	1.909 Å	1.906 Å	1.909 Å
Cu-C_3	1.854 Å	1.895 Å	1.909 Å	1.906 Å	1.909 Å
C_1-O_1	1.150 Å	1.146 Å	1.124 Å	1.121 Å	1.124 Å
C_2-O_2	1.150 Å	1.146 Å	1.124 Å	1.121 Å	1.124 Å
C_3-O_3	1.150 Å	1.146 Å	1.124 Å	1.121 Å	1.124 Å
∠C_1-Cu-C_2	119.6º	120.0º	120.0º	120.1º	120.0º
∠C_1-Cu-C_3	119.6º	120.0º	120.0º	120.0º	120.0º
∠C_2-Cu-C_3	119.6º	120.0º	119.9º	119.9º	120.1º
∠Cu-C_1-O_1	167.6º	180.0º	180.0º	180.0º	180.0º
∠Cu-C_2-O_2	167.6º	180.0º	180.0º	180.0º	180.0º
∠Cu-C_3-O_3	167.6º	180.0º	180.0º	180.0º	180.0º
D(O_1-C_1-Cu-C_2)	83.5º	-180.0º	0.0º	-180.0º	-180.0º
D(O_2-C_2-Cu-C_3)	-83.7º	0.0º	0.0º	0.0º	-180.0º
D(O_3-C_3-Cu-C_1)	83.7º	0.0º	-180.0º	-180.0º	0.0º
a_{63Cu}	77	43	48	52	48
a_{13C1} (C_1-C_3)	-2	-18	-22	-20	-22
a_{17O1} (O_1-O_3)	-14	-10	-9	-11	-9
ENERGY	-1980. 0483319	-1980. 1198896	-1980. 2758833	-1980. 3317738	-1980. 2758828

$Cu[C_2H_4]_2$

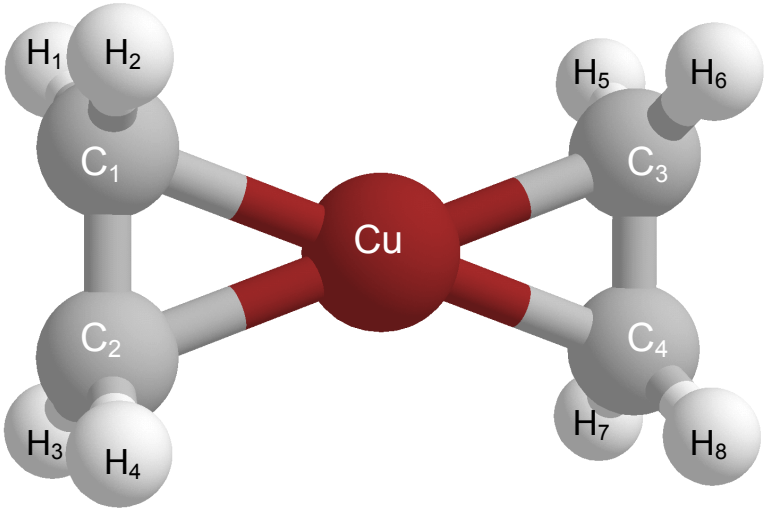

B3LYP	6-311G	6-311+G	6-311+G(d)	EPR-III	6-31++G(d,p)
$Cu\text{-}C_1$	2.014Å	2.062 Å	2.053 Å	2.053 Å	2.023 Å
$Cu\text{-}C_2$	2.014 Å	2.062 Å	2.053 Å	2.053 Å	2.023 Å
$Cu\text{-}C_3$	2.014 Å	2.062 Å	2.053 Å	2.053 Å	2.023 Å
$Cu\text{-}C_4$	2.014 Å	2.062 Å	2.053 Å	2.053 Å	2.023 Å
$C_1\text{-}C_2$	1.419 Å	1.412 Å	1.405 Å	1.402 Å	1.410 Å
$C_3\text{-}C_4$	1.419 Å	1.412 Å	1.405 Å	1.402 Å	1.410 Å
$C_1\text{-}H_1$	1.084 Å	1.084 Å	1.086 Å	1.083 Å	1.088 Å
$C_1\text{-}H_2$	1.084 Å	1.084 Å	1.086 Å	1.083 Å	1.088 Å
$C_2\text{-}H_3$	1.084 Å	1.084 Å	1.086 Å	1.083 Å	1.088 Å
$C_2\text{-}H_4$	1.084 Å	1.084 Å	1.086 Å	1.083 Å	1.088 Å
$C_3\text{-}H_5$	1.084 Å	1.084 Å	1.086 Å	1.083 Å	1.088 Å
$C_3\text{-}H_6$	1.084 Å	1.084 Å	1.086 Å	1.083 Å	1.088 Å
$C_4\text{-}H_7$	1.084 Å	1.084 Å	1.086 Å	1.083 Å	1.088 Å
$C_4\text{-}H_8$	1.084 Å	1.084 Å	1.086 Å	1.083 Å	1.088 Å
$\angle C_1\text{-}Cu\text{-}C_2$	41.3º	40.0º	40.0º	39.9º	40.2º
$\angle C_1\text{-}Cu\text{-}C_3$	138.7º	140.0º	140.0º	140.1º	139.8º
$\angle C_1\text{-}Cu\text{-}C_4$	180.0º	180.0º	180.0º	180.0º	180.0º
$\angle C_2\text{-}Cu\text{-}C_3$	180.0º	180.0º	180.0º	180.0º	180.0º
$\angle C_2\text{-}Cu\text{-}C_4$	138.7º	140.0º	140.0º	140.1º	139.8º
$\angle Cu\text{-}C_1\text{-}C_2$	69.4º	70.0º	70.0º	70.0º	69.9º
$\angle Cu\text{-}C_2\text{-}C_1$	69.4º	70.0º	670.0º	70.0º	69.9º
$\angle C_3\text{-}Cu\text{-}C_4$	41.3º	40.0º	40.0º	39.9º	40.2º
$\angle Cu\text{-}C_3\text{-}C_4$	69.4º	70.0º	70.0º	70.0º	69.9º
$\angle Cu\text{-}C_4\text{-}C_3$	69.4º	70.0º	70.0º	70.0º	69.9º
$\angle Cu\text{-}C_1\text{-}H_1$	110.9º	108.8º	108.7º	108.5º	108.6º
$\angle Cu\text{-}C_1\text{-}H_2$	110.9º	108.8º	108.7º	108.5º	108.6º
$\angle Cu\text{-}C_2\text{-}H_3$	110.9º	108.8º	108.7º	108.5º	108.6º
$\angle Cu\text{-}C_2\text{-}H_4$	110.9º	108.8º	108.7º	108.5º	108.6º

	6-311G	6-311+G	6-311+G(d)	EPR-III	6-31++G(d,p)
∠Cu-C_3-H_5	110.9º	108.8º	108.7º	108.5º	108.6º
∠Cu-C_3-H_6	110.9º	108.8º	108.7º	108.5º	108.6º
∠Cu-C_4-H_7	110.9º	108.8º	108.7º	108.5º	108.6º
∠Cu-C_4-H_8	110.9º	108.8º	108.7º	108.5º	108.6º
∠H_1-C_1-H_2	115.1º	115.3º	115.4º	115.6º	115.6º
∠H_5-C_3-H_6	115.1º	115.3º	115.4º	115.6º	115.6º
D(C_1-Cu-C_4-C_3)	39.4º	90.0º	180.0º	147.7º	147.7º
D(C_1-Cu-C_3-C_4)	180.0º	180.0º	180.0º	-180.0º	-180.0º
D(C_2-Cu-C_3-C_4)	-134.2º	90.0º	0.0º	-42.0º	-42.0º
D(C_2-Cu-C_4-C_3)	180.0º	180.0º	180.0º	180.0º	180.0º
D(Cu-C_2-C_1-H_1)	-102.9º	-100.6º	-100.4º	-100.2º	-100.2º
D(Cu-C_2-C_1-H_2)	102.9º	100.6º	100.4º	100.2º	100.2º
D(Cu-C_1-C_2-H_3)	102.9º	100.6º	100.4º	100.2º	100.2º
D(Cu-C_1-C_2-H_4)	-102.9º	-100.6º	-100.4º	-100.2º	-100.2º
D(Cu-C_4-C_3-H_5)	102.9º	100.6º	100.4º	100.2º	100.2º
D(Cu-C_4-C_3-H_6)	-102.9º	-100.6º	-100.4º	-100.2º	-100.2º
D(Cu-C_3-C_4-H_7)	-102.3º	-100.6º	-100.4º	-100.2º	-100.2º
D(Cu-C_3-C_4-H_8)	102.3º	100.6º	100.4º	100.2º	100.2º
D(H_1-C_1-C_2-H_3)	0.0º	0.0º	0.0º	0.0º	0.0º
D(H_2-C_1-C_2-H_3)	-154.2º	-158.9º	-159.3º	-159.6º	-159.6º
D(H_5-C_3-C_4-H_7)	0.0º	0.0º	0.0º	0.0º	0.0º
D(H_6-C_3-C_4-H_7)	154.2º	158.9º	159.3º	159.6º	159.6º
a_{63Cu}	-118	-99	-91	-90	-92
a_{13C} (C_1-C_4)	17	12	11	12	26
a_H (H_1-H_8)	0	-2	-3	-2	-3
Energy	-1797.6563660	-1797.6971307	-1797.7310890	-1797.7703570	-1797.7122873
M06					
Cu-C_1	1.986 Å	2.033 Å	2.023 Å	2.025 Å	2.023 Å
Cu-C_2	1.986 Å	2.033 Å	2.023 Å	2.025 Å	2.023 Å
Cu-C_3	1.986 Å	2.033 Å	2.023 Å	2.025 Å	2.023 Å
Cu-C_4	1.986 Å	2.033 Å	2.023 Å	2.025 Å	2.023 Å
C_1-C_2	1.415 Å	1.408 Å	1.401 Å	1.399 Å	1.406 Å
C_3-C_4	1.415 Å	1.408 Å	1.401 Å	1.399 Å	1.406 Å
C_1-H_1	1.085 Å	1.086 Å	1.089 Å	1.083 Å	1.089 Å
C_1-H_2	1.085 Å	1.086 Å	1.089 Å	1.083 Å	1.089 Å
C_2-H_3	1.085 Å	1.086 Å	1.089 Å	1.083 Å	1.089 Å
C_2-H_4	1.085 Å	1.086 Å	1.089 Å	1.083 Å	1.089 Å
C_3-H_5	1.085 Å	1.086 Å	1.089 Å	1.083 Å	1.089 Å
C_3-H_6	1.085 Å	1.086 Å	1.089 Å	1.083 Å	1.089 Å
C_4-H_7	1.085 Å	1.086 Å	1.089 Å	1.083 Å	1.089 Å
C_4-H_8	1.085 Å	1.086 Å	1.089 Å	1.083 Å	1.089 Å

	6-311G	6-311+G	6-311+G(d)	EPR-III	6-31++G(d,p)
$\angle C_1$-Cu-C_2	41.8º	40.5º	40.5º	40.4º	40.7º
$\angle C_1$-Cu-C_3	138.3º	139.5º	139.5º	139.6º	139.3º
$\angle C_1$-Cu-C_4	180.0º	180.0º	180.0º	180.0º	180.0º
$\angle C_2$-Cu-C_3	180.0º	180.0º	180.0º	180.0º	180.0º
$\angle C_2$-Cu-C_4	138.3º	139.5º	139.5º	139.6º	139.3º
$\angle$Cu-C_1-C_2	69.1º	69.7º	69.7º	69.8º	69.7º
$\angle$Cu-C_2-C_1	69.1º	69.7º	69.7º	69.8º	69.7º
$\angle C_3$-Cu-C_4	41.8º	40.5º	40.5º	40.4º	40.7º
$\angle$Cu-C_3-C_4	69.1º	69.7º	69.7º	69.8º	69.7º
$\angle$Cu-C_4-C_3	69.1º	69.7º	69.7º	69.8º	69.7º
$\angle$Cu-C_1-H_1	110.9º	108.7º	108.6º	108.5º	108.5º
$\angle$Cu-C_1-H_2	110.9º	108.7º	108.6º	108.5º	108.5º
$\angle$Cu-C_2-H_3	110.9º	108.7º	108.6º	108.5º	108.5º
$\angle$Cu-C_2-H_4	110.9º	108.7º	108.6º	108.5º	108.5º
$\angle$Cu-C_3-H_5	110.9º	108.7º	108.6º	108.5º	108.5º
$\angle$Cu-C_3-H_6	110.9º	108.7º	108.6º	108.5º	108.5º
$\angle$Cu-C_4-H_7	110.9º	108.7º	108.6º	108.5º	108.5º
$\angle$Cu-C_4-H_8	110.9º	108.7º	108.6º	108.5º	108.5º
$\angle H_1$-C_1-H_2	115.2º	115.4º	115.4º	115.6º	115.7º
$\angle H_5$-C_3-H_6	115.2º	115.4º	115.4º	115.6º	115.7º
D(C_1-Cu-C_4-C_3)	49.8º	63.1º	55.2º	90.7º	90.0º
D(C_1-Cu-C_3-C_4)	-180.0º	-179.9º	-180º	-180.0º	-180.0º
D(C_2-Cu-C_3-C_4)	-132.7º	-117.6º	-117.5º	-89.5º	-90.0º
D(C_2-Cu-C_4-C_3)	180.0º	179.9º	180.0º	180.0º	180.0º
D(Cu-C_2-C_1-H_1)	-102.8º	-100.3º	-100.1º	-100.0º	-100.0º
D(Cu-C_2-C_1-H_2)	102.8º	100.3º	100.1º	100.0º	100.0º
D(Cu-C_1-C_2-H_3)	102.8º	100.3º	100.1º	100.0º	100.0º
D(Cu-C_1-C_2-H_4)	-102.8º	-100.3º	-100.1º	-100.0º	-100.0º
D(Cu-C_4-C_3-H_5)	102.8º	100.3º	100.1º	100.0º	100.0º
D(Cu-C_4-C_3-H_6)	-102.8º	-100.3º	-100.1º	-100.0º	-100.0º
D(Cu-C_3-C_4-H_7)	-102.8º	-100.3º	-100.1º	-100.0º	-100.0º
D(Cu-C_3-C_4-H_8)	102.8º	100.3º	100.1º	100.0º	100.0º
D(H_1-C_1-C_2-H_3)	0.0º	0.0º	0.0º	0.0º	0.0º
D(H_2-C_1-C_2-H_3)	-154.5º	-154.4º	-159.7º	-160.0º	-160.1º
D(H_5-C_3-C_4-H_7)	0.0º	0.0º	0.0º	0.0º	0.0º
D(H_6-C_3-C_4-H_7)	154.5º	154.4º	159.7º	160.0º	160.1º
a_{63Cu} (MHz)	-122	-136	-129	-127	-130
a_{13C1} (MHz)	23	19	17	7	30
a_H (H_1-H_8)	-4	-7	-6	-9	-6
Energy	-1797.4191371	-1797.4617641	-1797.4889281	-1797.5337744	-1797.4706212

BHandHLYP	6-311G	6-311+G	6-311+G(d)	EPR-III	6-31++G(d,p)
$Cu\text{-}C_1$	2.013 Å	2.064 Å	2.056 Å	2.058 Å	2.055 Å
$Cu\text{-}C_2$	2.013 Å	2.064 Å	2.056 Å	2.058 Å	2.055 Å
$Cu\text{-}C_3$	2.013 Å	2.064 Å	2.056 Å	2.058 Å	2.055 Å
$Cu\text{-}C_4$	2.013 Å	2.064 Å	2.056 Å	2.058 Å	2.055 Å
$C_1\text{-}C_2$	1.405 Å	1.396 Å	1.391 Å	1.387 Å	1.394 Å
$C_3\text{-}C_4$	1.405 Å	1.396 Å	1.391 Å	1.387 Å	1.394 Å
$C_1\text{-}H_1$	1.075 Å	1.076 Å	1.078 Å	1.075 Å	1.079 Å
$C_1\text{-}H_2$	1.075 Å	1.076 Å	1.078 Å	1.075 Å	1.079 Å
$C_2\text{-}H_3$	1.075 Å	1.076 Å	1.078 Å	1.075 Å	1.079 Å
$C_2\text{-}H_4$	1.075 Å	1.076 Å	1.078 Å	1.075 Å	1.079 Å
$C_3\text{-}H_5$	1.075 Å	1.076 Å	1.078 Å	1.075 Å	1.079 Å
$C_3\text{-}H_6$	1.075 Å	1.076 Å	1.078 Å	1.075 Å	1.079 Å
$C_4\text{-}H_7$	1.075 Å	1.076 Å	1.078 Å	1.075 Å	1.079 Å
$C_4\text{-}H_8$	1.075 Å	1.076 Å	1.078 Å	1.075 Å	1.079 Å
$\angle C_1\text{-}Cu\text{-}C_2$	40.9º	39.6º	39.5º	39.4º	39.7º
$\angle C_1\text{-}Cu\text{-}C_3$	139.2º	140.5º	140.5º	140.6º	140.3º
$\angle C_1\text{-}Cu\text{-}C_4$	180.0º	180.0º	180.0º	180.0º	180.0º
$\angle C_2\text{-}Cu\text{-}C_3$	180.0º	180.0º	180.0º	180.0º	180.0º
$\angle C_2\text{-}Cu\text{-}C_4$	139.2º	140.5º	140.5º	140.6º	140.3º
$\angle Cu\text{-}C_1\text{-}C_2$	69.6º	70.2º	70.2º	70.3º	70.2º
$\angle Cu\text{-}C_2\text{-}C_1$	69.6º	70.2º	70.2º	70.3º	70.2º
$\angle C_3\text{-}Cu\text{-}C_4$	40.9º	39.6º	39.5º	39.4º	39.7º
$\angle Cu\text{-}C_3\text{-}C_4$	69.6º	70.2º	70.2º	70.3º	70.2º
$\angle Cu\text{-}C_4\text{-}C_3$	69.6º	70.2º	70.2º	70.3º	70.2º
$\angle Cu\text{-}C_1\text{-}H_1$	110.5º	108.4º	108.2º	108.0º	108.1º
$\angle Cu\text{-}C_1\text{-}H_2$	110.5º	108.4º	108.2º	108.0º	108.1º
$\angle Cu\text{-}C_2\text{-}H_3$	110.5º	108.4º	108.2º	108.0º	108.1º
$\angle Cu\text{-}C_2\text{-}H_4$	110.5º	108.4º	108.2º	108.0º	108.1º
$\angle Cu\text{-}C_3\text{-}H_5$	110.5º	108.4º	108.2º	108.0º	108.1º
$\angle Cu\text{-}C_3\text{-}H_6$	110.5º	108.4º	108.2º	108.0º	108.1º
$\angle Cu\text{-}C_4\text{-}H_7$	110.5º	108.4º	108.2º	108.0º	108.1º
$\angle Cu\text{-}C_4\text{-}H_8$	110.5º	108.4º	108.2º	108.0º	108.1º
$\angle H_1\text{-}C_1\text{-}H_2$	115.1º	115.4º	115.5º	115.7º	115.8º
$\angle H_5\text{-}C_3\text{-}H_6$	115.1º	115.4º	115.5º	115.7º	115.8º
$D(C_1\text{-}Cu\text{-}C_4\text{-}C_3)$	-42.6º	-180.0º	-180.0º	-48.6º	-144.7º
$D(C_1\text{-}Cu\text{-}C_3\text{-}C_4)$	180.0º	180.0º	180.0º	180.0º	180.0º
$D(C_2\text{-}Cu\text{-}C_3\text{-}C_4)$	137.4º	0.0º	0.0º	-8.6º	44.2º
$D(C_2\text{-}Cu\text{-}C_4\text{-}C_3)$	-180.0º	-180.0º	-180.0º	-180.0º	-180.0º
$D(Cu\text{-}C_2\text{-}C_1\text{-}H_1)$	-102.4º	-100.1º	-99.9º	-99.8º	-99.7º
$D(Cu\text{-}C_2\text{-}C_1\text{-}H_2)$	102.4º	100.1º	99.9º	99.8º	99.7º
$D(Cu\text{-}C_1\text{-}C_2\text{-}H_3)$	102.4º	100.1º	99.9º	99.8º	99.7º
$D(Cu\text{-}C_1\text{-}C_2\text{-}H_4)$	-102.4º	-100.1º	-99.9º	-99.8º	-99.7º
$D(Cu\text{-}C_4\text{-}C_3\text{-}H_5)$	102.4º	100.1º	99.9º	99.8º	99.7º

	6-311G	6-311+G	6-311+G(d)	EPR-III	6-31++G(d,p)
D(Cu-C_4-C_3-H_6)	-102.4º	-100.1º	-99.9º	-99.8º	-99.7º
D(Cu-C_3-C_4-H_7)	-102.4º	-100.1º	-99.9º	-99.8º	-99.7º
D(Cu-C_3-C_4-H_8)	102.4º	100.1º	99.9º	99.8º	99.7º
D(H_1-C_1-C_2-H_3)	0.0º	0.0º	0.0º	0.0º	0.0º
D(H_2-C_1-C_2-H_3)	-155.2º	-159.7º	-160.2º	-160.4º	-160.6º
D(H_5-C_3-C_4-H_7)	0.0º	0.0º	0.0º	0.0º	0.0º
D(H_6-C_3-C_4-H_7)	155.2º	159.7º	160.2º	160.4º	160.6º
a_{63Cu}	-128	-95	-76	-72	-79
a_{13C} (C_1-C_4)	22	15	14	14	27
a_H (H1-H_8)	-2	-5	-5	-4	-4
Energy	-1797. 4023714	-1797. 4403053	-1797. 4821245	-1797. 5201083	-1797. 4674359

$Cu[C_2H_2]_2$

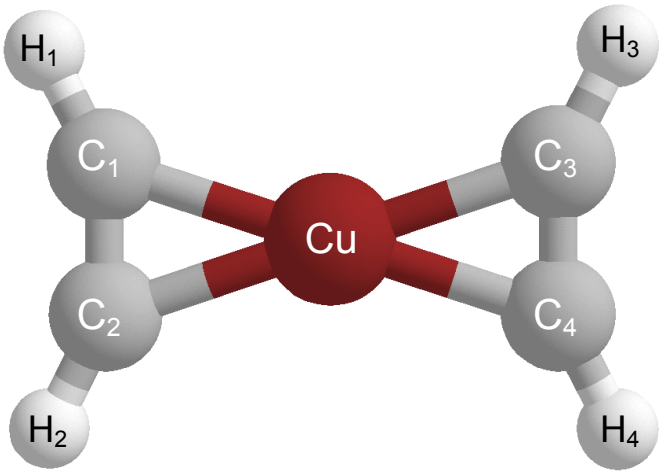

B3LYP	6-311G	6-311+G	6-311+G(d)	EPR-III	6-31++G(d,p)
$Cu\text{-}C_1$	1.974 Å	2.012 Å	1.997 Å	1.995 Å	1.992 Å
$Cu\text{-}C_2$	1.974 Å	2.012 Å	1.997 Å	1.995 Å	1.992 Å
$Cu\text{-}C_3$	1.974 Å	2.012 Å	1.997 Å	1.995 Å	1.992 Å
$Cu\text{-}C_4$	1.974 Å	2.012 Å	1.997 Å	1.995 Å	1.992 Å
$C_1\text{-}C_2$	1.263 Å	1.260 Å	1.254 Å	1.250 Å	1.261 Å
$C_3\text{-}C_4$	1.263 Å	1.260 Å	1.254 Å	1.250 Å	1.261 Å
$C_1\text{-}H_1$	1.074 Å	1.074 Å	1.077 Å	1.074 Å	1.078 Å
$C_1\text{-}H_2$	1.074 Å	1.074 Å	1.077 Å	1.074 Å	1.078 Å
$C_2\text{-}H_3$	1.074 Å	1.074 Å	1.077 Å	1.074 Å	1.078 Å
$C_2\text{-}H_4$	1.074 Å	1.047 Å	1.077 Å	1.074 Å	1.078 Å
$\angle C_1\text{-}Cu\text{-}C_2$	37.3º	36.5º	36.6º	36.5º	36.9º
$\angle C_1\text{-}Cu\text{-}C_3$	142.7º	143.5º	143.4º	143.5º	143.1º
$\angle C_1\text{-}Cu\text{-}C_4$	180.0º	180.0º	180.0º	180.0º	180.0º
$\angle C_2\text{-}Cu\text{-}C_3$	180.0º	180.0º	180.0º	180.0º	180.0º
$\angle C_2\text{-}Cu\text{-}C_4$	142.7º	143.5º	143.4º	143.5º	143.1º
$\angle Cu\text{-}C_1\text{-}C_2$	71.3º	71.8º	71.7º	71.7º	71.5º
$\angle Cu\text{-}C_2\text{-}C_1$	71.3º	71.8º	71.7º	71.7º	71.5º
$\angle C_3\text{-}Cu\text{-}C_4$	37.3º	36.5º	36.6º	36.5º	36.9º
$\angle Cu\text{-}C_3\text{-}C_4$	71.3º	71.8º	71.7º	71.7º	71.5º
$\angle Cu\text{-}C_4\text{-}C_3$	71.3º	71.8º	71.7º	71.7º	71.5º
$\angle Cu\text{-}C_1\text{-}H_1$	137.8º	135.1º	135.5º	135.1º	135.2º
$\angle Cu\text{-}C_2\text{-}H_2$	137.8º	135.1º	135.5º	135.1º	135.2º
$\angle Cu\text{-}C_3\text{-}H_3$	137.8º	135.1º	135.5º	135.1º	135.2º
$\angle Cu\text{-}C_4\text{-}H_4$	137.8º	135.1º	135.5º	135.1º	135.2º
$D(C_1\text{-}Cu\text{-}C_3\text{-}C_4)$	-180.0º	-180.0º	-180.0º	-180.0º	-180.0º
$D(C_2\text{-}Cu\text{-}C_4\text{-}C_3)$	-180.0º	-180.0º	-180.0º	-180.0º	-180.0º
$D(Cu\text{-}C_2\text{-}C_1\text{-}H_1)$	-180.0º	-180.0º	-180.0º	-180.0º	-180.0º
$D(Cu\text{-}C_1\text{-}C_2\text{-}H_2)$	-180.0º	-180.0º	-180.0º	-180.0º	-180.0º
$D(Cu\text{-}C_4\text{-}C_3\text{-}H_3)$	-180.0º	-180.0º	-180.0º	-180.0º	-180.0º

	6-311G	6-311+G	6-311+G(d)	EPR-III	6-31++G(d,p)
D(Cu-C_3-C_4-H_4)	-180.0º	-180.0º	-180.0º	-180.0º	-180.0º
D(H_1-C_1-C_2-H_2)	0.0º	0.0º	0.0º	0.0º	0.0º
D(H_3-C_3-C_4-H_4)	0.0º	0.0º	0.0º	0.0º	0.0º
a_{63Cu}	-111	-76	-74	-76	-75
a_{13C} (C_1-C_4)	73	62	60	60	67
a_H (H_1-H_4)	83	71	72	78	74
Energy	-1795. 1344268	-1795. 1827692	-1795. 2178376	-1795. 2546644	-1795. 1915599
M06					
Cu-C_1	1.950 Å	1.987 Å	1.972 Å	1.972 Å	1.969 Å
Cu-C_2	1.950 Å	1.987 Å	1.972 Å	1.972 Å	1.969 Å
Cu-C_3	1.950 Å	1.987 Å	1.972 Å	1.972 Å	1.969 Å
Cu-C_4	1.950 Å	1.987 Å	1.972 Å	1.972 Å	1.969 Å
C_1-C_2	1.262 Å	1.259 Å	1.252 Å	1.248 Å	1.260 Å
C_3-C_4	1.262 Å	1.258 Å	1.252 Å	1.248 Å	1.260 Å
C_1-H_1	1.075 Å	1.075 Å	1.080 Å	1.074 Å	1.079 Å
C_1-H_2	1.075 Å	1.075 Å	1.080 Å	1.074 Å	1.079 Å
C_2-H_3	1.075 Å	1.075 Å	1.080 Å	1.074 Å	1.079 Å
C_2-H_4	1.075 Å	1.045 Å	1.080 Å	1.074 Å	1.079 Å
∠C_1-Cu-C_2	37.7º	36.9º	37.0º	36.9º	37.3º
∠C_1-Cu-C_3	142.3º	143.1º	143.0º	143.1º	142.7º
∠C_1-Cu-C_4	180.0º	180.0º	180.0º	180.0º	180.0º
∠C_2-Cu-C_3	180.0º	180.0º	180.0º	180.0º	180.0º
∠C_2-Cu-C_4	142.3º	143.1º	143.0º	143.1º	142.7º
∠Cu-C_1-C_2	71.1º	71.5º	71.4º	71.5º	71.3º
∠Cu-C_2-C_1	71.1º	71.5º	71.4º	71.5º	71.3º
∠C_3-Cu-C_4	37.7º	36.9º	37.0º	36.9º	37.3º
∠Cu-C_3-C_4	71.1º	71.5º	71.4º	71.5º	71.3º
∠Cu-C_4-C_3	71.1º	71.5º	71.4º	71.5º	71.3º
∠Cu-C_1-H_1	137.0º	134.2º	134.3º	133.6º	134.2º
∠Cu-C_2-H_2	137.0º	134.2º	134.3º	133.6º	134.2º
∠Cu-C_3-H_3	137.0º	134.2º	134.3º	133.6º	134.2º
∠Cu-C_4-H_4	137.0º	134.2º	134.3º	133.6º	134.2º
D(C_1-Cu-C_3-C_4)	-180.0º	-180.0º	-180.0º	-180.0º	-180.0º
D(C_2-Cu-C_4-C_3)	-180.0º	-180.0º	-180.0º	-180.0º	-180.0º
D(Cu-C_2-C_1-H_1)	-180.0º	-180.0º	-180.0º	-180.0º	-180.0º
D(Cu-C_1-C_2-H_2)	-180.0º	-180.0º	-180.0º	-180.0º	-180.0º
D(Cu-C_4-C_3-H_3)	-180.0º	-180.0º	-180.0º	-180.0º	-180.0º
D(Cu-C_3-C_4-H_4)	-180.0º	-180.0º	-180.0º	-180.0º	-180.0º
D(H_1-C_1-C_2-H_2)	0.0º	0.0º	0.0º	0.0º	0.0º
D(H_3-C_3-C_4-H_4)	0.0º	0.0º	0.0º	0.0º	0.0º

	6-311G	6-311+G	6-311+G(d)	EPR-III	6-31++G(d,p)
a_{63Cu}	-106	-104	-105	-102	-106
a_{13C} (C_1-C_4)	74	65	62	60	68
a_H (H_1-H_4)	75	63	68	68	68
Energy	-1794.90349996	-1794.955917	-1794.9896756	-1795.0323996	-1794.9642975
BHandHLYP					
Cu-C_1	1.973 Å	2.012 Å	1.997 Å	1.995 Å	1.993 Å
Cu-C_2	1.973 Å	2.012 Å	1.997 Å	1.995 Å	1.993 Å
Cu-C_3	1.973 Å	2.012 Å	1.997 Å	1.995 Å	1.993 Å
Cu-C_4	1.973 Å	2.012 Å	1.997 Å	1.995 Å	1.993 Å
C_1-C_2	1.252 Å	1.247 Å	1.241 Å	1.237 Å	1.248 Å
C_3-C_4	1.252 Å	1.247 Å	1.241 Å	1.237 Å	1.248 Å
C_1-H_1	1.065 Å	1.064 Å	1.069 Å	1.066 Å	1.070 Å
C_1-H_2	1.065 Å	1.064 Å	1.069 Å	1.066 Å	1.070 Å
C_2-H_3	1.065 Å	1.064 Å	1.069 Å	1.066 Å	1.070 Å
C_2-H_4	1.065 Å	1.064 Å	1.069 Å	1.066 Å	1.070 Å
∠C_1-Cu-C_2	37.0º	36.1º	36.2º	36.1º	36.5º
∠C_1-Cu-C_3	143.0º	143.9º	143.8º	143.9º	143.5º
∠C_1-Cu-C_4	180.0º	180.0º	180.0º	180.0º	180.0º
∠C_2-Cu-C_3	180.0º	180.0º	180.0º	180.0º	180.0º
∠C_2-Cu-C_4	143.0º	143.9º	143.8º	143.9º	143.5º
∠Cu-C_1-C_2	71.5º	71.9º	71.9º	71.9º	71.8º
∠Cu-C_2-C_1	71.5º	71.9º	71.9º	71.9º	71.8º
∠C_3-Cu-C_4	37.0º	36.1º	36.2º	36.1º	36.5º
∠Cu-C_3-C_4	71.5º	71.9º	71.9º	71.9º	71.8º
∠Cu-C_4-C_3	71.5º	71.9º	71.9º	71.9º	71.8º
∠Cu-C_1-H_1	137.3º	133.9º	134.5º	134.0º	134.5º
∠Cu-C_2-H_2	137.3º	133.9º	134.5º	134.0º	134.5º
∠Cu-C_3-H_3	137.3º	133.9º	134.5º	134.0º	134.5º
∠Cu-C_4-H_4	137.3º	133.9º	134.5º	134.0º	134.5º
D(C_1-Cu-C_3-C_4)	-180.0º	-180.0º	-180.0º	-180.0º	-180.0º
D(C_2-Cu-C_4-C_3)	-180.0º	-180.0º	-180.0º	-180.0º	-180.0º
D(Cu-C_2-C_1-H_1)	-180.0º	-180.0º	-180.0º	-180.0º	-180.0º
D(Cu-C_1-C_2-H_2)	-180.0º	-180.0º	-180.0º	-180.0º	-180.0º
D(Cu-C_4-C_3-H_3)	-180.0º	-180.0º	-180.0º	-180.0º	-180.0º
D(Cu-C_3-C_4-H_4)	-180.0º	-180.0º	-180.0º	-180.0º	-180.0º
D(H_1-C_1-C_2-H_2)	0.0º	0.0º	0.0º	0.0º	0.0º
D(H_3-C_3-C_4-H_4)	0.0º	0.0º	0.0º	0.0º	0.0º
a_{63Cu}	-119	-58	-50	-50	-53
a_{13C} (C_1-C_4)	77	58	58	56	64
a_H (H_1-H_4)	90	73	75	80	78
Energy	-1794.8888638	-1794.932778	-1794.9754215	-1795.0111347	-1794.9528728

$HCuCH_3$

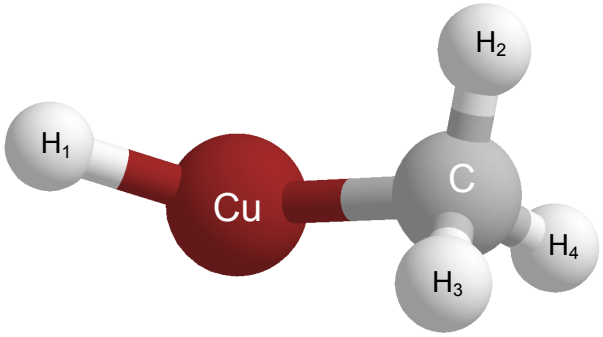

B3LYP	6-311G	6-311+G	6-311+G(d)	EPR-III	6-31++G(d,p)
Cu-C	1.926 Å	1.966 Å	1.963 Å	1.965 Å	1.963 Å
H_1-Cu	1.524 Å	1.535 Å	1.534 Å	1.525 Å	1.527 Å
C-H_2	1.089 Å	1.089 Å	1.090 Å	1.087 Å	1.092 Å
C-H_3	1.089 Å	1.089 Å	1.090 Å	1.087 Å	1.092 Å
C-H_4	1.097 Å	1.094 Å	1.095 Å	1.092 Å	1.097 Å
∠H_1-Cu-C	138.2º	127.4º	127.3º	127.8º	127.5º
∠Cu-C-H_2	110.8º	107.4º	107.9º	107.7º	107.7º
∠Cu-C-H_3	110.9º	107.4º	107.9º	107.7º	107.7º
∠Cu-C-H_4	104.9º	105.4º	105.5º	104.6º	104.9º
∠H_2-C-H_3	110.2º	112.0º	111.7º	112.1º	112.0º
∠H_2-C-H_4	109.9º	112.1º	111.7º	112.1º	112.0º
∠H_3-C-H_4	109.9º	112.1º	111.7º	112.1º	112.0º
D(H_1-Cu-C-H_2)	61.3º	60.1º	60.4º	60.6º	60.5º
D(H_1-Cu-C-H_3)	-61.4º	-60.5º	-60.9º	-60.6º	-60.5º
D(H_1-Cu-C-H_4)	180.0º	179.8º	179.9º	180.0º	180.0º
a_{63Cu}	-434	-521	-517	-518	-514
a_{13C}	80	91	92	91	107
a_{H1}	299	382	379	411	378
a_{H2}	-20	-22	-19	-19	-20
a_{H3}	-20	-22	-19	-19	-20
a_{H4}	33	23	25	27	24
Energy	-1680.898268	-1680.953159	-1680.9606147	-1680.9735694	-1680.9585393
BHandHLYP					
Cu-C	1.917 Å	1.950 Å	1.948 Å	1.949 Å	1.949 Å
H_1-Cu	1.542 Å	1.532 Å	1.532 Å	1.524 Å	1.525 Å
C-H_2	1.083 Å	1.082 Å	1.083 Å	1.081 Å	1.085 Å
C-H_3	1.083 Å	1.082 Å	1.083 Å	1.081 Å	1.085 Å
C-H_4	1.089 Å	1.087 Å	1.088 Å	1.086 Å	1.089 Å
∠H_1-Cu-C	140.7º	124.0º	123.7º	124.4º	124.0º
∠Cu-C-H_2	111.4º	107.9º	108.5º	108.3º	108.3º

	6-311G	6-311+G	6-311+G(d)	EPR-III	6-31++G(d,p)
∠Cu-C-H_3	111.4º	107.9º	108.5º	108.3º	108.3º
∠Cu-C-H_4	108.3º	107.7º	107.9º	107.1º	107.5º
∠H_2-C-H_3	108.8º	111.0º	110.6º	111.0º	110.9º
∠H_2-C-H_4	108.8º	111.1º	110.6º	111.0º	110.9º
∠H_3-C-H_4	108.4º	111.1º	110.6º	111.0º	110.9º
D(H_1-Cu-C-H_2)	70.0º	60.2º	60.3º	60.4º	60.3º
D(H_1-Cu-C-H_3)	-60.8º	-59.8º	-59.9º	-60.0º	-60.0º
D(H_1-Cu-C-H_4)	179.9º	179.8º	179.8º	179.8º	179.8º
a_{63Cu}	-425	-671	-664	-669	-658
a_{13C}	56	110	112	108	117
a_{H1}	178	333	329	350	326
a_{H2}	-18	-25	-23	-23	-23
a_{H3}	-18	-25	-23	-23	-23
a_{H4}	29	19	22	23	21
Energy	-1680.740274	-1680.7837748	-1680.7933059	-1680.8058748	-1680.7921704

$HCuNH_2$

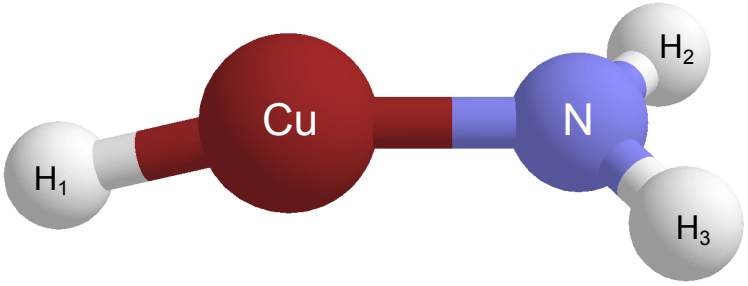

B3LYP	6-311G	6-311+G	6-311+G(d)	EPR-III	6-31++G(d,p)
Cu-N	1.785 Å	1.822 Å	1.826 Å	1.825 Å	1.824 Å
H_1-Cu	1.522 Å	1.518 Å	1.516 Å	1.509 Å	1.510 Å
N-H_2	1.016 Å	1.018 Å	1.017 Å	1.014 Å	1.019 Å
N-H_3	1.016 Å	1.018 Å	1.016 Å	1.014 Å	1.019 Å
∠H_1-Cu-N	180.0º	154.2º	152.6º	151.6º	152.4º
∠Cu-N-H_2	125.3º	124.1º	123.6º	123.4º	123.5º
∠Cu-N-H_3	125.3º	124.1º	123.6º	123.4º	123.5º
∠H_2-N-H_3	109.5º	110.0º	108.3º	108.0º	108.2º
D(H_1-Cu-N-H_2)	-88.2º	-81.7º	-76.7º	-75.9º	-76.4º
D(H_1-Cu-N-H_3)	91.8º	81.8º	76.6º	75.7º	76.4º
a_{63Cu}	-178	115	7	0	13
a_{14N}	18	19	18	20	31
a_{H1}	-15	89	104	125	106
a_{H2}	-38	-37	-37	-34	-36
a_{H3}	-38	-37	-37	-34	-36
Energy	-1696.9710947	-1697.0252968	-1697.0349429	-1697.0502765	-1697.0266065
M06					
Cu-N	1.772 Å	1.807 Å	1.814 Å	1.812 Å	1.811 Å
H_1-Cu	1.515 Å	1.516 Å	1.515 Å	1.512 Å	1.512 Å
N-H_2	1.016 Å	1.019 Å	1.018 Å	1.012 Å	1.018 Å
N-H_3	1.016 Å	1.019 Å	1.018 Å	1.012 Å	1.018 Å
∠H_1-Cu-N	180.0º	153.3º	151.7º	151.7º	151.5º
∠Cu-N-H_2	125.1º	123.7º	122.9º	123.0º	122.8º
∠Cu-N-H_3	125.2º	123.7º	122.9º	123.0º	122.8º
∠H_2-N-H_3	109.7º	110.3º	108.2º	108.0º	108.2º
D(H_1-Cu-N-H_2)	-89.2º	-80.5º	-74.8º	-74.8º	-74.7º
D(H_1-Cu-N-H_3)	90.9º	80.6º	74.7º	74.7º	74.6º
a_{63Cu}	-69	232	110	103	109
a_{14N}	23	24	24	26	33
a_{H1}	-19	109	126	137	124
a_{H2}	-48	-46	-45	-54	-39
a_{H3}	-48	-46	-45	-54	-39
Energy	-1696.815558	-1696.872690	-1696.8812288	-1696.897307	-1696.8751786

BHandHLYP	6-311G	6-311+G	6-311+G(d)	EPR-III	6-31++G(d,p)
Cu-N	1.762 Å	1.798 Å	1.799 Å	1.798 Å	1.798 Å
H_1-Cu	1.537 Å	1.528 Å	1.526 Å	1.520 Å	1.520 Å
N-H_2	1.004 Å	1.006 Å	1.005 Å	1.002 Å	1.007 Å
N-H_3	1.004 Å	1.006 Å	1.005 Å	1.001 Å	1.007 Å
∠H_1-Cu-N	179.9º	159.5º	157.4º	159.2º	158.0º
∠Cu-N-H_2	125.4º	125.0º	125.5º	125.7º	125.5º
∠Cu-N-H_3	125.4º	125.0º	125.5º	125.7º	125.5º
∠H_2-N-H_3	109.3º	110.0º	108.6º	108.5º	108.7º
D(H_1-Cu-N-H_2)	-89.9º	-88.9º	-85.8º	-88.7º	-86.8º
D(H_1-Cu-N-H_3)	90.1º	88.9º	85.7º	88.7º	86.8
a_{63Cu}	-250	234	105	252	162
a_{14N}	21	23	25	24	32
a_{H1}	-16	-8	7	-9	-1
a_{H2}	-30	-30	-34	-28	-31
a_{H3}	-30	-30	-34	-28	-31
Energy	-1696.8071082	-1696.8527625	-1696.8630698	-1696.8787159	-1696.8563288

Cu-$\overline{OCH_2CH_2}$

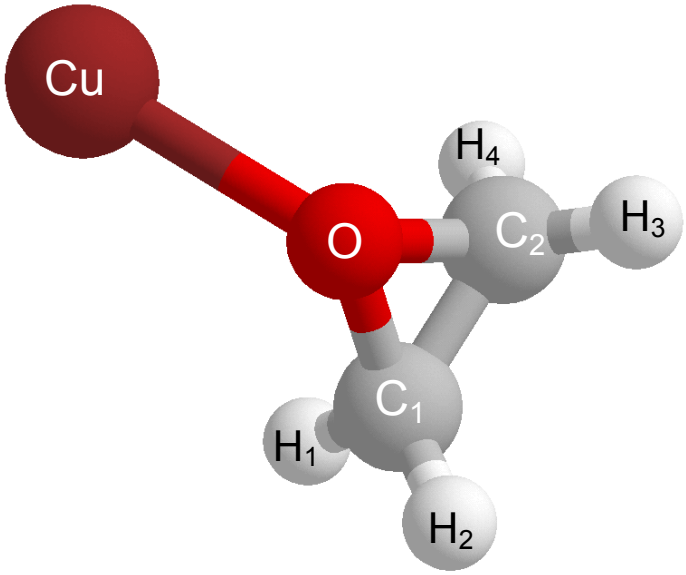

B3LYP	6-311G	6-311+G	6-311+G(d)	EPR-III	6-31++G(d,p)
Cu-O	2.038 Å	2.128 Å	2.256 Å	2.259 Å	2.259 Å
O-C_1	1.513 Å	1.513 Å	1.446 Å	1.444 Å	1.449 Å
O-C_2	1.513 Å	1.513 Å	1.446 Å	1.444 Å	1.449 Å
C_1-C_2	1.470 Å	1.473 Å	1.464 Å	1.461 Å	1.468 Å
C_1-H_1	1.080 Å	1.081 Å	1.086 Å	1.083 Å	1.088 Å
C_1-H_2	1.079 Å	1.080 Å	1.085 Å	1.083 Å	1.088 Å
C_2-H_3	1.079 Å	1.080 Å	1.085 Å	1.083 Å	1.088 Å
C_2-H_4	1.080 Å	1.081 Å	1.086 Å	1.083 Å	1.088 Å
∠Cu-O-C_1	117.5º	131.6º	124.9º	124.0º	123.7º
∠Cu-O-C_2	117.5º	131.6º	124.9º	124.0º	123.7º
∠C_1-O-C_2	58.2º	58.3º	60.8º	60.8º	60.8º
∠O-C_1-C_2	60.9º	60.9º	59.6º	59.6º	59.5º
∠C_1-C_2-O	60.9º	60.9º	59.6º	59.6º	59.5º
∠O-C_1-H_1	113.2º	113.5º	114.4º	114.6º	114.5º
∠O-C_1-H_2	113.3º	113.0º	113.9º	114.2º	114.0º
∠O-C_2-H_3	113.3º	113.0º	113.9º	114.2º	114.0º
∠O-C_2-H_4	113.1º	113.5º	114.4º	114.6º	114.5º
∠H_1-C_1-H_2	116.6º	116.4º	116.1º	116.1º	116.1º
D(Cu-O-C_1-C_2)	-106.8º	-119.7º	-114.2º	-113.3º	-113.0º
D(Cu-O-C_2-C_1)	106.8º	119.7º	114.2º	113.3º	113.0º
D(Cu-O-C_1-H_1)	4.9º	-7.7º	-2.9º	-2.0º	-1.8º
D(Cu-O-C_1-H_2)	140.5º	127.7º	134.0º	135.1º	135.2º
D(Cu-O-C_2-H_3)	-140.5º	-127.7º	-134.0º	-135.1º	-135.3º
D(Cu-O-C_2-H_4)	-4.9º	7.7º	2.9º	2.0º	1.8º
D(H_1-C_1-C_2-H_3)	156.7º	156.7º	155.7º	155.0º	155.4º
D(H_2-C_1-C_2-H_3)	0º	0º	0º	0º	0º

	6-311G	6-311+G	6-311+G(d)	EPR-III	6-31++G(d,p)
a_{63Cu}	2022	4310	4682	4690	4669
a_{17O}	-177	-156	-105	-108	-92
a_{13C} (C_1 & C_2)	1	3	0	0	0
a_H (H_1-H_4)	-1	-2	-1	-1	0
Energy	-1794.1735859	-1794.2599767	-1794.3075345	-1794.3384134	-1794.2761361
M06	6-311G	6-311+G	6-311+G(d)	EPR-III	6-31++G(d,p)
Cu-O	2.056 Å	2.205 Å	2.324 Å	2.343 Å	2.312 Å
O-C_1	1.481 Å	1.481 Å	1.423 Å	1.419 Å	1.428 Å
O-C_2	1.481 Å	1.481 Å	1.423 Å	1.419 Å	1.428 Å
C_1-C_2	1.466 Å	1.467 Å	1.454 Å	1.452 Å	1.458 Å
C_1-H_1	1.084 Å	1.084 Å	1.091 Å	1.087 Å	1.092 Å
C_1-H_2	1.081 Å	1.082 Å	1.089 Å	1.084 Å	1.089 Å
C_2-H_3	1.081 Å	1.082 Å	1.089 Å	1.084 Å	1.089 Å
C_2-H_4	1.084 Å	1.084 Å	1.091 Å	1.087 Å	1.092 Å
∠Cu-O-C_1	112.1º	115.8º	111.2º	109.9º	111.2º
∠Cu-O-C_2	112.1º	115.8º	111.2º	109.9º	111.2º
∠C_1-O-C_2	59.3º	59.3º	61.5º	61.5º	61.4º
∠O-C_1-C_2	60.3º	60.3º	59.3º	59.2º	59.3º
∠C_1-C_2-O	60.3º	60.3º	59.3º	59.2º	59.3º
∠O-C_1-H_1	113.5º	113.6º	114.4º	114.8º	114.4º
∠O-C_1-H_2	114.0º	113.8º	114.5º	114.8º	114.5º
∠O-C_2-H_3	114.0º	113.8º	114.5º	114.8º	114.5º
∠O-C_2-H_4	113.5º	113.6º	114.4º	114.8º	114.4º
∠H_1-C_1-H_2	116.6º	116.4º	116.0º	116.0º	116.1º
D(Cu-O-C_1-C_2)	-103.4º	-106.0º	-103.4º	-102.4º	-103.3º
D(Cu-O-C_2-C_1)	103.4º	106.0º	103.4º	102.4º	103.3º
D(Cu-O-C_1-H_1)	7.7º	5.4º	7.6º	8.1º	7.5º
D(Cu-O-C_1-H_2)	144.4º	141.6º	144.9º	146.2º	145.0º
D(Cu-O-C_2-H_3)	-144.4º	-141.6º	-144.9º	-146.2º	-145.0º
D(Cu-O-C_2-H_4)	-7.7º	-5.4º	-7.6º	-8.1º	-7.5º
D(H_1-C_1-C_2-H_3)	155.8º	156.1º	155.2º	154.2º	155.1º
D(H_2-C_1-C_2-H_3)	0º	0º	0º	0º	0º
a_{63Cu}	2248	4571	4958	5006	4920
a_{17O}	-136	-108	-77	-74	-68
a_{13C} (C_1 & C_2)	-2	0	1	1	0
a_H (H_1-H_4)	0	-2	-1	-3	-2
Energy	-1793.9660182	-1794.0543967	-1794.1033940	-1794.1386674	-1794.0751880
BHandHLYP					
Cu-O	2.0378 Å	2.1686 Å	2.3060 Å	2.3173 Å	2.3082 Å
O-C_1	1.4796 Å	1.4791 Å	1.4216 Å	1.4189 Å	1.4245 Å
O-C_2	1.4796 Å	1.4791 Å	1.4791 Å	1.4189 Å	1.4245 Å
C_1-C_2	1.4616 Å	1.4633 Å	1.4536 Å	1.4502 Å	1.4562 Å

	6-311G	6-311+G	6-311+G(d)	EPR-III	6-31++G(d,p)
C_1-H_1	1.071 Å	1.072 Å	1.078 Å	1.076 Å	1.079 Å
C_1-H_2	1.070 Å	1.071 Å	1.077 Å	1.075 Å	1.079 Å
C_2-H_3	1.070 Å	1.071 Å	1.077 Å	1.075 Å	1.079 Å
C_2-H_4	1.071 Å	1.072 Å	1.078 Å	1.076 Å	1.079 Å
∠Cu-O-C_1	123.3º	133.4º	127.2º	126.0º	125.8º
∠Cu-O-C_2	123.3º	133.4º	127.2º	126.0º	125.8º
∠C_1-O-C_2	59.2º	59.3º	61.5º	61.5º	61.5º
∠O-C_1-C_2	60.4º	60.4º	59.3º	59.3º	59.3º
∠C_1-C_2-O	60.4º	60.4º	59.3º	59.3º	59.3º
∠O-C_1-H_1	113.6º	113.9º	114.6º	114.9º	114.8º
∠O-C_1-H_2	113.4º	113.5º	114.3º	114.5º	114.3º
∠O-C_2-H_3	113.4º	113.5º	114.3º	114.5º	114.3º
∠O-C_2-H_4	113.6º	113.9º	114.6º	114.9º	114.8º
∠H_1-C_1-H_2	116.5º	116.3º	116.0º	115.9º	116.0º
∠H_3-C_2-H_4	116.5º	116.3º	116.0º	115.9º	116.0º
D(Cu-O-C_1-C_2)	-111.9º	-122.6º	-116.9º	-115.6º	-115.4º
D(Cu-O-C_2-C_1)	119.9º	122.6º	116.9º	115.6º	115.4º
D(Cu-O-C_1-H_1)	-0.4º	-10.9º	-5.8º	-4.7º	-4.4º
D(Cu-O-C_1-H_2)	135.6º	125.3º	131.5º	133.0º	133.1º
D(Cu-O-C_2-H_3)	-135.6º	-125.3º	-131.5º	-133.0º	-133.1º
D(Cu-O-C_2-H_4)	0.4º	10.9º	5.8º	4.7º	4.4º
D(H_1-C_1-C_2-H_3)	156.4º	156.1º	155.3º	154.5º	155.0º
D(H_2-C_1-C_2-H_3)	0.0º	0.0º	0.0º	0.0º	0.0º
a_{63Cu}	1244	4162	4505	4531	4497
a_{17O}	-163	-122	-86	-87	-73
a_{13C} (C_1 & C_2)	0	2	0	0	0
a_H (H_1-H_4)	-1	-2	-1.0	-1	-1
Energy	-1793. 9599803	-1794. 0382078	-1794. 0956796	-1794. 1256993	-1794. 0671541

Cu-$\overline{SCH_2CH_2}$

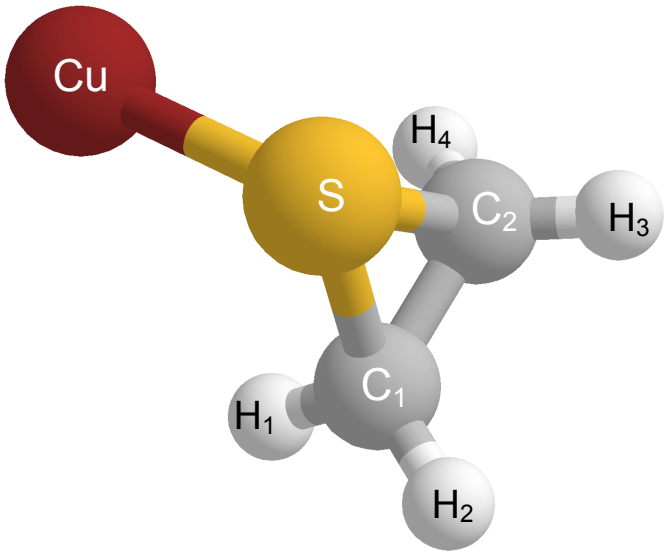

B3LYP	6-311G	6-311+G	6-311+G(d)	6-31++G(d,p)
Cu-S	2.468 Å	2.517 Å	2.445 Å	2.437 Å
S-C_1	1.940 Å	1.952 Å	1.850 Å	1.849 Å
S-C_2	1.940 Å	1.952 Å	1.850 Å	1.849 Å
C_1-C_2	1.467 Å	1.467 Å	1.473 Å	1.478 Å
C_1-H_1	1.080 Å	1.080 Å	1.084 Å	1.087 Å
C_1-H_2	1.078 Å	1.079 Å	1.084 Å	1.086 Å
C_2-H_3	1.078 Å	1.079 Å	1.084 Å	1.086 Å
C_2-H_4	1.080 Å	1.080 Å	1.084 Å	1.087 Å
∠Cu-S-C_1	90.8°	105.1°	103.0°	103.1°
∠Cu-S-C_2	90.8°	105.1°	103.0°	103.1°
∠C_1-S-C_2	44.4°	44.2°	44.9°	47.1°
∠S-C_1-C_2	67.8°	67.9°	66.5°	66.4°
∠C_1-C_2-S	67.8°	67.9°	66.5°	66.4°
∠S-C_1-H_1	111.9°	112.1°	114.0°	114.1°
∠S-C_1-H_2	112.8°	112.0°	113.7°	113.8°
∠S-C_2-H_3	112.8°	112.0°	113.7°	113.8°
∠S-C_2-H_4	111.9°	112.1°	114.0°	114.1°
∠H_1-C_1-H_2	116.5°	116.1°	115.5°	115.6°
D(Cu-S-C_1-C_2)	-90.3°	-96.2°	-95.7°	-95.8°
D(Cu-S-C_2-C_1)	90.3°	96.2°	95.7°	95.8°
D(Cu-S-C_1-H_1)	22.2°	17.3°	16.4°	16.1°
D(Cu-S-C_1-H_2)	156.0°	149.8°	151.6°	151.6°
D(Cu-S-C_2-H_3)	-156.0°	-149.8°	-151.6°	-151.6°
D(Cu-S-C_2-H_4)	-22.2°	-17.3°	-16.4°	-16.1°
D(H_1-C_1-C_2-H_3)	151.7°	152.4°	149.3°	149.1°
D(H_2-C_1-C_2-H_3)	0°	0°	0°	0°

	6-311G	6-311+G	6-311+G(d)	6-31++G(d,p)
a_{63Cu}	2731	4093	3956	3936
a_{33S}	63	88	73	64
a_{13C} (C_1 & C_2)	3	1	0	0
a_H (H_1-H_4)	1	1	2	3
Energy	-2117.1754152	-2117.2636995	-2117.3100565	-2117.2715795
M06				
Cu-S	2.439 Å	2.515 Å	2.548 Å	2.437 Å
S-C_1	1.903 Å	1.913 Å	1.825 Å	1.849 Å
S-C_2	1.903 Å	1.913 Å	1.825 Å	1.849 Å
C_1-C_2	1.465 Å	1.465 Å	1.465 Å	1.478 Å
C_1-H_1	1.084 Å	1.084 Å	1.076 Å	1.087 Å
C_1-H_2	1.080 Å	1.081 Å	1.075 Å	1.086 Å
C_2-H_3	1.080 Å	1.081 Å	1.075 Å	1.086 Å
C_2-H_4	1.084 Å	1.084 Å	1.076 Å	1.087 Å
∠Cu-S-C_1	87.5º	94.7º	103.0º	101.5º
∠Cu-S-C_2	87.5º	94.7º	103.0º	101.5º
∠C_1-S-C_2	45.3º	45.0º	44.9º	47.3º
∠S-C_1-C_2	67.4º	67.5º	66.5º	66.3º
∠C_1-C_2-S	67.4º	67.5º	66.5º	66.3º
∠S-C_1-H_1	112.7º	112.3º	114.0º	114.4º
∠S-C_1-H_2	113.4º	112.8º	113.7º	114.0º
∠S-C_2-H_3	113.4º	112.8º	113.7º	114.0º
∠S-C_2-H_4	112.7º	112.3º	114.0º	114.4º
∠H_1-C_1-H_2	116.5º	116.3º	115.5º	115.4º
D(Cu-S-C_1-C_2)	-89.0º	-92.0º	-95.7º	-95.1º
D(Cu-S-C_2-C_1)	89.0º	92.0º	95.7º	95.1º
D(Cu-S-C_1-H_1)	22.8º	20.7º	16.4º	16.7º
D(Cu-S-C_1-H_2)	157.8º	154.4º	151.6º	152.5º
D(Cu-S-C_2-H_3)	-157.8º	-154.4º	-151.6º	-152.5º
D(Cu-S-C_2-H_4)	-22.8º	-20.7º	-16.4º	-16.7º
D(H_1-C_1-C_2-H_3)	150.3º	151.5º	149.3º	148.5º
D(H_2-C_1-C_2-H_3)	0º	0º	0º	0º
a_{63Cu}	2791	4153	4039	4013
a_{33S}	55	65	62	54
a_{13C} (C_1 & C_2)	6	2	1	2
a_H (H_1-H_4)	1	1	1	1
Energy	-2116.9734288	-2117.0647358	-2117.112992	-2117.0742644
BHandHLYP				
Cu-S	2.528 Å	2.622 Å	2.548 Å	2.546 Å
S-C_1	1.911 Å	1.918 Å	1.825 Å	1.823 Å
S-C_2	1.911 Å	1.918 Å	1.825 Å	1.823 Å
C_1-C_2	1.457 Å	1.458 Å	1.465 Å	1.469 Å
C_1-H_1	1.071 Å	1.071 Å	1.076 Å	1.078 Å
C_1-H_2	1.069 Å	1.070 Å	1.075 Å	1.078 Å

	6-311G	6-311+G	6-311+G(d)	6-31++G(d,p)
C_2-H_3	1.069 Å	1.070 Å	1.075 Å	1.078 Å
C_2-H_4	1.071 Å	1.071 Å	1.076 Å	1.078 Å
∠Cu-S-C_1	90.3º	102.0º	103.0º	101.8º
∠Cu-S-C_2	90.3º	102.0º	103.0º	101.8º
∠C_1-S-C_2	44.8º	44.7º	47.3º	47.5º
∠S-C_1-C_2	67.6º	67.7º	66.5º	66.2º
∠C_1-C_2-S	67.6º	67.7º	66.5º	66.2º
∠S-C_1-H_1	112.6º	112.7º	114.4º	114.5º
∠S-C_1-H_2	113.0º	112.4º	113.8º	114.1º
∠S-C_2-H_3	113.0º	112.7º	113.8º	114.1º
∠S-C_2-H_4	112.6º	112.4º	114.4º	114.5º
∠H_1-C_1-H_2	116.1º	116.0º	115.3º	115.4º
D(Cu-S-C_1-C_2)	-90.1º	-95.0º	-97.1º	-95.3º
D(Cu-S-C_2-C_1)	90.1º	95.0º	97.1º	95.3º
D(Cu-S-C_1-H_1)	22.3º	18.1º	16.4º	16.3º
D(Cu-S-C_1-H_2)	156.4º	151.3º	150.6º	152.1º
D(Cu-S-C_2-H_3)	-156.4º	-151.3º	-150.6º	-152.1º
D(Cu-S-C_2-H_4)	-22.3º	-18.1º	-16.4º	-16.3º
D(H_1-C_1-C_2-H_3)	150.8º	151.5º	148.1º	148.8º
D(H_2-C_1-C_2-H_3)	0º	0º	0º	0º
a_{63Cu}	3120	4169	4039	4039
a_{33S}	64	65	62	53
a_{13C} (C_1 & C_2)	5	0	1	0
a_H (H_1-H_4)	0	0	1	1
Energy	-2116.9774943	-2117.0586497	-2117.112992	-2117.0790626

Cu-$\overline{NHCH_2CH_2}$

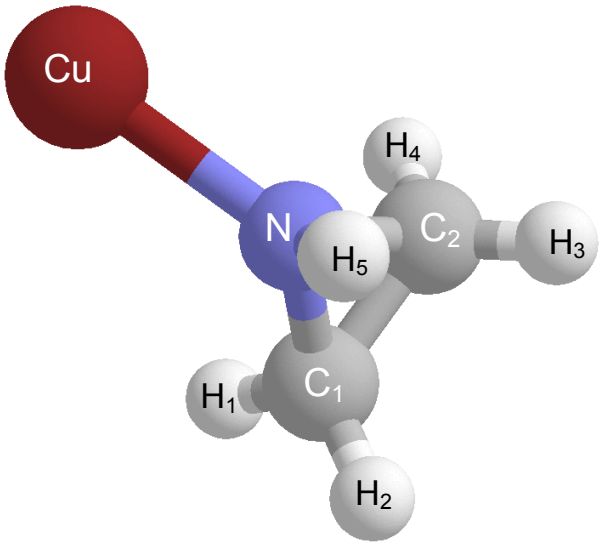

B3LYP	6-311G	6-311+G	6-311+G(d)	EPR-III	6-31++G(d,p)
Cu-N	1.964 Å	2.041 Å	2.084 Å	2.082 Å	2.083 Å
N-C_1	1.499 Å	1.507 Å	1.482 Å	1.479 Å	1.483 Å
N-C_2	1.499 Å	1.507 Å	1.482 Å	1.479 Å	1.483 Å
N-H_5	1.017 Å	1.019 Å	1.016 Å	1.014 Å	1.019 Å
C_1-C_2	1.492 Å	1.492 Å	1.481 Å	1.477 Å	1.484 Å
C_1-H_1	1.079 Å	1.079 Å	1.083 Å	1.081 Å	1.086 Å
C_1-H_2	1.080 Å	1.081 Å	1.084 Å	1.082 Å	1.086 Å
C_2-H_3	1.080 Å	1.081 Å	1.084 Å	1.082 Å	1.086 Å
C_2-H_4	1.079 Å	1.079 Å	1.083 Å	1.081 Å	1.086 Å
∠Cu-N-C_1	119.6º	124.0º	124.9º	124.7º	124.4º
∠Cu-N-C_2	119.6º	124.0º	124.9º	124.7º	124.4º
∠Cu-N-H_5	116.7º	113.3º	113.4º	113.9º	113.9º
∠C_1-N-C_2	59.7º	59.3º	59.9º	59.9º	60.0º
∠N-C_1-C_2	60.2º	60.3º	60.0º	60.0º	60.0º
∠C_1-C_2-N	60.2º	60.3º	60.0º	60.0º	60.0º
∠C_1-N-H_5	114.5º	112.9º	111.7º	111.5º	113.9º
∠C_2-N-H_5	114.5º	112.9º	111.7º	111.5º	113.9º
∠N-C_1-H_1	113.7º	114.2º	114.2º	113.1º	114.2º
∠N-C_1-H_2	113.7º	114.2º	114.2º	113.1º	114.2º
∠N-C_2-H_3	113.7º	114.2º	114.2º	113.1º	114.2º
∠N-C_2-H_4	113.7º	114.2º	114.2º	113.1º	114.2º
∠H_1-C_1-H_2	115.7º	115.4º	115.3º	115.9º	115.4º
D(Cu-N-C_1-C_2)	-109.0º	-112.6º	-113.7º	-113.5º	-113.3º
D(Cu-N-C_2-C_1)	109.0º	112.6º	113.7º	113.5º	113.3º
D(Cu-N-C_1-H_1)	2.6º	-0.8º	-2.0º	-2.1º	-1.8º
D(Cu-N-C_1-H_2)	142.0º	138.2º	137.1º	137.4º	137.6º

	6-311G	6-311+G	6-311+G(d)	EPR-III	6-31++G(d,p)
D(Cu-N-C_2-H_3)	-142.0º	-138.2º	-137.1º	-137.4º	-137.6º
D(Cu-N-C_2-H_4)	-2.6º	0.8º	2.0º	2.1º	1.8º
D(H_5-N-C_1-C_2)	105.2º	103.9º	103.3º	103.6º	103.3º
D(H_1-C_1-C_2-H_3)	151.2º	151.2º	151.1º	151.3º	151.3º
D(H_2-C_1-C_2-H_3)	0.0º	0.0º	0º	0º	0º
a_{63Cu}	1341	3209	3469	3461	3447
a_{14N}	98	85	77	80	68
a_{13C1}	3	2	2	2	-1
a_{13C2}	3	2	2	2	-1
a_{H1}	2	1	1	1	1
a_{H2}	2	1	1	1	1
a_{H3}	2	1	1	1	1
a_{H4}	2	1	1	1	1
a_{H5}	1	1	1	1	1
Energy	-1774.3233366	-1774.4027038	-1774.4436898	-1774.4726086	-1774.4227888
M06					
Cu-N	1.951 Å	2.032 Å	2.086 Å	2.088 Å	2.088 Å
N-C_1	1.483 Å	1.489 Å	1.466 Å	1.463 Å	1.469 Å
N-C_2	1.483 Å	1.489 Å	1.466 Å	1.463 Å	1.469 Å
N-H_5	1.016 Å	1.019 Å	1.017 Å	1.012 Å	1.017 Å
C_1-C_2	1.483 Å	1.492 Å	1.469 Å	1.466 Å	1.471 Å
C_1-H_1	1.083 Å	1.083 Å	1.089 Å	1.083 Å	1.089 Å
C_1-H_2	1.082 Å	1.083 Å	1.087 Å	1.081 Å	1.088 Å
C_2-H_3	1.082 Å	1.083 Å	1.087 Å	1.081 Å	1.088 Å
C_2-H_4	1.083 Å	1.073 Å	1.089 Å	1.083 Å	1.089 Å
∠Cu-N-C_1	116.1º	119.1º	118.9º	118.3º	118.6º
∠Cu-N-C_2	116.1º	119.1º	118.9º	118.3º	118.6º
∠Cu-N-H_5	116.7º	113.2º	119.6º	120.8º	120.1º
∠C_1-N-C_2	59.1º	59.3º	60.1º	60.2º	60.1º
∠N-C_1-C_2	60.5º	60.3º	59.9º	59.9º	59.9º
∠C_1-C_2-N	60.5º	60.3º	59.9º	59.9º	59.9º
∠C_1-N-H_5	115.1º	112.7º	112.6º	112.3º	112.6º
∠C_2-N-H_5	115.1º	112.7º	112.6º	112.3º	112.6º
∠N-C_1-H_1	113.4º	114.3º	113.9º	114.0º	113.8º
∠N-C_1-H_2	113.4º	114.3º	113.9º	114.0º	113.8º
∠N-C_2-H_3	113.4º	114.3º	113.9º	114.0º	113.8º
∠N-C_2-H_4	113.4º	114.3º	113.9º	114.0º	113.8º
∠H_1-C_1-H_2	115.9º	115.8º	115.5º	115.6º	115.5º
D(Cu-N-C_1-C_2)	-102.0º	-112.6º	-108.7º	-108.1º	-108.4º
D(Cu-N-C_2-C_1)	102.0º	112.6º	108.7º	108.1º	108.4º
D(Cu-N-C_1-H_1)	2.2º	1.8º	3.0º	3.2º	3.2º
D(Cu-N-C_1-H_2)	145.0º	138.2º	142.3º	143.0º	142.6º

	6-311G	6-311+G	6-311+G(d)	EPR-III	6-31++G(d,p)
D(Cu-N-C_2-H_3)	-145.0º	-138.2º	-142.3º	-143.0º	-142.6º
D(Cu-N-C_2-H_4)	-2.2º	-1.8º	-3.0º	-3.2º	-3.2º
D(H_5-N-C_1-C_2)	105.2º	103.9º	103.9º	103.8º	103.9º
D(H_1-C_1-C_2-H_3)	151.2º	151.2º	151.2º	151.1º	151.3º
D(H_2-C_1-C_2-H_3)	0.0º	0.0º	0º	0º	0º
a_{63Cu}	1554	3290	3617	3605	3606
a_{14N}	89	85	78	78	67
a_{13C1}	4	2	2	2	2
a_{13C2}	4	2	2	2	2
a_{H1}	3	1	1	1	1
a_{H2}	3	1	1	1	1
a_{H3}	3	1	1	1	1
a_{H4}	3	1	1	1	1
a_{H5}	3	1	1	2	0
Energy	-1774.1204844	-1774.2011143	-1774.2387317	-1774.2722802	-1774.2195956
BHandHLYP					
Cu-N	1.986 Å	2.075 Å	2.130 Å	2.128 Å	2.134 Å
N-C_1	1.479 Å	1.484 Å	1.464 Å	1.460 Å	1.463 Å
N-C_2	1.479 Å	1.484 Å	1.464 Å	1.460 Å	1.463 Å
N-H_5	1.005 Å	1.007 Å	1.005 Å	1.003 Å	1.008 Å
C_1-C_2	1.480 Å	1.480 Å	1.470 Å	1.466 Å	1.472 Å
C_1-H_1	1.071 Å	1.071 Å	1.076 Å	1.074 Å	1.078 Å
C_1-H_2	1.072 Å	1.072 Å	1.077 Å	1.074 Å	1.078 Å
C_2-H_3	1.072 Å	1.072 Å	1.077 Å	1.074 Å	1.078 Å
C_2-H_4	1.071 Å	1.071 Å	1.076 Å	1.074 Å	1.078 Å
∠Cu-N-C_1	120.1º	123.3º	124.3º	124.2º	123.9º
∠Cu-N-C_2	120.1º	123.3º	124.3º	124.2º	123.9º
∠Cu-N-H_5	115.1º	113.0º	113.6º	114.0º	113.9º
∠C_1-N-C_2	60.0º	59.8º	60.3º	60.3º	60.4º
∠N-C_1-C_2	60.0º	60.1º	59.8º	59.9º	59.8º
∠C_1-C_2-N	60.0º	60.1º	59.8º	59.9º	59.8º
∠C_1-N-H_5	115.2º	113.7º	112.0º	111.9º	112.2º
∠C_2-N-H_5	115.2º	113.7º	112.0º	111.9º	112.2º
∠N-C_1-H_1	114.3º	114.6º	114.5º	114.6º	114.5º
∠N-C_1-H_2	114.3º	114.6º	114.5º	114.6º	114.5º
∠N-C_2-H_3	114.3º	114.6º	114.5º	114.6º	114.5º
∠N-C_2-H_4	114.3º	114.6º	114.5º	114.6º	114.5º
∠H_1-C_1-H_2	115.5º	115.3º	115.2º	115.2º	115.2º
D(Cu-N-C_1-C_2)	-109.6º	-112.2º	-113.4º	-113.2º	-113.0º
D(Cu-N-C_2-C_1)	109.6º	112.2º	113.4º	113.2º	113.0º
D(Cu-N-C_1-H_1)	2.0º	-0.5º	-3.2º	-1.8º	-1.6º
D(Cu-N-C_1-H_2)	141.6º	138.9º	137.7º	138.0º	138.2º

	6-311G	6-311+G	6-311+G(d)	EPR-III	6-31++G(d,p)
D(Cu-N-C_2-H_3)	-141.6º	-138.9º	-137.7º	-138.0º	-138.2º
D(Cu-N-C_2-H_4)	-2.0º	0.5º	3.2º	1.8º	-1.6º
D(H_5-N-C_1-C_2)	105.8º	104.6º	103.6º	103.5º	103.7º
D(H_1-C_1-C_2-H_3)	150.9º	150.6º	150.7º	150.3º	150.5º
D(H_2-C_1-C_2-H_3)	0.0º	0.0º	0º	0º	0º
a_{63Cu}	844	3199	3473	3469	3478
a_{14N}	82	68	62	64	52
a_{13C1}	3	1	1	1	1
a_{13C2}	3	1	1	1	1
a_{H1}	2	1	1	0	0
a_{H2}	2	1	1	0	0
a_{H3}	2	1	1	0	0
a_{H4}	2	1	1	0	0
a_{H5}	4	2	3	2	1
Energy	-1774.114344	-1774.1852179	-1774.2340621	-1774.2619648	-1774.2163269

CuOCH2CH2

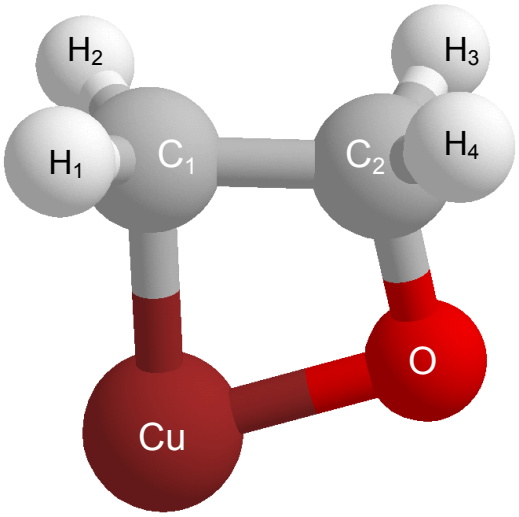

B3LYP	6-311G	6-311+G	6-311+G(d)	EPR-III	6-31++G(d,p)
Cu-C_1	1.943 Å	1.999 Å	1.991 Å	1.991 Å	1.989 Å
Cu-O	1.877 Å	1.897 Å	1.870 Å	1.858 Å	1.862 Å
O-C_2	1.491 Å	1.503 Å	1.441 Å	1.439 Å	1.444 Å
C_1-C_2	1.535 Å	1.517 Å	1.520 Å	1.518 Å	1.523 Å
C_1-H_1	1.088 Å	1.087 Å	1.089 Å	1.086 Å	1.090 Å
C_1-H_2	1.088 Å	1.087 Å	1.089 Å	1.086 Å	1.090 Å
C_2-H_3	1.093 Å	1.090 Å	1.097 Å	1.095 Å	1.099 Å
C_2-H_4	1.092 Å	1.090 Å	1.097 Å	1.095 Å	1.099 Å
∠C_1-Cu-O	78.0º	77.4º	74.5º	74.7º	75.0º
∠Cu-O-C_2	90.0º	93.0º	94.1º	94.2º	94.0º
∠O-C_2-C_1	105.1º	103.6º	104.4º	104.5º	104.5º
∠C_2-C_1-Cu	86.3º	88.0º	87.0º	86.6º	86.6º
∠Cu-C_1-H_1	111.8º	108.6º	108.9º	108.9º	108.8º
∠Cu-C_1-H_2	113.7º	108.5º	108.9º	108.9º	108.8º
∠O-C_2-H_3	109.4º	108.4º	109.6º	109.7º	109.7º
∠O-C_2-H_4	108.7º	108.4º	109.6º	109.7º	109.7º
∠H_1-C_1-H_2	112.1º	113.9º	113.8º	114.1º	114.0º
∠H_3-C_2-H_4	109.5º	110.1º	109.0º	109.0º	109.1º
D(C_1-Cu-O-C_2)	-5.1º	0.0º	0.0º	0.0º	0.0º
D(Cu-O-C_2-C_1)	6.6º	0.0º	0.0º	0.0º	0.0º
D(Cu-C_1-C_2-O)	-6.4º	0.0º	0.0º	0.0º	0.0º
D(O-Cu-C_1-C_2)	5.0º	0.0º	0.0º	0.0º	0.0º
D(O-Cu-C_1-H_1)	110.5º	-109.9º	117.7º	117.5º	117.6º
D(O-Cu-C_1-H_2)	-121.3º	109.8º	-117.7º	-117.5º	-117.6º
D(Cu-O-C_2-H_3)	113.3º	120.3º	120.2º	120.2º	120.1º
D(Cu-O-C_2-H_4)	-127.2º	-120.2º	-120.2º	-120.2º	-120.2º
D(H_1-C_1-C_2-H_4)	12.1º	7.2º	8.9º	9.2º	9.1º
D(H_1-C_1-C_2-H_3)	135.5º	133.0º	131.7º	131.9º	131.9º

	6-311G	6-311+G	6-311+G(d)	EPR-III	6-31++G(d,p)
a_{63Cu}	-495	-336	-305	-316	-314
a_{17O}	-15	-14	-23	-31	-51
a_{13C1}	98	99	104	104	115
a_{13C2}	-18	-19	-17	-16	-16
a_{H1}	1	-1	1	2	1
a_{H2}	-2	-1	1	2	1
a_{H3}	2	1	1	1	1
a_{H4}	3	1	1	1	1
Energy	-1794. 2158458	-1794. 2878538	-1794. 3214831	-1794. 3516911	-1794. 2902768
M06					
Cu-C_1	1.924 Å	1.979 Å	1.973 Å	1.972 Å	1.972 Å
Cu-O	1.868 Å	1.870 Å	1.859 Å	1.845 Å	1.851 Å
O-C_2	1.465 Å	1.476 Å	1.421 Å	1.420 Å	1.426 Å
C_1-C_2	1.528 Å	1.511 Å	1.510 Å	1.508 Å	1.514 Å
C_1-H_1	1.090 Å	1.089 Å	1.091 Å	1.086 Å	1.092 Å
C_1-H_2	1.090 Å	1.089 Å	1.091 Å	1.086 Å	1.092 Å
C_2-H_3	1.097 Å	1.093 Å	1.101 Å	1.096 Å	1.101 Å
C_2-H_4	1.095 Å	1.093 Å	1.101 Å	1.096 Å	1.101 Å
∠C_1-Cu-O	77.0º	74.9º	74.2º	74.5º	74.7º
∠Cu-O-C_2	90.8º	93.5º	94.5º	94.4º	94.3º
∠O-C_2-C_1	104.1º	103.3º	104.2º	104.4º	104.2º
∠C_2-C_1-Cu	86.8º	88.2º	87.2º	86.7º	86.9º
∠Cu-C_1-H_1	111.4º	108.0º	108.2º	108.1º	108.0º
∠Cu-C_1-H_2	114.2º	108.0º	108.2º	108.1º	108.0º
∠O-C_2-H_3	110.3º	109.1º	110.2º	110.3º	110.2º
∠O-C_2-H_4	109.5º	109.1º	110.2º	110.3º	110.2º
∠H_1-C_1-H_2	112.1º	114.3º	114.0º	114.4º	114.1º
∠H_3-C_2-H_4	108.8º	109.6º	108.3º	108.3º	108.3º
D(C_1-Cu-O-C_2)	7.8º	0.0º	0.0º	0.0º	0.0º
D(Cu-O-C_2-C_1)	-9.8º	0.0º	0.0º	0.0º	0.0º
D(Cu-C_1-C_2-O)	-9.8º	0.0º	0.0º	0.0º	0.0º
D(O-Cu-C_1-C_2)	9.6º	0.0º	0.0º	0.0º	0.0º
D(O-Cu-C_1-H_1)	107.6º	118.0º	118.0º	117.8º	117.9º
D(O-Cu-C_1-H_2)	-124.0º	-118.0º	-118.0º	-117.8º	-117.9º
D(Cu-O-C_2-H_3)	109.4º	120.1º	120.3º	120.2º	120.1º
D(Cu-O-C_2-H_4)	-130.9º	-120.1º	-120.3º	-120.2º	-120.1º
D(H_1-C_1-C_2-H_3)	116.3º	133.0º	131.9º	132.1º	132.2º
D(H_1-C_1-C_2-H_4)	6.3º	8.3º	8.3º	10.5º	10.4º

	6-311G	6-311+G	6-311+G(d)	EPR-III	6-31++G(d,p)
a_{63Cu}	-495	-162	-124	-131	-122
a_{17O}	-28	-25	-33	-51	-58
a_{13C1}	118	116	120	97	121
a_{13C2}	-14	-27	-24	-21	-8
a_{H1}	0	-8	-6	-9	-6
a_{H2}	-6	-8	-6	-9	-6
a_{H3}	2	2	1	2	1
a_{H4}	3	2	1	2	1
Energy	-1794.0048666	-1794.077902	-1794.1093446	-1794.1419868	-1794.0812379
BHandHLYP					
Cu-C_1	1.943 Å	2.001 Å	1.994 Å	1.989 Å	1.988 Å
Cu-O	1.832 Å	1.856 Å	1.842 Å	1.828 Å	1.833 Å
O-C_2	1.468 Å	1.476 Å	1.419 Å	1.418 Å	1.423 Å
C_1-C_2	1.531 Å	1.509 Å	1.514 Å	1.513 Å	1.517 Å
C_1-H_1	1.079 Å	1.079 Å	1.080 Å	1.078 Å	1.082 Å
C_1-H_2	1.079 Å	1.079 Å	1.080 Å	1.078 Å	1.082 Å
C_2-H_3	1.083 Å	1.082 Å	1.089 Å	1.087 Å	1.090 Å
C_2-H_4	1.083 Å	1.082 Å	1.089 Å	1.087 Å	1.090 Å
∠C_1-Cu-O	78.7º	74.9º	74.5º	75.0º	75.1º
∠Cu-O-C_2	90.6º	93.9º	94.7º	94.5º	94.3º
∠O-C_2-C_1	105.9º	103.8º	104.8º	105.1º	105.0º
∠C_2-C_1-Cu	84.7º	87.3º	85.9º	85.3º	85.5º
∠Cu-C_1-H_1	114.0º	109.1º	109.7º	109.9º	109.9º
∠Cu-C_1-H_2	114.0º	109.1º	109.7º	109.9º	109.9º
∠O-C_2-H_3	109.1º	108.7º	109.8º	109.9º	109.8º
∠O-C_2-H_4	109.1º	108.7º	109.8º	109.9º	109.8º
∠H_1-C_1-H_2	111.5º	113.7º	113.5º	113.7º	113.6º
∠H_3-C_2-H_4	109.3º	109.7º	108.6º	108.5º	108.7º
D(C_1-Cu-O-C_2)	0.0º	0.0º	0.0º	0.0º	0.0º
D(Cu-O-C_2-C_1)	0.0º	0.0º	0.0º	0.0º	0.0º
D(Cu-C_1-C_2-O)	0.0º	0.0º	0.0º	0.0º	0.0º
D(O-Cu-C_1-C_2)	0.0º	0.0º	0.0º	0.0º	0.0º
D(O-Cu-C_1-H_1)	115.2º	117.6º	117.4º	117.1º	117.1º
D(O-Cu-C_1-H_2)	-115.2º	-117.6º	-117.4º	-117.1º	-117.1º
D(Cu-O-C_2-H_3)	120.4º	120.3º	120.3º	120.3º	120.3º
D(Cu-O-C_2-H_4)	-120.4º	-120.3º	-120.3º	-120.3º	-120.3º
D(H_1-C_1-C_2-H_3)	127.3º	132.4º	131.0º	130.8º	132.9º
D(H_1-C_1-C_2-H_4)	4.6º	7.4º	8.9º	9.2º	8.9º

	6-311G	6-311+G	6-311+G(d)	EPR-III	6-31++G(d,p)
a_{63Cu}	-819	-731	-702	-702	-697
a_{17O}	-30	-29	-40	-45	-62
a_{13C1}	105	131	132	127	139
a_{13C2}	-20	-27	-21	-19	-20
a_{H1}	-6	-10	-7	-6	-7
a_{H2}	-6	-10	-7	-6	-7
a_{H3}	3	3	2	2	2
a_{H4}	3	3	2	2	2
Energy	-1793.9965674	-1794.056492	-1794.0970784	-1794.1264824	-1794.0689812

$\overline{OCuCH_2CHCH_2CH_3}$

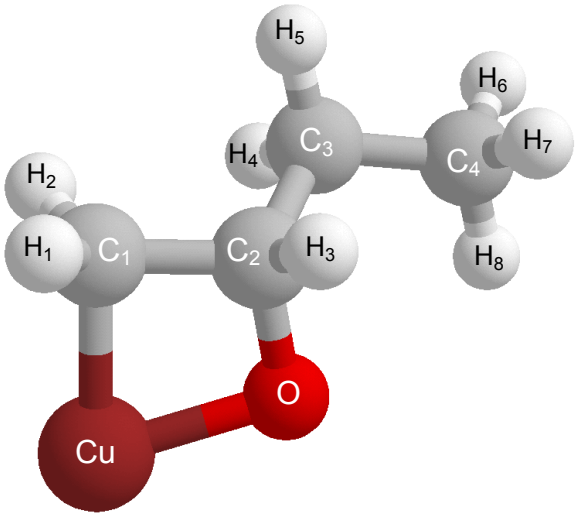

B3LYP	6-311G	6-311+G	6-311+G(d)	EPR-III	6-31++G(d,p)
Cu-C_1	1.937 Å	1.996 Å	1.989 Å	1.988 Å	1.987 Å
Cu-O	1.873 Å	1.876 Å	1.868 Å	1.857 Å	1.861 Å
O-C_2	1.498 Å	1.494 Å	1.446 Å	1.443 Å	1.448 Å
C_1-C_2	1.537 Å	1.537 Å	1.523 Å	1.520 Å	1.526 Å
C_2-C_3	1.528 Å	1.521 Å	1.528 Å	1.526 Å	1.531 Å
C_3-C_4	1.533 Å	1.535 Å	1.530 Å	1.527 Å	1.533 Å
C_1-H_1	1.088 Å	1.087 Å	1.089 Å	1.086 Å	1.090 Å
C_1-H_2	1.088 Å	1.088 Å	1.089 Å	1.087 Å	1.092 Å
C_2-H_3	1.096 Å	1.094 Å	1.100 Å	1.098 Å	1.102 Å
C_3-H_4	1.095 Å	1.095 Å	1.097 Å	1.095 Å	1.099 Å
C_3-H_5	1.096 Å	1.097 Å	1.098 Å	1.095 Å	1.099 Å
C_4-H_6	1.092 Å	1.093 Å	1.094 Å	1.091 Å	1.096 Å
C_4-H_7	1.092 Å	1.093 Å	1.095 Å	1.093 Å	1.097 Å
C_4-H_8	1.089 Å	1.090 Å	1.092 Å	1.090 Å	1.094 Å
∠C_1-Cu-O	78.0º	75.1º	74.3º	74.5º	74.7º
∠Cu-O-C_2	90.5º	93.7º	94.7º	94.7º	94.6º
∠O-C_2-C_1	104.5º	102.4º	103.4º	103.6º	103.5º
∠C_2-C_1-Cu	87.0º	87.3º	87.6º	87.2º	87.3º
∠C_1-C_2-C_3	113.8º	115.4º	114.3º	114.2º	114.2º
∠C_2-C_3-C_4	113.0º	113.0º	113.0º	113.0º	113.0º
∠Cu-C_1-H_1	112.9º	109.3º	109.6º	109.5º	109.6º
∠Cu-C_1-H_2	112.9º	108.5º	108.6º	108.5º	108.5º
∠O-C_2-H_3	107.7º	106.7º	108.0º	108.2º	108.1º
∠C_2-C_3-H_4	108.9º	108.3º	108.4º	108.3º	108.3º
∠C_2-C_3-H_5	112.1º	108.3º	108.4º	108.3º	108.3º
∠C_3-C_4-H_6	111.3º	111.0º	111.2º	111.1º	111.1º
∠C_3-C_4-H_7	111.3º	111.1º	111.3º	111.1º	111.1º

B3LYP	6-311G	6-311+G	6-311+G(d)	EPR-III	6-31++G(d,p)
$\angle C_3\text{-}C_4\text{-}H_8$	107.8º	111.4º	110.8º	110.7º	110.6º
$D(C_1\text{-}Cu\text{-}O\text{-}C_2)$	0.6º	0.9º	1.0º	1.2º	0.9º
$D(C_1\text{-}C_2\text{-}C_3\text{-}C_4)$	175.6º	174.7º	176.0º	176.5º	176.0º
$D(O\text{-}Cu\text{-}C_1\text{-}H_1)$	115.4º	119.1º	119.0º	118.8º	118.9º
$D(O\text{-}Cu\text{-}C_1\text{-}H_2)$	-116.2º	-116.2º	-116.2º	-116.1º	-116.1º
$D(Cu\text{-}O\text{-}C_2\text{-}H_3)$	-118.8º	-116.0º	-115.6º	-115.8º	-115.9º
$D(C_1\text{-}C_2\text{-}C_3\text{-}H_4)$	-62.1º	-62.4º	-62.5º	-62.2º	-62.4º
$D(C_1\text{-}C_2\text{-}C_3\text{-}H_5)$	-177.8º	-178.1º	-178.1º	-177.9º	-178.2º
$D(C_2\text{-}C_3\text{-}C_4\text{-}H_6)$	-176.5º	-179.1º	-179.0º	-179.0º	-179.0º
$D(C_2\text{-}C_3\text{-}C_4\text{-}H_7)$	63.3º	61.0º	61.1º	61.1º	61.1º
$D(C_2\text{-}C_3\text{-}C_4\text{-}H_8)$	-56.1º	-58.7º	-58.7º	-58.6º	-58.7º
a_{63Cu}	-446	-310	-272	-284	-282
a_{17O}	-19	-16	-25	-32	-52
a_{13C1}	93	98	102	102	114
a_{13C2}	-16	-17	-15	-14	-15
a_{13C3}	-1	-1	-1	-1	-1
a_{13C4}	3	3	3	3	3
a_{H1}	1	1	1	2	1
a_{H2}	1	0	3	4	1
a_{H3}	3	2	1	1	2
a_{H4}	1	1	0	1	0
a_{H5}	1	1	2	2	2
a_{H6}	1	1	1	0	0
a_{H7}	-1	-1	-1	-1	-1
a_{H8}	0	1	1	1	1
Energy	-1872. 8508024	-1872. 9196493	-1872. 9715957	-1873. 0179653	-1872. 9302374
M06					
$Cu\text{-}C_1$	1.922 Å	1.977 Å	1.973 Å	1.973 Å	1.971 Å
Cu-O	1.865 Å	1.866 Å	1.857 Å	1.843 Å	1.849 Å
$O\text{-}C_2$	1.471 Å	1.483 Å	1.427 Å	1.424 Å	1.443 Å
$C_1\text{-}C_2$	1.528 Å	1.513 Å	1.512 Å	1.510 Å	1.516 Å
$C_2\text{-}C_3$	1.517 Å	1.516 Å	1.516 Å	1.514 Å	1.519 Å
$C_3\text{-}C_4$	1.520 Å	1.522 Å	1.516 Å	1.514 Å	1.519 Å
$C_1\text{-}H_1$	1.090 Å	1.089 Å	1.091 Å	1.085 Å	1.092 Å
$C_1\text{-}H_2$	1.092 Å	1.091 Å	1.093 Å	1.088 Å	1.094 Å
$C_2\text{-}H_3$	1.096 Å	1.098 Å	1.106 Å	1.101 Å	1.106 Å
$C_3\text{-}H_4$	1.099 Å	1.098 Å	1.102 Å	1.096 Å	1.102 Å
$C_3\text{-}H_5$	1.098 Å	1.098 Å	1.101 Å	1.095 Å	1.101 Å
$C_4\text{-}H_6$	1.093 Å	1.093 Å	1.095 Å	1.090 Å	1.096 Å
$C_4\text{-}H_7$	1.095 Å	1.095 Å	1.098 Å	1.092 Å	1.097 Å
$C_4\text{-}H_8$	1.092 Å	1.092 Å	1.095 Å	1.090 Å	1.094 Å

	6-311G	6-311+G	6-311+G(d)	EPR-III	6-31++G(d,p)
$\angle C_1$-Cu-O	70.1º	74.8º	74.0º	74.3º	74.5º
$\angle$Cu-O-C_2	90.9º	93.9º	94.8º	94.9º	94.7º
$\angle$O-C_2-C_1	103.8º	102.5º	103.4º	103.6º	103.4º
$\angle C_2$-C_1-Cu	87.1º	88.7º	87.6º	87.1º	87.3º
$\angle C_1$-C_2-C_3	112.7º	114.4º	113.5º	113.3º	113.5º
$\angle C_2$-C_3-C_4	112.4º	112.3º	112.4º	112.4º	112.4º
$\angle$Cu-C_1-H_1	111.9º	108.7º	108.4º	109.5º	108.3º
$\angle$Cu-C_1-H_2	113.4º	108.2º	108.3º	108.1º	108.2º
$\angle$O-C_2-H_3	108.2º	107.5º	108.5º	108.6º	108.6º
$\angle C_2$-C_3-H_4	107.3º	107.8º	108.0º	107.8º	107.8º
$\angle C_2$-C_3-H_5	109.1º	108.6º	108.7º	108.6º	108.6º
$\angle C_3$-C_4-H_6	111.8º	111.6º	111.8º	111.6º	111.1º
$\angle C_3$-C_4-H_7	110.9º	110.9º	111.1º	110.9º	111.0º
$\angle C_3$-C_4-H_8	109.6º	110.2º	110.7º	110.5º	110.4º
D(C_1-Cu-O-C_2)	8.9º	1.0º	2.0º	3.0º	2.0º
D(C_1-C_2-C_3-C_4)	174.3º	174.5º	175.1º	176.5º	175.2º
D(O-Cu-C_1-H_1)	108.7º	117.7º	116.5º	115.3º	116.3
D(O-Cu-C_1-H_2)	-122.5º	-117.7º	-119.2º	-119.9º	-119.0º
D(Cu-O-C_2-H_3)	-128.3º	-118.9º	-120.4º	-121.7º	-120.5º
D(C_1-C_2-C_3-H_4)	-61.9º	-61.7º	-62.6º	-62.6º	-62.3º
D(C_1-C_2-C_3-H_5)	-177.5º	-177.3º	-177.9º	-178.2º	-177.8º
D(C_2-C_3-C_4-H_6)	-176.6º	-179.3º	-179.3º	-179.1º	-179.2º
D(C_2-C_3-C_4-H_7)	62.9º	60.2º	60.6º	60.7º	60.7º
D(C_2-C_3-C_4-H_8)	-56.0º	-59.0º	-58.7º	-58.6º	-58.6º
a_{63Cu}	-163	-146	-105	-112	-104
a_{17O}	-29	-25	-33	-52	-58
a_{13C1}	114	115	118	95	120
a_{13C2}	-23	-25	-22	-19	-21
a_{13C3}	-2	-1	-2	-2	-2
a_{13C4}	2	3	3	2	2
a_{H1}	-7	3	2	3	2
a_{H2}	3	-9	-8	-12	-8
a_{H3}	3	-6	-4	-5	-3
a_{H4}	0	-1	0	0	0
a_{H5}	0	0	2	2	2
a_{H6}	0	0	0	0	0
a_{H7}	1	1	1	0	0
a_{H8}	1	1	1	1	1
Energy	-1872.5780298	-1872.6475995	-1872.6940098	-1872.7445542	-1872.6548239

BHandHLYP	6-311G	6-311+G	6-311+G(d)	EPR-III	6-31++G(d,p)
$Cu\text{-}C_1$	1.938 Å	2.000 Å	1.993 Å	1.987 Å	1.986 Å
Cu-O	1.830 Å	1.854 Å	1.842 Å	1.829 Å	1.833 Å
$O\text{-}C_2$	1.473 Å	1.481 Å	1.423 Å	1.421 Å	1.426 Å
$C_1\text{-}C_2$	1.533 Å	1.512 Å	1.516 Å	1.515 Å	1.519 Å
$C_2\text{-}C_3$	1.517 Å	1.516 Å	1.518 Å	1.516 Å	1.520 Å
$C_3\text{-}C_4$	1.522 Å	1.523 Å	1.520 Å	1.517 Å	1.519 Å
$C_1\text{-}H_1$	1.080 Å	1.079 Å	1.081 Å	1.078 Å	1.082 Å
$C_1\text{-}H_2$	1.081 Å	1.080 Å	1.082 Å	1.080 Å	1.084 Å
$C_2\text{-}H_3$	1.087 Å	1.085 Å	1.092 Å	1.091 Å	1.094 Å
$C_3\text{-}H_4$	1.087 Å	1.086 Å	1.090 Å	1.087 Å	1.091 Å
$C_3\text{-}H_5$	1.087 Å	1.089 Å	1.090 Å	1.087 Å	1.091 Å
$C_4\text{-}H_6$	1.084 Å	1.084 Å	1.086 Å	1.084 Å	1.088 Å
$C_4\text{-}H_7$	1.085 Å	1.086 Å	1.087 Å	1.085 Å	1.089 Å
$C_4\text{-}H_8$	1.081 Å	1.082 Å	1.084 Å	1.082 Å	1.086 Å
$\angle C_1\text{-}Cu\text{-}O$	78.6º	74.6º	74.1º	74.6º	74.5º
$\angle Cu\text{-}O\text{-}C_2$	91.0º	94.6º	95.4º	95.1º	94.7º
$\angle O\text{-}C_2\text{-}C_1$	105.1º	102.8º	103.9º	104.2º	103.8º
$\angle C_2\text{-}C_1\text{-}Cu$	85.3º	88.0º	86.6º	86.0º	87.3º
$\angle C_1\text{-}C_2\text{-}C_3$	113.6º	115.1º	114.0º	113.8º	113.5º
$\angle C_2\text{-}C_3\text{-}C_4$	112.8º	112.8º	112.8º	112.8º	112.4º
$\angle Cu\text{-}C_1\text{-}H_1$	114.0º	109.8º	110.2º	110.4º	110.3º
$\angle Cu\text{-}C_1\text{-}H_2$	113.8º	109.0º	109.2º	109.5º	109.2º
$\angle O\text{-}C_2\text{-}H_3$	107.7º	107.2º	107.8º	108.6º	108.6º
$\angle C_2\text{-}C_3\text{-}H_4$	107.7º	108.2º	108.4º	108.3º	107.8º
$\angle C_2\text{-}C_3\text{-}H_5$	109.0º	108.5º	108.7º	108.6º	108.6º
$\angle C_3\text{-}C_4\text{-}H_6$	111.4º	111.2º	111.3º	111.2º	111.1º
$\angle C_3\text{-}C_4\text{-}H_7$	111.1º	111.1º	111.2º	111.0º	111.0º
$\angle C_3\text{-}C_4\text{-}H_8$	109.7º	110.3º	110.7º	110.6º	110.4º
$D(C_1\text{-}Cu\text{-}O\text{-}C_2)$	0.6º	1.3º	1.0º	1.0º	1.0º
$D(C_1\text{-}C_2\text{-}C_3\text{-}C_4)$	175.9º	174.6º	176.0º	176.7º	175.2º
$D(O\text{-}Cu\text{-}C_1\text{-}H_1)$	114.7º	119.0º	118.8º	115.3º	116.3
$D(O\text{-}Cu\text{-}C_1\text{-}H_2)$	-115.5º	-115.9º	-115.9º	-118.4º	-119.0º
$D(Cu\text{-}O\text{-}C_2\text{-}H_3)$	-118.9º	-116.1º	-115.8º	-115.9º	-115.5º
$D(C_1\text{-}C_2\text{-}C_3\text{-}H_4)$	-62.2º	-62.5º	-62.6º	-62.3º	-62.3º
$D(C_1\text{-}C_2\text{-}C_3\text{-}H_5)$	-178.1º	-178.3º	-178.3º	-178.2º	-178.8º
$D(C_2\text{-}C_3\text{-}C_4\text{-}H_6)$	-176.2º	-178.6º	-178.7º	-178.7º	-178.2º
$D(C_2\text{-}C_3\text{-}C_4\text{-}H_7)$	62.6º	61.4º	61.4º	60.5º	60.7º
$D(C_2\text{-}C_3\text{-}C_4\text{-}H_8)$	-55.6º	-58.2º	-58.3º	-58.7º	-58.6º

	6-311G	6-311+G	6-311+G(d)	EPR-III	6-31++G(d,p)
a_{63Cu}	-778	-708	-676	-679	-673
a_{17O}	-34	-32	-42	-48	-63
a_{13C1}	103	132	131	127	140
a_{13C2}	-18	-25	-20	-18	-19
a_{13C3}	0	0	-1	-1	-1
a_{13C4}	2	3	3	3	2
a_{H1}	-5	3	2	-5	-6
a_{H2}	-7	-9	-7	-6	-7
a_{H3}	4	3	-6	2	-6
a_{H4}	-1	-8	1	-1	-1
a_{H5}	0	0	2	2	2
a_{H6}	0	0	0	0	0
a_{H7}	0	1	0	0	0
a_{H8}	1	1	1	1	1
Energy	-1872.572671	-1872.6299286	-1872.6933274	-1872.738112	-1872.6569337

$\overline{CuOCH_2CHCH_2CH_3}$

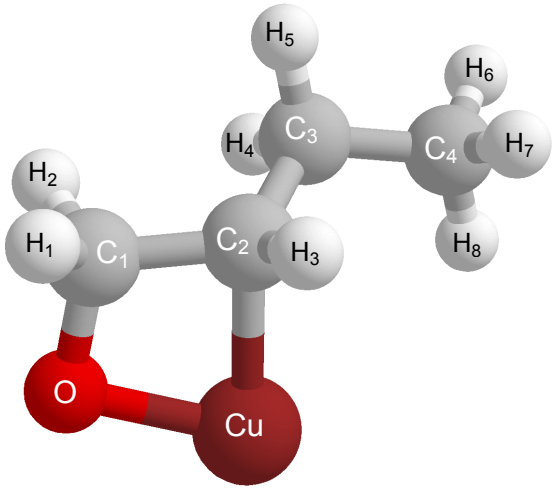

B3LYP	6-311G	6-311+G	6-311+G(d)	EPR-III	6-31++G(d,p)
O-C_1	1.474 Å	1.482 Å	1.423 Å	1.421 Å	1.426 Å
Cu-O	1.830 Å	1.856 Å	1.842 Å	1.829 Å	1.833 Å
Cu-C_2	1.938 Å	2.001 Å	1.993 Å	1.987 Å	1.986 Å
C_1-C_2	1.533 Å	1.516 Å	1.516 Å	1.515 Å	1.519 Å
C_2-C_3	1.517 Å	1.516 Å	1.518 Å	1.516 Å	1.520 Å
C_3-C_4	1.523 Å	1.523 Å	1.520 Å	1.517 Å	1.519 Å
C_1-H_1	1.080 Å	1.079 Å	1.081 Å	1.078 Å	1.082 Å
C_1-H_2	1.082 Å	1.081 Å	1.082 Å	1.080 Å	1.084 Å
C_2-H_3	1.086 Å	1.086 Å	1.092 Å	1.091 Å	1.094 Å
C_3-H_4	1.086 Å	1.086 Å	1.090 Å	1.087 Å	1.091 Å
C_3-H_5	1.086 Å	1.090 Å	1.090 Å	1.087 Å	1.091 Å
C_4-H_6	1.083 Å	1.085 Å	1.086 Å	1.084 Å	1.088 Å
C_4-H_7	1.084 Å	1.087 Å	1.087 Å	1.085 Å	1.089 Å
C_4-H_8	1.082 Å	1.083 Å	1.084 Å	1.082 Å	1.086 Å
∠C_1-O-Cu	79.2º	77.6º	74.1º	74.6º	74.5º
∠O-Cu-C_2	91.0º	94.6º	95.4º	95.1º	94.7º
∠Cu-C_2-C_1	85.3º	88.0º	86.6º	86.0º	87.3º
∠C_2-C_1-O	105.1º	102.8º	103.9º	104.2º	103.8º
∠C_1-C_2-C_3	113.6º	115.1º	114.0º	113.8º	113.5º
∠C_2-C_3-C_4	112.8º	112.8º	112.8º	112.8º	112.4º
∠O-C_1-H_1	114.0º	109.8º	110.2º	110.4º	110.3º
∠O-C_1-H_2	113.8º	109.0º	109.2º	109.5º	109.2º
∠Cu-C_2-H_3	107.7º	107.2º	107.8º	108.6º	108.6º
∠C_2-C_3-H_4	107.7º	108.2º	108.4º	108.3º	107.8º
∠C_2-C_3-H_5	109.0º	108.5º	108.7º	108.6º	108.6º
∠C_3-C_4-H_6	111.4º	111.2º	111.3º	111.2º	111.1º
∠C_3-C_4-H_7	111.1º	111.1º	111.2º	111.0º	111.0º
∠C_3-C_4-H_8	109.7º	110.3º	110.7º	110.6º	110.4º

	6-311G	6-311+G	6-311+G(d)	EPR-III	6-31++G(d,p)
D(C_1-O-Cu-C_2)	0.6º	1.1º	0.0º	0.0º	0.0º
D(C_1-C_2-C_3-C_4)	175.9º	174.6º	176.0º	176.7º	175.2º
D(Cu-O-C_1-H_1)	114.7º	119.0º	118.8º	115.3º	116.3
D(Cu-O-C_1-H_2)	-115.5º	-115.9º	-115.9º	-118.4º	-119.0º
D(O-Cu-C_2-H_3)	-118.9º	-116.1º	-115.8º	-115.9º	-115.5º
D(C_1-C_2-C_3-H_4)	-62.2º	-62.5º	-62.6º	-62.3º	-62.3º
D(C_1-C_2-C_3-H_5)	-178.1º	-178.3º	-178.3º	-178.2º	-178.8º
D(C_2-C_3-C_4-H_6)	-176.2º	-178.6º	-178.7º	-178.7º	-178.2º
D(C_2-C_3-C_4-H_7)	62.6º	61.4º	61.4º	60.5º	60.7º
D(C_2-C_3-C_4-H_8)	-55.6º	-58.2º	-58.3º	-58.7º	-58.6º
a_{63Cu}	-415	-276	-236	-244	-242
a_{17O}	-18	-15	-24	-31	-49
a_{13C1}	-17	-19	-16	-15	-16
a_{13C2}	97	105	107	109	123
a_{H1}	1	2	1	1	1
a_{H2}	4	2	3	3	3
a_{H3}	5	5	7	8	6
a_{H4}	6	13	13	15	13
a_{H5}	27	47	49	54	49
a_{H6}	0	-1	-1	-1	-1
a_{H7}	-1	-1	-1	-1	-1
a_{H8}	0	-1	-1	-1	-1
Energy	-1872. 8446886	-1872. 9133313	-1872. 9665983	-1873. 0127084	-1872. 9247057
M06					
O-C_1	1.463 Å	1.491 Å	1.435 Å	1.433 Å	1.438 Å
Cu-O	1.873 Å	1.876 Å	1.869 Å	1.858 Å	1.862 Å
Cu-C_2	1.944 Å	2.031 Å	2.024 Å	2.023 Å	2.020 Å
C_1-C_2	1.521 Å	1.521 Å	1.524 Å	1.521 Å	1.523 Å
C_2-C_3	1.519 Å	1.520 Å	1.513 Å	1.509 Å	1.516 Å
C_3-C_4	1.524 Å	1.535 Å	1.530 Å	1.527 Å	1.533 Å
C_1-H_1	1.097 Å	1.092 Å	1.098 Å	1.096 Å	1.100 Å
C_1-H_2	1.097 Å	1.092 Å	1.098 Å	1.096 Å	1.101 Å
C_2-H_3	1.095 Å	1.092 Å	1.093 Å	1.090 Å	1.095 Å
C_3-H_4	1.093 Å	1.094 Å	1.096 Å	1.093 Å	1.098 Å
C_3-H_5	1.101 Å	1.102 Å	1.104 Å	1.101 Å	1.105 Å
C_4-H_6	1.093 Å	1.092 Å	1.094 Å	1.091 Å	1.095 Å
C_4-H_7	1.094 Å	1.093 Å	1.095 Å	1.092 Å	1.096 Å
C_4-H_8	1.093 Å	1.094 Å	1.095 Å	1.093 Å	1.097 Å
∠C_1-O-Cu	90.2º	93.5º	94.4º	94.5º	94.2º
∠O-Cu-C_2	77.0º	75.1º	74.3º	74.5º	74.7º
∠Cu-C_2-C_1	86.0º	86.8º	85.8º	85.5º	85.6º

	6-311G	6-311+G	6-311+G(d)	EPR-III	6-31++G(d,p)
$\angle C_2\text{-}C_1\text{-}O$	104.7º	105.4º	105.4º	105.3º	105.3º
$\angle C_1\text{-}C_2\text{-}C_3$	116.9º	116.9º	118.9º	119.0º	118.9º
$\angle C_2\text{-}C_3\text{-}C_4$	114.2º	114.2º	114.9º	114.8º	115.1º
$\angle O\text{-}C_1\text{-}H_1$	110.1º	110.1º	109.7º	109.8º	109.6º
$\angle O\text{-}C_1\text{-}H_2$	108.6º	108.2º	109.8º	109.8º	109.7º
$\angle Cu\text{-}C_2\text{-}H_3$	111.7º	110.7º	103.7º	103.7º	103.2º
$\angle C_2\text{-}C_3\text{-}H_4$	108.7º	109.7º	109.9º	109.9º	109.9º
$\angle C_2\text{-}C_3\text{-}H_5$	109.3º	109.3º	107.7º	107.7º	107.7º
$\angle C_3\text{-}C_4\text{-}H_6$	111.8º	111.6º	111.4º	111.3º	111.3º
$\angle C_3\text{-}C_4\text{-}H_7$	111.3º	111.7º	111.4º	111.2º	111.3º
$\angle C_3\text{-}C_4\text{-}H_8$	109.9º	109.1º	111.1º	110.9º	111.1º
$D(C_1\text{-}O\text{-}Cu\text{-}C_2)$	-16.5º	-0.9º	-0.2º	-0.3º	-0.3º
$D(C_1\text{-}C_2\text{-}C_3\text{-}C_4)$	160.5º	168.4º	168.8º	168.7º	168.8º
$D(Cu\text{-}O\text{-}C_1\text{-}H_1)$	107.2º	120.0º	120.1º	120.2º	120.1º
$D(Cu\text{-}O\text{-}C_1\text{-}H_2)$	-133.0º	-120.6º	-121.0º	-119.8º	-121.0º
$D(O\text{-}Cu\text{-}C_2\text{-}H_3)$	-124.7º	-114.7º	-115.2º	-115.1º	-115.2º
$D(C_1\text{-}C_2\text{-}C_3\text{-}H_4)$	-58.1º	-56.6º	-56.7º	-56.7º	-56.7º
$D(C_1\text{-}C_2\text{-}C_3\text{-}H_5)$	-173.5º	-171.2º	-170.5º	-170.5º	-170.5º
$D(C_2\text{-}C_3\text{-}C_4\text{-}H_6)$	180.0º	176.1º	178.3º	178.4º	178.3º
$D(C_2\text{-}C_3\text{-}C_4\text{-}H_7)$	-59.1º	-56.0º	-56.2º	-56.2º	-56.2º
$D(C_2\text{-}C_3\text{-}C_4\text{-}H_8)$	-59.7º	-63.8º	-52.9º	-62.3º	-63.6º
a_{63Cu}	-125	-96	-55	-62	-47
a_{17O}	-29	-24	-32	-50	-54
a_{13C1}	-24	-26	-23	-20	-22
a_{13C2}	116	120	20	95	127
a_{H1}	1	2	1	1	0
a_{H2}	2	3	3	3	2
a_{H3}	2	-4	-4	-6	-3
a_{H4}	7	14	16	18	15
a_{H5}	29	50	55	61	54
a_{H6}	0	-1	-1	0	0
a_{H7}	-1	-1	-2	-3	-2
a_{H8}	0	-1	-1	-1	-1
Energy	-1872.571843	-1872.6417646	-1872.6893694	-1872.7397033	-1872.6494403

BHandHLYP	6-311G	6-311+G	6-311+G(d)	EPR-III	6-31++G(d,p)
O-C_1	1.474 Å	1.482 Å	1.423 Å	1.421 Å	1.426 Å
Cu-O	1.830 Å	1.856 Å	1.842 Å	1.829 Å	1.833 Å
Cu-C_2	1.938 Å	2.001 Å	1.993 Å	1.987 Å	1.986 Å
C_1-C_2	1.533 Å	1.516 Å	1.516 Å	1.515 Å	1.519 Å
C_2-C_3	1.517 Å	1.516 Å	1.518 Å	1.516 Å	1.520 Å
C_3-C_4	1.523 Å	1.523 Å	1.520 Å	1.517 Å	1.519 Å
C_1-H_1	1.080 Å	1.079 Å	1.081 Å	1.078 Å	1.082 Å
C_1-H_2	1.082 Å	1.081 Å	1.082 Å	1.080 Å	1.084 Å
C_2-H_3	1.086 Å	1.086 Å	1.092 Å	1.091 Å	1.094 Å
C_3-H_4	1.086 Å	1.086 Å	1.090 Å	1.087 Å	1.091 Å
C_3-H_5	1.086 Å	1.090 Å	1.090 Å	1.087 Å	1.091 Å
C_4-H_6	1.083 Å	1.085 Å	1.086 Å	1.084 Å	1.088 Å
C_4-H_7	1.084 Å	1.087 Å	1.087 Å	1.085 Å	1.089 Å
C_4-H_8	1.082 Å	1.083 Å	1.084 Å	1.082 Å	1.086 Å
∠C_1-O-Cu	79.2º	77.6º	74.1º	74.6º	74.5º
∠O-Cu-C_2	91.0º	94.6º	95.4º	95.1º	94.7º
∠Cu-C_2-C_1	85.3º	88.0º	86.6º	86.0º	87.3º
∠C_2-C_1-O	105.1º	102.8º	103.9º	104.2º	103.8º
∠C_1-C_2-C_3	113.6º	115.1º	114.0º	113.8º	113.5º
∠C_2-C_3-C_4	112.8º	112.8º	112.8º	112.8º	112.4º
∠O-C_1-H_1	114.0º	109.8º	110.2º	110.4º	110.3º
∠O-C_1-H_2	113.8º	109.0º	109.2º	109.5º	109.2º
∠Cu-C_2-H_3	107.7º	107.2º	107.8º	108.6º	108.6º
∠C_2-C_3-H_4	107.7º	108.2º	108.4º	108.3º	107.8º
∠C_2-C_3-H_5	109.0º	108.5º	108.7º	108.6º	108.6º
∠C_3-C_4-H_6	111.4º	111.2º	111.3º	111.2º	111.1º
∠C_3-C_4-H_7	111.1º	111.1º	111.2º	111.0º	111.0º
∠C_3-C_4-H_8	109.7º	110.3º	110.7º	110.6º	110.4º
D(C_1-O-Cu-C_2)	0.6º	1.1º	0.0º	0.0º	0.0º
D(C_1-C_2-C_3-C_4)	175.9º	174.6º	176.0º	176.7º	175.2º
D(Cu-O-C_1-H_1)	114.7º	119.0º	118.8º	115.3º	116.3
D(Cu-O-C_1-H_2)	-115.5º	-115.9º	-115.9º	-118.4º	-119.0º
D(O-Cu-C_2-H_3)	-118.9º	-116.1º	-115.8º	-115.9º	-115.5º
D(C_1-C_2-C_3-H_4)	-62.2º	-62.5º	-62.6º	-62.3º	-62.3º
D(C_1-C_2-C_3-H_5)	-178.1º	-178.3º	-178.3º	-178.2º	-178.8º
D(C_2-C_3-C_4-H_6)	-176.2º	-178.6º	-178.7º	-178.7º	-178.2º
D(C_2-C_3-C_4-H_7)	62.6º	61.4º	61.4º	60.5º	60.7º
D(C_2-C_3-C_4-H_8)	-55.6º	-58.2º	-58.3º	-58.7º	-58.6º

	6-311G	6-311+G	6-311+G(d)	EPR-III	6-31++G(d,p)
a_{63Cu}	-415	-276	-236	-244	-242
a_{17O}	-18	-15	-24	-31	-49
a_{13C1}	-17	-19	-16	-15	-16
a_{13C2}	97	105	107	109	123
a_{H1}	1	2	1	1	1
a_{H2}	4	2	3	3	3
a_{H3}	5	5	7	8	6
a_{H4}	6	13	13	15	13
a_{H5}	27	47	49	54	49
a_{H6}	0	-1	-1	-1	-1
a_{H7}	-1	-1	-1	-1	-1
a_{H8}	0	-1	-1	-1	-1
Energy	-1872.8446886	-1872.9133313	-1872.9665983	-1873.0127084	-1872.9247057

CuSCH2CH2

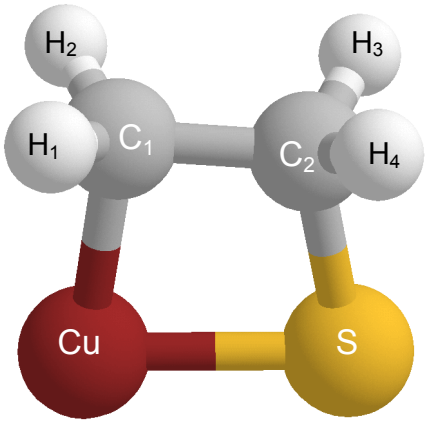

B3LYP	6-311G	6-311+G	6-311+G(d)	6-31++G(d,p)
Cu-C_1	1.944 Å	2.018 Å	2.012 Å	2.011 Å
Cu-S	2.264 Å	2.235 Å	2.203 Å	2.198 Å
S-C_2	1.987 Å	1.988 Å	1.895 Å	1.896 Å
C_1-C_2	1.516 Å	1.501 Å	1.509 Å	1.513 Å
C_1-H_1	1.089 Å	1.088 Å	1.089 Å	1.091 Å
C_1-H_2	1.089 Å	1.088 Å	1.089 Å	1.091 Å
C_2-H_3	1.086 Å	1.085 Å	1.090 Å	1.092 Å
C_2-H_4	1.086 Å	1.085 Å	1.090 Å	1.092 Å
∠C_1-Cu-S	84.0º	81.8º	80.4º	80.6º
∠Cu-S-C_2	72.9º	76.9º	79.0º	78.9º
∠S-C_2-C_1	106.8º	105.4º	105.7º	105.7º
∠C_2-C_1-Cu	93.4º	95.8º	95.0º	94.7º
∠Cu-C_1-H_1	112.2º	105.9º	106.8º	106.8º
∠Cu-C_1-H_2	112.2º	105.9º	106.8º	106.8º
∠S-C_2-H_3	105.6º	105.6º	107.7º	107.8º
∠S-C_2-H_4	105.6º	105.6º	107.7º	107.8º
D(C_1-Cu-S-C_2)	12.8º	0.0º	0.0º	0.0º
D(S-Cu-C_1-H_1)	131.2º	119.5º	119.2º	119.0º
D(S-Cu-C_1-H_2)	-103.9º	-119.5º	-119.2º	-119.0º
D(Cu-S-C_2-H_3)	135.8º	120.9º	120.9º	120.8º
D(Cu-S-C_2-H_4)	-106.8º	-120.9º	-120.9º	-120.8º
a_{63Cu}	-229	-226	-272	-272
a_{33S}	-4	-6	0	13
a_{13C1}	89	96	106	123
a_{13C2}	-13	-17	-12	-12
a_{H1}	7	4	1	1
a_{H2}	7	4	1	1
a_{H3}	1	6	4	4
a_{H4}	8	6	4	4
Energy	-2117.2286206	-2117.2975923	-2117.329459	-2117.2909135

M06	6-311G	6-311+G	6-311+G(d)	6-31++G(d,p)
Cu-C_1	1.931 Å	2.005 Å	2.000 Å	1.999 Å
Cu-S	2.239 Å	2.208 Å	2.177 Å	2.172 Å
S-C_2	1.949 Å	1.955 Å	1.881 Å	1.886 Å
C_1-C_2	1.508 Å	1.494 Å	1.496 Å	1.500 Å
C_1-H_1	1.091 Å	1.090 Å	1.092 Å	1.093 Å
C_1-H_2	1.091 Å	1.090 Å	1.092 Å	1.093 Å
C_2-H_3	1.089 Å	1.088 Å	1.093 Å	1.094 Å
C_2-H_4	1.089 Å	1.088 Å	1.093 Å	1.094 Å
∠C_1-Cu-S	82.8º	81.6º	80.4º	80.6º
∠Cu-S-C_2	73.4º	77.4º	79.2º	79.0º
∠S-C_2-C_1	105.6º	105.5º	105.6º	105.7º
∠C_2-C_1-Cu	93.2º	95.5º	94.8º	94.4º
∠Cu-C_1-H_1	112.8º	105.2º	105.9º	105.7º
∠Cu-C_1-H_2	112.8º	105.2º	105.9º	105.7º
∠S-C_2-H_3	106.0º	106.2º	107.9º	107.8º
∠S-C_2-H_4	106.0º	106.2º	107.9º	107.8º
D(C_1-Cu-S-C_2)	16.9º	0.0º	0.0º	0.0º
D(S-Cu-C_1-H_1)	135.7º	119.6º	119.4º	119.3º
D(S-Cu-C_1-H_2)	-99.2º	-119.6º	-119.4º	-119.3º
D(Cu-S-C_2-H_3)	140.4º	120.9º	120.9º	120.8º
D(Cu-S-C_2-H_4)	-101.8º	-120.9º	-120.9º	-120.8º
a_{63Cu}	-229	-226	-272	-272
a_{33S}	-4	-6	0	13
a_{13C1}	89	96	106	123
a_{13C2}	-13	-17	-12	-12
a_{H1}	7	4	1	1
a_{H2}	7	4	1	1
a_{H3}	1	6	4	4
a_{H4}	8	6	4	4
Energy	-2117.2286206	-2117.2975923	-2117.329459	-2117.2909135
BHandHLYP				
Cu-C_1	1.940 Å	2.073 Å	2.066 Å	2.065 Å
Cu-S	2.236 Å	2.230 Å	2.201 Å	2.196 Å
S-C_2	1.965 Å	1.959 Å	1.869 Å	1.867 Å
C_1-C_2	1.511 Å	1.485 Å	1.495 Å	1.498 Å
C_1-H_1	1.081 Å	1.079 Å	1.081 Å	1.082 Å
C_1-H_2	1.081 Å	1.079 Å	1.081 Å	1.082 Å
C_2-H_3	1.076 Å	1.077 Å	1.082 Å	1.084 Å
C_2-H_4	1.076 Å	1.077 Å	1.082 Å	1.084 Å
∠C_1-Cu-S	84.8º	79.0º	78.0º	78.3º
∠Cu-S-C_2	73.7º	79.6º	81.1º	81.1º

	6-311G	6-311+G	6-311+G(d)	6-31++G(d,p)
∠S-C_2-C_1	108.1º	105.5º	105.6º	105.7º
∠C_2-C_1-Cu	93.4º	96.0º	95.3º	94.9 º
∠Cu-C_1-H_1	111.2º	103.7º	104.7º	104.6º
∠Cu-C_1-H_2	111.2º	103.7º	104.7º	104.6º
∠S-C_2-H_3	105.2º	106.0º	108.2º	108.3º
∠S-C_2-H_4	105.2º	106.0º	108.2º	108.3º
D(C_1-Cu-S-C_2)	0.1º	0.0º	0.0º	0.0º
D(S-Cu-C_1-H_1)	117.8º	119.9º	119.7º	119.6º
D(S-Cu-C_1-H_2)	-117.8º	-119.9º	-119.7º	-119.6º
D(Cu-S-C_2-H_3)	121.4º	120.9º	115.6º	120.7º
D(Cu-S-C_2-H_4)	-121.4º	-120.9º	-115.6º	-120.7º
a_{63Cu}	-507	-495	-560	-564
a_{33S}	-5	-10	1	14
a_{13C1}	111	134	144	163
a_{13C2}	-17	-29	-20	-15
a_{H1}	-7	-20	-15	-19
a_{H2}	-7	-20	-15	-15
a_{H3}	6	12	9	9
a_{H4}	6	12	9	9
Energy	-2117.0254649	-2117.0879098	-2117.125905	-2117.0920516